Engineering Environmentally Friendly Dielectrics for use in Capacitors and Thin Film Transistors

By

Mathieu Tousignant

A THESIS

SUBMITTED TO THE UNIVERSITY OF OTTAWA

IN PARTIAL FULFILMENT OF THE REQUIRMENTS FOR THE

DOCTORAL OF PHILOSOPHY DEGREE

IN CHEMICAL ENGINEERING

DEPARTMENT OF CHEMICAL AND BIOLOGICAL ENGINEERING

UNIVERSITY OF OTTAWA

Abstract

Electronic devices are used for tasks such as keeping people connected, figuring out the contents of a package or detecting impurities in the air. The use of electronic sensors in short life cycle products has also begun to increase with the field of smart packaging. For example, RFID tags are used everyday in sorting facilities to identify packages and then discarded when the packaging is thrown away. Every year the world generates millions of tons of E-waste and most of it is exported, incinerated, or put in landfills. To mitigate the impact of electronics on the environment, it is essential that the next generation of disposable electronic devices are fabricated using environmentally friendly materials. For these materials to be considered for high throughput fabrication they need to be solution processable and biodegradable, all while having the necessary mechanical and electrical properties.

This thesis focuses on the development of novel environmentally friendly dielectrics that can be used in capacitors and thin film transistors. A common environmentally friendly and biodegradable material used as a polymer dielectric is poly(vinyl alcohol) (PVA). Although PVA has a high capacitance it also has its drawbacks. Being mostly processed from aqueous solutions it is hard to form uniform thin films of PVA and it is sensitive to moisture which changes its capacitance. PVA is also a polar material which can cause charge trapping at the semiconductor/dielectric interface when used as a dielectric in the fabrication of organic thin film transistors (OTFTs). In this thesis we use different strategies such as blending dielectrics and stacking them to help improve the performance of PVA as a dielectric in OTFTs. In the first study, I demonstrate how low weight percentages of cellulose nanocrystals can be used to increase the viscosity of PVA without negatively impacting its dielectric properties. This led to better film uniformity and a larger number of functioning OTFTs. The second study focused on using a toluene diisocyanate terminated polycaprolactone (TPCL) polymer as a low-*k* barrier between PVA and the semiconductor. The TPCL led to an increase in OTFT performance and a large reduction in moisture sensitivity. For the third study, I improved the shelf life of the TPCL materials by replacing the toluene diisocyanate end units with UV crosslinking end units. The UV end units were protected unlike the TPCL end units allowing the polymer to remain stable under ambient conditions. The UV-PCL demonstrates similar resistance to moisture and dielectric properties to TPCL while being more stable and easier to use in traditional printing processes. My last study, investigates the use of a poly(lactic acid) (PLA) layer as a third layer in

the TPCL/PVA/PLA dielectric system. The PLA layer acted as an intermediate between the substrate and PVA increasing the adhesion of PVA. Further the PLA layer improved OTFT performance and allowed for n-type single walled carbon nanotube transistors under ambient conditions.

Finally, this work has demonstrated ways to improve the performance of PVA so that it can be used as an environmentally friendly dielectric in thin film, flexible and printed electronic applications.

Abstrait

Les appareils électroniques sont utilisés pour des tâches telles que garder les gens connectés, déterminer le contenu d'un colis ou détecter les impuretés dans l'air. L'utilisation de capteurs électroniques dans les produits à cycle de vie court a également commencé à augmenter avec le domaine des emballages intelligents. Par exemple, les étiquettes RFID sont utilisées quotidiennement dans les installations de tri pour identifier les colis, puis jetées lorsque l'emballage est jeté. Chaque année, le monde génère des millions de tonnes de déchets électroniques et la plupart d'entre eux sont exportés, incinérés ou jeté. Pour atténuer l'impact de l'électronique sur l'environnement, il est essentiel que la prochaine génération d'appareils électroniques jetables soit fabriquée à l'aide de matériaux écologique. Pour que ces matériaux soient considérés pour la fabrication à haut débit, ils doivent être traitables par solution et biodégradables, tout en ayant les propriétés mécaniques et électriques nécessaires.

Cette thèse porte sur le développement de nouveaux diélectriques écologique pouvant être utilisés dans les condensateurs et les transistors à couches minces. Un matériau écologique et biodégradable couramment utilisé comme diélectrique est le poly(vinyl alcohol) (PVA). Bien que le PVA ait une capacitance élevée, il a aussi ses inconvénients. Étant principalement traité à partir de solutions aqueuses, il est difficile de former des films minces uniformes de PVA et il est sensible à l'humidité qui modifie sa capacitance. Le PVA est également un matériau polaire qui peut provoquer un piégeage de charge à l'interface semi-conducteur/diélectrique lorsqu'il est utilisé comme diélectrique dans la fabrication de transistors à couches minces organiques (OTFT). Dans cette thèse, nous utilisons différentes stratégies telles que le mélange de diélectriques et leur empilement pour aider à améliorer la performance du PVA en tant que diélectrique dans les OTFT. Dans la première étude, je démontre comment de faibles pourcentages en poids de nanocristaux de cellulose peuvent être utilisés pour augmenter la viscosité du PVA sans impact négatif sur ses propriétés diélectriques. Cela a permis une meilleure uniformité du film et à un plus grand nombre d'OTFT fonctionnels. La deuxième étude s'est concentrée sur l'utilisation d'un polymère de polycaprolactone à terminaison diisocyanate de toluène (TPCL) comme barrière à faible-*k* entre le PVA et le semi-conducteur. Le TPCL a entraîné une augmentation des performances OTFT et une forte réduction de la sensibilité à l'humidité. Pour la troisième étude, j'ai amélioré la durée de conservation des matériaux TPCL en remplaçant les unités terminales de diisocyanate de toluène par des unités terminales de

réticulation UV. Les unités terminales UV étaient protégées contrairement aux unités terminales TPCL permettant au polymère de rester stable dans les conditions ambiantes. L'UV-PCL présente une résistance à l'humidité et des propriétés diélectriques similaires à celles du TPCL tout en étant plus stable et plus facile à utiliser dans les processus d'impression traditionnels. Ma dernière étude porte sur l'utilisation d'une couche de poly(lactic acide) (PLA) comme troisième couche dans le système diélectrique TPCL/PVA/PLA. La couche de PLA agi comme un intermédiaire entre le substrat et le PVA augmentant l'adhérence du PVA. En outre, la couche PLA a amélioré les performances OTFT et a permis des transistors à nanotubes de carbone à n-type dans des conditions ambiantes.

Finalement, ce travail a démontré des moyens d'améliorer les performances du PVA afin qu'il puisse être utilisé comme diélectrique écologique dans les applications électroniques à couches minces, flexibles et imprimées.

Acknowledgements

First off, I would like to thank my supervisor professor Benoit Lessard for giving me the opportunity to learn and grow as a researcher within his group. Professor Lessard gave me the opportunity to do a thesis project with his group during my undergraduate studies. This work began to fuel my passion for research in organic electronics. Throughout my academic journey professor Lessard has continuously provided me with support and helped me grow and improve my skills as a researcher. It has been a pleasure to work with the Lessard Research Group and see the groups knowledge and skills grow over the years.

I would also like to thank all of my group members from the Lessard Research Group for providing a research environment where I felt I could continuously grow and learn. I would like to give a special thank you to Dr. Nicole Rice for her mentorship and help early on in my graduate studies. Her guidance and help created the foundation of my skills as a researcher. I would also like to thank Dr. Alexander Peltekoff, Dr. Owen Melville, Dr. Jukka Niskanen, Dr. Sonia Lin and Dr. Brendan Mirka for all their support and collaboration on projects over the years. Further I would like to thank my fellow lab mates Benjamin, Kaitlin, Mario, Rosemary and Samantha for their support and friendship throughout my graduate studies.

I would like to thank the support staff James MacDermid, Gerard Nina, Franco Ziraldo and Patrick Pageau. The members of the support staff were essential to helping me build the necessary equipment during my graduate studies.

I would like to thank my friends for their support and encouragement, especially Phillip Williams for your collaborations and help. I would also like to thank all the members of my family for their support and a special thanks to my father Eric Tousignant for encouraging me to pursue my passion in research. Your encouragement to learn new things and step out of my comfort zone has helped me grow as both a person and researcher.

Finally, I would like to thank my partner, Rosalie. Her continued support, love and encouragement has helped me through both my undergraduate and graduate studies. Both your work ethic and caring heart have served as an inspiration for me during my studies and I’m excited to start the next chapter of our lives and continue growing with you.

List of Peer Reviewed Journal Article Contributions

Statement of contributions are found preceding each chapter.

1. **M.N. Tousignant**, N.A. Rice, A. Peltekoff, C. Sundaresan, C. Miao, W.Y. Hamad, B.H. Lessard, Improving Thin-Film Properties of Poly(vinyl alcohol) by the Addition of Low-Weight Percentages of Cellulose Nanocrystals, Langmuir. 36 (2020) 3550–3557.

2. **Mathieu N Tousignant**, Nicole A Rice, Jukka Niskanen, Chloé M Richard, Dialia Ritaine, Alex Adronov, Benoît H Lessard. High Performance Organic Electronic Devices Based on a Green Hybrid Dielectric. Adv. Electron. Mater. 7, 1–10 (2021).

3. **Mathieu N Tousignant**, Zheng Sonia Lin, Jaclyn Brusso, Benoît H Lessard. Interfacial Ultraviolet Cross-Linking of Green Bilayer Dielectrics. ACS Appl. Mater. Interfaces 15, 2, 3680–3688 (2023).

4. **Tousignant, M. N.**, Ronnasi, B., Tischler, V. & Lessard, B. H. N-Type Single Walled Carbon Nanotube Thin Film Transistors Using Green Tri-Layer Polymer Dielectric. Adv. Mater. Interfaces 2300079, 1–8 (2023)

The full abstract, links to the publications and statement contributions are found in chapter 7.

5. A.J. Peltekoff, **M.N. Tousignant**, V.E. Hiller, O.A. Melville, B.H. Lessard, Controlled synthesis of poly(pentafluorostyrene-ran-methyl methacrylate) copolymers by nitroxide mediated polymerization and their use as dielectric layers in organic thin-film transistors, Polymers (Basel). 12 (2020).
6. O.A. Melville, T.M. Grant, K. Lochhead, B. King, R. Ambrose, N.A. Rice, N.T. Boileau, A.J. Peltekoff, **M.Tousignant**, I.G. Hill, B.H. Lessard, Contact Engineering Using Manganese, Chromium, and Bathocuproine in Group 14 Phthalocyanine Organic Thin-Film Transistors, ACS Appl. Electron. Mater. 2 (2020) 1313–1322.
7. Jukka Niskanen, **Mathieu N. Tousignant**, Alexander J. Peltekoff, and Benoît H. Lessard, 1,2,3-triazole based poly(ionic liquids) as solid dielectric materials. Polymer 212,123144
8. Mirka, B., Rice, N.A., Williams, P., **Tousignant, M.N.**, Boileau, N.T., Bodnaryk, W.J., Fond, D., Adronov, A., Lessard, B.H. Excess Polymer in Single-Walled Carbon Nanotube Field-Effect Transistors: Does It Really Need to be Removed Prior to Fabrication? ACS Nano 15, 8252–8266 (2021).
9. Vida A Gabriel, **Mathieu N Tousignant**, Sean MW Wilson, Marie DM Faure, Emily D Cranston, Michael F Cunningham, Benoît H Lessard, Marc A Dubé. Improving Latex-Based Pressure-Sensitive Adhesive Properties Using Carboxylated Cellulose Nanocrystals. Macromol. React. Eng. 16, 2100051 (2022).
10. Jukka Niskanen, **Mathieu N Tousignant**, Alexander J Peltekoff, Benoît H Lessard. Poly (ethylene glycol)-Based Poly (ionic liquid) Block Copolymers through 1, 2, 3-Triazole Click Reactions. ACS Appl. Polym. Mater. 4, 1559–1564 (2022).
11. Samantha Brixi, Chase L Radford, **Mathieu N Tousignant**, Alexander J Peltekoff, Joseph G Manion, Timothy L Kelly, Benoît H Lessard. Poly (ionic liquid) Gating Materials for High-

Performance Organic Thin-Film Transistors: The Role of Block Copolymer Self-Assembly at the Semiconductor Interface. ACS Appl. Mater. Interfaces 14, 40361–40370 (2022).

12. **Mathieu N Tousignant**, May Ourabi, Brendan Mirka, William Bodnaryk, Alex Adronov, Benoit Lessard. Poly (ionic liquid) Dielectric for High performing P-and N-type Single Walled Carbon Nanotube Transistors. Flex. Print. Electron. 7, 034004 (2022).
13. Ronnasi, B., **Tousignant, M.** & Lessard, B. H. Chitosan based dielectrics for use in single walled carbon nanotube-based thin film Transistors. *J. Mater. Chem. C* (2023)
14. Vebber, M. C.; King, B.; French, C.; **Tousignant, M.**; Ronnasi, B.; Dindault, C.; Wantz, G.; Hirsch, L.; Brusso, J.; Lessard, B. H. From P-type to N-type: Peripheral Fluorination of Axially Substituted Silicon Phthalocyanines Enables Fine Tuning of Charge Transport. *Can. J. Chem. Eng.* 2023, No. January, 1–13.

Table of Contents

List of Figures

List of Tables

List of Abbreviations

AFM: atomic force microscope

AL_2O_3: aluminium oxide

BGBC: bottom gate bottom contact

BGTC: bottom gate top contact

C: capacitance

C_i: capacitance density

CNC: cellulose nanocrystals

Cr: chromium

CuPc: copper phthalocyanine

DMA: dynamic mechanical analysis

DOS: density of states

DSC: differential scanning calorimetry

E-waste: electronic waste

EDL: electrical double layer

EIS: electrochemical impedance spectroscopy

EMIM: 1-ethyl-3-methylimidazolium

F: farads

f: frequency

γ_{SD}: dispersive component of the surface energy

γ_{SP}: polar component of the surface energy

g_m: transconductance

H: Hysteresis

high-*k*: Dielectric constant > 3.9

$I_{on/off}$: on/off current ratio

ILs: ionic liquids

I_{SD}: source-drain current

I_{GS}: source-gate current

IS: Impedance Spectroscopy

ITO: indium tin oxide

k: dielectric constant (relative permittivity)

L: length of the source drain electrodes

low-*k*: dielectric constant < 3.9

MIM: metal-insulator-metal

m-SWCNTs: metallic single walled carbon nanotubes

NMR: nuclear magnetic resonance

ω: angular frequency

OLED: organic light emitting diode

OPV: organic photovoltaic

OTFT: organic thin film transistor

OTS: trichloro(octadecyl)*silane*

PBS: polybutylene succinate

PCF: poly(carbazole-*co*-*alt*-fluorene)

PCF-SWCNT: poly(carbazole-*co*-*alt*-fluorene) - single walled carbon nanotubes

PCL: polycaprolactone

Φ: phase angle

PILs: polymer-ionic liquids

PLA: poly(lactic acid)

PMMA: polymethyl methacrylate

PS: polystyrene

PVA: poly(vinyl alcohol)

PVAc : poly(vinyl alcohol)/cellulose nanocrytals

PVD: physical vapor deposition

PVP: polyvinyl phenol

P3HT: poly-3-hexylthiophene

RH: relative humidity

RFID: radio frequency identification

RMS: root mean square

sc-SWCNT: semiconducting single walled carbon nanotubes

SiO_2: silicon dioxide

SWCNT: Single walled carbon nanotubes

t: thickness of the dielectric layer

Tanφ: tangent loss

TDI: toluene-2, 4-diisocianate

TFSI: bis(trifluoromethylsulfonyl)imide

T_g: glass transition temperature

TGA: thermogravimetric analysis

TGBC: top gate bottom contact

TGTC: top gate top contact

TiO_2: titanium dioxide

TLC: thin layer chromatography

T_m: melting temperature

TPCL: toluene diisocianate terminated polycaprolactone

μ: mobility

μ_h: hole mobility

UV-PCL: Benzodioxinone terminated polycaprolactone

V_{GS}: gate-source voltage

V_{SD}: source-drain voltage

V_T: threshold voltage

W: width between the source drain electrodes

Z: impedance

Z': real portion of the impedance

Z": imaginary portion of the impedance

ZnO: zinc oxide

Chapter 1 : Introduction

1.1 Overview

1.1.1 Electronic Waste

Electronics are used in everything from smart phones to product packaging. This increase in applications for electronic devices has also brought along the problem of electronic waste or E-waste. The lifespan of electronics continues to decrease as consumers replace their devices more frequently. For example, in 2014 the world produced 41 million tonnes of electronic waste, in 2022 we produced 59.4 million tonnes and it is predicted that the world will produce over 70 million tonnes of e-waste by 2030.[1,2] At the end of an electronic devices lifecycle they end up in landfills, being incinerated or exported.[3] One way to reduce waste is to produce biodegradable electronics. This can be done through the use of organic electronic materials. Another advantage of organic electronics is that they can be printed using solution processing techniques, for example: roll to roll printing, reducing the cost of production.[3] There are many types of organic electronics, the most popular being organic light emitting diodes (OLEDs), organic photovoltaics (OPVs) and organic thin film transistors (OTFTs). Each of these types of devices can have a variety of architectures and applications.[4] For instance, OTFTs can be used in a wide variety of disposable packaging and sensing applications.[3] For many of these sensing applications the OTFTs are one-time or short term use increasing their environmental impact.[5–8]

1.2 Organic-Thin-Film Transistors

1.2.1 OTFT Architecture and Equations

OTFTs are logic gate operators that consist of five main components: the substrate, the gate, the dielectric, the organic semiconductor, and the source-drain electrodes. The order in which these components are stacked together will determine the architecture of the fabricated device. For example, OTFTs can have a bottom gate top contact (BGTC) or a bottom gate bottom contact (BGBC) configuration. The difference between these architectures is the position of the source drain electrodes as demonstrated in **Figure 1.1A** and **1.1B**. Other OTFT architectures include top gate bottom contact (TGBC) and top gate top contact (TGTC) also demonstrated in **Figure 1.1C** and **1.1D**. Each of these architectures has their own advantages and can be selected depending on the processing steps used during OTFT fabrication. For example, top gate architectures encapsulate the semiconducting materials with the dielectric which can improve device performance. This is especially true in the case of n-type materials which are

usually sensitive to oxygen and moisture.[9] Bottom gate architectures expose the semiconductor to the ambient environment which is good if the semiconductor is going to be the active sensing layer.[10]

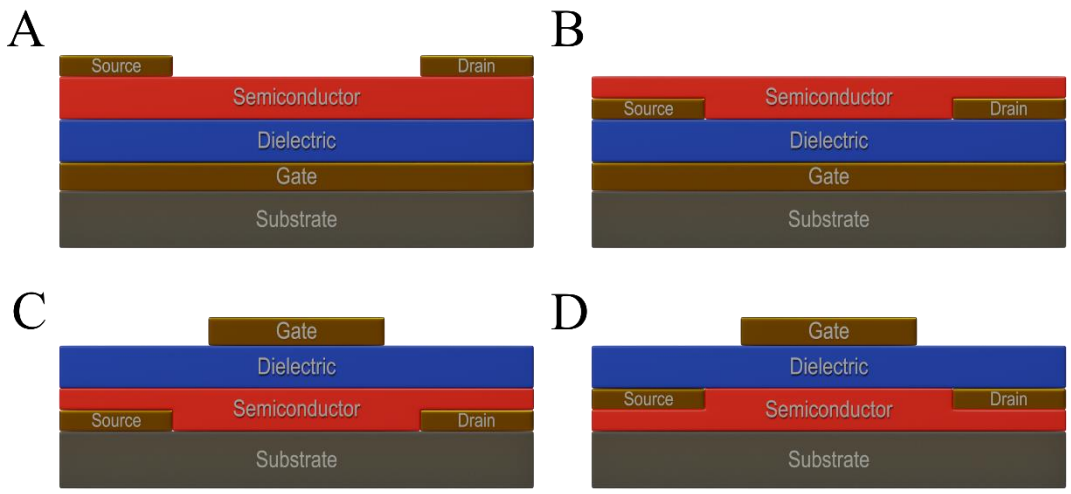

Figure 1.1. Various OTFT architectures: A) bottom gate top contact B) bottom gate bottom contact C) top gate bottom contact D) top gate top contact

OTFTs function by applying a voltage bias between the source-drain electrodes and the source-gate electrodes while measuring the current between the source-drain electrodes. As the gate voltage exceeds the threshold voltage (V_T), the device turns on and charge carriers flow from the source to the drain electrode. The charge mobility (μ) describes the drift velocity of an average charge carrier per unit of an electrical field as either a positive (hole, p-type) or negative (electron, n-type) charge moves through the semiconducting layer from the source to the drain.[4] There are also some organic semiconducting materials where both holes and electrons can move with the appropriately applied bias, these materials are called ambipolar and a common example is semiconducting single walled carbon nanotubes.[11] The on/off ratio ($I_{on/off}$), is the difference between the current being measured from the device in an off state versus in a on state. Gate leakage (I_{GS}) is the amount of current passing between the gate and the source electrodes when a bias is applied.[4] Transconductance (g_m) is the measure of the slope of the transfer curve and this gives you information on the amplification effect of the fabricated OTFT. A field effect is observed when the source gate voltage bias is increased and change in current is measured

between the source and drain electrodes. This information is typically plotted as an output curve where the source-drain current (I_{SD}) vs source-drain voltage (V_{SD}) at varying source-gate voltages (V_{GS}) is plotted as seen in **Figure 1.2A**. There are two sections of an output curve, the linear region where $V_{SD} < (V_{GS} - V_T)$. In the linear region I_{SD} will increase linearly with V_{SD}. Once $V_{SD} > (V_{GS} - V_T)$ the OTFT is in the saturation region, as the name states past this threshold the I_{SD} no longer increases linearly with V_{SD} and eventually becomes saturated. To properly characterize and OTFT the output curve is used to determine the linear and saturation regions and select a V_{SD} either in the linear or saturation regime. Next, the V_{SD} is held constant and the V_{GS} is swept and the I_{SD} is measured. With this information a transfer curve can be plotted as seen in **Figure 1.2B**.

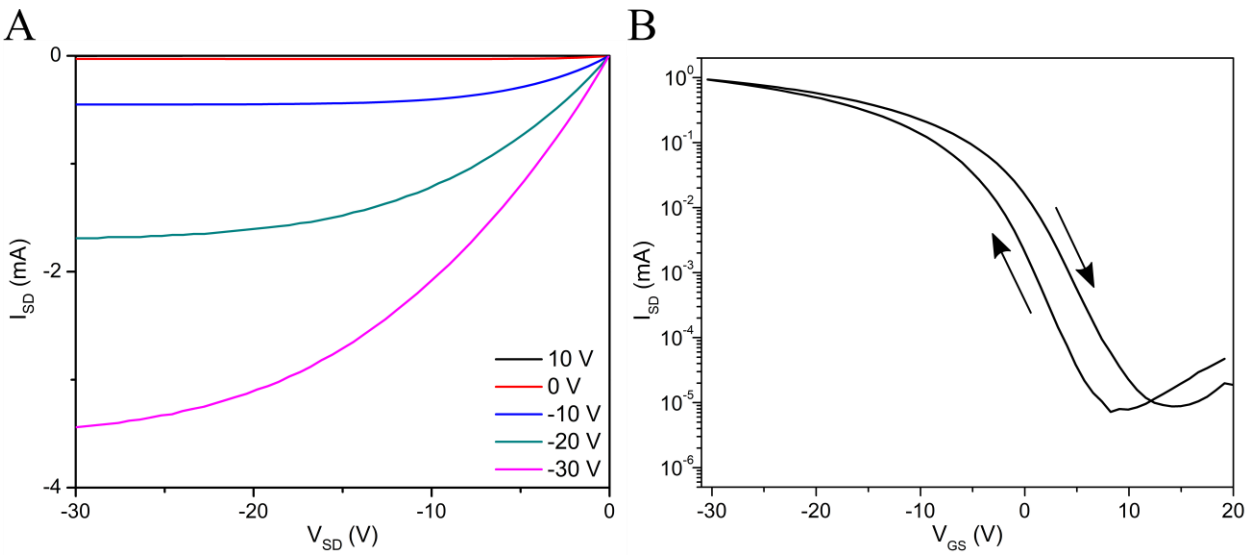

Figure 1.2. (A) Output curve and (B) Transfer curve for a single walled carbon nanotube semiconductor (SWCNTs) with a silicon dioxide (SiO2) dielectric. The black arrows represent the forwards and backwards sweep direction for the transfer curve.

The transfer curve is a plot of I_{SD} vs V_{GS} at a fixed V_{SD} and can be used to calculate the electrical properties of an OTFT with the following equations:

Linear region $V_{SD} < (V_{GS} - V_T)$:

$$I_{SD} = \frac{W\mu C_i}{L}\left(V_{Gs} - V_T - \frac{V_{DS}}{2}\right)V_{DS} \qquad Eq\ 1.1$$

$$\mu = \frac{L}{WC_iV_{Ds}}\frac{\partial I_{DS}}{\partial V_{Gs}} \qquad Eq\ 1.2$$

$$V_T = V_{GS}(x - intecerpt) - \frac{V_{SD}}{2} \qquad Eq\ 1.3$$

Saturation region $V_{SD} > (V_{GS} - V_T)$:

$$I_{SD} = \frac{W\mu C_i}{2L}(V_{Gs} - V_T)^2 \qquad Eq\ 1.4$$

$$\mu = \frac{2L}{WC_i}\left(\frac{\partial\sqrt{I_{DS}}}{\partial V_{Gs}}\right)^2 \qquad Eq\ 1.5$$

$$V_T = V_{GS}(x - intercept) \qquad Eq\ 1.6$$

From the equations 1.1, 1.2, 1.4 and 1.5 : C_i is the capacitance density, L is the length of the source-drain electrodes and W is the width between the source-drain electrodes.

1.2.2 Organic Semiconductors

Within literature there are a wide variety of organic semiconducting materials ranging from small molecules to polymers. The common theme is that all these materials have pi conjugation allowing for electron delocalization. This electron delocalization is what gives these materials their semiconducting properties. Some of the first organic semiconductors were naphthalenes and anthracenes discovered back in the 1940 -1950s.[12] Since that time, lots of research has gone into understanding the impact of crystal structure and packing motifs on the performance of both small molecule and polymer semiconductors.

Another emerging material for organic semiconductors is semiconducting single walled carbon nanotubes (sc-SWCNTs). These materials are rolled up sp2 hybridized carbon sheets where both the angle that the sheet is rolled up and the diameter will determine if the SWCNTs have metallic or semiconducting properties.[13,14] SWCNTs can be fabricated through arc discharge, laser ablation and chemical vapor deposition.[15] Most techniques produce semiconducting and metallic SWCNTs in a ratio of 30% metallic and 70% semiconducting.[16,17] For SWCNTs to be used as semiconductors the metallic SWCNTs need to be separated from the sc-SWCNTs. This can be done using a variety of techniques such as density gradient ultracentrifugation, selective polymers, gel chromatography, gel electrophoresis and ion exchange chromatography.[17–19] Conjugated polymer sorting techniques are where a polymer will selectively wrap around the sc-SWCNTs, enabling their separation from the metallic SWCNTs

with purities upwards of 99%.[20] This technique is one of the most effective ways to obtain sc-SWCNTS with purities upwards of 99%, which is necessary for their use as a semiconductor. The advantage of using sc-SWCNTs as a semiconducting material versus small molecules is that they can be easily dispersed in solution and have recorded μs upwards of 100 cm^2/Vs for p-type performance and theoretical performances of up to 100,000 cm^2/Vs.[11,17,21] Because sc-SWCNTs can be processed in solution they have the potential to be mass produced using traditional printing techniques such as aerosol jet printing, inkjet printing and gravure.[19,22–24] Once sorted, sc-SWCNTs are ambipolar meaning they can be integrated into devices which operate in either p or n-type characteristics. However, sc-SWCNTs are more commonly used in p-type devices because unless they are encapsulated they become doped with oxygen supressing any n-type performance.[19] For fully n-type OTFTs the sc-SWCNTS are typically doped with positively charged ions increasing the accumulation of electrons within the SWCNTs and amplifying n-type performance.[25–27]

1.2.3 Single Walled Carbon Nanotubes Environmental Impact

The main toxicity concern associated to the use of sc-SWCNTs is primarily due to inhalation of the dry nanotube powder. One study led by Maynard et al analyzed the impact of exposure to SWCNTs during their fabrication. Their findings determined that the high aspect ratios pose a toxicity risk however, processing the raw materials did not produce large amounts of airborn SWCNTs.[28] This study shows that the risk of aerosol release of nanotubes during their fabrication exists but is limited. These risks can be further limited using proper PPE during the fabrication and dispersing the fabricated nanotubes in a solvent. Other studies have also demonstrated that SWCNTs can pose toxicity risk to many other organs if they are absorbed into your body. When extending these studies into marine life both Zhu et al and da Rocha et al have reported negative impacts to artemia salina and zebra fish when SWCNTs were introduced.[29,30] The general consensus for SWCNTs is that there are many factors that effect their environmental impact such as absorbed pollutants or conjugation and more studies need to be performed.[31,32] This means more detailed studies on the toxicity and environmental impact of polymer wrapped SWCNTs need to be performed to fully understand their risk on humans and the environment. However, SWCNTs can be biodegraded through enzymatic, cell or bacterial degradation.[31] If proper systems are put in place to reclaim electronics containing SWCNTs they have the

potential to be biodegraded under a controlled environment limiting their environmental impact and toxicity.

1.3 Printed Electronics

OTFTs have been used in a wide variety of sensing applications such as: gas sensing, ion sensing, humidity, temperature and biosensing.[6,33,34] The potential for low cost manufacturing of OTFTs paired with their relatively short lifespan, makes them attractive for disposable applications, such as: bio sensors, flexible RFID tags and smart packaging.[4] Furthermore, OTFTs can be used as artificial skin or as implantable sensors when biocompatible materials are selected. Wu et al. demonstrated the use of biocompatible PLA, Gold and 3 different biocompatible organic semiconductors for the fabrication of a flexible temperature sensor.[35] For most of the proposed sensing applications OTFTs would have a short lifetime further highlighting the need to reduce their environmental impact.

1.3.1 Disposable Sensors and Printing Techniques

One of the benefits of organic electronics is that their low processing temperatures and ability to be dissolved in solution facilitate fabrication using traditional printing techniques, such as: inkjet printing, aerosol jet printing, screen printing and gravure.[36,37] An example of printed electronics through gravure and screen printing can be seen in **Figure 1.3**.

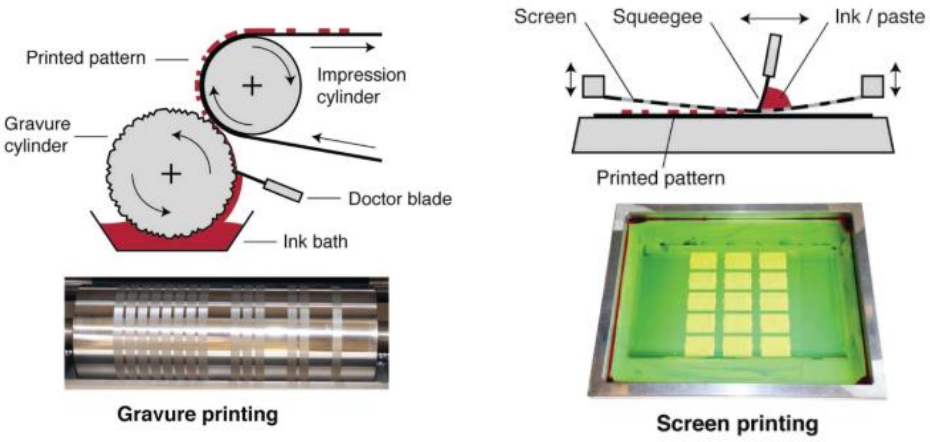

Figure 1.3. Illustration of both gravure and screen printing techniques, from Søndergaard et al.[36]

Another advantage is that the low processing temperatures enable the use of flexible plastic substrates.[38] Grau et al. have reviewed various printing techniques and have demonstrated that gravure techniques can be used to print transistors that have features sizes in the range of 1 – 10 μm at throughput speeds anywhere from 10 to 100 m^2/s.[38] Grau et al. also highlight some of the shortcomings of these printing techniques including electrode roughness, solvent compatibility, and film thickness. All of these factors can impact the performance of printed OTFTs.[38]

Ink jet printing has been used to print poly-3-hexylthiophene (P3HT)/polystyrene (PS) blended semiconductors. In this work by Lim et al., an inkjet printer was used to deposit the P3HT/PS semiconducting material between the source-drain electrodes. The deposited PS helped the P3HT semiconductor form nanowires enabling mobilities as high as 6.3×10^{-3} cm^2/Vs.[39] Similarly, Cho et al. have demonstrated a technique using inkjet printing to deposit a dielectric layer while fabricating OTFTs. This technique uses aerosol jet printing to print a poly(styrene-block-ethylene oxide-block-styrene) (PS-PEO-PS)/1-ethyl-3-methylimidazolium bis(trifluoromethylsulfonyl)imide ([EMIM][TFSI]) ion gel dielectric that achieved capacitance densities as high as 10 $\mu F/cm^2$ at 10 Hz.[40] Aerosol jet printing is a promising technique because it can help mitigate issues caused by the solvents used to dissolve materials. For example, when screen printing, blade coating or using a gravure printing method, the layer underneath must provide suitable surface wetting to evenly distribute the next layer.[41] Aerosol jet printing atomizes the ink being used and sprays a thin line of the atomized ink on the substrate. This technique can help mitigate wetting issues caused by the solvent. Aerosol jet printing techniques have also been widely used with single walled carbon nanotubes (SWCNTs) to print dense networks on a variety of substrates.[16,42,43] The high throughput speeds of these various printing techniques facilitate the mass production of electronics enabling their incorporation into short term and disposable products. This highlights the need for electronically active environmentally friendly materials. These techniques will never be industrially viable with the toxic and chlorinated solvents that are used to dissolve most organic materials.[36] By using solvents that have lower environmental impacts and choosing green substrates it is possible to further offset the environmental impact of these materials. For example using paper/cellulose as the substrate and a solvent such as water, ethanol or anisole.[36,44,45] Using pre-existing printing techniques,

green materials and green solvents, the mass production of disposable electronics can be achieved while minimizing the impact on the environment.

1.3.2 Printed Sensors and their Environmental Impact

The use of printed electronics for sensor development can already be seen within literature. Although organic electronic sensors are still new, they offer many benefits when compared against traditional silicon-based sensors. For example, they can have a low elastic modulus due to being printed on plastic materials, they can be scalable and can have high throughput speeds both of which reduce the cost of production.[46] **Figure 1.4** reproduce from Khan et al. highlights the benefits and applications of organic printed sensors.

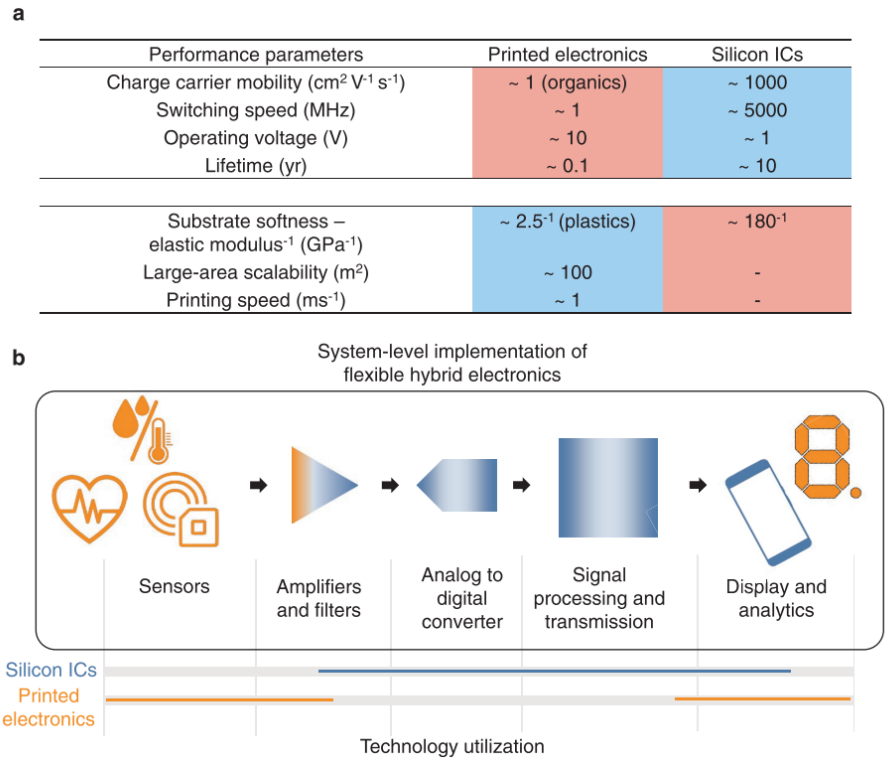

Figure 1.4. A) Difference in performance parameter for printed and silicon base sensors. B). Chart showing where silicon based (blue line) and printed electronics (orange line) can be used in the fabrication of printed sensors. Copied from Khan et al.[46]

Organic electronic sensors often cannot outperform silicon-based sensors, however not all applications require such high performances and longevity. Short-term sensors can be used to measure information such as temperature, pressure, analyte concentration, light and even DNA.[7,47,48] These sensors can be used in a wide variety of applications from medical sensors to

sensors for monitoring the structural integrity of buildings.[49,50] When discussing printed electronics and sensors Wilkund et al. mention that "*The current trend of adding intelligence into everyday objects and discarding their environmental impact is not sustainable and requires alternative solutions that aims at reducing the looming e-waste stream*".[51] This statement is true for electronics in general, but especially for short life cycle printed electronic sensors. Therefore, when developing inks for printed electronic applications it is important to keep the complete life cycle of the fabricated devices in mind.[3] For example Williams et al. fabricated fully printed and recyclable electronics using a paper substrate with graphene electrodes, a cellulose nanocrystal dielectric and carbon nanotube based semiconductor.[52] Low cost and high throughput sensors have the potential to enable point of care medical testing and smart packaging/sensors within everyday life however, these devices can also lead to a large increase in electronic waste if the proper fabrication guidelines are not implemented.

1.4 Capacitors and Dielectric Materials

1.4.1 Dielectric Equations

One of the active layers within an OTFT is the dielectric layer. The dielectric is an insulating layer between the gate electrode and the organic semiconductor. The dielectric facilitates charge accumulation at the semiconductor dielectric interface following the application of a bias between the source and the gate electrodes. By applying a $V_{GS,}$ mobile charge carriers within the semiconductor accumulate at the interface. This facilitates current flow through the semiconductor once a source-drain bias is applied.[53,54] An important property of a dielectric material is the capacitance. A high capacitance increases the charge accumulation at the dielectric/semiconductor interface and will lead to increased μ while reducing threshold voltage.[55] In order to characterize the electrical properties such as capacitance, metal-insulator-metal (MIM) capacitors are fabricated. MIM capacitors consist of an insulating layer sandwiched between two electrodes. **Figure 1.5** is an example of a substrate with 10 MIM capacitors with areas varying from 0.35-2.88 mm^2.

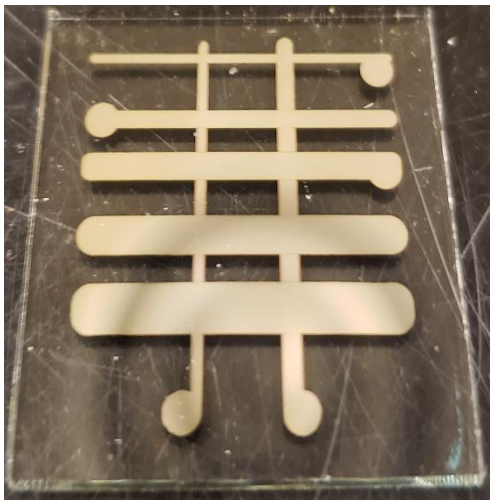

Figure 1.5. 10 MIM capacitors with areas from 0.35-2.88 mm^2 fabricated on 1 in^2 glass substrate.

The dielectric properties of the insulating layer are characterized using electrochemical impedance spectroscopy (EIS). Impedance is the measurement of a current in response to an applied voltage bias (~10 mV) in a sinsuadal form. Impedance can be expressed using the following equation:

$$Z(f) = \frac{V(f)}{I(f)} \qquad Eq\ 1.7$$

Equation 1.7 uses the principles of ohms law but there are two main differences: the resistance (R) is replaced with impedance (Z) and the impedance is dependant on the frequency at which the potential is oscilating.[56] These properties are commonly expressed through nyquist and bode plots **Figure 1.6.**

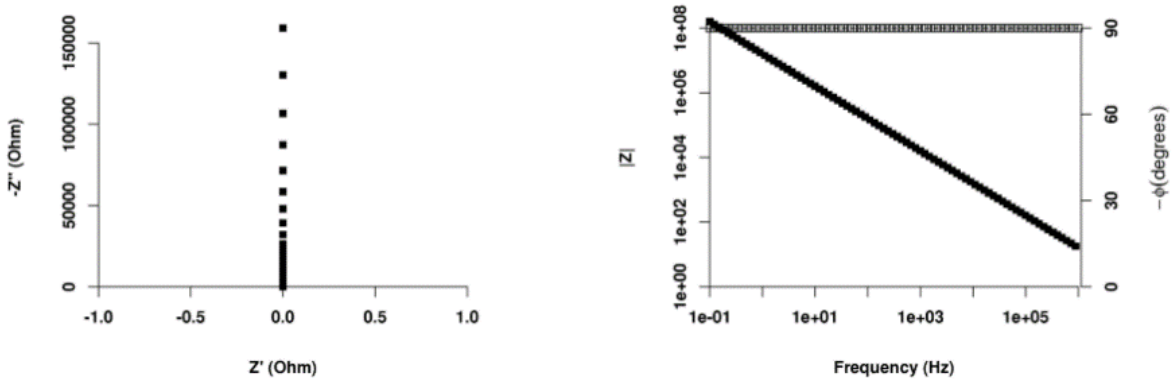

Figure 1.6. Impedance spectra of an ideal capacitor (left) in a Nyquist and (right) in a Bode plot.[56]

The nyquist plot from **Figure 1.6** represents both the imaginary (y-axis, *-Z''*) and the real (x-axis, *Z'*) portion of the impedance (*Z*). The sum of these portions describes the impedance and can be represented as:

$$Z = Z' + jZ'' \qquad Eq\ 1.8$$

The phase angle (*-φ* in **Figure 1.6**) can then be calculated from the imaginary and real portions of the impedance using the equation below:

$$\varphi = Tan^{-1}\left(\frac{Z''}{Z'}\right) \qquad Eq\ 1.9$$

Using the imaginary portion of the impedance *(-Z'')* and the frequency (f) the capacitance (*C*) can be calculated:

$$c = \frac{1}{2\pi \times f \times -Z''} \qquad Eq\ 1.10$$

Equation 1.10 is used to calculate the capacitance of a dielectric material that is behaving as an ideal capacitor. For a capacitor to be considered ideal it needs to have a *Z'* value of zero, as seen in **Figure 1.6**. This 0 value for *Z'* means that the dielectric material does not have any resistive behaviour. However, when working with polymer dielectrics this is usually not the case. Dipole polarization can contribute towards the dielectric constant and the dielectric loss.[57] Polymer dielectrics can have a dipole along the backbone, a dipole on rigid pendant groups or a

dipole on flexible pendant groups. These dipoles will impact the polarization of the dielectric due to local reorientation of the pendant or the main polymer chain.[58] To improve the fidelity of the calculations, the relative permitivity of a dielectric material (dielectric constant) can be expressed by both the imaginarry (*-Z''*) and the real (*Z'*) portions. When a bias is applied the polymer dielectric will polarize, this is not an instantanious process and a certain amount of time is needed once the bias is removed for the polymer to return to its random orientation. This causes what is called tangent loss (*Tanφ*) which is the ratio between *-Z''* and *Z'*. The tangent loss is at a minimum when relaxation time for the polymer dielectric is smaller or equal to the frequency of the applied voltage bias.[57] In order to consider the impact of polarization, the following equations are used to calculate the relative permitivity (dielectric constant) and capacitance with a higher degree of precision.[57,59]

$$k = \frac{t}{\omega A \epsilon_0} \frac{Z''}{Z'^2 + Z''^2} \qquad Eq\ 1.11$$

$$Tan\varphi = \frac{Z''}{Z'} \qquad Eq\ 1.12$$

$$c = \frac{k \epsilon_0 A}{t} \qquad Eq\ 1.13$$

For equations 1.11 through 1.13, k is the dielectric constant, ω is the angular frequency ($2\pi f$), ϵ_0 is the relative permitivity of a vacuum, A is the area of the metal electrode and t is the thickness of the dielectric. Using the above equations both the dielectric constant and the capacitance of a polymer dielectric can be calculated for a given frequency. The calculated capacitance can then be divided by the area of the capacitors electrode giving c_i. The calculation of capacitance density is important to be able to accurately calculate the μ of an OTFT. The electrical properties of a dielectric material can have a large impact on the performance of an OTFT. For example, higher capacitance densities give higher μ*'s* and a lower V_T. Therefore, the fabrication of MIM capacitors allows for the isolation and optimization of the dielectric material and its properties before these materials are integrated into OTFTs.

1.4.2 Organic and Inorganic Dielectrics

Inorganic dielectrics are typically oxide based dielectrics, for example: SiO_2, Al_2O_3 and HfO_2.[54,60] From these examples, SiO_2 is commonly used as a standard with a dielectric constant

(*k*) of approximately 3.9. Materials with a dielectric constant lower than this value are considered low-*k* materials and higher than 3.9 are considered high-*k* materials.[54] The benefit of these oxide based dielectrics is that they typically have lower leakage currents (I_{GS}), higher capacitance values (high-*k* materials) and lower operating voltages. However, oxides are brittle and require high processing temperatures.[54] Inorganic dielectrics are still commonly used when studying OTFTs. The reason for this is that it is easier to make meaningful comparisons between the performance of semiconductors if all studies are done using SiO_2.[61] In contrast, organic dielectrics such as polymer dielectrics are flexible and can be processed at low temperatures, although they have a higher I_{GS} and lower capacitance (typically low-*k* materials). **Table 1.1.** highlights the advantages and disadvantages of both organic and inorganic dielectric materials as well as the optimal properties for a dielectric.

Table 1.1. Comparison of organic and inorganic dielectrics, taken from B.Karri et al.[62]

Property	Inorganic dielectrics	Organic dielectrics	Desired aspect of a gate dielectric material
Dielectric constant	High-*k* (>7.2)	Low-*k* (<3.9)	Higher-*k* is desired
Deposition techniques	Vacuum deposition techniques	Solution processing	Solution processing
Temperature	Ranges from 200 to 500°C which is necessary for annealing	Ranges from 100 to 300°C, which is determined by curing temperature	Low temperature
Impact on threshold voltage	Clean interfaces, lower and stable V_T	Variable V_T due to interface states	Stable V_T
Impact on mobility	Surface energy mismatch between the dielectric material and OSC leads to poor mobility	Surface energy matching between the OSC and dielectric enhances the mobility	High mobility
Impact on current modulation ratio (I_{ON}/I_{OFF})	No structural defects and has good dielectric strength and hence large current modulation ratio	Structural defects are common in thin layers and tend to increase I_{OFF} thereby reducing current modulation ratio	Large current modulation ratio
Impact on reliability	Hysteresis is rarely observed	Hysteresis is common	No hysteresis

Although many polymer dielectric materials are considered low-*k*, it is possible to obtain high-*k* polymer dielectrics. For example, poly(vinyl alcohol) (PVA) is a high-*k* organic dielectric material. These high-*k* properties are usually from polar pendant groups or polar groups on the polymer backbone that increase the capacitance.[63] The disadvantage of these polar dielectrics are that the polymer groups along side impurities within the polymers tend to increase the observed device hysteresis.[64–66] I_{GS} tends to be elevated for organic materials due to poor thin film and surface characteristics, however there are approaches that can reduce I_{GS}. For example, thicker dielectric materials will reduce I_{GS} but also tend to reduce device performance, another approach

is using a dielectric with a lower dielectric constant to increase the band gap, which would also reduce the device performance.[67,68] The main differences between the organic and inorganic materials are the processing temperatures, the deposition methods, and overall stability. For mass produced printed sensors, inorganic materials pose more challenges and are not easily processed onto flexible substrates using solution processing techniques, increasing fabrication time and cost. Furthermore, inorganic dielectrics require high processing temperatures which are also incompatible with many flexible substrates that melt at temperatures as low as 115 °C.[69–71]. Finally, most applications which we are targeting, such as disposable electronics, do not require long lifetimes making long term stability less important. These key points make polymer dielectrics an attractive solution for use in printed electronics for sensing applications.

1.4.3 Environmentally Friendly Dielectrics

Polymer dielectrics are gaining popularity within the field of organic electronics. This is due to both their flexibility and ability to be printed expanding their applications and reducing their costs of manufacturing. **Table 1.2** contains some of the most commonly used polymer dielectrics within OTFTs and their dielectric constant.[54,72]

Table 1.2. Commonly used polymer dielectrics for OTFT fabrication, taken from Guo et al.[72]

Dielectric	Dielectric constant	Reference
CYTOP	2.1	[40]
Polystyrene	2.6	[68]
BCB	2.65	[69]
Polyimide	3.4	[70]
PVC	3.4	[71]
PMMA	3.5	[40]
SU8	3.9	[72]
PVP	4.5	[73]
PVA	7.8 - 10	[74]
CYEL	12	[75]
PVDF-TrFE	-	[76]
PVDF-TrFE-CTFE	>60	[78]

Many of the dielectrics within **Table 1.2** are still considered low-*k* (dielectric constant < 3.9), and PVA is the only polymer dielectric in **Table 1.2** that can be considered environmentally friendly. Apart from the dielectrics shown in **Table 1.2** there are also environmentally friendly natural and synthetic polymers. These materials also have the necessary electrical and mechanical properties to be used as a dielectric within OTFTs and should be further explored for sustainable printed electronics.

Natural and synthetic polymers that are compostable or biodegradable can still demonstrate favorable dielectric properties. These are some examples of natural polymers: chitosan, natural rubber, almond gum, glucose, cytosine, chicken albumen and cellulose.[3,73,74] Many of these natural polymers have high capacitances and are high-*k* materials. Furthermore, their performance as dielectrics within OTFTs are comparable to non-biodegradable synthetic polymers.[3,75–77] Apart from natural polymers, PVA, polycaprolactone (PCL), PLA and polybutylene succinate (PBS) are examples of environmentally friendly and biocompatible synthetic polymers.[3] However, it should be noted that although some synthetic polymers are still environmentally friendly and labeled as biodegradable, they often only decompose with the presence of certain microorganisms. This makes the term compostable more appropriate for these materials.[3] Some examples of these compostable materials are PLA and PVA. For PLA, *Bacillus licheniformis* is responsible for the biodegradation and for PVA the enzymes secreted from various soil bacteria are responsible for its biodegradation.[78,79] More examples of both natural and synthetic polymers along with their mechanisms for biodegradation are shown in **Figure 1.7** from Hosseini et al.[80]

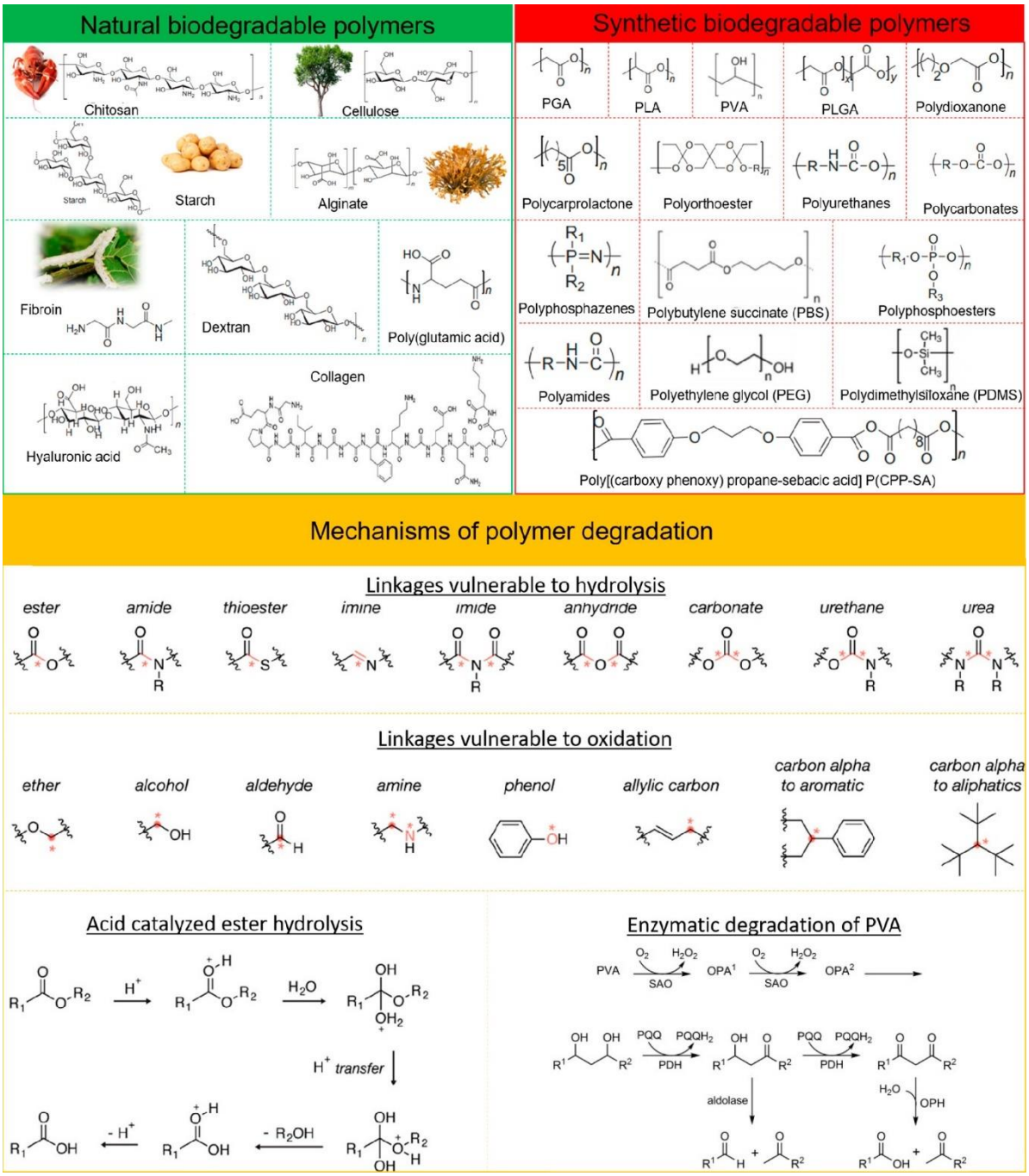

Figure 1.7. Chemical structures of natural and synthetic polymers. The various linkages vulnerable to hydrolysis or oxidation. The mechanisms of both enzymatic degradation of PVA and acid catalyzed ester hydrolysis. Copied from Hosseini et al.[80]

Many of the reported natural and synthetic polymers have been used as flexible substrates for OTFTs. Some of these polymers have even been applied as both a substrate and dielectric, for

example: cellulose, cellulose nanocrystals and PLA.[81–83] Cellulose is an example of a versatile dielectric material, it can be processed into cellulose nanocrystals (CNCs) and used as an additive for increasing the viscosity of PVA.[84] CNCs can also be used with sodium ions as high capacitance ionic conductive nanopapers.[17] The cylindrical surface of CNCs have a large number of hydroxyl groups making it easy to graft polymers to the surface and change the properties of the material.[86,87] Additionally, Cellulose is low-cost, flexible, environmentally friendly, easily obtained through renewable forestry and has good mechanical properties. All of these factors have helped cellulose gain popularity within the field of flexible electronics.[81,88] Unfortunately, environmentally friendly materials do not always outperform other traditional polymer dielectrics and can have issues with material processing, electrical properties and mass production. However, there are strategies that can be used to improve the processing and electrical properties of environmentally friendly dielectrics.

1.4.4 Strategies for Improving the Performance of Environmentally Friendly Dielectrics

There are a few ways to increase the capacitance of a dielectric material: by increasing the dielectric constant of a material (using a high-*k* material), by decreasing the thickness of the dielectric or by using additives to increase the dielectric constant. For a low-*k* material to have a high capacitance the dielectric needs to be very thin as capacitance scales inversely with thickness. Unfortunately, ultra thin dielectric materials can lead to increased leakage currents and can lead to shorted devices from pinholes (**Figure 1.8**) or dielectric breakdown. Furthermore, thin dielectrics are hard to manufacture at scale due to challenges with high throughput printing processes. Many commercial printing techniques use conductive nanoparticles as inks for their conductive electrodes which tend to have high surface roughness's leading to greater I_{GS} and short circuits.[14] Because of this, low-*k* dielectrics are usually thicker and by consequence have higher operating voltages. A promising approach is to create polymer blends to take advantage of the complementary properties leading to both high-*k* properties and thickness independent performance. These blends can also change the mechanical properties, for instance making the polymer dielectric less brittle or increasing its viscosity in solution.[53,85,91,92] The following sub section outline the potential for blending different materials to combine desired material properties:

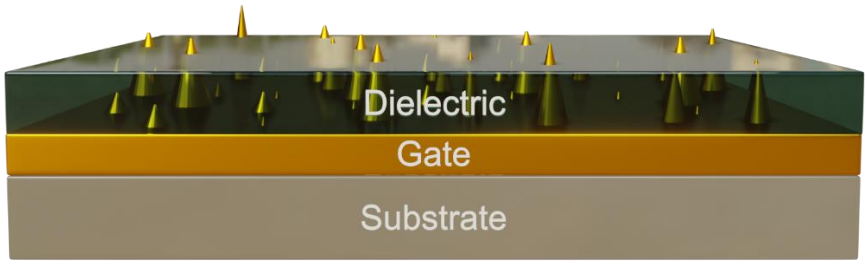

Figure 1.8. Example of pinholes caused by the surface roughness of the metal electrodes and how they can cause short circuits.

1.4.4.1 PIL Dielectrics

One of the approaches to improve dielectric performance involves blending dielectrics with unbound ions usually from inorganic salts. The free moving ions from these salts can greatly increase the capacitance of the dielectric. Researchers have explored the use of ionic liquids (ILs) and polymer-ionic liquids (PILs). For example, studies by Ono et al. used various ILs from the imidazolium family to create high performance low voltage OTFTs.[91,92] The advantage of ILs is that they have free moving charges that can diffuse towards the semiconductor/gate electrode and form an electrical double layer (EDL) with a high capacitance density.[93] In spite of these high capacitance densities, having a liquid dielectric leads to manufacturing challenges and limits their potential applications. Alternatively, polymers can be blended with *ILs* causing the polymer to swell but remain solid. The swollen polymer forms a gel dielectric instead of a liquid dielectric with limited applications. For example, polystyrene and poly(ethylene oxide) triblock copolymers have been applied with a wide range of ILs. Capacitance densities as high as 43 μF cm^{-2} at 10 Hz could be achieved with EMIM/TFSI as the *IL* and an operating frequency as high as 1000 Hz.[94] Dai et al. have also demonstrated this principle with an environmentally friendly ion gel dielectric. They combined sodium ions with cellulose nanofibers creating a high capacitance green dielectric. The sodium ions could diffuse through the cellulose nanofibers and form an EDL allowing for capacitances as high as 220 nF cm^{-2} at 0.1 Hz.[85] Nanocellulose is often blended with either organic, metallic or inorganic particles such as silver nanoparticles and wires.[95] The use of blended nanoparticles or ions to form and EDL has a large impact on the performance of the dielectric layer. **Figure 1.9** highlights the change in capacitance as an EDL forms. This starts with the dipolar relaxation in

region (i) followed by the ionic relaxation in region (ii) and finally the EDL formation in region (iii). ion gel dielectrics, are semi-solid, taking advantage of the *IL* while reducing some manufacturing challenges.

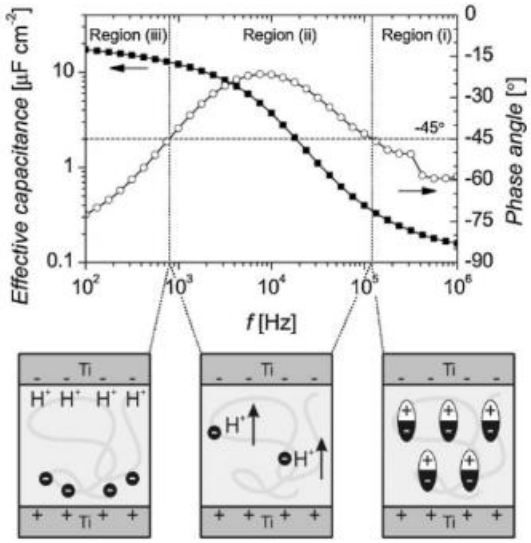

Figure 1.9. Increase in capacitance at various stages in EDL formation. Taken from Larsson et al.[96]

These blends of polymer dielectrics with salts are advantageous but have certain pitfalls. For example, the free moving charges or nanoparticles can diffuse into the semiconducting layer affecting device performance. Therefore, when using ion gels both ions are free to diffuse and form an EDL.[40,94] One way to get around this is to use unipolar polymerized ionic liquids also called PILs. For PILs, one of the charges is bound to the polymer backbone while the other is free to diffuse through the dielectric and form an EDL.[96–101] Peltekoff et al. has fabricated various *PILs* where one of the charges is bound to the polymer by immobilizing it. By tailoring the semiconductor to the dielectric charge it is possible to stop the free moving ions from diffusing into the semiconductor.[97] This means an n-type semiconductor would be paired with an immobilized positive charge and a p-type semiconductor would be paired with an immobilized negative charge. Further, ILs, PILs and ion gels have the potential to be environmentally friendly when green materials and chemistry are used.[102,103]

1.4.4.2 Polymer Blended Dielectrics

Blends can also be used to try and exploit the high-*k* properties of one material as well as the favorable low-*k* properties of the other material. For instance, low-*k* PMMA has been blended with poly(vinylidenefluoride trifluoroethylene) which resulted in a decrease in hysteresis and an enhancement in both electron and hole concentration. This was due to the reduction of dipolar disorder at the dielectric semiconductor interface.[54] Another approach is to use crosslinked polymer blends. Blending a polymer dielectric with a crosslinker allows for the thickness of the dielectric layer to be reduced by increasing film uniformity which reduces leakage currents caused by defects.[104] For non-*IL* and non-*PIL* dielectrics the capacitance will increase as the thickness of the dielectric is decreased and the crosslinking will help reduce gate leakage currents for these thin dielectrics.[105,106] Yoon et al. has reported capacitance densities as high as 200 - 300 nF cm^{-2} and dielectric thickness as thin as 10 – 20 nm through the use of both PVP and PS blends with crosslinking reagents.[107] Crosslinked polymer dielectrics are also beneficial for the fabrication of fully solution processed electronics. Crosslinking the dielectric layer makes it insoluble and prevents it from being removed during orthogonal processing. However, reliably printing 10 – 20 nm dielectric films is still challenging even when crosslinking additives are being used. Blended dielectrics can exploit the high capacitances of high-*k* dielectrics as well as the improved insulating properties by using low-*k* dielectric materials. Blended dielectrics can also be used to improve the mechanical properties of the dielectric materials and reduce leakage currents. Therefore, using blending strategies can lead to increased capacitances, increased device performance and increased device stability.

1.4.4.2 Bilayer and Stacked Dielectrics

Another approach is orthogonal processing of different dielectric layers to improve OTFT performance. For instance, high-*k* dielectrics tend to have a higher surface roughness and this can lead to lower μ.[3] High-*k* dielectrics also tend to have higher dipolar disorder which also leads to a decrease in μ and device performance.[53,54] It has been demonstrated in literature that increases in dipolar disorder at the semiconductor dielectric interface broadens the density of states (DOS). Increasing the polarity of the dielectric will increase capacitance but it also broadens the DOS increasing the amount of trap states and lowering μ.[109] In a study by Masillamani et al. it was demonstrated that changing the dielectric from PS (k ~ 2.0) to PMMA (k ~ 3.6), the hole μ was decreased by a factor of 20 and this was most likely due to a broadening of the DOS.[110] Apart

from reductions in μ, high-*k* dielectrics also have higher leakage currents and off state currents. One of the reasons for this is the presence of free moving charges in the form of impurities or polarizable groups for example, hydroxyl groups.[111] Alternatively, there are low- *k* polymer dielectrics which have reduced leakage current and less polar disorder, but have lower capacitances. Hence, both high-*k* and low-*k* materials have their advantages and disadvantages when being used separately.

By creating a high-*k*/low-*k* bilayer structure with a thin low-*k* dielectric layer on top of a high-*k* dielectric it is possible to mitigate the disadvantages of both high-*k* and low-*k* dielectrics. High-*k*/low-*k* bilayer structures have demonstrated reductions in gate leakage, charge traps and improved OTFT μs.[53,54,112,113] The bilayer approach will also reduce the surface roughness as well as narrow the DOS, both of which will improve μ.[3] Many studies have also shown that using a high-*k*/low-*k* bilayer structures can reduce the I_{GS}.[54,62,114] There are a wide range of low-*k* polymers that can be used to improve device performance. For example, crosslinked polyvinyl phenol (PVP), PMMA and trichloro(octadecyl)silane (OTS) have been used as low-*k* layers for reduced I_{GS} and V_T.[112,114–116] Sun et al. have used PVA with an OTS treatment to form a low-*k* monolayer leading to a reduction in I_{GS}.[115] This same principle also applies for environmentally friendly polymers. Rullyani et al. used natural rubber as a low-*k* layer on top of chitosan, reducing I_{GS} and improving semiconductor growth by adjusting the surface energy of the dielectric.[75]

It has also been demonstrated that a low-*k* layer between the gate electrode and the dielectric layer can improve OTFT performance. Lee et al. found that charge injection from the gate into the dielectric layer can increase the hysteresis of devices.[117] Hysteresis causes issues because it shifts V_T and leads to unpredictable OTFT behaviour. Taking this into account, Wang et al. fabricated OTFTs using a PMMA/PVA/PMMA trilayer dielectric which drastically reduced the hysteresis of the native PVA dielectric improving the $I_{on/off}$ ratios to 10^4, V_T to -0.55V and μs to as high as 1.83 cm^2/Vs with a pentacene semiconductor.[118] High-*k*/low-*k* bilayer polymer dielectric systems have also been demonstrated to improve the performance of SWCNT based OTFTs leading to higher μs and better $I_{on/off}$ current ratios.[119] Many studies have also used combinations of organic and in organic bilayer dielectrics such as Al_2O_3, SiO_2 and TiO_2.[68,105,120–122] Although these high-*k*/low-*k* systems using metal oxides demonstrate lower leakage currents

they still have the disadvantages caused by traditional inorganic dielectrics. Therefore, when trying to improve dielectric performance for printable and environmentally friendly materials it's important to select high-*k* and low-*k* materials that meet these criteria. Although a lot of literature combines inorganic with organic or uses non-environmentally friendly polymers, there are still many examples of environmentally friendly bilayer systems within literature. For example, Combinations of Chicken albumen/Gelatin, Chitosan/PLA, Chitosan/Gelatin, PVA/PCL have all been used as bilayer dielectrics for improved OTFT performance.[77,123–126] The combination of a thin low-*k* layer on top of a high-*k* dielectric layer has demonstrated improved properties such as higher μs, lower gate leakage, less hysteresis, and improved stability. The use of layered dielectrics also allows dielectrics to be deposited at higher thicknesses further simplifying their mass production through traditional printing techniques.

Within literature there are few examples of bi-layer dielectric systems that are not a combination of organic/inorganic dielectrics. Within the few examples of bilayer polymer systems there are even fewer that use biodegradable or compostable polymers for both materials in these bilayers systems. The few examples that have been demonstrated within literature also use materials that are not currently being mass produced on the ton scale. This thesis addresses this gap in literature by engineering environmentally friendly bilayer dielectrics using commercially available biodegradable and compostable polymer materials.

1.5 Scope of Thesis

The focus of this thesis is to improve the performance of PVA as a dielectric layer in thin film electronics. PVA is a commercially available compostable polymer that is water soluble and already being produced on the ton scale making it an ideal candidate material to be quickly incorporated into the growing printed electronics industry.

The following chapters will address the current issues with PVA by investigating the following questions:

1. How can the film forming properties of PVA be improved making it easier to form uniform films on substrates? (Chapter 2)
2. Can the semiconductor/dielectric interface be improved through the addition of a low-*k* dielectric material and can PVA be encapsulated to reduce its sensitivity to moisture in the ambient environment? (Chapter 3)

3. Can the thermally activated crosslinking reaction between PVA and the low-*k* polycaprolactone dielectric be replaced with an ultraviolet reaction to increase the shelf life of the polymer and make it easier to implement with traditional printing processes? (Chapter 4)
4. Can a third low-*k* layer of poly(lactic acid) be used to fabricate tri-layer dielectrics with increased thin film transistor performance while enabling n-type transistors? (Chapter 5)

References

1. Kumar, A., Holuszko, M. & Espinosa, D. C. R. E-waste: An overview on generation, collection, legislation and recycling practices. *Resour. Conserv. Recycl.* **122**, 32–42 (2017).
2. Rajesh, R., Kanakadhurga, D. & Prabaharan, N. Electronic waste: A critical assessment on the unimaginable growing pollutant, legislations and environmental impacts. *Environ. Challenges* **7**, 100507 (2022).
3. Tan, M. J. *et al.* Biodegradable electronics: cornerstone for sustainable electronics and transient applications. *J. Mater. Chem. C* **4**, 5531–5558 (2016).
4. Kumar, B., Kaushik, B. K. & Negi, Y. S. Organic Thin Film Transistors: Structures, Models, Materials, Fabrication, and Applications: A Review. *Polym. Rev.* **54**, 33–111 (2014).
5. Elkington, D., Cooling, N., Belcher, W., Dastoor, P. & Zhou, X. Organic Thin-Film Transistor (OTFT)-Based Sensors. *Electronics* **3**, 234–254 (2014).
6. Mabeck, J. T. & Malliaras, G. G. Chemical and Biological Sensors Based on Organic Thin-film Transistors. *Anal. Bioanal. Chem.* **384**, 343–353 (2006).
7. Comeau, Z. J. *et al.* On-the-Spot Detection and Speciation of Cannabinoids Using Organic Thin-Film Transistors. *ACS Sensors* **4**, 2706–2715 (2019).
8. Lin, P. & Yan, F. Organic Thin-Film Transistors for Chemical and Biological Sensing. *Adv. Mater.* **24**, 34–51 (2012).
9. Li, H. *et al.* Effects of Ambient Air and Temperature on Ionic Gel Gated Single-Walled Carbon Nanotube Thin-Film Transistor and Circuits. *ACS Appl. Mater. Interfaces* **7**, 22881–22887 (2015).
10. Nketia-Yawson, B. & Noh, Y. Y. Organic thin film transistor with conjugated polymers for highly sensitive gas sensors. *Macromol. Res.* **25**, 489–495 (2017).
11. Ha, M. *et al.* Printed, sub-3V digital circuits on plastic from aqueous carbon nanotube inks. *ACS Nano* **4**, 4388–4395 (2010).
12. Wang, C., Dong, H., Jiang, L. & Hu, W. Organic semiconductor crystals. *Chem. Soc. Rev.* **47**, 422–500 (2018).
13. Dresselhaus, M. S., Dresselhaus, G., Saito, R. & Jorio, A. Raman spectroscopy of carbon nanotubes. *Phys. Rep.* **409**, 47–99 (2005).
14. Liu, C. & Cheng, H. M. Carbon nanotubes: Controlled growth and application. *Mater. Today* **16**, 19–28 (2013).
15. Wang, H. & Bao, Z. Conjugated polymer sorting of semiconducting carbon nanotubes and their

electronic applications. *Nano Today* **10**, 737–758 (2015).

16. Lefebvre, J. *et al.* High-Purity Semiconducting Single-Walled Carbon Nanotubes: A Key Enabling Material in Emerging Electronics. *Acc. Chem. Res.* **50**, 2479–2486 (2017).

17. Zorn, N. F. & Zaumseil, J. Charge transport in semiconducting carbon nanotube networks. *Appl. Phys. Rev.* **8**, (2021).

18. Qiu, S. *et al.* Solution-Processing of High-Purity Semiconducting Single-Walled Carbon Nanotubes for Electronics Devices. *Adv. Mater.* **31**, 1–21 (2019).

19. Li, H. & Zhou, L. Effects of Ambient Air and Temperature on Ionic Gel Gated Single-Walled Carbon Nanotube Thin-Film Transistor and Circuits. *ACS Appl. Mater. Interfaces* **7**, 22881–22887 (2015).

20. Rice, N. A. *et al.* Organic Thin Film Transistors: Polycarbazole-Sorted Semiconducting Single-Walled Carbon Nanotubes for Incorporation into Organic Thin Film Transistors. *Adv. Electron. Mater.* **5**, 1970002 (2019).

21. Han, J. *et al.* A photodegradable hexaaza-pentacene molecule for selective dispersion of large-diameter semiconducting carbon nanotubes. *Chem. Commun.* **52**, 7683–7686 (2016).

22. Okimoto, H. *et al.* Tunable carbon nanotube thin-film transistors produced exclusively via inkjet printing. *Adv. Mater.* **22**, 3981–3986 (2010).

23. Homenick, C. M. *et al.* Fully Printed and Encapsulated SWCNT-Based Thin Film Transistors via a Combination of R2R Gravure and Inkjet Printing. *ACS Appl. Mater. Interfaces* **8**, 27900–27910 (2016).

24. Noh, J. *et al.* Fully Gravure-Printed D Flip-Flop on Plastic Foils Using Single-Walled Carbon-Nanotube-Based TFTs. *IEEE Electron Device Lett.* **32**, 638–640 (2011).

25. Aikawa, S. *et al.* Carrier polarity engineering in carbon nanotube field-effect transistors by induced charges in polymer insulator. *Appl. Phys. Lett.* **112**, (2018).

26. Kim, S., Baek, G. W., Jeong, J., Seo, S. G. & Jin, S. H. Scalable and selective N-type conversion for carbon nanotube transistors via patternable polyvinyl alcohol stacked with hydrophobic layers and their application to complementary logic circuits. *J. Mater. Res. Technol.* **12**, 243–256 (2021).

27. Geier, M. L., Moudgil, K., Barlow, S., Marder, S. R. & Hersam, M. C. Controlled n-type doping of carbon nanotube transistors by an organorhodium dimer. *Nano Lett.* **16**, 4329–4334 (2016).

28. Maynard, A. D. *et al.* Exposure to carbon nanotube material: Aerosol release during the handling of unrefined single-walled carbon nanotube material. *J. Toxicol. Environ. Heal. - Part A* **67**, 87–107 (2004).

29. Zhu, B., Zhu, S., Li, J., Hui, X. & Wang, G.-X. The developmental toxicity, bioaccumulation and distribution of oxidized single walled carbon nanotubes in Artemia salina. *Toxicol. Res. (Camb).* **7**, 897–906 (2018).

30. da Rocha, A. M. *et al.* Neurotoxicity in zebrafish exposed to carbon nanotubes: Effects on neurotransmitters levels and antioxidant system. *Comp. Biochem. Physiol. Part C Toxicol. Pharmacol.* **218**, 30–35 (2019).

31. Peng, Z. *et al.* Advances in the application, toxicity and degradation of carbon nanomaterials in environment: A review. *Environ. Int.* **134**, 105298 (2020).

32. Mohanta, D., Patnaik, S., Sood, S. & Das, N. Carbon nanotubes: Evaluation of toxicity at biointerfaces. *J. Pharm. Anal.* **9**, 293–300 (2019).

33. Subbarao, N. V. V., Gedda, M., Iyer, P. K. & Goswami, D. K. Organic field-effect transistors as high performance humidity sensors with rapid response, recovery time and remarkable ambient stability. *Org. Electron.* **32**, 169–178 (2016).

34. Guo, C. *et al.* Enrichment of Semiconducting Single-Walled Carbon Nanotubes with Indigo-Fluorene-Based Copolymers and Their Use in Printed Thin-Film Transistors and Carbon Dioxide Gas Sensors. *ACS Sensors* **5**, 2136–2145 (2020).

35. Wu, X. *et al.* Thermally Stable, Biocompatible, and Flexible Organic Field-Effect Transistors and Their Application in Temperature Sensing Arrays for Artificial Skin. *Adv. Funct. Mater.* **25**, 2138–2146 (2015).

36. Søndergaard, R. R., Hösel, M. & Krebs, F. C. Roll-to-Roll fabrication of large area functional organic materials. *J. Polym. Sci. Part B Polym. Phys.* **51**, 16–34 (2013).

37. Ha, M. *et al.* Aerosol jet printed, low voltage, electrolyte gated carbon nanotube ring oscillators with sub-5 μs stage delays. *Nano Lett.* **13**, 954–960 (2013).

38. Grau, G. & Subramanian, V. Dimensional scaling of high-speed printed organic transistors enabling high-frequency operation. *Flex. Print. Electron.* **5**, 014013 (2020).

39. Lim, J. A. *et al.* Inkjet-printed Single-droplet Organic Transistors Based on Semiconductor Nanowires Embedded in Insulating Polymers. *Adv. Funct. Mater.* **20**, 3292–3297 (2010).

40. Cho, J. H. *et al.* Printable Ion-gel Gate Dielectrics for Low-Voltage Polymer Thin-Film Transistors on Plastic. *Nat. Mater.* **7**, 900–906 (2008).

41. Guo, X., Han, L. & Hou, X. Insights into the device structure, processing and material design for an organic thin-film transistor towards functional circuit integration. *Mater. Chem. Front.* **5**, 6760–6778 (2021).

42. Cao, C., Andrews, J. B. & Franklin, A. D. Completely Printed, Flexible, Stable, and Hysteresis-Free Carbon Nanotube Thin-Film Transistors via Aerosol Jet Printing. *Adv. Electron. Mater.* **3**, 1700057 (2017).

43. Heimfarth, D. *et al.* Enhancing Electrochemical Transistors Based on Polymer-Wrapped (6,5) Carbon Nanotube Networks with Ethylene Glycol Side Chains. *ACS Appl. Mater. Interfaces* **14**, 8209–8217 (2022).

44. Irimia-Vladu, M., Głowacki, E. D., Voss, G., Bauer, S. & Sariciftci, N. S. Green and biodegradable electronics. *Mater. Today* **15**, 340–346 (2012).

45. Larsen, C. *et al.* A tool for identifying green solvents for printed electronics. *Nat. Commun.* **12**, 1–7 (2021).

46. Khan, Y. *et al.* A New Frontier of Printed Electronics: Flexible Hybrid Electronics. *Adv. Mater.* **32**, 1–29 (2020).

47. Boileau, N. T., Melville, O. A., Mirka, B., Cranston, R. & Lessard, B. H. P and N type copper phthalocyanines as effective semiconductors in organic thin-film transistor based DNA biosensors at elevated temperatures. *RSC Adv.* **9**, 2133–2142 (2019).

48. Fattori, M. *et al.* A Fully-Printed Organic Smart Temperature Sensor for Cold Chain Monitoring Applications. in *2020 IEEE Custom Integrated Circuits Conference (CICC)* vols 2020-March 1–4

(IEEE, 2020).

49. Zymelka, D., Yamashita, T., Takamatsu, S., Itoh, T. & Kobayashi, T. Thin-film flexible sensor for omnidirectional strain measurements. *Sensors Actuators A Phys.* **263**, 391–397 (2017).

50. Kuzma, M., Gerhard, E., Shan, D. & Yang, J. Advances in Bioresorbable Electronics and Uses in Biomedical Sensing. in *Interfacing Bioelectronics and Biomedical Sensing* 29–72 (Springer International Publishing, 2020). doi:10.1007/978-3-030-34467-2_2.

51. Wiklund, J. *et al.* A Review on Printed Electronics: Fabrication Methods, Inks, Substrates, Applications and Environmental Impacts. *J. Manuf. Mater. Process.* **5**, 89 (2021).

52. Williams, N. X., Bullard, G., Brooke, N., Therien, M. J. & Franklin, A. D. Printable and recyclable carbon electronics using crystalline nanocellulose dielectrics. *Nat. Electron.* **4**, 261–268 (2021).

53. Li, J. *et al.* Solution-processable organic and hybrid gate dielectrics for printed electronics. *Mater. Sci. Eng. R Reports* **127**, 1–36 (2018).

54. Nketia-Yawson, B. & Noh, Y.-Y. Recent Progress on High-Capacitance Polymer Gate Dielectrics for Flexible Low-Voltage Transistors. *Adv. Funct. Mater.* **28**, 1802201 (2018).

55. Lee, E. *et al.* Gate Capacitance-Dependent Field-Effect Mobility in Solution-Processed Oxide Semiconductor Thin-Film Transistors. *Adv. Funct. Mater.* **24**, 4689–4697 (2014).

56. Bardini, L. EIS 101 , an introduction to electrochemical spectroscopy . *ResearchGate* 44 (2015) doi:10.13140/RG.2.1.2248.5600.

57. Ahmad, Z. Polymer Dielectric Materials. in *Polymer Dielectric Materials* vol. i 25 (InTech, 2012).

58. Schönhals, A. Dielectric Spectroscopy on the Dynamics of Amorphous Polymeric Systems. 1–17 (1974).

59. Joshi, J. H., Kanchan, D. K., Joshi, M. J., Jethva, H. O. & Parikh, K. D. Dielectric relaxation, complex impedance and modulus spectroscopic studies of mix phase rod like cobalt sulfide nanoparticles. *Mater. Res. Bull.* **93**, 63–73 (2017).

60. Xiongfei Yu *et al.* A High-Density MIM Capacitor (13 fF/um^2) Using ALD HfOP Dielectrics. *IEEE Electron Device Lett.* **24**, 63–65 (2003).

61. Facchetti, A., Yoon, M. H. & Marks, T. J. Gate Dielectrics for Organic Field-effect Transistors: New Opportunities for Organic Electronics. *Adv. Mater.* **17**, 1705–1725 (2005).

62. TEJA KARRI, B. R. & GUPTA, N. Hybrid bilayer gate dielectric-based organic thin film transistors. *Bull. Mater. Sci.* **42**, 2 (2019).

63. Lopinski, G. *et al.* Cyanoethylated pullulan as a high-k solution processable polymer gate dielectric for SWCNT TFTs. *Org. Electron.* **42**, 329–336 (2017).

64. Georgiou, V. *et al.* Ferroelectricity in Polar Polymer-Based FETs: A Hysteresis Analysis. *Adv. Funct. Mater.* **28**, 1705250 (2018).

65. Egginger, M., Bauer, S., Schwödiauer, R., Neugebauer, H. & Sariciftci, N. S. Current versus gate voltage hysteresis in organic field effect transistors. *Monatshefte fur Chemie* **140**, 735–750 (2009).

66. Egginger, M. *et al.* Mobile ionic impurities in poly (vinyl alcohol) gate dielectric: Possible source of the hysteresis in organic field-effect transistors. *Adv. Mater.* **20**, 1018–1022 (2008).

67. Su, Y. *et al.* Low-Voltage Organic Field-Effect Transistors (OFETs) with Solution-Processed Metal-Oxide as Gate Dielectric. 4662–4667 (2011).

68. Subbarao, N. V. V, Gedda, M., Iyer, P. K. & Goswami, D. K. Enhanced environmental stability induced by effective polarization of a polar dielectric layer in a trilayer dielectric system of organic field-effect transistors: A quantitative study. *ACS Appl. Mater. Interfaces* **7**, 1915–1924 (2015).

69. Cruz, S. M. F., Rocha, L. A. & Viana, J. C. *Flexible Electronics*. *Flexible Electronics* (InTech, 2018). doi:10.5772/intechopen.72522.

70. Douglas, S. P., Mrig, S. & Knapp, C. E. MODs vs. NPs: Vying for the Future of Printed Electronics. *Chem. - A Eur. J.* **27**, 8062–8081 (2021).

71. Matsui, H., Takeda, Y. & Tokito, S. Flexible and printed organic transistors: From materials to integrated circuits. *Org. Electron.* **75**, 105432 (2019).

72. Guo, X. *et al.* Current Status and Opportunities of Organic Thin-Film Transistor Technologies. *IEEE Trans. Electron Devices* **64**, 1906–1921 (2017).

73. Chang, J.-W. *et al.* Chicken Albumen Dielectrics in Organic Field-Effect Transistors. *Adv. Mater.* **23**, 4077–4081 (2011).

74. Irimia-Vladu, M. *et al.* Environmentally sustainable organic field effect transistors. *Org. Electron.* **11**, 1974–1990 (2010).

75. Rullyani, C., Ramesh, M., Sung, C.-F., Lin, H.-C. & Chu, C.-W. Natural polymers for disposable organic thin film transistors. *Org. Electron.* **54**, 154–160 (2018).

76. Seck, M. *et al.* Organic FETs using biodegradable almond gum as gate dielectric: A promising way towards green electronics. *Org. Electron.* **83**, 105735 (2020).

77. Ronnasi, B., Tousignant, M. N. & Lessard, B. H. Chitosan based dielectrics for use in single walled carbon nanotube-based thin film transistors. *J. Mater. Chem. C* **11**, 3197–3205 (2023).

78. Chiellini, E., Corti, A., D'Antone, S. & Solaro, R. Biodegradation of poly (vinyl alcohol) based materials. *Prog. Polym. Sci.* **28**, 963–1014 (2003).

79. Fukushima, K., Abbate, C., Tabuani, D., Gennari, M. & Camino, G. Biodegradation of poly(lactic acid) and its nanocomposites. *Polym. Degrad. Stab.* **94**, 1646–1655 (2009).

80. Hosseini, E. S., Dervin, S., Ganguly, P. & Dahiya, R. Biodegradable Materials for Sustainable Health Monitoring Devices. *ACS Appl. Bio Mater.* **4**, 163–194 (2021).

81. Zhao, D. *et al.* Cellulose-Based Flexible Functional Materials for Emerging Intelligent Electronics. *Adv. Mater.* **2000619**, 2000619 (2020).

82. Mattana, G., Briand, D., Marette, A., Vásquez Quintero, A. & de Rooij, N. F. Polylactic acid as a biodegradable material for all-solution-processed organic electronic devices. *Org. Electron.* **17**, 77–86 (2015).

83. Gaspar, D. *et al.* Nanocrystalline Cellulose Applied Simultaneously as the Gate Dielectric and the Substrate in Flexible Field Effect Transistors. *Nanotechnology* **25**, 1–11 (2014).

84. Tousignant, M. N. *et al.* Improving Thin-Film Properties of Poly(vinyl alcohol) by the Addition of Low-Weight Percentages of Cellulose Nanocrystals. *Langmuir* **36**, 3550–3557 (2020).

85. Dai, S. *et al.* Intrinsically ionic conductive cellulose nanopapers applied as all solid dielectrics for low voltage organic transistors. *Nat. Commun.* **9**, 2737 (2018).

86. Hamad, W. Y., Miao, C. & Beck, S. Growing the Bioeconomy: Advances in the Development of Applications for Cellulose Filaments and Nanocrystals. *Ind. Biotechnol.* **15**, 133–137 (2019).

87. George, J. & Sabapathi, S. N. Cellulose Nanocrystals: Synthesis, Functional Properties, and Applications. *Nanotechnol. Sci. Appl.* **8**, 45–54 (2015).

88. Hoeng, F., Denneulin, A. & Bras, J. Use of Nanocellulose in Printed Electronics: A Review. *Nanoscale* **8**, 13131–13154 (2016).

89. Wang, P., Xu, P., Wei, H., Fang, H. & Ding, Y. Effect of block copolymer containing ionic liquid moiety on interfacial polarization in PLA/PCL blends. *J. Appl. Polym. Sci.* **135**, 46161 (2018).

90. Tousignant, M. N. *et al.* Improving Thin-Film Properties of Poly(vinyl alcohol) by the Addition of Low-Weight Percentages of Cellulose Nanocrystals. *Langmuir* **36**, (2020).

91. Ono, S., Miwa, K., Seki, S. & Takeya, J. A comparative study of organic single-crystal transistors gated with various ionic-liquid electrolytes. *Appl. Phys. Lett.* **94**, 1–4 (2009).

92. Ono, S., Seki, S., Hirahara, R., Tominari, Y. & Takeya, J. High-mobility, low-power, and fast-switching organic field-effect transistors with ionic liquids. *Appl. Phys. Lett.* **92**, 90–93 (2008).

93. Fujimoto, T. & Awaga, K. Electric-double-layer field-effect transistors with ionic liquids. *Phys. Chem. Chem. Phys.* **15**, 8983–9006 (2013).

94. Cho, J. H. *et al.* High-capacitance ion gel gate dielectrics with faster polarization response times for organic thin film transistors. *Adv. Mater.* **20**, 686–690 (2008).

95. Hoeng, F., Denneulin, A. & Bras, J. Use of nanocellulose in printed electronics: a review. *Nanoscale* **8**, 13131–13154 (2016).

96. Larsson, O., Said, E., Berggren, M. & Crispin, X. Insulator polarization mechanisms in polyelectrolyte-gated organic field-effect transistors. *Adv. Funct. Mater.* **19**, 3334–3341 (2009).

97. Peltekoff, A. J., Hiller, V. E., Lopinski, G. P., Melville, O. A. & Lessard, B. H. Unipolar Polymerized Ionic Liquid Copolymers as High-Capacitance Electrolyte Gates for n-Type Transistors. *ACS Appl. Polym. Mater.* **1**, 3210–3221 (2019).

98. Niskanen, J., Tousignant, M. N., Peltekoff, A. J. & Lessard, B. H. 1,2,3-Triazole based poly(ionic liquids) as solid dielectric materials. *Polymer (Guildf).* **212**, 123144 (2021).

99. Peltekoff, A. J., Brixi, S., Niskanen, J. & Lessard, B. H. Ionic Liquid Containing Block Copolymer Dielectrics: Designing for High-Frequency Capacitance, Low-Voltage Operation, and Fast Switching Speeds. *JACS Au* **1**, 1044–1056 (2021).

100. Tousignant, M. N. *et al.* Poly(ionic liquid) dielectric for high performing P- and N-type single walled carbon nanotube transistors. *Flex. Print. Electron.* **7**, 034004 (2022).

101. Niskanen, J., Tousignant, M. N., Peltekoff, A. J. & Lessard, B. H. Poly(ethylene glycol)-Based Poly(ionic liquid) Block Copolymers through 1,2,3-Triazole Click Reactions. *ACS Appl. Polym. Mater.* **4**, 1559–1564 (2022).

102. Costa, S. P. F., Azevedo, A. M. O., Pinto, P. C. A. G. & Saraiva, M. L. M. F. S. Environmental Impact of Ionic Liquids: Recent Advances in (Eco)toxicology and (Bio)degradability. *ChemSusChem* **10**, 2321–2347 (2017).

103. Messali, M. An Efficient and Green Sonochemical Synthesis of Some New Eco-Friendly Functionalized Ionic Liquids. *Arab. J. Chem.* **7**, 63–70 (2014).

104. Aleeva, Y. & Pignataro, B. Recent advances in upscalable wet methods and ink formulations for printed electronics. *J. Mater. Chem. C* **2**, 6436–6453 (2014).

105. Ortiz, R. P., Facchetti, A. & Marks, T. J. High-k organic, inorganic, and hybrid dielectrics for low-voltage organic field-effect transistors. *Chem. Rev.* **110**, 205–239 (2010).

106. Kim, C. *et al.* Printable cross-linked polymer blend dielectrics. Design strategies, synthesis, microstructures, and electrical properties, with organic field-effect transistors as testbeds. *J. Am. Chem. Soc.* **130**, 6867–6878 (2008).

107. Yoon, M. H., Yan, H., Facchetti, A. & Marks, T. J. Low-voltage organic field-effect transistors and inverters enabled by ultrathin cross-linked polymers as gate dielectrics. *J. Am. Chem. Soc.* **127**, 10388–10395 (2005).

108. She, X.-J., Liu, J., Zhang, J.-Y., Gao, X. & Wang, S.-D. Operational stability enhancement of low-voltage organic field-effect transistors based on bilayer polymer dielectrics. *Appl. Phys. Lett.* **103**, 133303 (2013).

109. Veres, J., Ogier, S. D., Leeming, S. W., Cupertino, D. C. & Khaffaf, S. M. Low-k insulators as the choice of dielectrics in organic field-effect transistors. *Adv. Funct. Mater.* **13**, 199–204 (2003).

110. Merari Masillamani, A., Orgiu, E. & Samorì, P. Effect of the molecular weight of the polymer gate dielectric on the performances of solution-processed ambipolar OTFTs. *J. Mater. Chem. C* **1**, 7725–7730 (2013).

111. Lee, S. *et al.* Effects of hydroxyl groups in polymeric dielectrics on organic transistor performance. *Appl. Phys. Lett.* **88**, (2006).

112. Yang, F. Y., Chang, K. J., Hsu, M. Y. & Liu, C. C. Low-operating-voltage polymeric transistor with solution-processed low-k polymer/high-k metal-oxide bilayer insulators. *Org. Electron.* **9**, 925–929 (2008).

113. Zhang, H. *et al.* Solution-processed organic field-effect transistors with cross-linked poly(4-vinylphenol)/polyvinyl alcohol bilayer dielectrics. *Appl. Surf. Sci.* **478**, 699–707 (2019).

114. Faraji, S., Hashimoto, T., Turner, M. L. & Majewski, L. A. Solution-processed nanocomposite dielectrics for low voltage operated OFETs. *Org. Electron.* **17**, 178–183 (2015).

115. Sun, Y. *et al.* Polymer gate dielectrics with self-assembled monolayers for high-mobility organic thin-film transistors based on copper phthalocyanine. *Appl. Phys. A* **95**, 777–780 (2009).

116. Jin, S. H. *et al.* 34.2: PMMA Buffer-Layer Effects on Electrical Performance of Pentacene OTFTs with a Cross-linked PVA Gate Insulator on a Flexible Substrate. *SID Symp. Dig. Tech. Pap.* **34**, 1088 (2003).

117. Lee, C. A. *et al.* Hysteresis mechanism and reduction method in the bottom-contact pentacene thin-film transistors with cross-linked poly(vinyl alcohol) gate insulator. *Appl. Phys. Lett.* **88**, (2006).

118. Wang, W., Ma, D., Pan, S. & Yang, Y. Hysteresis mechanism in low-voltage and high mobility pentacene thin-film transistors with polyvinyl alcohol dielectric. *Appl. Phys. Lett.* **101**, (2012).

119. Lee, S. H., Kim, D. Y. & Noh, Y. Y. Solution-processed polymer-sorted semiconducting carbon nanotube network transistors with low- k/high- k bilayer polymer dielectrics. *Appl. Phys. Lett.*

111, (2017).

120. Li, Q. *et al.* Designing hybrid gate dielectric for fully printing high-performance carbon nanotube thin film transistors. *Nanotechnology* **28**, (2017).

121. Wang, C. Y. *et al.* Stable Low-voltage Operation Top-gate Organic Field-effect Transistors on Cellulose Nanocrystal Substrates. *ACS Appl. Mater. Interfaces* **7**, 4804–4808 (2015).

122. Subbarao, N. V. V., Mandal, S., Gedda, M., Iyer, P. K. & Goswami, D. K. Effect of temperature on hysteresis of dipolar dielectric layer based organic field-effect transistors: A temperature sensing mechanism. *Sensors Actuators, A Phys.* **269**, 491–499 (2018).

123. Tousignant, M. N., Lin, Z. S., Brusso, J. & Lessard, B. H. Interfacial Ultraviolet Cross-Linking of Green Bilayer Dielectrics. *ACS Appl. Mater. Interfaces* **15**, 3680–3688 (2023).

124. Tousignant, M. N. *et al.* High Performance Organic Electronic Devices Based on a Green Hybrid Dielectric. *Adv. Electron. Mater.* **7**, 2100700 (2021).

125. Konwar, G., Saxena, P., Raghuwanshi, V., Rahi, S. & Tiwari, S. P. High Performance Flexible Organic Transistors with Biodegradable Natural-Protein based Gate Dielectrics. *Proc. AM-FPD 2022 - 29th Int. Work. Act. Flatpanel Displays Devices TFT Technol. FPD Mater.* **1**, 190–193 (2022).

126. Konwar, G., Saxena, P., Raghuwanshi, V., Rahi, S. & Tiwari, S. P. Solution-processed biopolymer dielectric based organic field-effect transistors for sustainable electronics. *6th IEEE Electron Devices Technol. Manuf. Conf. EDTM 2022* 107–109 (2022) doi:10.1109/EDTM53872.2022.9798041.

127. Peppas, N. A. & Merrill, E. W. Differential scanning calorimetry of crystallized PVA hydrogels. *J. Appl. Polym. Sci.* **20**, 1457–1465 (1976).

Chapter 2 : Improving Polyvinyl Alcohol (PVA) Thin Film Properties Through the Addition of Low Weight Percentages of Cellulose Nanocrystals

This chapter was published in the journal "Langmuir": M.N. Tousignant, N.A. Rice, A. Peltekoff, C. Sundaresan, C. Miao, W.Y. Hamad, B.H. Lessard, Improving Thin-Film Properties of Poly(vinyl alcohol) by the Addition of Low-Weight Percentages of Cellulose Nanocrystals, Langmuir. 36 (2020) 3550–3557.

Context

For this work I investigated how varying low weight percentages of cellulose nanocrystals would impact the film forming properties of PVA. Dr. Hamad from FP Innovations provided our group with a 2 wt% suspension of cellulose nanocrystals which we could then use to create PVA/CNC dispersions with low weight percentages of CNCs. As outlined in Chapter 1, the main issue with polymer dielectrics is having the right mechanical and electrical properties. Although PVA is a high-*k* dielectric material it has poor film forming properties. We surmised that the addition of low weight percentages of CNCs could help increase the viscosity of the PVA solutions allowing for better film forming properties. We were interested in characterizing these PVA/CNC dispersions at various weight percentages to see if the addition of low weight percentages of CNCs would lead to more uniform films of PVA without negatively impacting its performance when used as a dielectric in capacitors and organic thin film transistors.

Contribution

I prepared all the PVA/CNC dispersions using the stock CNC dispersion provided by Dr.Hamad. Dr.Sundaresan performed all the viscosity measurements. Dr. Miao performed the storage and loss modulus calculations and Dr. Rice performed the AFM imaging. I performed all profilometry measurements, contact angle measurements and aided with the AFM film analysis. I was responsible for all the capacitor and thin film transistor fabrication and characterization. I wrote the manuscript with input and revisions from Dr. Lessard and Dr. Rice.

2.1 Abstract

The increased demand for electronic devices, combined with a desire to minimize the environmental impact, necessitates the development of new eco-friendly materials. One promising approach is the incorporation of renewable and green materials that possess the

desired mechanical and electrical properties, while allowing for more ecologically friendly disposal of these devices. The addition of low weight percentages (0.25 – 0.75 wt %) of CNCs was investigated as an environmentally friendly additive in aqueous dispersions of PVA. It was found that these low CNC loadings were sufficient to induce a favorable increase in viscosity, which in turn dramatically enhanced the film quality of the PVA blends through an improvement in the critical radius of the spun film, overall film thickness and homogeneity of the thin film. This corresponded to an increase in the number of functioning organic electronic devices that could be fabricated by spin coating, including MIM capacitors and OTFTs. Most importantly, the incorporation of CNCs into PVA did not significantly alter the native dielectric properties of the polymer thin films when incorporated into both MIM capacitors and OTFTs.

2.2 Introduction

Electronic devices are ubiquitous and diverse, with applications ranging from long-lasting computers and televisions to short-lived disposable sensors for the biomedical and wearables fields. As global demand continues to increase for basic electronic components like transistors and capacitors, consideration of the environmental impact of these materials, both in production and during disposal, is becoming increasingly imperative. Recent work in the field of organic electronics has focused on finding carbon-based materials that are both environmentally friendly and retain the necessary electrical properties for consumer applications.[1] Inexpensive, single-use sensors are a particularly attractive application of organic electronics, further underscoring the need for these devices to be environmentally friendly.[2] Various architectures have been reported in the literature for sensors comprised of carbon-based components, including OTFTs and chemiresistors.[3,4] OTFTs can be utilized in simple and complex circuitry, with disposable electronics like sensors for biomedical and environmental monitoring emerging as promising applications.[5] OTFTs are comprised of four major components: a gate, the dielectric, an organic semiconductor and source-drain electrodes.[6] The dielectric is an insulating layer that can accumulate charge along the interface with the semiconductor, effectively turning "on" the transistor.[7] This occurs by applying a bias through the gate, inducing the opposite charge of that bias to accumulate on the dielectric in proximity to the gate and the same charge as the bias applied to the gate to accumulate on the opposite side of the dielectric, near the semiconductor. This facilitates either hole (for p-type semiconductors) or electron (for n-type) transport through the organic semiconductor from the source to the drain.[8] Common dielectric

materials utilized in OTFTs include polymers like PMMA, PVP and PS;[7] while these polymers offer the potential to produce light-weight and flexible electronics, they are not biodegradable materials and (with the exception of PVP) often solubilized in organic solvents. For single-use disposable applications, it is necessary to develop dielectrics that are cost-effective, utilize environmentally friendly solvents during manufacturing, and can be effortlessly disposed of after use with minimal environmental impact.

PVA is a low-cost polymer that is used in the textiles, adhesives and coatings industries. It is readily soluble in environmentally friendly solvents like water, and is biodegradable in the presence of the proper microorganisms.[9] PVA has previously been incorporated into organic electronics as a dielectric, both as a neat homopolymer as well as in composites.[10,11] PVA has a dielectric constant ranging from 5 – 10, classifying it as a high-*k* dielectric. One of the major drawbacks to PVA is its sensitivity to moisture, which can drastically alter its dielectric properties. Cross-linking chemistries have shown great promise in mitigating this moisture sensitivity and decreasing leakage current, however this methodology has the drawback of lowering the capacitance density of PVA.[10,12] Additionally, neat PVA has a low viscosity in solution, which can effect film formation during spin coating, resulting in inhomogeneous thin films.

CNCs are renewable nanomaterials derived from lignocellulosic biomass found in wood, cotton, or tunicate (a sea animal); the CNCs can be obtained from these natural sources using strong acid hydrolysis, typically sulfuric acid hydrolysis.[13] As-produced CNCs are spindle-like, negatively-charged nanoparticles with an electrical double layer influenced by both external mechanical energy and ionic strength.[14] The negative charge is critical to create a stable steric suspension in compatible liquids, like water. The young's modulus for individual CNCs has been experimentally determined to be ~ 145 GPa,[15] and as such can significantly improve the mechanical performance when incorporated into polymer blends.[16] CNC polymer blends with PMMA and PVA have demonstrated improved rheological properties compared to the native polymer.[17,18] Neat CNCs have previously been utilized within organic electronics as ultra-smooth paper-like substrates, but there are relatively few reports of incorporation of CNCs as a dielectric.[19,20]

PVA-CNC blends have previously been reported in the literature, with a focus on improving the mechanical properties of the PVA.[21] In a study performed by Zhou et al., blends of PVA with CNCs were fabricated with an increasing weight percentage of CNCs from 3 to 9 wt %.[17] An increase in viscoelastic properties of the solution, as well as a transition from a viscoelastic fluid towards either viscoelastic gel or solid, was observed as the weight percent of CNCs was increased.[17] This shift from a low viscosity solution towards a more viscoelastic fluid behaviour drastically altered the fluid properties, which in turn affected the thin film properties obtained during spin coating.[22] Increases in the viscoelastic properties of a dispersion is known to result in more uniform thin films during spin coating by increasing the amount of time that the droplet can spread before rivulets begin to form.[23] The change in viscoelastic properties will also affect what printing processes can be used during large-scale fabrication of organic electronic devices.[24–26]

Almost all previous literature reports of PVA-CNC dispersions have primarily focused on incorporating large amounts of CNCs, in excess of 1 wt %.[21,27,28] Furthermore, to our knowledge, there are relatively few reports of incorporating low loading of CNCs into PVA,[17] and only one report of a PVA-CNC blend employed as a dielectric.[28] To more thoroughly investigate the practicality of CNCs as an environmentally friendly additive with PVA for incorporation into biodegradable organic electronics, we prepared blends at much lower CNC weight loadings (under 1 wt %). Viscosity measurements confirmed that small additions of CNCs were sufficient to improve the viscoelastic properties of PVA, resulting in more homogeneous thin films. MIM capacitors were fabricated to measure dielectric properties of the blends, and OTFTs were prepared and characterized. It was found that the addition of small amounts of CNCs did not affect the dielectric constant of the PVA blends; μ, V_T and $I_{on/off}$ ratios of the OTFTs incorporating PVA-CNC blends were also not significantly altered compared to neat PVA. Furthermore, the improved thin film uniformity during spin coating resulted in a significant increase in the number of functioning MIM and OTFT devices.

2.3 Results and Discussion

Blends of PVA with CNCs were prepared in water/methanol co-solvent such that the final loading of CNCs was 0, 0.25, 0.5 or 0.75 wt % in 80 mg/mL of PVA. Our PVA-CNC dispersions were limited to a maximum weight percentage of 0.75 % due to the stock suspension

of CNCs being 2 wt % in distilled water, as well as the prerequisite to completely dissolve and filter the PVA before the addition of the CNCs.

It is well known in the literature that incorporation of CNCs into PVA can increase solution viscosity due to the hydrogen bonding interaction between the CNCs and pendant alcohols on PVA, with 1 – 3 wt % of CNCs sufficient to induce notable changes in viscosity.[17] This viscosity change is attributed to entanglement and hydrogen bonding between the CNCs and PVA.[17] The viscosity of our PVA-CNC solutions as a function of increasing weight percentage of CNCs was investigated using a rheometer, shown in **Figure 2.1A**. Despite the relatively low loadings of CNCs, the amount of CNCs present in our blends was sufficient to induce noticeable viscosity changes. Our PVA-CNC blends follow the same trend reported in literature for higher CNC loadings, with viscosity increasing from 0.008 to 0.046 Pa·s at a shear rate of 90 s^{-1} and at 63 s^{-1} which is approximately 4000 rpm the viscosity is increased from 0.008 to 0.051 Pa·s which is a 6 fold increase as the weight percent of CNCs increased from 0 to 0.75 %. Increasing the percentage of CNCs in PVA also had an impact on film thickness. Film thickness measurements were performed on thin films spin coated onto glass substrates. As shown in **Figure 2.1B**, the neat PVA film had the lowest average thickness of 234 ± 3.3 nm, which increased to 319 ± 12 nm for 0.75 wt % CNCs.

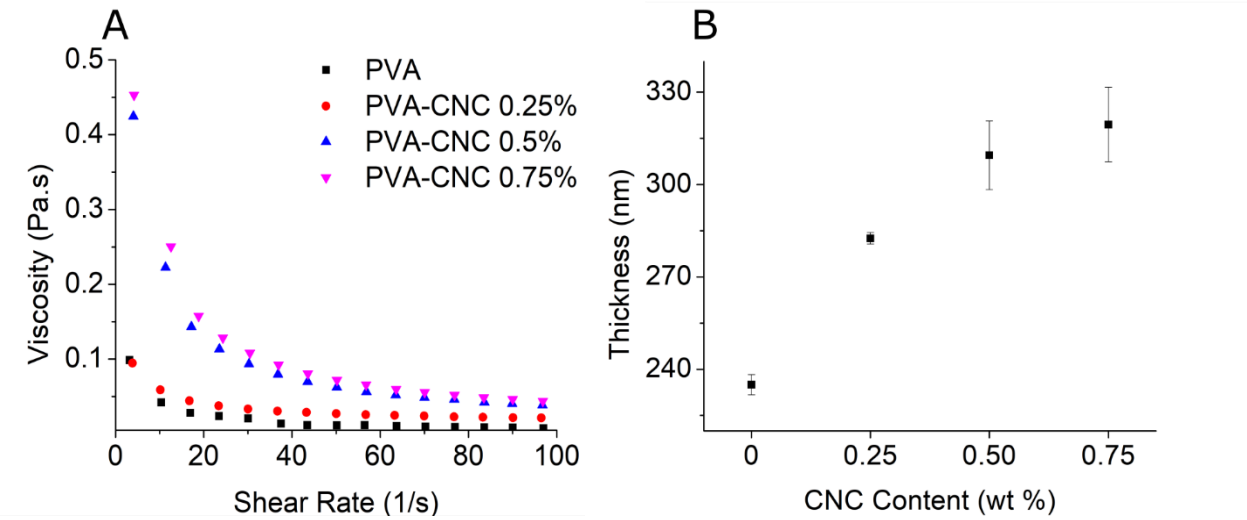

Figure 2.1. A) Viscosity as a function of shear rate for pure PVA polymer and PVA-CNC blends and B) thickness of PVA-CNC films spin coated onto glass substrates.

DSC measurements were performed on solid polymer-CNC materials, obtained by evaporating off the solvent to yield the bulk PVA-CNC materials. It has been reported that the addition of CNCs into polymer blends can induce changes in crystallinity, but the majority of these reports in the literature are at much higher CNC loadings, upwards of 10%.[29] Electrospun nanofibers of PVA with 2 – 5 wt % CNCs have shown a decrease in crystallinity with increasing incorporation of CNCs.[30] The results from our very low additions of CNCs are inconclusive with glass transition temperatures from 65-75 °C, crystallinities from 11-22 % and temperatures of 261- 270 for 90% of the polymers original weight. However, it does appear that low CNC loadings cause an increase in both storage and loss moduli (**Figure 2.2**). The addition of CNCs into polymer blends has been shown in literature to increase the mechanical properties of PVA-CNC blends and have shown increases in storage and loss moduli with increased loading. [17,31] This increase is caused by hydrogen bond interactions between PVA and the CNCs which increase the mechanical properties of the CNCs as well as the viscoelastic properties by restricting the movement of PVA. [17,31]

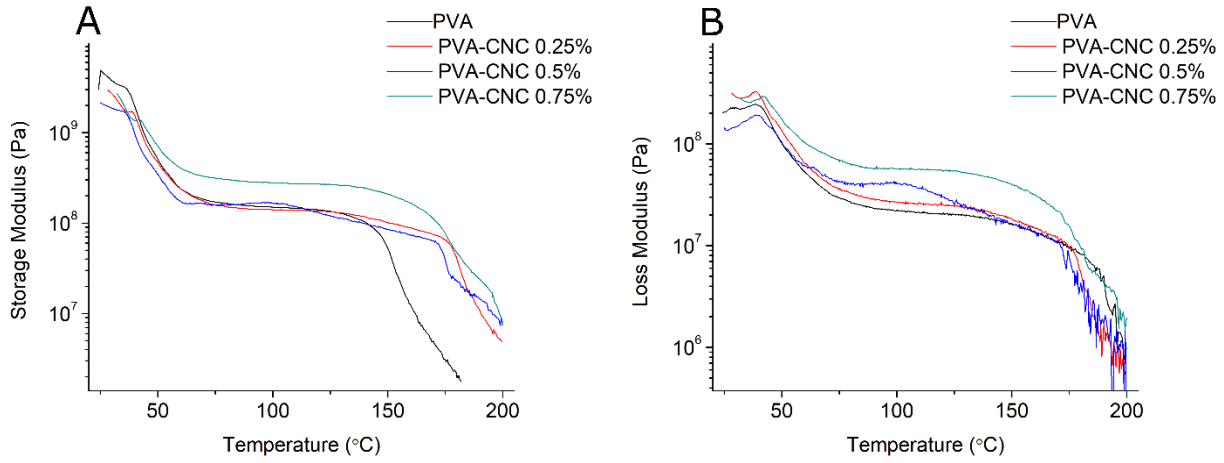

Figure 2.2. DMA data from PVA and PVA-CNC polymer blends between 20 and 200 °C. A) storage modulus and B) loss modulus.

AFM measurements were performed on PVA and PVA-CNC thin films spun onto glass substrates, with representative images shown in **Figure 2.3**. Rod-like CNC features are clearly visible in **Figures 2.3B-D**, with significant amounts of CNCs dispersed relatively evenly throughout the films at all loadings. Linear height profiles below each of the four AFM images

confirm the surface roughness trends determined by optical profilometry in **Figure 2.4B**. The neat PVA film is relatively flat, with no discerning features. Upon the addition of 0.25 wt % CNCs (**Figure 2.3B**), there is a substantial increase in surface features and roughness. Subsequent additions of 0.5 wt % (**Figure 2.3C**) and 0.75 wt % (**Figure 2.3D**) of CNCs show linear features very similar to the 0.25 wt % films, with no large increases in surface features.

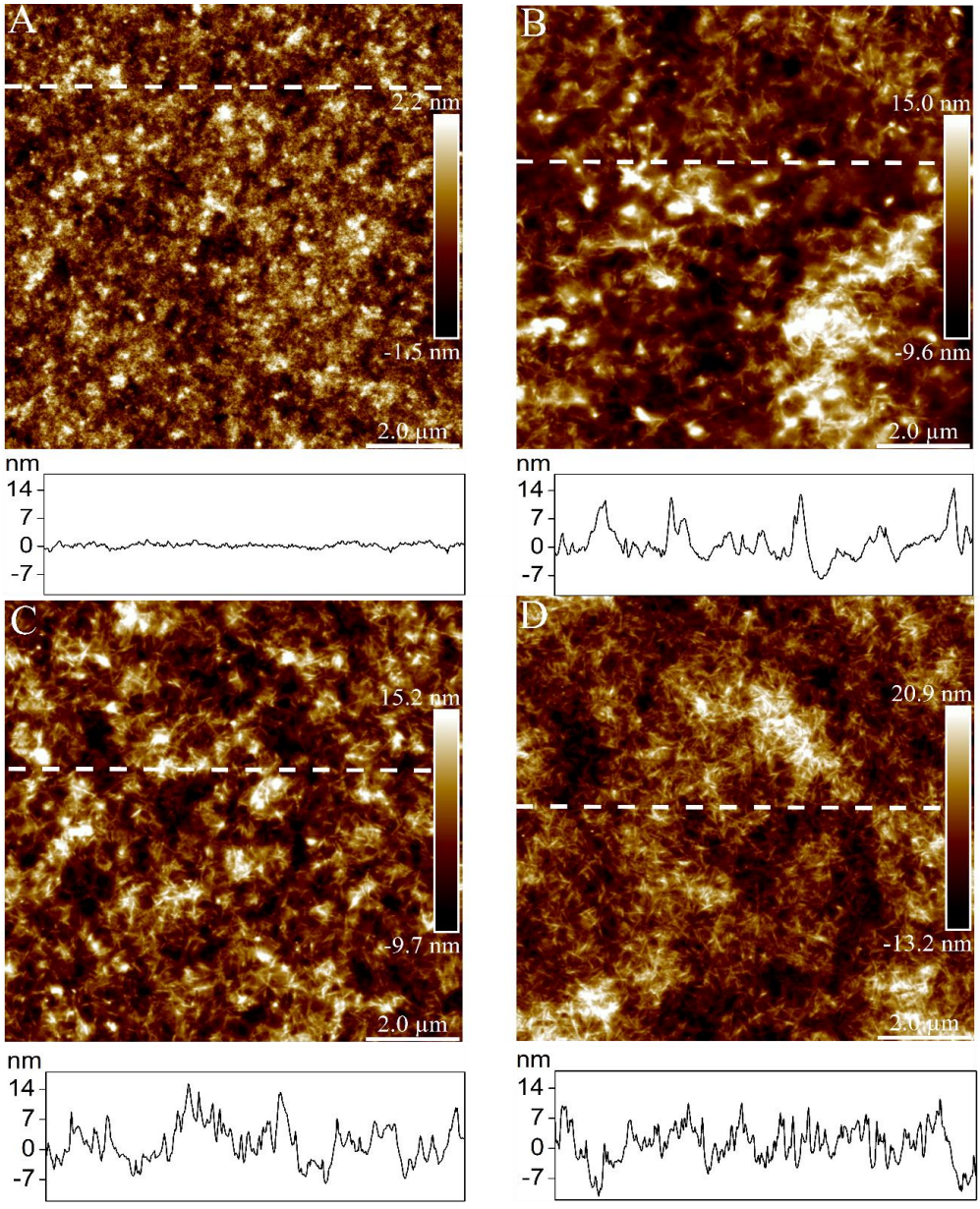

Figure 2.3. Representative AFM images and height profiles of (A) neat PVA (B) 0.25 wt % PVA-CNCs (C) 0.5 wt % PVA-CNCs and (D) 0.75 wt % PVA-CNCs. The white dashed lines represent the location of the linear surface profile below each image.

Contact angle measurements (**Figure 2.4A**) performed on thin films spin coated onto glass substrates initially show only minor changes in contact angle for the 0.25 and 0.5 wt % additions of CNCs compared to neat PVA, but a minor loss of hydrophilicity upon the addition of 0.75 wt % CNCs to PVA. Experiments were also performed where the drop was permitted to settle for 5 seconds before measurement; a significant drop in the contact angle was observed for all thin films, with a minor increase in hydrophobicity for all PVA-CNC samples compared to PVA observed, with little statistical difference between the three loadings. Micro level surface roughness measurements were also performed on these composite thin films using AFM. Surface roughness increased dramatically with the addition of 0.25 wt % of CNCs compared to neat PVA, with subsequent additions of small amounts of CNCs resulting in slight increases in surface roughness (**Figure 2.4B**).

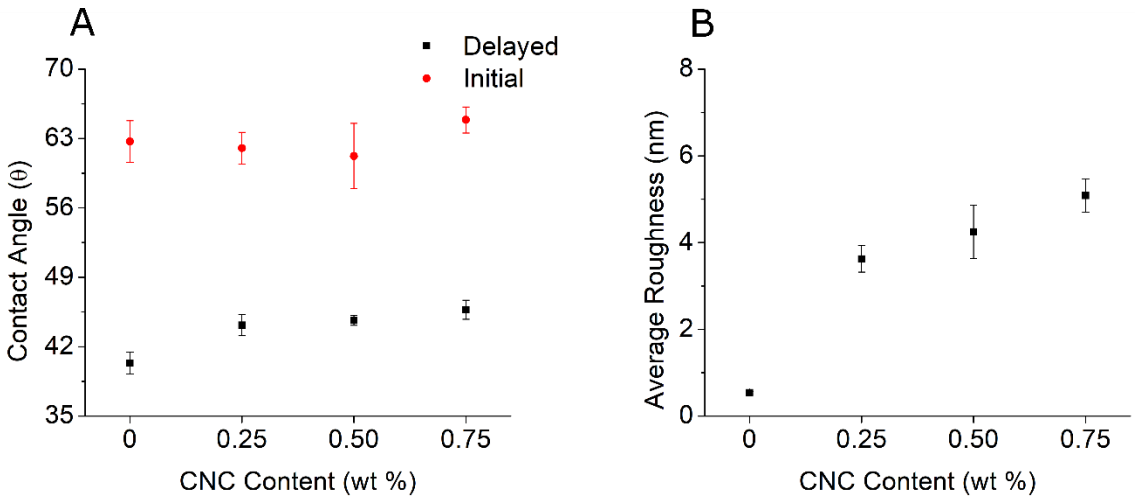

Figure 2.4. A) Contact angle measurements of PVA and PVA-CNC films, measured immediately after the drop was cast (red circles) and after allowing the drop to settle for 5 seconds (black squares) and B) average surface roughness of PVA-CNC films at all CNC loadings measured with AFM.

MIM capacitors were fabricated by spin coating PVA and PVA-CNC dispersions between silver electrodes that were deposited through a shadow mask using physical vapor deposition (PVD). The MIM architecture and mask alignment was designed to yield 10 capacitors of varying areas on a 1 in^2 glass substrate, as shown in **Figure 2.5A** (details of capacitor areas can be found in **Figure 2.9,** supporting information). The spin coating conditions

used were identical to those used to prepare PVA-CNC films for the characterization experiments discussed previously. Three different substrates were prepared from each dispersion to yield a total of 30 potential capacitors for testing. All capacitors were tested using EIS, with measurements taken in frequency range of 10^{-2} – 10^{5} Hz with an AC amplitude of 10 mV. From the EIS measurements the capacitance can be calculated using Equation 2.1 where C is capacitance, f is the frequency, and $-Z''$ is the imaginary portion of the impedance.

$$C = \frac{1}{2\pi \times f \times -Z''} \qquad Eq\ 2.1$$

Using the capacitance value obtained from Equation 2.1 the dielectric constant can be found through Equation 2.2, where k is the dielectric constant, d is the thickness of the polymer film, A is the surface area of the capacitor and ε_0 is the permittivity constant.

$$k = \frac{C \times d}{\varepsilon_0 \times A} \qquad Eq\ 2.2$$

Increasing the weight percentage of CNCs in the PVA dispersion resulted in a substantial increase in the number of functioning devices (**Figure 2.5B**). Devices prepared from neat PVA had either no working capacitors (due to electrical shorting from the silver electrodes making contact) or on average 2 functioning devices per wafer. Upon addition of just 0.25 wt % CNCs, the number of working capacitors increased to an average of 5 per sample, however significant variability was still observed between substrates. This variability decreased upon the addition of 0.5 wt % CNCs. At 0.75 wt % CNCs, an average of 7 of the 10 capacitors were functional, with one substrate having 9 working capacitors.

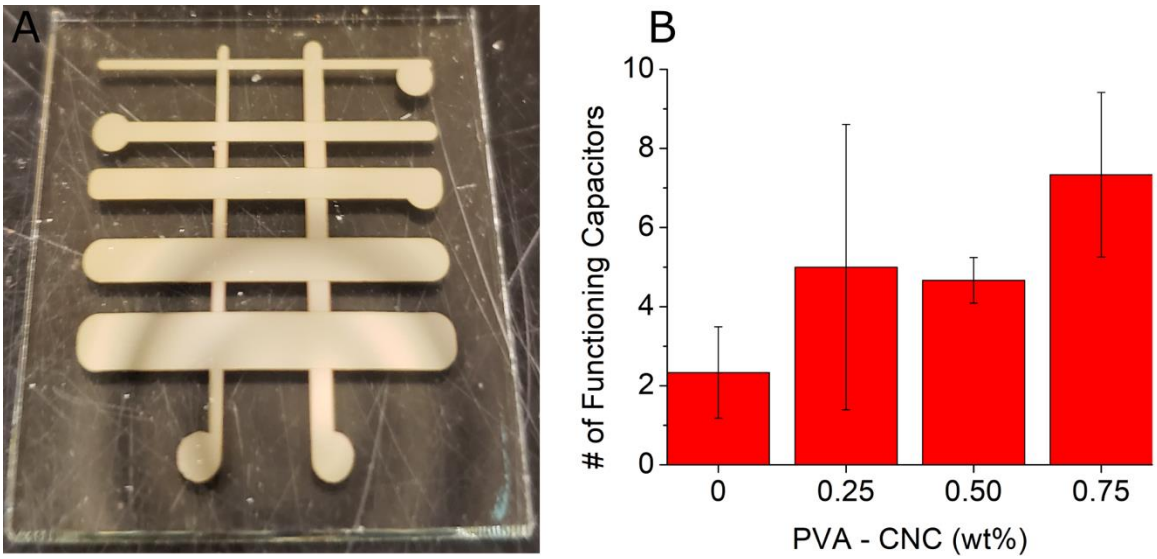

Figure 2.5. A) Photo of glass substrate with 10 capacitors, with the dielectric sandwiched between the silver electrodes. B) The number of functioning capacitors per substrate at various CNC loadings.

Surprisingly, the addition of CNCs to the PVA films did not cause a statistically significant change to the dielectric constant of PVA itself. PVA is considered to be a high *k* organic dielectric material, with a *k* value within the range of 5 – 10. As shown in **Figure 2.6A**, at 100,000 Hz the value of *k* is consistently centred around 6 for PVA and 5.3 for all three PVA-CNC blends. When the frequency is decreased to 1000 Hz, the dielectric constant rises to an average of 7.4 for PVA and 6.5 for the PVA-CNC films. The retention of a high *k* value for the PVA-CNC blends, combined with the substantial improvement in the number of functioning devices, corroborates the potential benefits of adding low-weight percentages of CNCs into the polymer matrix.

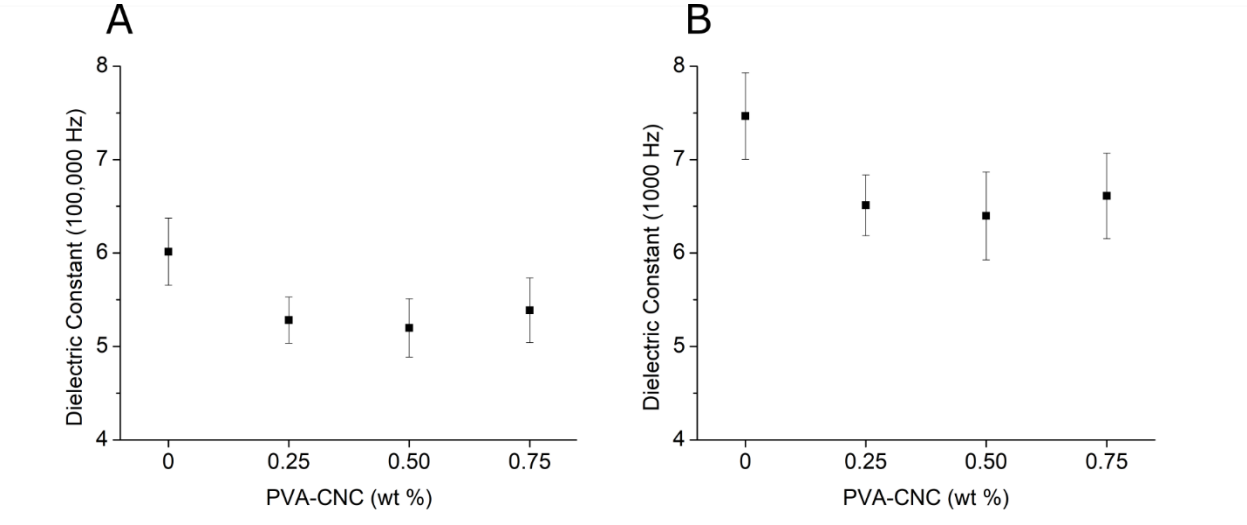

Figure 2.6. Dielectric constants (*k*) with varying CNC loading at A) 100,000 Hz and B) 1000 Hz.

Each set of 30 capacitors were further characterized by imaging under a backlit microscope with 4X magnification, which facilitated the visual observation of defects in the polymer films. Example images are shown in **Figures 2.7A** and **2.7D** for 0.75 wt % CNC loading and neat PVA, respectively. For neat PVA, there are distinct ripples visible in the film, indicating that the polymer is not forming a homogeneous film across the device. In contrast, **Figure 2.7A** for PVA with 0.75 wt % CNCs does not have any ripples and possesses a uniform colour when visually inspected, indicating a much more homogeneous film. To further quantify the macro level film uniformity and coverage a profilometer was utilized to do a macroscopic scan over the surface of these capacitors. 2D and 3D scans of a 0.15 x 1.00 mm^2 area were imaged on the surface of a PVA-CNC capacitor with 0.75 wt % CNCs (**Figures 2.7B** and **2.7C**, respectively). Smaller height features, on the order of a few nanometers, are observed over this extended range, corresponding with the roughness of a PVA-CNC film as previously discussed. **Figures 2.7E** and **2.7F** show the 2D and 3D profiles, respectively, of the PVA film in **Figure 2.7D**. These scans show that while there are some regions of low surface roughness, there are also large defects present in the film. The visible rippling on the PVA film near the top of **Figure 2.7D** corresponds to a large step edge, beyond which the film is increasingly thin or non-existent, resulting in electrical contact and a shorted MIM capacitor.

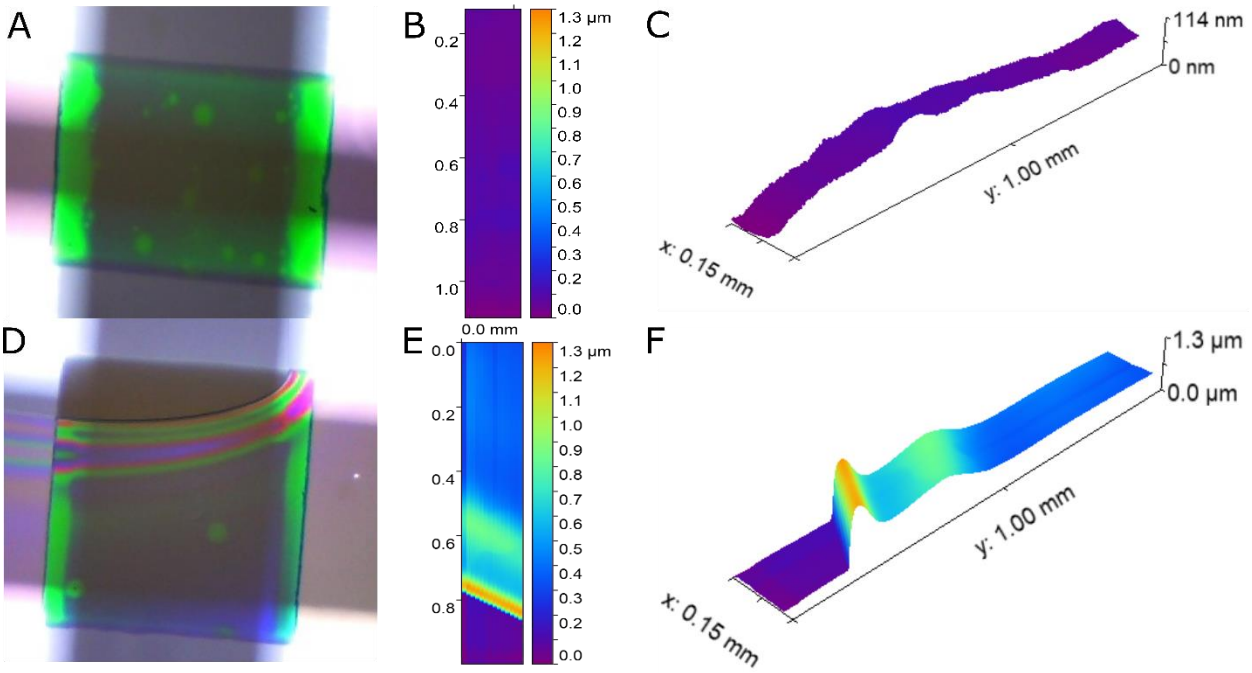

Figure 2.7. A) Macroscopic image (4X lens) of PVA-CNCs (0.75 wt %) thin films, sandwiched between two silver electrodes with the corresponding B) 2D and C) 3D surface profile scans of the same capacitor. D) Macroscopic image (4X lens) of neat PVA sandwiched between two silver electrodes with E) 2D and F) 3D surface profile scans of the PVA capacitor.

BGTC OTFTs (insert, **Figure 2.8A**) were fabricated by spin coating the four different PVA dispersions on top of silver gate electrodes that were deposited using PVD onto quartz-coated glass substrates. After drying the dielectric layer to remove residual solvent, the organic semiconductor (CuPc) was deposited by PVD on top of the PVA-CNC polymer blends using a shadow mask; silver source-drain electrodes were deposited via PVD on top of the semiconductor to yield 20 individual transistors per substrate. Two substrates were fabricated for each PVA dispersion, with μ_h, V_T and $I_{on/off}$ ratios characterized for each individual OTFT. A summary of these results can be found in **Table 2.1**, with an example output and transfer curve for PVA-CNC (0.75 wt %) shown in Figure 8. After correcting for film thickness, the fabricated OTFTs showed no statistically significant changes in μ_h, V_T or $I_{on/off}$ with increasing weight percentages of CNCs. Although the $I_{on/off}$ ratios are relatively low this has been reported in literature for PVA dielectrics.[32] These results corroborate the findings from the MIM capacitor study: incorporation of small amounts of CNCs into PVA does not drastically affect the electrical properties of organic electronic devices prepared from these composites. It is particularly

interesting that OTFT device performance remained consistent, despite the slight increase in surface roughness of the PVA-CNC thin films.

Table 2.1. OTFT electrical data with varying CNC loading.

PVA-CNC wt %	μ_h (cm^2/Vs) (x10^{-3})	V_T (V)	$I_{on/off}$
0	6.71 ± 3.3	5.55 ± 3.2	10
0.25	8.76 ± 5.8	4.26 ± 2.3	10
0.5	5.70 ± 9.5	4.72 ± 3.2	10
0.75	7.15 ± 1.7	6.16 ± 2.8	10

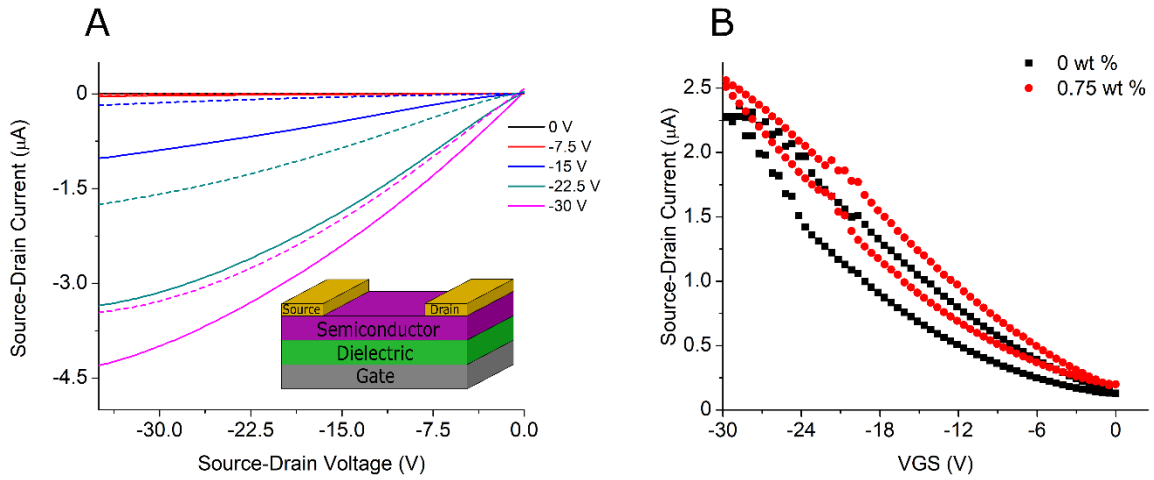

Figure 2.8. A) Example output curve for both neat PVA (dashed lines) and 0.75 wt % PVA-CNC (lines) transistors with CuPc as the semiconductor, and an insert showing schematic of the BGTC OTFT architecture and (B) example transfer curves of both neat PVA and 0.75 wt % PVA-CNC blend.

The drastic improvement in device fabrication and reproducibility can be directly related to the increase in solution viscosity and corresponding increase in film thickness shown previously in **Figures 2.1A** and **2.1B**. The inclusion of a small amount of CNCs (0.25 wt %) into the PVA solution was sufficient to result in a two-fold increase in the viscosity in the water/methanol co-solvent mixture. When the amount of CNCs added was increased slightly to 0.75 wt %, viscosity increased over six-fold compared to neat PVA. Increasing the viscoelastic

properties of the solution increased both the uniformity and the surface coverage of these films over the substrates, resulting in a larger number of functioning devices. This is a result of an extension of the critical radius of the spun film before fingering is observed.[23] This effect has previously been observed in the literature for PVA-CNC blends, where through rheological studies it was observed that increasing the CNC content would increase the viscoelastic properties of the solutions. However, we are the first to show this effect can still be exploited at much lower CNC loadings, and the benefit this protocol has on improving performances in organic electronic devices. While the addition of CNCs to PVA also increased both the hydrophobicity and surface roughness of the films, neither of these appear to negatively impact the performance of the blends in capacitors or OTFTs.

2.4 Conclusion

The addition of extremely low weight percentages of CNCs (0.25 – 0.75 wt %) into PVA solutions is sufficient to augment the viscosity of the dispersion by increasing the amount of hydrogen bonding in the blend. This change in viscoelastic properties results in increased critical radius before fingering, eliciting more uniform and homogeneous surfaces, corresponding to a reduction in the number of electrically shorted capacitors. Most importantly, the addition of CNCs was sufficiently low as to preserve the dielectric properties of the high-*k* PVA and did not alter the electrical properties of BGTC OTFTs compared to neat PVA. This study confirms that CNCs can be utilized as an environmentally friendly additive to PVA to improve the processability of this water-soluble polymer for organic electronic devices. Furthermore, the ability to tune the viscosity through minor changes in CNC loading could be beneficial for the development of printing applications with this dielectric blend.

2.5 Experimental

PVA (M_w = 13,000 – 23,000 Da; 98 % hydrolyzed) was purchased from Sigma Aldrich; a 2 wt % aqueous suspension of CNCs was prepared according to a procedure detailed elsewhere,[13] and provided by FPInnovations. Silver (99.99 %) was purchased from Angstrom Engineering, glass substrates (pre-cut to 1 in^2) were obtained from University Wafers and 15 x 20 mm^2 quartz coated glass substrates were purchased from Ossila. CuPc was purchased from Sigma Aldrich and purified by double sublimation All other solvents and reagents were purchased from Caledon Chemicals.

A Laurell WS-650-23 Spin coater was used for depositing the polymer thin films. The impedance properties of the capacitors were measured using EIS with a Metrohm PGSTAT204. Potentiostatic impedance measurements were done under ambient conditions within the frequency range of 10^{-2} – 10^{5} Hz with an AC amplitude of 10 mV. The devices were imaged using a backlit microscope with a 4x optical zoom. The electrical properties of the OTFTs were characterized using a Keithley 2614B. Measurements of the μ, V_T and $I_{on/off}$ were taken under ambient conditions. Contact angle measurements were obtained using a VSA Optima goniometer by AST Products Inc and were performed on polymer films spun onto glass substrates cleaned following the procedure outlined in Device Fabrication section; 0.1 µL of distilled water was dropped onto the films for measurements. The viscosity measurements were performed using an ATS Rheosystems Stresstech HR rheometer operated with parallel plates. Differential scanning calorimetry (DSC) analysis was performed using a TA DSC Q100, with a power ramp from 20 °C to 250 °C at 10 °C min^{-1} to remove moisture and thermal history, followed by cool down to 20 °C at 10 °C min^{-1} before a second ramp from 20 °C to 250 °C at 10 °C min^{-1} for the analysis. Thermogravimetric analysis (TGA) was performed using a TA Q50 with a power ramp from 25 °C to 600 °C at 20 °C min^{-1}. Both DSC and TGA data were analyzed using TA universal analysis 2000 software. Dynamic mechanical analysis (DMA) tests were performed on a PekinElmer DMA 8000 using tension mode. Samples were scanned from 25 ^{o}C to 200 ^{o}C at a ramp rate of 5 °C min^{-1} and frequency of 1 Hz, two runs were performed for each sample. The silver electrodes were deposited through a shadow mask using a physical vapor deposition chamber fabricated by Angstrom Engineering. Film thickness measurements and macro level profile scans were performed using a Bruker Dektak XT profilometer. Atomic force microscopy (AFM) measurements were performed using a Bruker Dimension Icon AFM, with ScanAsyst-Air probes. Several 10 x 10 μm^2 images were obtained for each sample at a scan rate of 1 Hz. AFM image processing was performed with NanoScope Analysis v1.9. Surface roughness measurement were taken from the 10 x 10 μm^2 area imaged through AFM using NanoScope Analysis.

2.5.1 Polymers Blends

PVA-CNC dispersions were prepared so that the final solution concentration of PVA was 80 mg/mL. The required amount of PVA (~ 90 mg) to achieve this final concentration was weighed into a 1 dr vial, dissolved in distilled water, and heated to 90 °C for 3 h to ensure all

polymer was dissolved. The solutions were allowed to cool to room temperature before dilution with 60 – 120 μL of methanol (with the purpose of making the final total volume of methanol in the dispersion 5 wt %), and filtration through a 0.45 μm filter. CNCs (2 wt % stock dispersion in distilled water) were then added to the filtered polymer solution to achieve a final loading of: 0, 0.25, 0.5 or 0.75 wt % of CNCs.

Table 2.2. Weight break down, weight percent ratios and viscosities of Native PVA and PVA blends with varying CNCs loadings.

CNC wt%	PVA (mg)	CNCs (mg)	Methanol (mg)	Water (mg)	Ratio (%) (PVA/CNC/Solvent)	Viscosity at 63 s^{-1}
0	80	0	54	930	(7.52/0/92.48)	0.008
0.25	80	2.67	55	932	(7.48/0.25/92.27)	0.023
0.5	80	5.36	55	932	(7.46/0.5/92.04)	0.043
0.75	80	8.06	55	932	(7.44/0.75/91.81)	0.051

2.5.2 Polymer blends for DSC, TGA and DMA

PVA was dissolved in a mixture of deionized water and methanol (95:5 v/v) at 80 mg/mL by stirring at 90 ^{o}C. Films were prepared by casting 10 mL of the PVA solution in Petri dishes (dia. ~ 9cm) at room temperature. Prior to casting a calculated amount of CNC suspension (4.3% wt. in water) was added into the PVA solution to achieve four films with CNC loadings of: 0, 0.25 wt %, 0.5 wt %, and 0.75 wt %.

2.5.3 Device Fabrication and Characterization

Metal-insulator-metal (MIM) capacitors were fabricated on 1 in^2 glass substrates under ambient conditions. The glass substrates were cleaned by sonicating sequentially for 5 minutes with: soapy water, distilled water, acetone and methanol. The substrates were dried under nitrogen and a 60 nm silver electrode was deposited onto the glass substrate by PVD with a shadow mask. The PVA-CNC solutions were spin coated onto the substrates at 4000 rpm for 1.5 min. The polymer films were then annealed at 90 °C under vacuum for 30 min to remove any residual solvent before the top electrode (silver, 60 nm) was deposited again by PVD with a

shadow mask. The final MIM configuration yielded 10 individual capacitors, with areas ranging from 0.35 – 2.88 mm^2 (see **Figure 2.9** in Supporting Information). After impedance characterization, insulator thickness and roughness were measured by profilometry. A macro-level scan of the surface area of certain capacitors was also performed using a profilometer.

BGTC OTFTs were fabricated on 15 x 20 mm^2 quartz coated glass substrates under ambient conditions. The quartz coated substrates were cleaned by sonication sequentially for 5 minutes using: soapy water, distilled water, acetone and methanol. The substrates were then dried under a stream of nitrogen and gate electrodes (silver, 60 nm) were deposited onto the substrate using a shadow mask and PVD. The PVA-CNC solutions were spin coated onto the substrates at 4000 rpm for 1.5 min. The polymers films were then annealed at 90 °C under vacuum for 30 min to remove any residual solvent. A 30 nm layer of copper phthalocyanine (CuPc, a p-type organic semiconductor) was deposited on top of the polymer films by PVD at a rate of 0.3 A s^{-1} using a shadow mask. The top source-drain electrodes (silver, 60 nm) were deposited over top of the CuPc layer by PVD using a shadow mask. This process yielded 20 individual TGBC OTFTs per substrate. After the OTFT devices were characterized, the thickness of the dielectric layer was obtained through profilometry and used to adjust the measured mobilities.

2.6 Acknowledgement

This work was supported by the NSERC Green Electronics Network (GreEN) (grant number: NETGP 508526-17) and NSERC Engage Grant (grant number: 513849-17). We also thank the Ontario government for the Queen Elizabeth II Graduate Scholarships in Science & Technology (AP). We are grateful to the NRC for their use of the rheometer operated with parallel plates, and A. Adronov (McMaster Univesity) for the use of his AFM.

2.7 Supporting Information

Crystallinity calculation:

$$X_c = \frac{\Delta H_m}{w \Delta H_m^0} \qquad Eq\ 2.3$$

where w is the weight fraction of PVA in the samples, ΔH_m is the melting enthalpy of the samples, and ΔH^o_m is the theoretical 100% crystalline heat fusion of PVA, which is 138.7 J/g for PVA.[127]

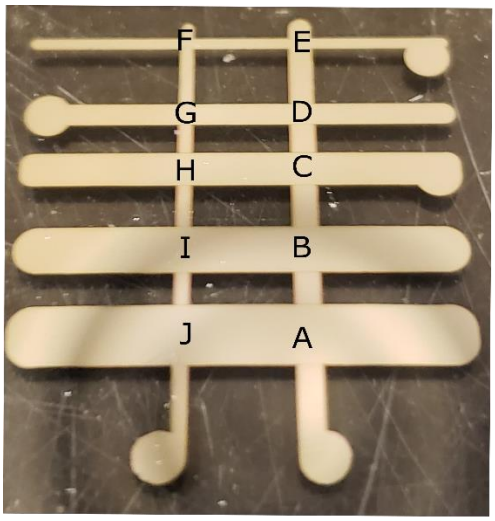

Capacitor Site	Capacitor Area (mm^2)
A	2.879
B	2.382
C	1.775
D	1.199
E	0.632
F	0.353
G	0.682
H	1.020
I	1.355
J	1.621

Figure 2.9. Capacitor areas for all 10 capacitor sites A-J.

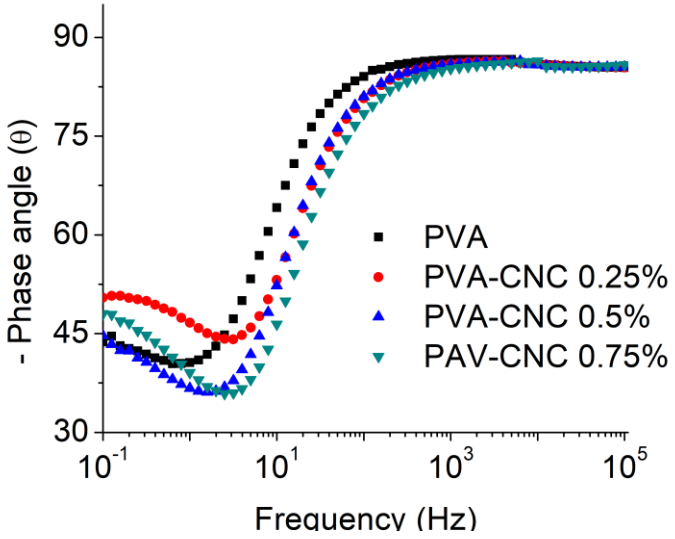

Figure 2.10. Representative phase angles of PVA-CNC capacitors between 10^{-2} – 10^5 Hz.

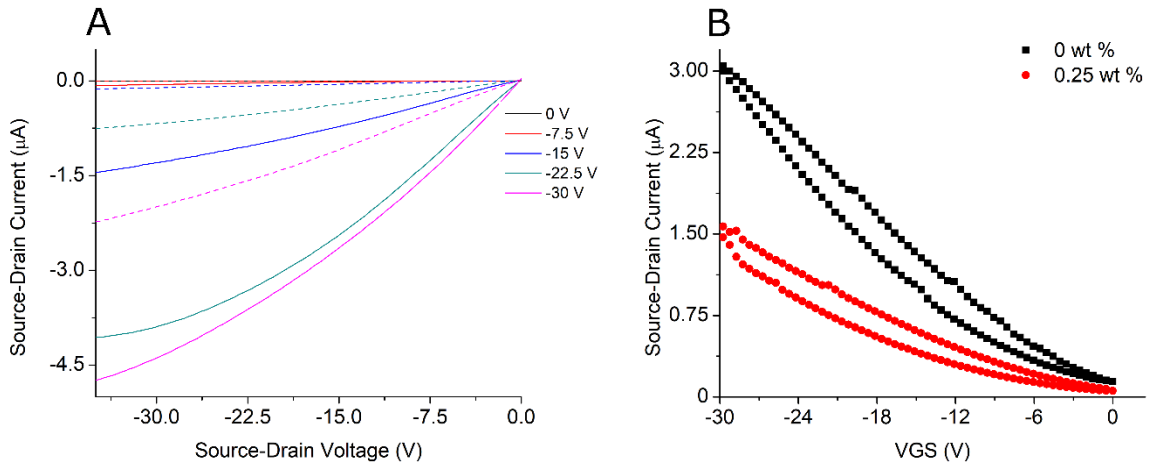

Figure 2.11. A) Example output curve for both 0.25 wt % PVA-CNC (dashed lines) and 0.5 wt % PVA-CNC (lines) transistors with CuPc as the semiconductor and (B) example transfer curves of both 0.25 wt % PVA-CNC and 0.5 wt % PVA-CNC blends.

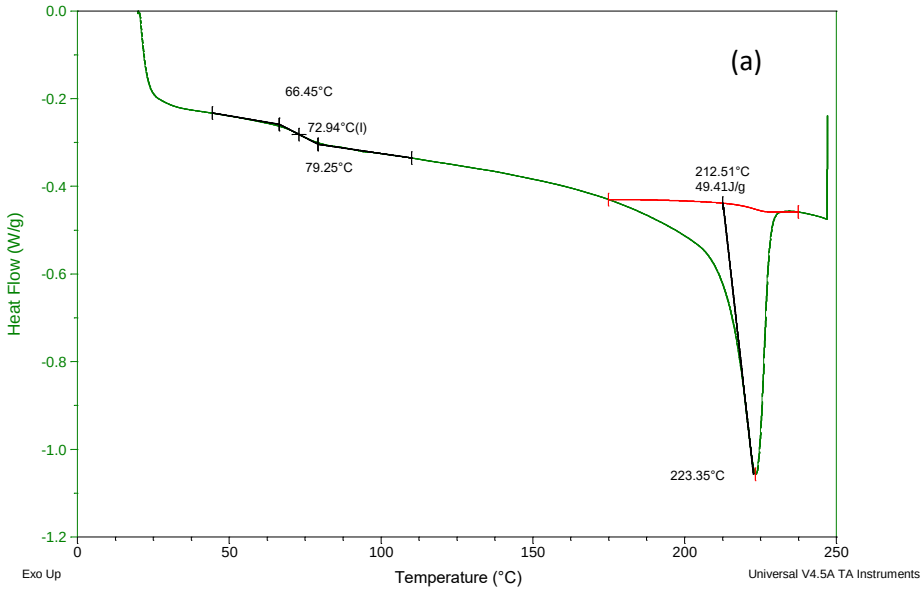
(a)
66.45°C
72.94°C(I)
79.25°C
212.51°C
49.41J/g
223.35°C
Heat Flow (W/g)
Temperature (°C)
Exo Up
Universal V4.5A TA Instruments

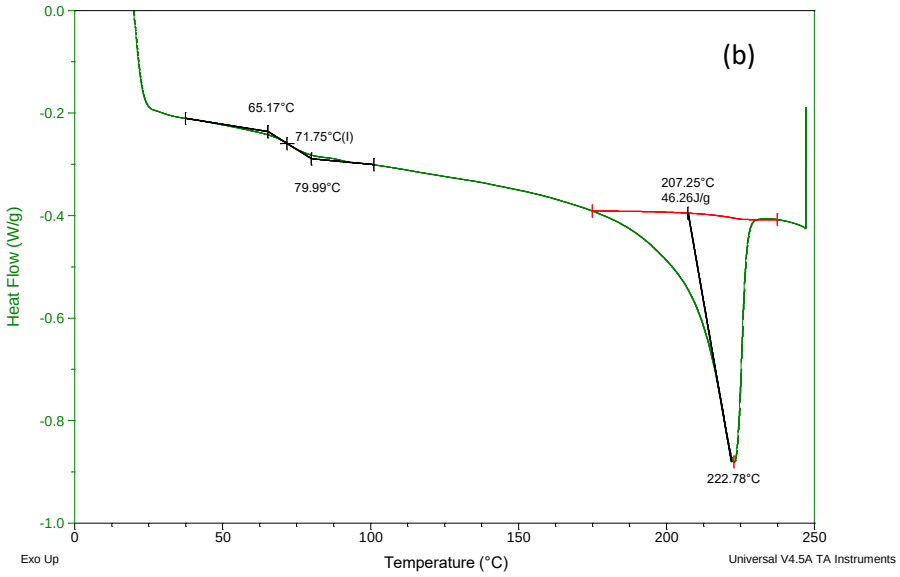
(b)
65.17°C
71.75°C(I)
79.99°C
207.25°C
46.26J/g
222.78°C
Heat Flow (W/g)
Temperature (°C)
Exo Up
Universal V4.5A TA Instruments

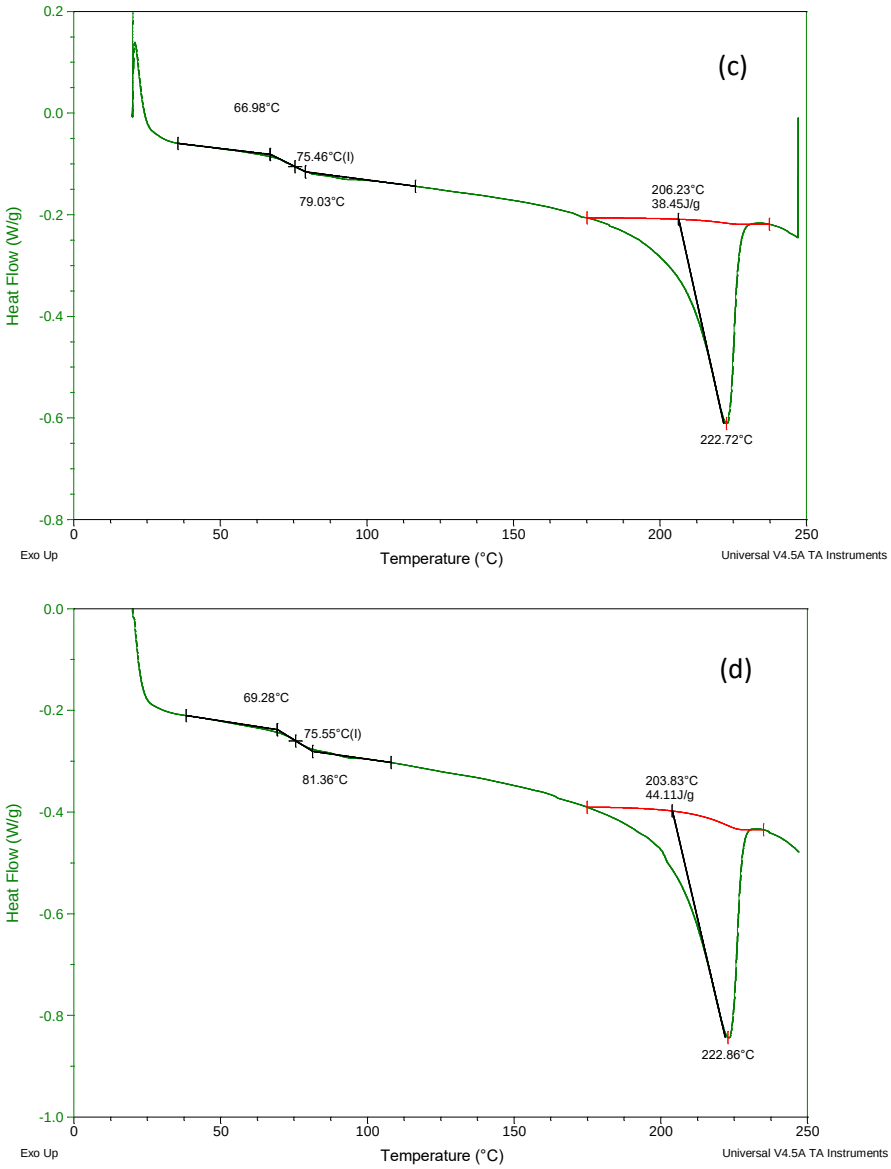

Figure 2.12. DSC results of (a) pure PVA, (b) PVA-CNC 0.25 wt %, (c) PVA-CNC 0.5 wt %, and (d) PVA-CNC 0.75 wt %.

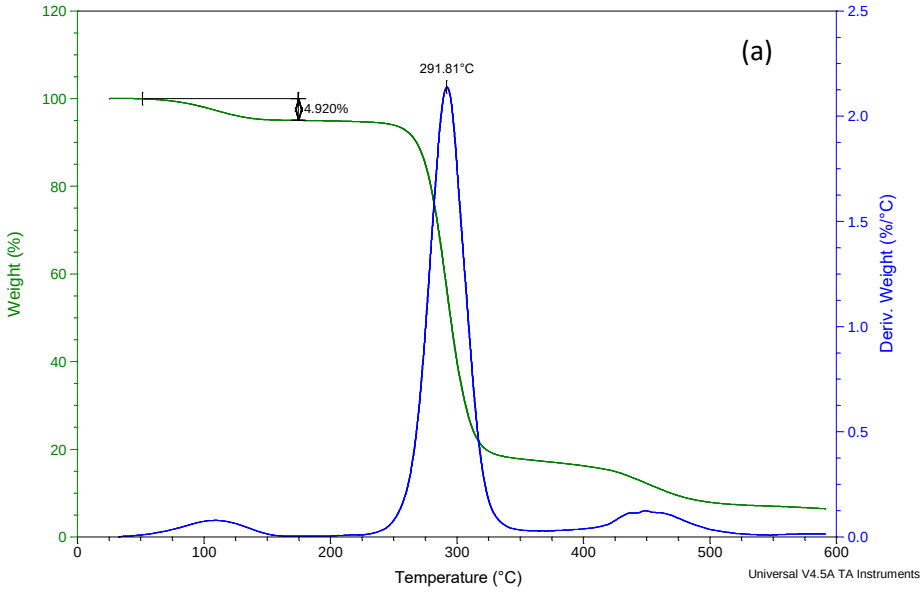
(a)
291.81°C
4.920%
Weight (%)
Deriv. Weight (%/°C)
Temperature (°C)
Universal V4.5A TA Instruments

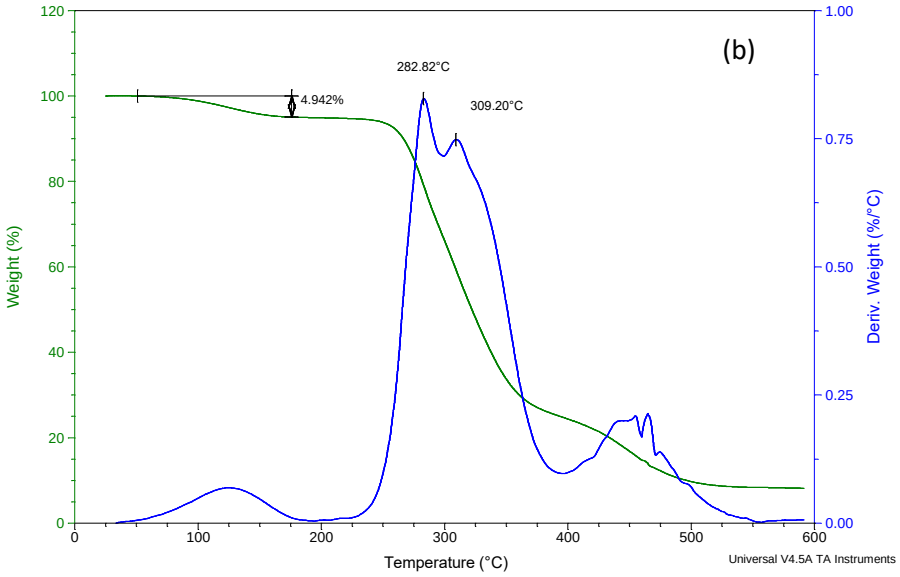
(b)
282.82°C
309.20°C
4.942%
Weight (%)
Deriv. Weight (%/°C)
Temperature (°C)
Universal V4.5A TA Instruments

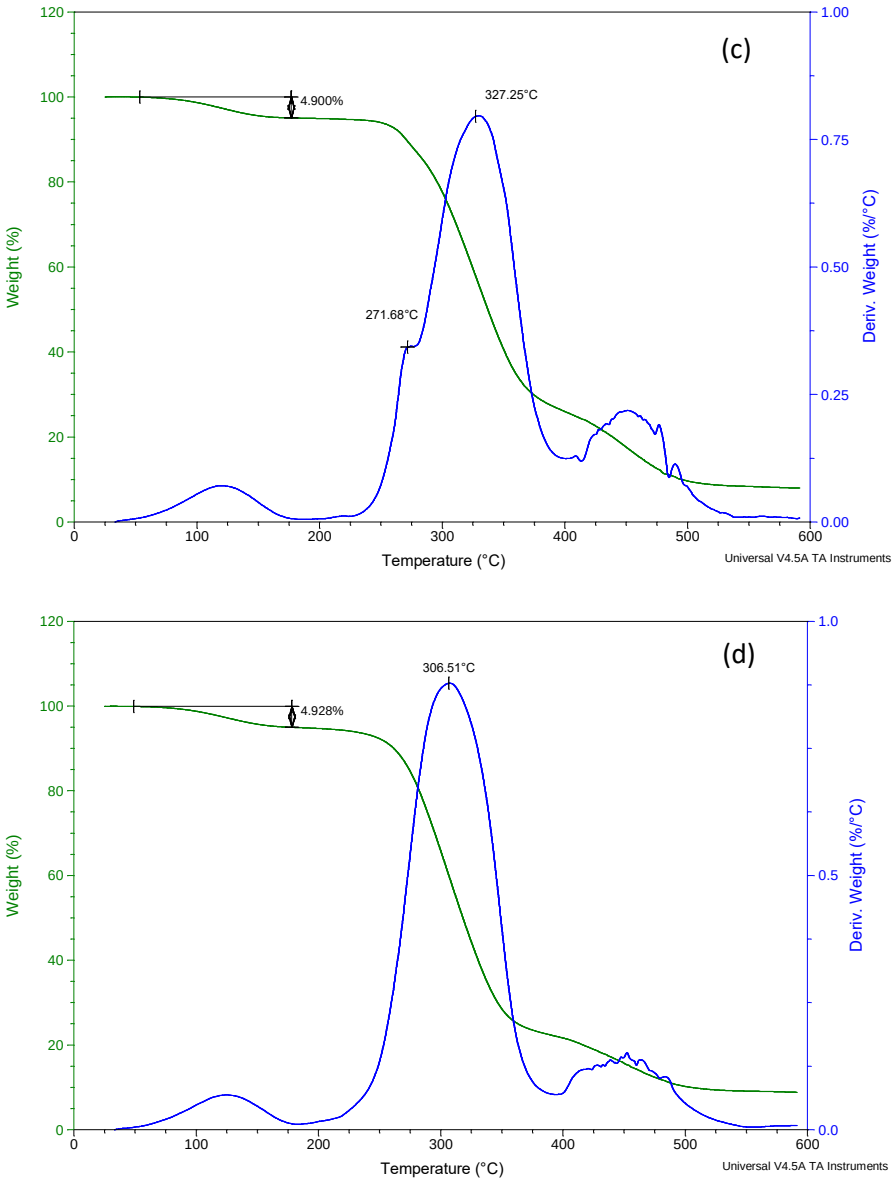

Figure 2.13. TGA results of (a) pure PVA, (b) PVA-CNC 0.25 wt %, (c) PVA-CNC 0.5 wt %, and (d) PVA-CNC 0.75 wt %.

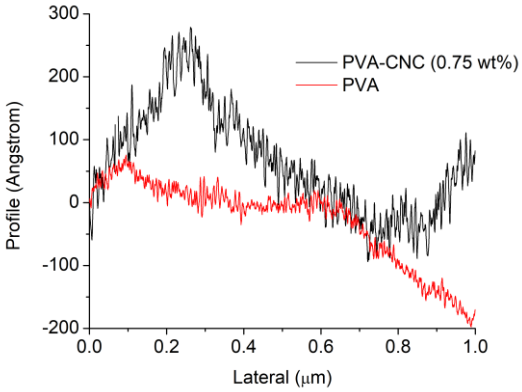

Figure 2.14. Profilometry measurement over 1 μm of the surface for both neat PVA and PVA-CNC 0.75 wt% films.

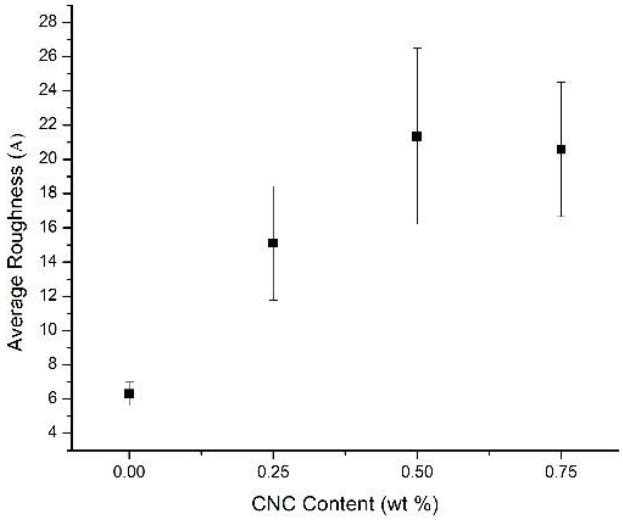

Figure 2.15. Profilometry measurement of average surface roughness of PVA-CNC films at all CNC loadings.

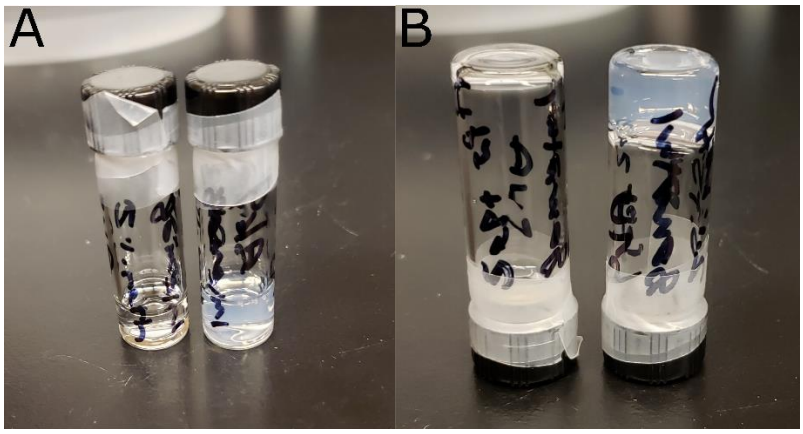

Figure 2.16. Visual demonstration of the polymer solution viscosity (A). vials Standing vertically left: neat PVA solution. Right: PVA-CNC 0.75 wt% solution (B). vials placed upside down Left: neat PVA solution. Right: PVA-CNC 0.75 wt% solution.

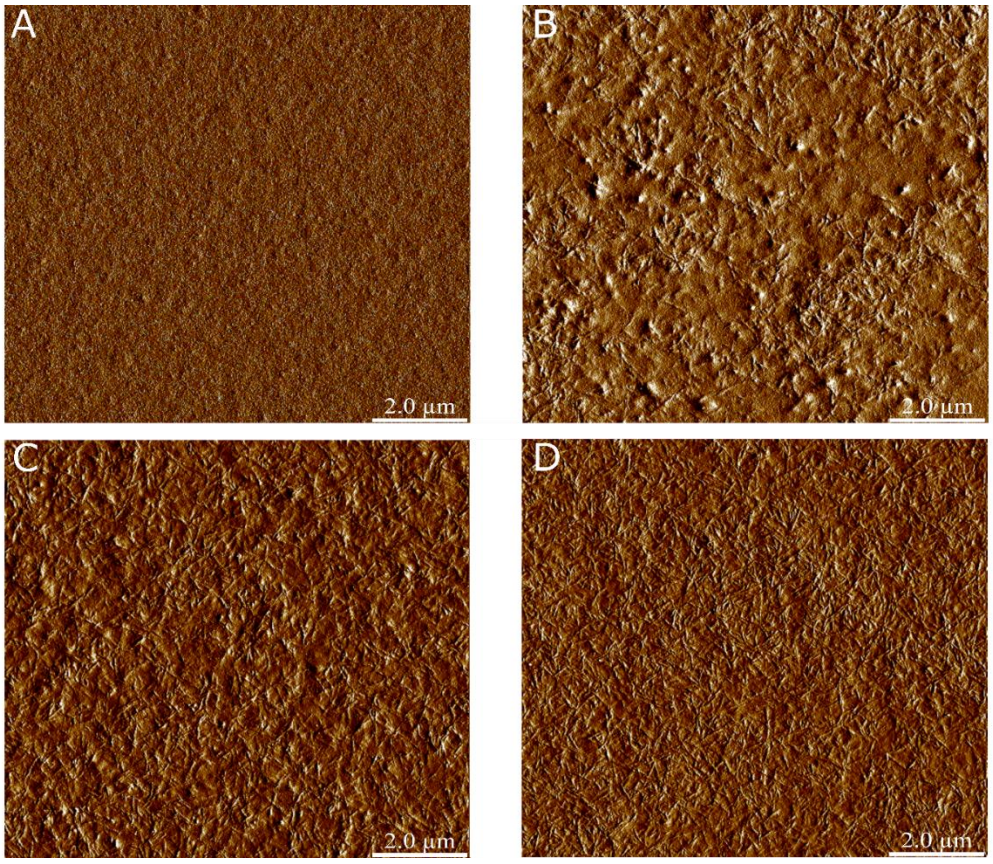

Figure 2.17. Representative AFM phase images of (A) neat PVA (B) 0.25 wt % PVA-CNCs (C) 0.5 wt % PVA-CNCs and (D) 0.75 wt % PVA-CNCs.

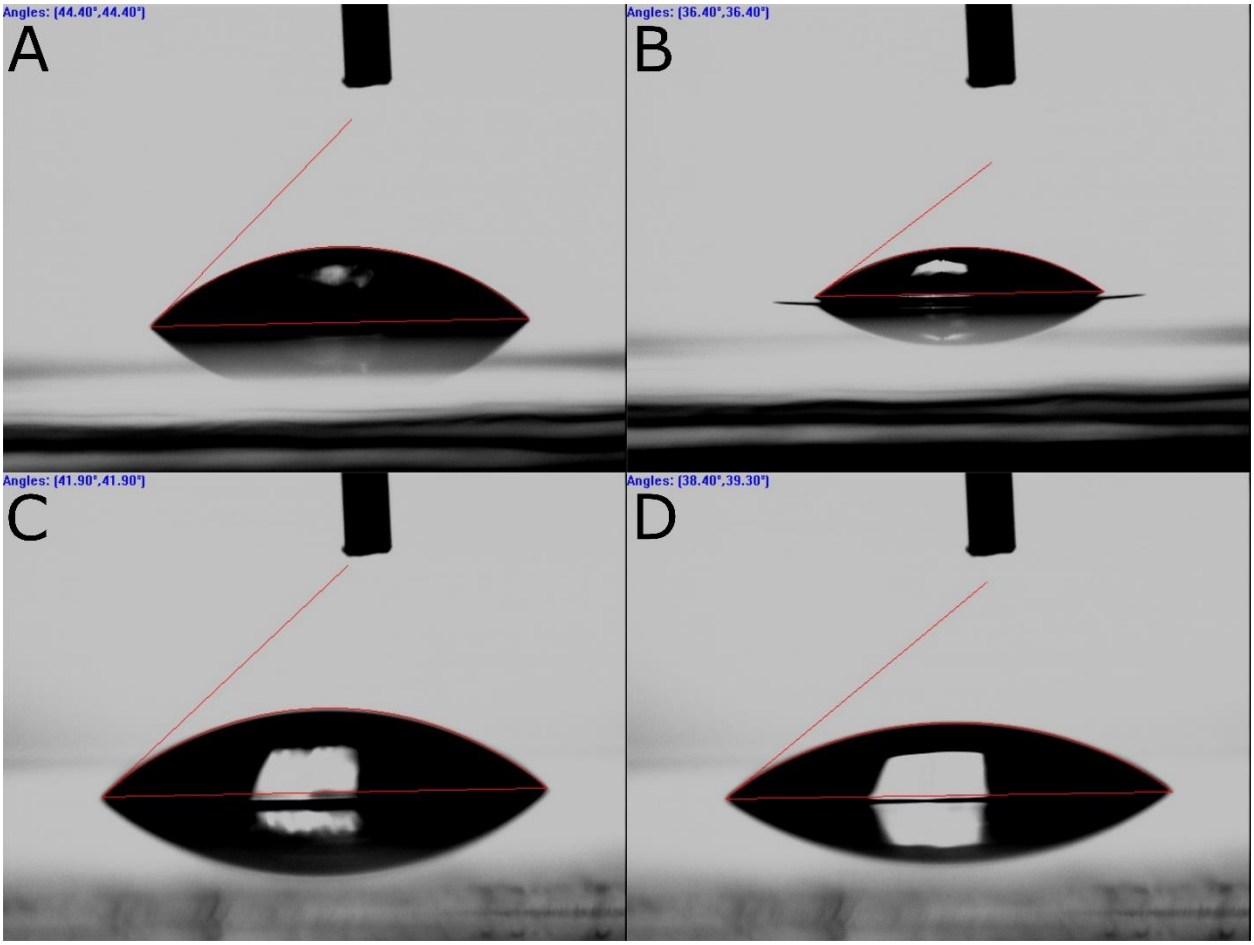

Figure 2.18. Captured images of the apparent contact angle of two polymer solutions on cleaned glass substrates (A) 0.75 wt % PVA-CNCs (B) 0.75 wt % PVA-CNCs after a 5 second delay (C) neat PVA and (D) Neat-PVA after a 5 second delay.

2.8 References

1. Irimia-Vladu, M., Głowacki, E. D., Voss, G., Bauer, S. & Sariciftci, N. S. Green and biodegradable electronics. *Mater. Today* **15**, 340–346 (2012).

2. Mabeck, J. T. & Malliaras, G. G. Chemical and Biological Sensors Based on Organic Thin-film Transistors. *Anal. Bioanal. Chem.* **384**, 343–353 (2006).

3. Comeau, Z. J. *et al.* On-the-Spot Detection and Speciation of Cannabinoids Using Organic Thin-Film Transistors. *ACS Sensors* **4**, 2706–2715 (2019).

4. Mirica, K. A., Azzarelli, J. M., Weis, J. G., Schnorr, J. M. & Swager, T. M. Rapid Prototyping of Carbon-based Chemiresistive Gas Sensors on Paper. *Proc. Natl. Acad. Sci. U. S. A.* **110**, 3265–3270 (2013).

5. Katz, H. E. & Huang, J. Thin-film organic electronic devices. *Annu. Rev. Mater. Res.* **39**, 71–92 (2009).

6. Kumar, B., Kaushik, B. K. & Negi, Y. S. Organic Thin Film Transistors: Structures, Models, Materials, Fabrication, and Applications: A Review. *Polym. Rev.* **54**, 33–111 (2014).

7. Facchetti, A., Yoon, M. H. & Marks, T. J. Gate Dielectrics for Organic Field-effect Transistors: New Opportunities for Organic Electronics. *Adv. Mater.* **17**, 1705–1725 (2005).

8. Melville, O. A., Lessard, B. H. & Bender, T. P. Phthalocyanine-Based Organic Thin-Film Transistors: A Review of Recent Advances. *ACS Appl. Mater. Interfaces* **7**, 13105–13118 (2015).

9. Chiellini, E., Corti, A., D'Antone, S. & Solaro, R. Biodegradation of poly (vinyl alcohol) based materials. *Prog. Polym. Sci.* **28**, 963–1014 (2003).

10. Van Etten, E. A. *et al.* Insulating characteristics of polyvinyl alcohol for integrated electronics. *Thin Solid Films* **568**, 111–116 (2014).

11. Li, J. *et al.* Solution-processable organic and hybrid gate dielectrics for printed electronics. *Mater. Sci. Eng. R Reports* **127**, 1–36 (2018).

12. Zocco, A. T., You, H., Hagen, J. A. & Steckl, A. J. Pentacene Organic Thin-film Transistors on Flexible Paper and Glass Substrates. *Nanotechnology* **25**, (2014).

13. Hamad, W. Y. & Hu, T. Q. Structure-process-yield Interrelations in Nanocrystalline Cellulose Extraction. *Can. J. Chem. Eng.* **88**, 392–402 (2010).

14. Foster, E. J. *et al.* Current Characterization Methods for Cellulose Nanomaterials. *Chem.*

Soc. Rev. **47**, 2609–2679 (2018).

15. Šturcová, A., Davies, G. R. & Eichhorn, S. J. Elastic Modulus and Stress-Transfer Properties of Tunicate Cellulose Whiskers. *Biomacromolecules* **6**, 1055–1061 (2005).

16. Marcos Mariano, Nadia El Kissi, A. D. Cellulose Nanocrystals and Related Nanocomposites: Review of some Properties and Challenges. *Transfus. Apher. Sci.* **27**, 83–92 (2002).

17. Zhou, L. *et al.* Morphological Influence of Cellulose Nanoparticles (CNs) from Cottonseed Hulls on Rheological Properties of Polyvinyl Alcohol/CN Suspensions. *Carbohydr. Polym.* **153**, 445–454 (2016).

18. Anju, V. P. & Narayanankutty, S. K. Impact of Bis-(3-Triethoxysilylpropyl)tetrasulphide on the Properties of PMMA/Cellulose Composite. *Polymer (Guildf).* **119**, 224–237 (2017).

19. Valentini, L., Bittolo Bon, S., Cardinali, M., Fortunati, E. & Kenny, J. M. Cellulose Nanocrystals Thin Films as Gate Dielectric for Flexible Organic Field-effect Transistors. *Mater. Lett.* **126**, 55–58 (2014).

20. Zhou, Y. *et al.* Recyclable Organic Solar Cells on Cellulose Nanocrystal Substrates. *Sci. Rep.* **3**, 24–26 (2013).

21. Abitbol, T., Johnstone, T., Quinn, T. M. & Gray, D. G. Reinforcement with Cellulose Nanocrystals of Poly(vinyl alcohol) Hydrogels Prepared by Cyclic Freezing and Thawing. *Soft Matter* **7**, 2373–2379 (2011).

22. Ching, Y. C. *et al.* Rheological properties of cellulose nanocrystal-embedded polymer composites: a review. *Cellulose* **23**, 1011–1030 (2016).

23. Spaid, M. A. & Homsy, G. M. Stability of Viscoelastic Dynamic Contact Lines: An Experimental Study. *Phys. Fluids* **9**, 823–832 (1997).

24. Hambsch, M. *et al.* Uniformity of Fully Gravure Printed Organic Field-effect Transistors. *Mater. Sci. Eng. B Solid-State Mater. Adv. Technol.* **170**, 93–98 (2010).

25. Jung, S., Hoath, S. D. & Hutchings, I. M. The Role of Viscoelasticity in Drop Impact and Spreading for Inkjet Printing of Polymer Solution on a Wettable Surface. *Microfluid.*

Nanofluidics **14**, 163–169 (2013).

26. Søndergaard, R. R., Hösel, M. & Krebs, F. C. Roll-to-Roll fabrication of large area functional organic materials. *J. Polym. Sci. Part B Polym. Phys.* **51**, 16–34 (2013).

27. Lee, S. Y. *et al.* Nanocellulose reinforced PVA composite films: Effects of acid treatment and filler loading. *Fibers Polym.* **10**, 77–82 (2009).

28. Jayaramudu, T. *et al.* Electroactive Hydrogels Made with Polyvinyl Alcohol / Cellulose Nanocrystals. *Materials (Basel).* **11**, 1–11 (2018).

29. Miao, C. & Hamad, W. Y. Critical Insights into the Reinforcement Potential of Cellulose Nanocrystals in Polymer Nanocomposites. *Curr. Opin. Solid State Mater. Sci.* **23**, 100761 (2019).

30. Park, Y. *et al.* Thermal conductivity Enhancement in Electrospun Poly(vinyl alcohol) and Poly(vinyl alcohol)/Cellulose Nanocrystal Composite Nanofibers. *Sci. Rep.* **9**, 1–10 (2019).

31. Ago, M., Jakes, J. E. & Rojas, O. J. Thermomechanical properties of lignin-based electrospun nanofibers and films reinforced with cellulose nanocrystals: A dynamic mechanical and nanoindentation study. *ACS Appl. Mater. Interfaces* **5**, 11768–11776 (2013).

32. Vasimalla, S., Subbarao, N. V. V., Gedda, M., Goswami, D. K. & Iyer, P. K. Effects of Dielectric Material, HMDS Layer, and Channel Length on the Performance of the Perylenediimide-Based Organic Field-Effect Transistors. *ACS Omega* **2**, 2552–2560 (2017).

Chapter 3 : High Performance Organic Electronic Devices Based on a Green Hybrid Dielectric

This chapter was published in the journal "Advanced Electronic Materials": Mathieu N. Tousignant, Nicole A. Rice, Jukka Niskanen, Chloé M. Richard, Dialia Ritaine, Alex Adronov, and Benoît H. Lessard, High Performance Organic Electronic Devices Based on a Green Hybrid Dielectric. Adv. Electron. Mater. 7, 1–10 (2021)

Context

For this work I looked at ways of improving the performance of PVA when used as a dielectric in organic thin film transistors. As mentioned in Chapter 1, PVA is a high-*k* environmentally friendly material that is water soluble. Being soluble in water is an advantage for green processing however it also makes this material extremely hygroscopic. This can cause issues because the dielectric properties of PVA vary depending on the moisture of the ambient environment. Another issue is that PVA is a polar dielectric which is not ideal for the semiconductor/dielectric interface. Therefor I wanted to find a biodegradable low-*k* polymer that I could put on top of PVA/cellulose nanocrystal blends (PVAc) to take advantage of a high-*k*/low-*k* bilayer dielectric structure as discussed in Chapter 1. Toluene diisocyanate terminated polycaprolactone (TPCL) had been blended with PVA and crosslinked with PVA in literature to be used as solarizing films in agricultural applications. The TPCL was crosslinked with the hydroxy groups of PVA and remained fully biodegradable. In literature PCL is commonly referred to as a possible biodegradable substrate or dielectric for organic electronics. However, there were very few applications of PCL as a dielectric within literature. Therefore, I decided to investigate the dielectric properties of TPCL and determine if it could be used as a low-*k* dielectric to enhance the performance of PVAc. We found that the TPCL layer both reduced the moisture sensitivity of PVA and improved its performance when used as a low-*k* dielectric in a bilayer system for OTFTs. The crosslinking between PVAc and TPCL also allowed for further orthogonal processing and helped mitigate issues cause by the low melting temperature of PCL.

Contribution

Dr. Niskanen synthesized the TPCL used within this study and performed all polymer characterization. I prepared all the thin films used within this study. I performed the AFM measurements and cleaned up the raw AFM images with the guidance of Dr. Rice. I performed

all the contact angle measurements for this study. I performed all profilometry measurements and microscope imaging. I fabricated, characterized and interpreted all the capacitor data. Dialia Ritaine performed the TGA measurements. Chloe Richard prepared and characterized all the organic thin film transistors under the supervision of myself and Dr. Rice. I interpreted the thin film, capacitor and OTFT data and made all the figures used within the study. Chloe Richard, Dr. Niskanen, Dr. Rice, Dr. Lessard and Dr. Adronov reviewed the manuscript. I wrote and reviewed the submitted manuscript.

3.1 Abstract

As the cost of electronics decreases, the demand for short-term and single-use applications, such as smart packaging, increases. Consequently, there is significant need for electronically active biodegradable materials to reduce the environmental impact of disposable electronic devices. We have developed a bilayer dielectric based on environmentally friendly, low-cost solution-processable polymers, fabricated by thermally crosslinking a TPCL layer with the hydroxyl groups of PVA_C. MIM capacitors were fabricated and characterized under ambient and humid conditions. The incorporation of a TPCL layer in the bilayer dielectric resulted in a large reduction in moisture sensitivity when compared to neat PVA_C without significantly altering the dielectric constant. When utilized as a dielectric in OTFTs, the transistors prepared with the PVA_C/TPCL dielectric had greater $I_{on/off}$ ratios and μ_h, with reduced hysteresis compared to devices fabricated with PVA_C. Furthermore, the fabricated OTFTs function at operating voltages six times lower when compared against a traditional SiO_2 dielectric. The facile processing, combined with superior device performance, make this green bilayer dielectric a promising candidate material for biodegradable disposable electronic applications.

3.2 Introduction

As the manufacturing cost of electronic devices decreases, the potential for emerging applications increases, such as the use of smart packaging. Some examples of these applications include the incorporation of electronic sensors within product packaging, such as radio-frequency identification (RFID) tags that enable consumers to access supplemental product information or temperature sensors to alert distributors and consumers that a product has been exposed to unsafe temperatures.[1] Smart packaging has quickly become a multi billion-dollar industry,[2] with the potential to dramatically reduce food waste and improve consumer experience

and confidence. However, for smart packaging to be viable, the electronically active materials need to be environmentally friendly to reduce the footprint of the waste created, inexpensive, and amenable to low-cost printing processes.[1]

OTFTs can address the complex and variable demands of smart packaging. If the proper materials are selected, OTFTs can be low-cost, environmentally friendly, and solution processable, with the capability to be fabricated on flexible substrates. OTFTs have also been demonstrated in a wide variety of sensing applications, including temperature and cannabinoid sensors.[3–5] OTFT architectures vary, however all designs are comprised of multiple layers, including electrodes, a semiconductor, and a dielectric. Dielectric materials can be classified into two main categories: organic or inorganic, both of which have their advantages and disadvantages. Organic dielectrics have the potential to yield flexible and biodegradable devices through low-temperature and solution processing techniques, however they typically suffer from higher leakage currents, a larger number of defects, and lower capacitances.[6–9] In contrast, inorganic dielectrics have lower leakage currents with well characterized performance metrics, but these materials require higher processing temperatures, higher operating voltages, and are not amenable to printing processes or many flexible applications.[10] An "ideal" dielectric material for OTFTs would need to possess a high-*k*, low leakage currents, and no hysteresis.[9,11] Many of the polymer dielectrics that are commonly used within literature cannot fulfill all these requirements. For example, PMMA, PVP and PS are commonly used dielectrics within OTFTs that have low leakage currents, but these materials are low-*k* and have low capacitance densities.[12] Additionally, these polymer dielectrics are non-biodegradable and their polymer films need to be extremely thin to obtain capacitance densities comparable to high-*k* dielectric materials.[12]

PVA is a high-*k* dielectric that is water soluble, environmentally friendly, and has been utilized as a dielectric for OTFTs.[13] However, neat PVA is moisture sensitive and suffers from large leakage currents, poor film forming capabilities, and large hysteresis. Previously, we reported that low wt % of CNCs could be used to increase the viscosity of the PVA solutions, dramatically improving the thin-film properties without negatively impacting the dielectric properties of PVA.[14] Problems related to hysteresis and gate leakage in PVA dielectrics could result from charge trapping caused by the hydroxyl groups at the organic semiconductor/dielectric interface.[9,15] Tsai et al. demonstrated that hysteresis in PVA dielectrics

could be manipulated by changing the moisture content of the films.[16] The excess moisture interacts with the hydroxyl groups of PVA, limiting the concentration of hydroxyl groups available to trap charges, effectively reducing the hysteresis.

There are two approaches commonly used in the literature to reduce gate leakage in organic dielectrics: crosslinking or using bilayer dielectrics.[8,11] Crosslinking PVA can reduce both the leakage current and moisture sensitivity of the dielectric by limiting the concentration of available hydroxyl groups. However, reducing the concentration of hydroxyl groups within the PVA dielectric film also negatively influences capacitance and decreases the measured μ of the fabricated OTFTs.[17] A bilayer dielectric combines the beneficial properties of a high-*k* and a low-*k* dielectric while optimizing overall device performance. By covering a high-*k* polymer dielectric with a thin-film of a low-*k* material it is possible to reduce the dipolar disorder at the dielectric/organic semiconductor interface, reducing charge trapping and the leakage current, while preserving the large capacitance values obtained when using just the high-*k* polymer dielectric.[12,18–20] Within the literature there are several examples of improved device performance through the use of a low-*k*/PVA bilayer dielectric.[15,21–23] However, all these examples use non-environmentally friendly low-*k* materials that cannot be orthogonally processed for example: poly(methyl methacrylate) (PMMA) and polystyrene.

To fabricate a fully biodegradable dielectric we chose to combine both methods, crosslinking and a bilayer structure, incorporating PCL as our low-*k* top-layer dielectric. PCL is a biodegradable, hydrophobic, insulating polymer that has been used as a substrate in organic electronic devices, with relatively few reports regarding dielectric applications,[24–27] mostly due to its poor thermal stability.[28,29] To improve the thermal stability of PCL within devices we followed a procedure by Prisco et al. where hydroxyl terminated PCL is reacted with toluene diisocyanate to synthesize TPCL.[30] Malinconico et al. demonstrated that blends of PVA and TPCL could be thermally crosslinked together to create biodegradable plastic films for solarization applications.[31] When compared against the previous PVA/bilayer structures, TPCL has the advantages of being environmentally friendly and orthogonally processable when used as a low-*k* dielectric atop PVA.[6,32,33]

In this report we investigate how crosslinking a low-*k* TPCL layer on top of a high-*k* blend of PVA and CNCs (PVA_C) affects dielectric performance in both capacitor and OTFT

architectures. The TPCL layer was thermally crosslinked with hydroxyl groups in the PVA_C blend at the bilayer interface after film deposition. Optical profilometry and microscopy studies were performed to determine the optimal TPCL concentration to yield consistent thin-films. MIM capacitors were fabricated with and without the TPCL layer and characterized under ambient conditions and after 30 minutes of exposure to 99% relative humidity (RH). Incorporation of the TPCL layer significantly decreased moisture sensitivity compared to neat PVA_C. Finally, the utility of our novel bilayer dielectric was demonstrated in an OTFT architecture with sc-SWCNTs. The bilayer dielectric devices had higher μ_h, reduced hysteresis, larger $I_{on/off}$ ratios, and reduced variation in device performance compared to PVA_C devices. Furthermore, the OTFTs operated at voltages six times lower compared to a SiO_2 dielectric.

3.3 Discussion

3.3.1 Film studies

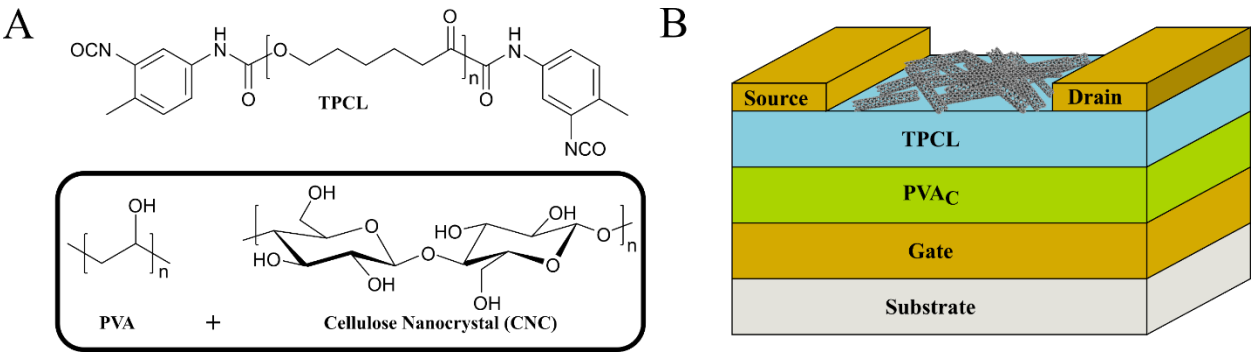

Figure 3.1. (a) Chemical structures of materials incorporated into dielectrics, including PVA, CNCs and TPCL and (b) schematic of BGTC OTFT structure with the bilayer dielectric.

Previously, we demonstrated that incorporating 0.75 wt % CNCs into PVA (PVA_C) could dramatically improve MIM device reliability without significantly altering the dielectric constant.[14] However, PVA_C films are hydroscopic, with device performance sensitive to moisture in ambient conditions. Incorporating PCL, a hydrophobic biodegradable polymer, in a bilayer architecture with PVA_C could act as a moisture barrier to protect the PVA_C film. A significant drawback of using PCL is that it is soluble in many organic solvents, limiting orthogonal processing of the organic semiconductor layer, which limits the practicality of this polymer in

organic electronics. To overcome this limitation, we investigated crosslinking the PCL layer to PVA_C with toluene diisocyanate functional end-groups (TPCL, **Figure 3.1**).

Three different polymer thin-films were spin-coated on glass substrates: PVA_C, PVA_C/PCL (no crosslinking moiety present), and PVA_C/TPCL. The water contact angle was measured for the pristine films, as shown in **Figure 3.2**, before the films were subjected to two rinsing steps with toluene for 10 s, with the contact angle of the films remeasured after each rinsing step. The contact angle of PVA_C, which is insoluble in toluene, was measured to be approximately 46º, matching values reported for PVA with CNCs in the literature.[36] The water contact angle of PVA_C remains relatively consistent after each rinsing step, confirming the toluene rinse was not sufficient to remove the polymer film. The contact angle of the pristine PVA_C/PCL film was much larger at 78º, but dropped to 47º after the first rinse, matching the values achieved for neat PVA_C. PCL is soluble in toluene, therefore the dramatic change in contact angle is attributed to complete removal of the PCL layer, exposing the PVA_C film underneath. In contrast, the contact angle of PVA_C/TPCL bilayer films remained unchanged after rinsing, with a contact angle of approximately 62º persisting after both rinsing steps, which is sufficiently different from PVA_C to confirm the presence of TPCL on the surface. This substantiates that the TPCL layer has successfully crosslinked with hydroxyl groups at the PVA_C/TPCL interface, stabilizing the polymer layer, which will facilitate the deposition of the semiconductor from an organic solvent without the risk of damaging the TPCL layer.

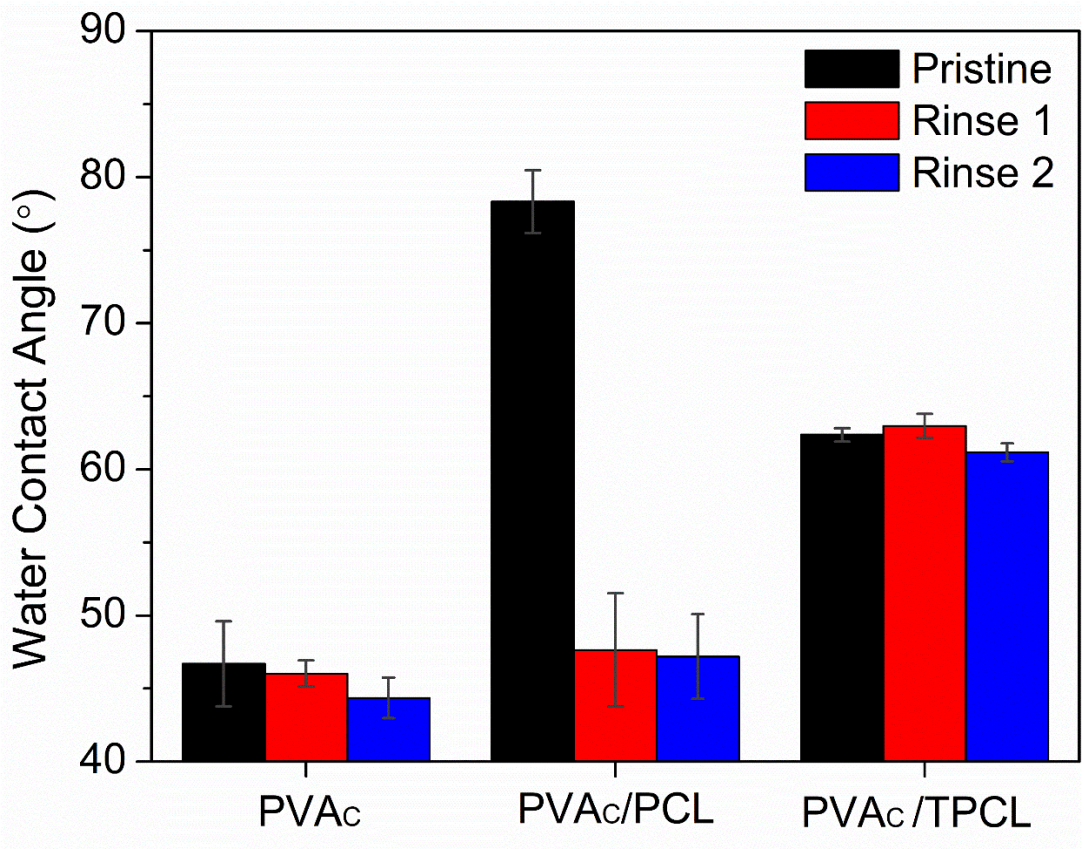

Figure 3.2. Water contact angle for PVAC, PVAC/PCL, and PVAC/TPCL thin-films. The films were subjected to sequential rinses with toluene (10 s, then dried with nitrogen).

Neat PCL has a low melting temperature (T_m) of 60 ºC and a glass transition temperature of -61 ºC;[37] additionally, PCL is immiscible with PVA, promoting phase separation of the polymer layers.[38] When a PCL film is heated above its T_m, it rapidly shrinks and aggregates with itself,[39] a phenomenon that has been reported in the literature for a variety of PCL/polymer blends.[40] We observed similar behaviour with our annealed PCL/PVA_C films (**Figure 5.12,** in the supporting information), with PCL aggregates forming an uneven coating on the surface of the PVA_C. However, this aggregation can be prevented through crosslinking the PCL layer. Thermally crosslinking the TPCL polymer with the hydroxyl groups of PVA_C enables annealing above the T_m of PCL as the crosslinked TPCL films can no longer move freely on the surface of the PVA_C film and self-aggregate. However, if the concentration of TPCL is too high (10 mg/ml) there is an excess of TPCL, resulting in incomplete crosslinking at the PVA_C/TPCL interface. The excess TPCL aggregates with itself, increasing the surface roughness as shown in **Figure 3.3D** and **Figure 3.13** in the supporting information. It is widely accepted in the literature that an

increase in surface roughness negatively impacts OTFT performance.[9,18,41] To avoid deleterious aggregation of the TPCL layer we decreased the concentration of the TPCL solution to 2 mg/mL. This resulted in smoother surfaces without large aggregates, as shown in **Figure 3.3B**. Further, thermal gravimetric analysis was performed for both the PVA_C and PVA_C/TPCL samples. This included a heat and hold at 200 ºC. Both the crosslinking and the annealing for the OSC takes place at 200 ºC. Therefore, these results confirm that the polymer dielectric remained stable at 200 ºC **(Figure 3.14,** in the supporting information).

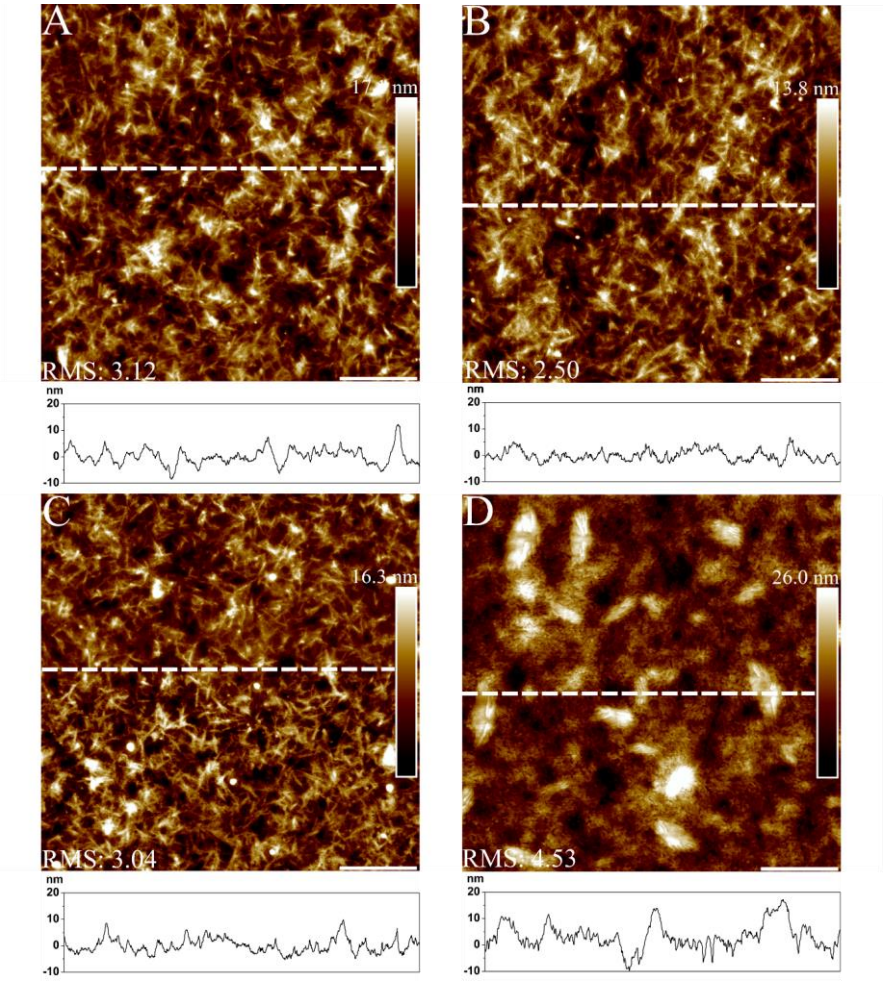

Figure 3.3. AFM height and linear surface profiles of (A) PVAC (B) PVAC/TPCL 2mg/ml (C) PVAC/TPCL 4mg/ml and (D) PVAC/TPCL 10mg/ml. The root mean square (RMS) surface roughness is included on the images and the white dashed lines show the location where the linear surface profiles were measured. The white scale bar in the lower right corner represents 1 µm

3.3.2 Capacitors

The dielectric properties of spin-coated PVA_C, PVA_C/TPCL, and PCL polymer thin-films were characterized using MIM capacitors. The PVA_C/PCL films were not further characterized due to the poor thermal stability of neat PCL. PVA_C was deposited via spin-coating onto substrates that were pre-patterned with the bottom electrodes and annealed at 150 ºC under vacuum to remove any excess moisture.[42] For the bilayer devices, a TPCL (2 mg/ml) solution was spun on top of the PVA_C thin-films in an oxygen and moisture free environment. Next, the films were annealed at 200 ºC for 15 minutes to thermally crosslink the TPCL layer with PVA_C. We were not successful in fabricating neat TPCL dielectrics, therefore PCL (35mg/mL) without annealing were used for comparison.

The fabricated MIM capacitors were characterized through EIS under ambient conditions. The dielectric properties of PVA_C, PVA_C/TPCL and PCL at a frequency of 10 Hz are summarized in **Table 3.1**; this frequency was chosen as it is representative of the operating frequency at which the fabricated OTFTs were characterized. The dielectric constant of neat PVA has been reported to be between 5-10,[43,44] while the dielectric constant of PCL (~3) is not widely reported in the literature due to PCL being more commonly utilized as a substrate material for organic electronics.[45] Our measured dielectric constants for PVA_C and PCL (12 and 4, respectively) match well with values reported in the literature. The addition of the TPCL layer above the PVA_C film caused a very minor decrease in dielectric constant (11) and capacitance density compared to PVA_C. These changes are minimal allowing for the high-*k* properties of PVA_C to be preserved despite the addition of a thin low-*k* TPCL layer.

Table 3.1. Dielectric constant (κ) and capacitance density (nF/cm2) of PVAC, PVAC/TPCL, and PCL, measured at 10 Hz.

Dielectric Material	Dielectric Constant (κ)	Capacitance Density (nF/cm^2)
PVA_C	12.2 ± 0.8	25.7 ± 0.8
PVA_C /TPCL	11.1 ± 0.6	22.6 ± 1.5
PCL	4.1 ± 0.1	9.3 ± 0.2

We explored the stability of the polymer dielectric materials by exposing PVA_C and PVA_C/TPCL MIM capacitors to 99 % relative humidity (99RH) for 30 min in a humidity chamber followed by immediate characterization through EIS. PVA is a water-soluble, hygroscopic polymer with moisture significantly impacting the dielectric properties. This has been demonstrated through its use as a humidity sensor.[46–48] However, this results in PVA slowly absorbing moisture in ambient environments, negatively impacting the electrical performance of fabricated unencapsulated electronic devices,[32] through an increase in both off state currents and gate leakage.[16,49]

Figure 3.4 shows the impact of moisture on the capacitance density of PVA_C and PVA_C/TPCL MIM capacitors. After exposure to 99RH, the capacitance density of the PVAc capacitors at 10 Hz is 40 times greater than devices characterized under ambient conditions, while the capacitance density of the PVA_C/TPCL MIM capacitors is only 3 times greater after exposure to 99RH. The moisture absorbed by the PVA_C films acts as a plasticizer and increases polymer chain mobility leading to an increase in capacitance density and dielectric constant.[42] The addition of a thin crosslinked TPCL layer acts as a barrier to moisture, significantly improving the stability of the fabricated devices. The observed small increase in capacitance density for PVA_C/TPCL capacitors is caused by the presence of ester groups within the TPCL layer (**Figure 3.1**) permitting some moisture to permeate the TPCL films.[50] Changes on the same order of magnitude were also observed for the frequency dependant dielectric constants before and after RH99 (**Figure 3.16,** in the supporting information).

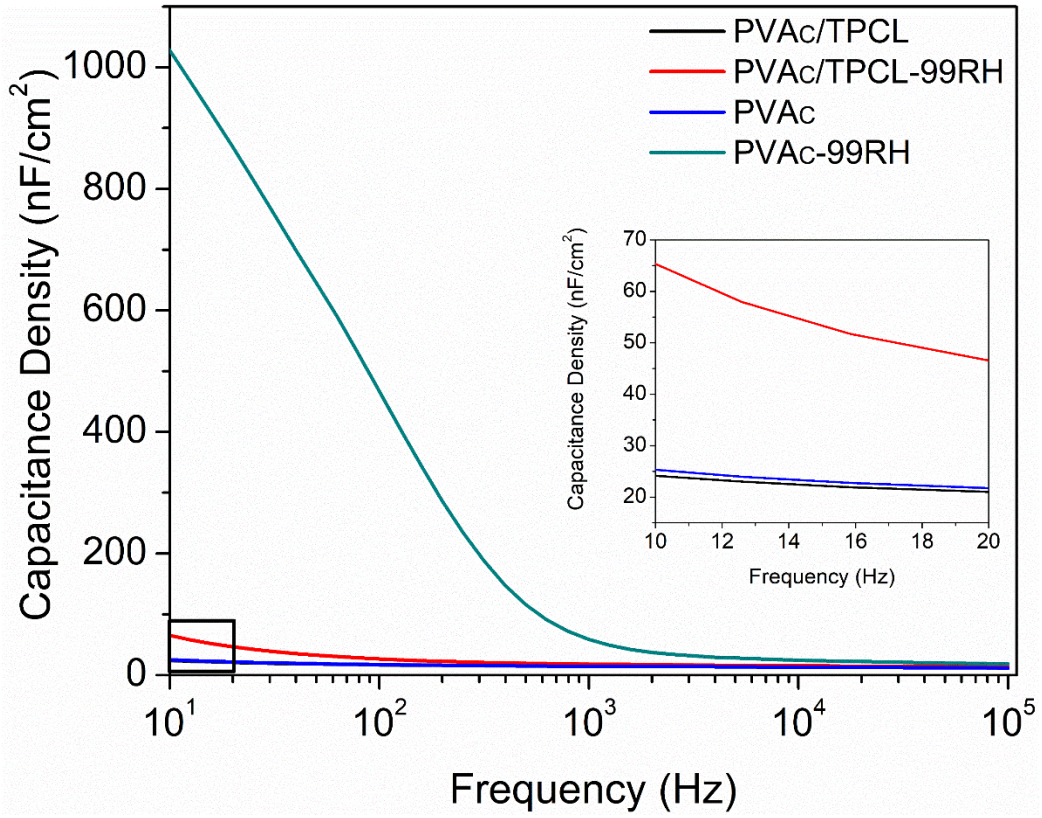

Figure 3.4. Frequency dependant capacitance density of PVAC and PVAC/TPCL capacitors before and after exposure to 99 % relative humidity (99RH). The black box indicates the location of the inset graph.

3.3.3 Organic Thin film transistors

BGTC OTFTs were fabricated on glass substrates, using our novel PVA$_C$/TPCL bilayer as the dielectric and polymer-sorted SWCNTs as the semiconductor. For comparison, OTFTs were also constructed with the same semiconductor on PVA$_C$ and SiO_2. The ultrapure sc-SWCNT dispersion was prepared using a poly(carbazole-*co*-*alt*-fluorene) polymer (PCF, **Figure 3.11,** in the supporting information), which we have previously demonstrated produces semiconducting enriched nanotube dispersions with greater than 99.9 % purity.[34] The sc-SWCNT layer was deposited on top of the various dielectric surfaces through sequential drop-casting and rinsing with toluene to remove excess unbound PCF polymer from the surface. The devices were then annealed in air at 200 ºC for one hour before deposition of gold source-drain electrodes (channel length of 30 μm) through PVD.

Representative output and transfer curves of OTFTs prepared on PVA_C, PVA_C/TPCL and SiO_2 are shown in **Figure 3.5**. The output curves for OTFTs with the PVA_C dielectric did not achieve saturation (**Figure 3.5A**), which can be attributed to the hydroxyl groups of PVA interacting with the sc-SWCNT, limiting its ability to saturate.[51] Additionally, the transfer curves for OTFTs with PVA_C have significant hysteresis between the forward and reverse sweeps (**Figure 3.5B**). In contrast, output curves for PVA_C/TPCL bilayer dielectric OTFTs have a well-defined saturation regime, and achieved higher I_{SD} (**Figure 3.5C**) compared to those prepared on PVA_C. Transfer curves for the PVA_C/TPCL OTFTs also have greater I_{SD} and significantly reduced H (**Figure 3.5D**) when compared to those fabricated with PVA_C. OTFTs were also fabricated with an SiO_2 dielectric (**Figures 3.5E** and **3.5F)**, a common dielectric material used in the literature for sc-SWCNT OTFTs. When operated in the same voltage range as OTFTs prepared on PVA_C and PVA_C/TPCL (V_{SD} = 1 to -5 V, V_{GS} from 1 to -5 V), the output and transfer curves do not have a defined off and on state for the transistor. When the devices fabricated with the SiO_2 dielectric are operated at potentials six times larger than those shown in **Figure 3.5**, we observe characteristic output and transfer behaviour values similar (**Figure 3.17,** in the supporting information**)** to those reported in the literature for polymer-sorted sc-SWCNT networks on SiO_2 dielectrics.[35]

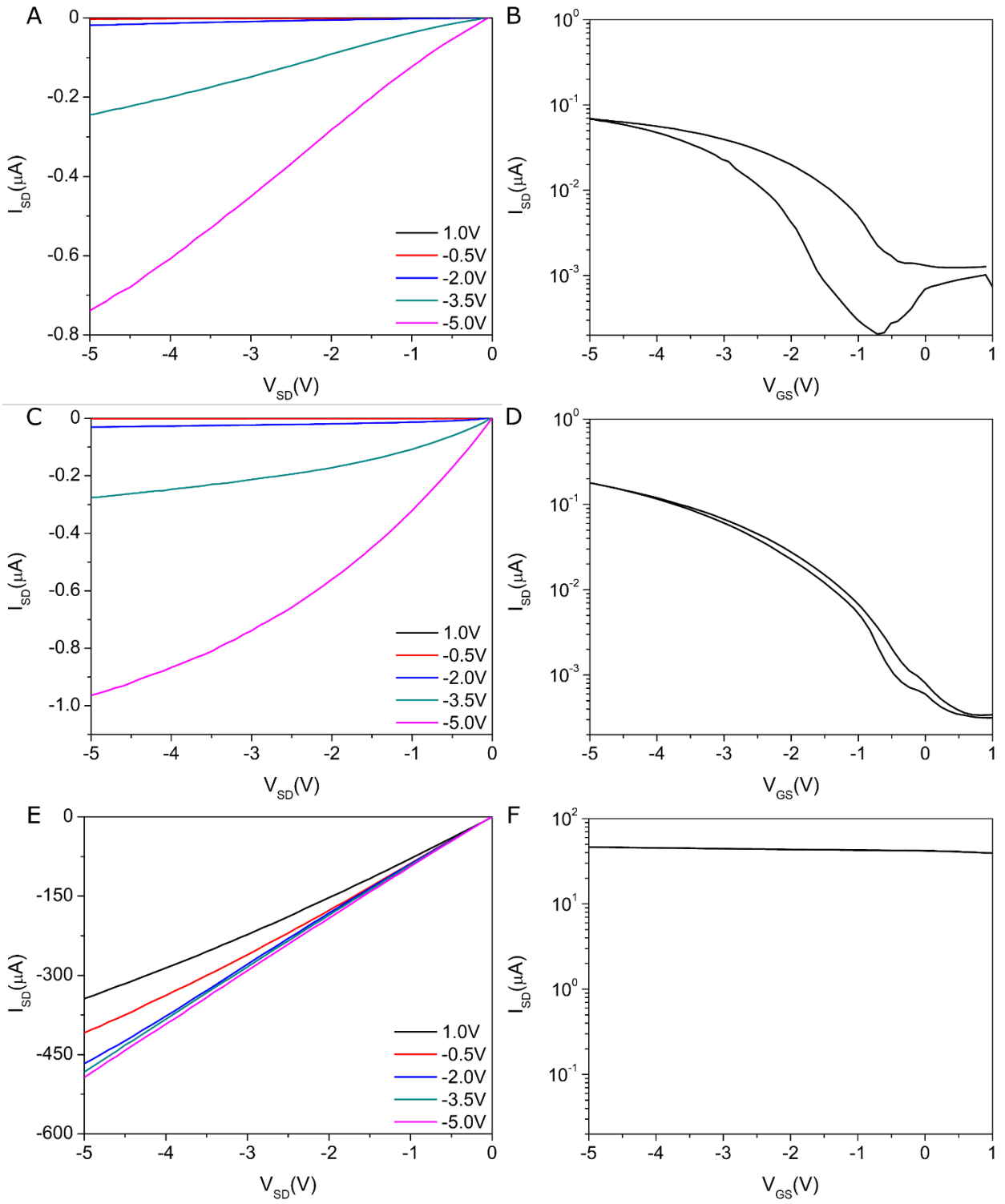

Figure 3.5. Output and transfer curves of PCF-SWCNT OTFTs fabricated on a: PVAc dielectric (A and B), PVAc/TPCL bilayer dielectric (C and D), and a SiO_2 dielectric (E and F). The transfer curve measurements were performed using a V_{SD} of -0.5 V.

μ_h, V_T, $I_{on/off}$ and H values were calculated from the transfer curves of the fabricated PVA_C and PVA_C/TPCL OTFTs, with the results summarized using box plots in **Figure 3.6**. Data for OTFTs prepared on the SiO_2 dielectric was not included as they did not behave as transistors in the same voltage range. Charge trapping, moisture absorption, and surface roughness are some of the properties that will impact performance at the semiconductor/dielectric interface.[52] The PVA_C/TPCL OTFTs had an average and maximum μ_h (0.42 cm^2/Vs and 2.42 cm^2/Vs, respectively) that was over a magnitude greater compared to OTFTs with only PVA_C (0.032 cm^2/Vs and 0.078 cm^2/Vs, respectively). The improved performance can be attributed to the TPCL layer acting as a barrier between PVA_C and the sc-SWCNTs, preventing charge trapping by the hydroxyl groups of PVA_C. Improved μ values have been observed for other bilayer PVA dielectrics due to the reduction of charge trapping at the semiconductor/dielectric interface.[22] In the literature, OTFTs prepared from sc-SWCNTS in combination with a polymer dielectric have reported μ_h values between 1 – 10 cm^2/Vs. However, in all these reports the sc-SWCNTs were deposited using aerosol printing techniques, resulting in a much denser network of sc-SWCNTs and, therefore, greater μ_h.[53–56] AFM images revealed that our drop-cast methodology resulted in lower sc-SWCNT network densities (**Figure 3.7** and **Figure 3.18,** in the supporting information) and therefore lower average μ_h values.

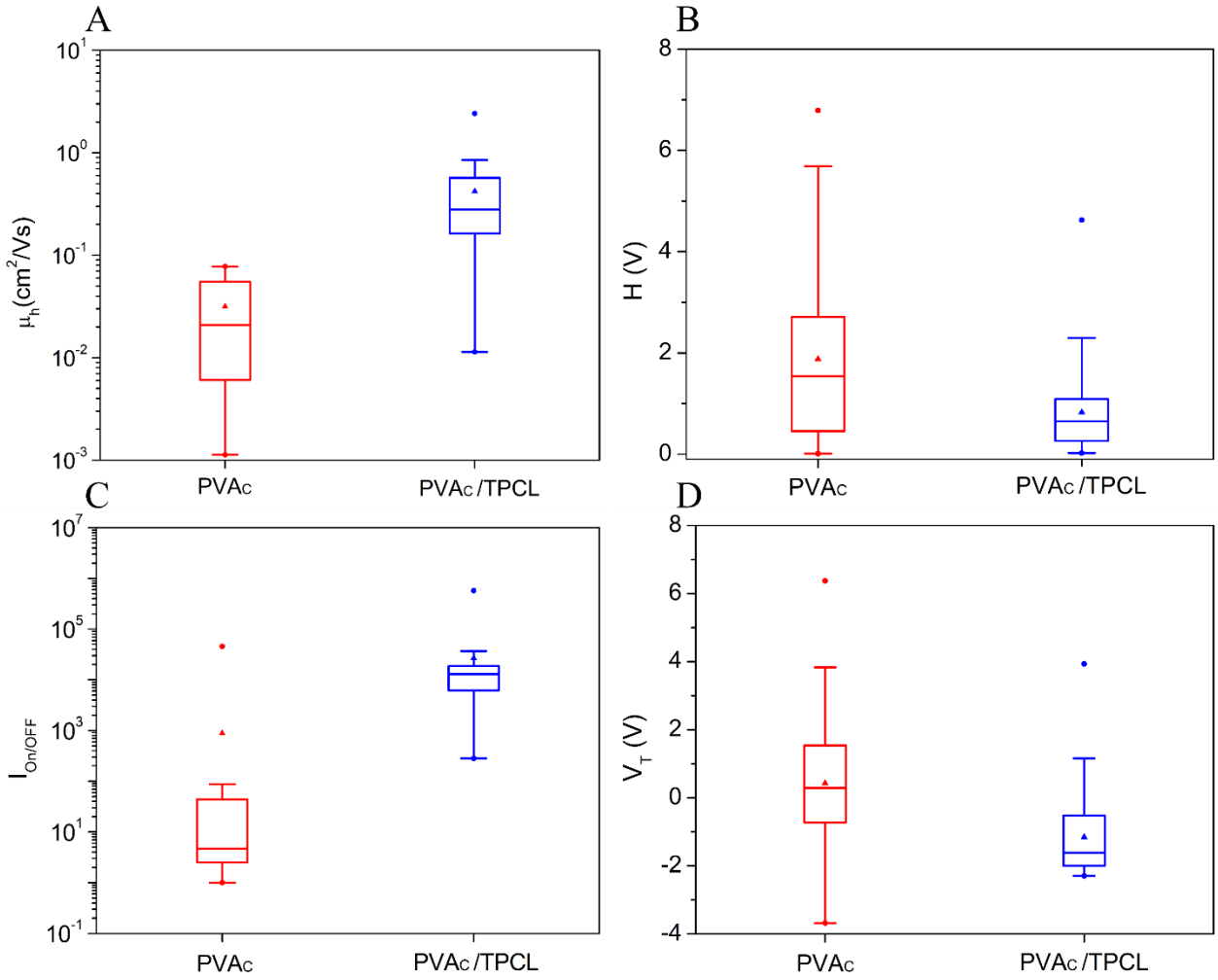

Figure 3.6. Box plots of the μ_h, V_T, $I_{on/off}$ and H for all fabricated PVAc and PVAc/TPCL OTFTs. The rectangle represents the interquartile range, the "T" lines represent the 95th and 5th percentile, and the circles represent the minimum and maximum values, while the horizontal line and triangle within the box represents the median and mean, respectively.

The PVA$_C$/TPCL OTFTs also had dramatically reduced H, with less variation between devices (**Figure 3.6B**). The reduction in hysteresis is most likely due to the TPCL layer preventing the hydroxyl groups from interacting with the semiconductor at the semiconductor/dielectric interface and trapping charges.[9,13,16] The TPCL layer also reduces the quantity of moisture absorbed by the PVA$_C$ film in the ambient environment. Both these factors help reduce the hysteresis and device to device variance. A significant improvement in the average $I_{on/off}$ ratio for PVA$_C$/TPCL (10^4) compared with PVA$_C$ (10^2) was also observed. These findings are in agreement with literature, where the use of a low-k dielectric material between

PVA and the semiconductor reduces leakage currents and improves device performance.[8,32] The improved insulating properties of the TPCL layer also reduces the off-state current of the fabricated OTFTs, resulting in reduced power consumption in the off state. A minor shift in the average V_T was observed for OTFTs prepared with the bilayer dielectric compared to neat PVA_C (-1.15 V and 0.42 V respectively), indicating V_T was still dominated by the high-*k* PVA. Similarly, negative shifts in threshold voltage have been reported in literature for PVA/PMMA bilayer devices.[21] Importantly, the incorporation of the TPCL layer above PVA_C also resulted in improved reproducibility, as indicated by the lower variance in data values that were measured for all OTFT parameters shown in **Figure 3.6**. Further, the TPCL film leads to a decrease in the surface roughness at the OSC/dielectric interface. For the samples fabricated with a 2mg/ml TPCL solution the RMS surface roughness decreased to 2.50 nm from 3.12 nm for neat PVA_C (**Figure 3.3**). A lower surface roughness is beneficial as increases in surface roughness have been shown to decrease the performance of sc-SWCNTs.[57] Our novel bilayer architecture enables the use of the high-*k* PVA_C layer for low voltage operation, while the TPCL layer improves the semiconductor/dielectric interface, stabilizing the devices and enhancing the performance of the fabricated OTFTs.

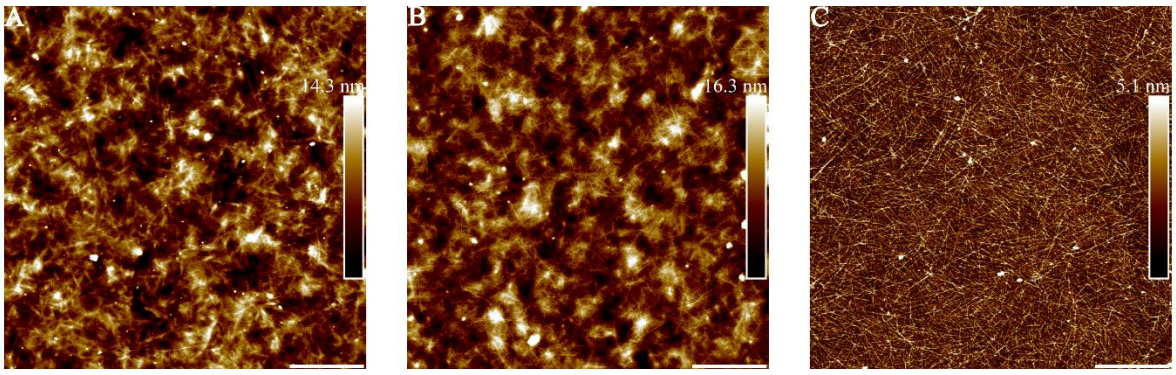

Figure 3.7. AFM height profiles demonstrating sc-SWCNTs network density on (A) PVAC, (B) PVAC/TPCL and (C) SiO2 dielectrics. The white scale bar in the lower right corner represents 1 µm.

3.4 Conclusion

PVA_C is an inexpensive, accessible synthetic polymer blend that is a very promising green polymer dielectric candidate material. However, it has yet to see widespread adoption due to devices suffering from large hysteresis, leakage currents, and moisture sensitivity. We have shown here that the facile addition of a thermally crosslinked TPCL layer on top of PVA_C enables the fabrication of a novel, orthogonally processable, and environmentally friendly bilayer dielectric. Previously, PCL has seen limited incorporation into dielectric applications due to its poor thermal stability. TGA experiments demonstrated that incorporation of a thermally cross-linkable toluene diisocyanate unit dramatically improves the thermal stability of PCL, while simultaneously forming a stable, thin hydrophobic barrier above PVA_C. This novel PVA_C/TPCL bilayer dielectric showed a significant reduction in moisture sensitivity while maintaining most of the favorable dielectric properties of the high-*k* PVA_C. OTFTs fabricated with PVA_C/TPCL demonstrated improved μ_h, increased $I_{on/off}$, reduced H, and lower device to device variance when compared with OTFTs fabricated using a monolayer PVA_C dielectric. Furthermore, the PVA_C/TPCL bilayer dielectric facilitates the operation of sc-SWCNT OTFT devices at voltages 6 times lower when compared to a traditional SiO_2 dielectric. These factors make the PVA_C/TPCL bilayer dielectric a viable option as an inexpensive, green, low operating voltage dielectric for disposable electronic applications such as smart packaging.

3.5 Experimental

PCL, M_w = 80,000 Da, PCL diol (M_w = 2,000 Da), PVA, M_w = 31,000 – 50,000 Da; 98-99% hydrolyzed and tolylene-2,4-diisocyanate (95%) were purchased from Sigma-Aldrich. 2 wt % aqueous dispersion of CNCs was donated by FP Innovations. Gold (Au, 99.99%) and chromium-coated tungsten rods (Cr) were purchased from Angstrom Engineering. Pre-diced (1 in^2) glass substrates were purchased from University Wafers, and 15 x 20 mm^2 quartz coated glass substrates were purchased from Ossila Limited. Chloroform, dichloromethane, and petroleum ether were obtained from Fischer, with all other solvents and reagents purchased from Caledon Chemicals. TPCL structure and purity was analyzed using an Agilent Technologies Cary 630 FT-IR spectrometer and a Bruker 400 MHz NMR spectrometer.

3.5.1 TPCL synthesis

The synthesis of difunctionalized diisocyanate polycaprolactone was conducted as described by Prisco et al.[30] Polycaprolactone diol (PCL, 0.98 g, 0.5 mmol) was dissolved in chloroform (10 mL) and placed under nitrogen atmosphere. Tolylene-2,4-diisocyanate (0.97 g, 5.6 mmol), dissolved in chloroform (3 mL), was added to the PCL solution. The reaction mixture was refluxed at 65 °C for 5 hours. The chloroform was evaporated under reduced pressure, and the obtained viscous oil was washed three times with petroleum ether. The product was dissolved in dichloromethane (2 mL) and precipitated in petroleum ether (50 mL). The precipitation was repeated twice. The product (0.9 g) was obtained as a viscous oil, which was dried *in vacuo*. ^{1}H-NMR (400 MHz. $CDCl_3$): 1.30, 1.39, and 1.64 ($-CH_2-$); 2.27 ($-CH_3$); 2.31 ($-CH_2-$); 3.88 and 4.06 ($-CH_2-O-$); 6.56, 6.77, and 7.08 (C-H, arom) ppm. FT-IR: 1220 (C-N), 1553 (N-H), 1724 (C=O), and 2270 (N=C=O) cm^{-1}.

3.5.2 Preparation of dielectric and semiconductor materials

PVA_C dispersions were prepared in ambient conditions following previously reported procedures[14], with a final concentration of 80 mg/ml PVA and 0.75 wt % CNCs. Briefly, 320 mg of PVA was dissolved in 2400 µL of distilled water at 90 ºC and filtered using a 0.45 µm filter, after which 1650 µL of a 2 wt % dispersion of CNCs in water was added. TPCL solutions in anhydrous toluene were prepared at concentrations of 10, 4 and 2 mg/ml in a nitrogen-filled glovebox. PCL 80K MW was dissolved at 35 mg/ml. PCL was weighed under ambient environment and dissolved in toluene.

Ultrapure semiconducting-enriched dispersions of sc-SWNTs were prepared with a PCF polymer) in toluene following a previously reported procedure.[34] The synthesis of PCF (M_n = 65 kDa, $Đ$ = 2.7) has previously been reported[34], with dispersions prepared using plasma grown SWCNTs (Batch: RNB781-120, diameter: 0.9 – 1.5 nm) purchased from Raymor NanoIntegris. The PCF-SWCNT dispersion was not filtered to remove excess polymer prior to fabricating OTFT devices,[35] with concentration of sc-SWCNTs adjusted so that the peak at 937 nm had an absorbance value of 2.0 a.u (**Figure 3.10,** in the supporting information).

3.5.3 Thin film fabrication and characterization

A Laurell WS-650-23 spin coater was used to deposit the PVA_C and PCL films. A specialty coating systems G3P-8 spin coater was used to deposit the TPCL films. PVA_C,

PVA_C/TPCL, and PVA_C/PCL films were deposited on 1 in^2 glass substrates. The substrates were cleaned in a bath sonicator for 5 minutes using detergent, distilled water, acetone, and methanol, sequentially. The PVA_C films were deposited by spin coating (200 µL) at 3000 rpm for 90 s under ambient conditions, then annealed under vacuum at 150 ºC for 1h to remove excess moisture. PCL layers were deposited (200 µL) at 2000 rpm for 90 s under ambient conditions. TPCL layers were deposited (200 µL) at 2000 rpm for 60 s in an inert environment, then annealed for 15 minutes at 200 ºC under vacuum to thermally crosslink the TPCL to the PVA_C film.

Water contact angle measurements were acquired using a VSA Optima goniometer with a 1 µL drop size. The measurements were repeated after rinsing the films with toluene for 10 seconds and drying the films with nitrogen. AFM was used to determine the surface roughness of the films at various concentrations and determine the network density of single-walled carbon nanotubes on the fabricated OTFTs.

TGA measurements were performed on PVA_C and PVA_C/TPCL using a Mettler Toledo TGA/DSCA 3+. An alumina sample holder was used to heat the sample at a rate of 10 °C/min. Heat and hold measurements were also performed heating at 10 °C /min and holding the temperature at 200 ºC for 260 min.

A Laxco LMC4MT7 microscope was used to image the PVA_C, PCL and PVA_C /TPCL films with a 10x optical zoom.

3.5.4 Device fabrication and characterization

MIM capacitors were fabricated on cleaned 1 in^2 glass substrates. The bottom electrodes, 5 nm of Cr (0.5 Å/s) followed by 50 nm of Au (1 Å/s), were deposited through a shadow mask using PVD. The PVA_C and PVA_C/TPCL dispersions were spun onto the patterned substrate using the conditions described in the previous section. Next, the top electrode (50 nm Au, 1 Å/s) was deposited onto the polymer films using PVD and a shadow mask. This yielded 10 individual MIM capacitors with areas ranging from 0.35 – 2.88 mm^2. The MIM capacitors were characterized through electrochemical impedance spectroscopy using a Methrom PGSTAT204 using an AC amplitude of 10 mV, between the frequencies of 10^{-2} - 10^5 Hz and under ambient

conditions. Film thicknesses were measured through profilometry using a Bruker Dektak XT profilometer.

BGTC OTFTs were fabricated on 15 mm x 20 mm quartz coated glass substrates. The substrates were cleaned through sequential sonication in detergent, distilled water, acetone, and methanol, then dried and the gate electrode (5 nm Cr and 50 nm Au, same deposition rates as stated above) were deposited through a shadow mask using PVD. Polymer dielectric films were spun onto the surface using the same procedure described in the fabrication of the MIM capacitors. The PCF-SWCNT dispersion was sonicated for 10 min prior to drop casting 0.5 μL of the dispersion onto the polymer dielectric in the regions where the transistor channels would be located using a custom 3D printed holder. The entire chip was rinsed with 1 mL of toluene at a 45° angle to rinse off unbound polymer, dried with nitrogen, and a second 0.5 μL drop of PCF-SWCNT was deposited in the same locations. The entire chip was rinsed with 2 mL of toluene in 1 mL increments (at a 45° angle), drying with nitrogen after each rinse, and then annealed in air at 200 ºC for 1h.[35] Source-drain electrodes (50 nm of Au) were deposited using a shadow mask to yield 20 BGTC OTFTs per chip (L = 30 μm, W = 1000 μm). Control devices were also prepared on Si wafers (15 mm x 20 mm) with 210 nm thermal SiO_2 layer. The Si/SiO_2 chips were cleaned through sequential 5 min bath sonication with detergent, distill water, acetone, and methanol, then plasma treated for 15 min. The chips were rinsed sequentially with water and isopropyl alcohol, dried, and then submerged in a 1 % v/v octyltrichlorosilane solution in toluene and heated to 70 °C overnight. The silane-treated wafers were then rinsed with toluene and dried in a vacuum oven at 70 °C for 1 hr. The PCF-SWCNT semiconducting layer and Au source-drain electrodes were then deposited following the procedures previously discussed.

A Keithley 2614B with custom LabVIEW software was used to characterize the electrical properties of the OTFTs. The OTFTs were characterized using a custom-built probe station (oesProbe A10000- P290) from Element Instrumentation Inc. & Kreus Design Inc. All measurements were performed under ambient conditions, with seven transfer curves (linear regime) collected for each transistor. The I_{SD} was calculated using the following equation:

$$I_{SD} = \frac{W\mu_h C_i}{L}\left((V_{GS} - V_T)V_{SD} - \frac{V_{SD}^2}{2}\right) \qquad Eq\ 3.1$$

where L is the channel length, W is the channel width, μ_h is the hole field-effect mobility, C_i is the dielectric capacitance density, V_T is the threshold voltage, and V_{SD} and V_{GS} are the source-drain and gate-source voltages, respectively. The value of C_i had to be adjusted after electrical characterization of the OTFTs, using profilometry to determine the true thickness of the polymer films. μ_h and V_T were calculated from the following equations:

$$\mu = \frac{L}{WC_iV_{SD}}\frac{dI_{SD}}{dV_{GS}} \qquad Eq\ 3.2$$

$$V_T = V_{GS}(x\text{-}intercept) - \frac{V_{SD}}{2} \qquad Eq\ 3.3$$

while H was the absolute difference between the forward and reverse sweep V_T values. $I_{on/off}$ were calculated using the current at the maximum voltage (V_{GS} = -5 V for polymer dielectrics, -30 V for SiO_2) and the minimum recorded current. At least 20 MIM capacitors and 40 OTFTs were characterized for each condition.

3.6 Acknowledgements

This work was supported by the NSERC Green Electronics Network (GreEN) (grant number: NETGP 508526-17).

3.7 Supporting Information

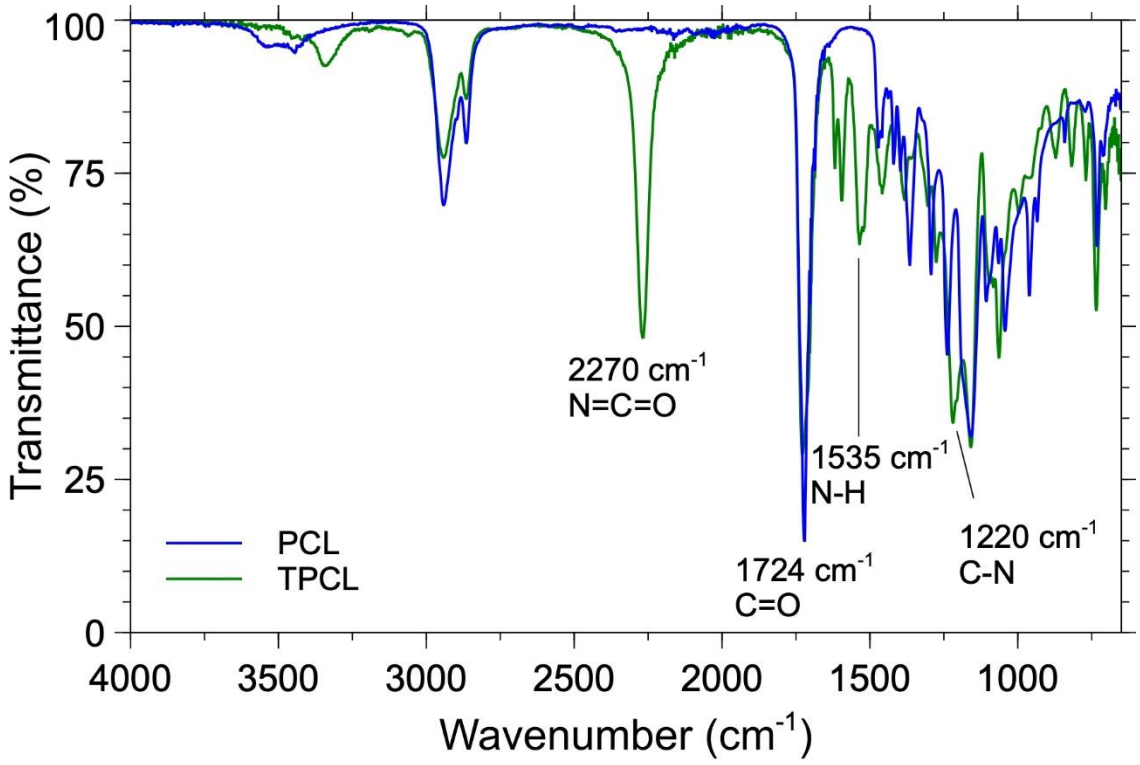

Figure 3.8. FT-IR spectra of polycaprolactone diol (PCL, blue) and tolylene-2,4-diisocyanate difunctionalized polycaprolactone (TPCL, green).

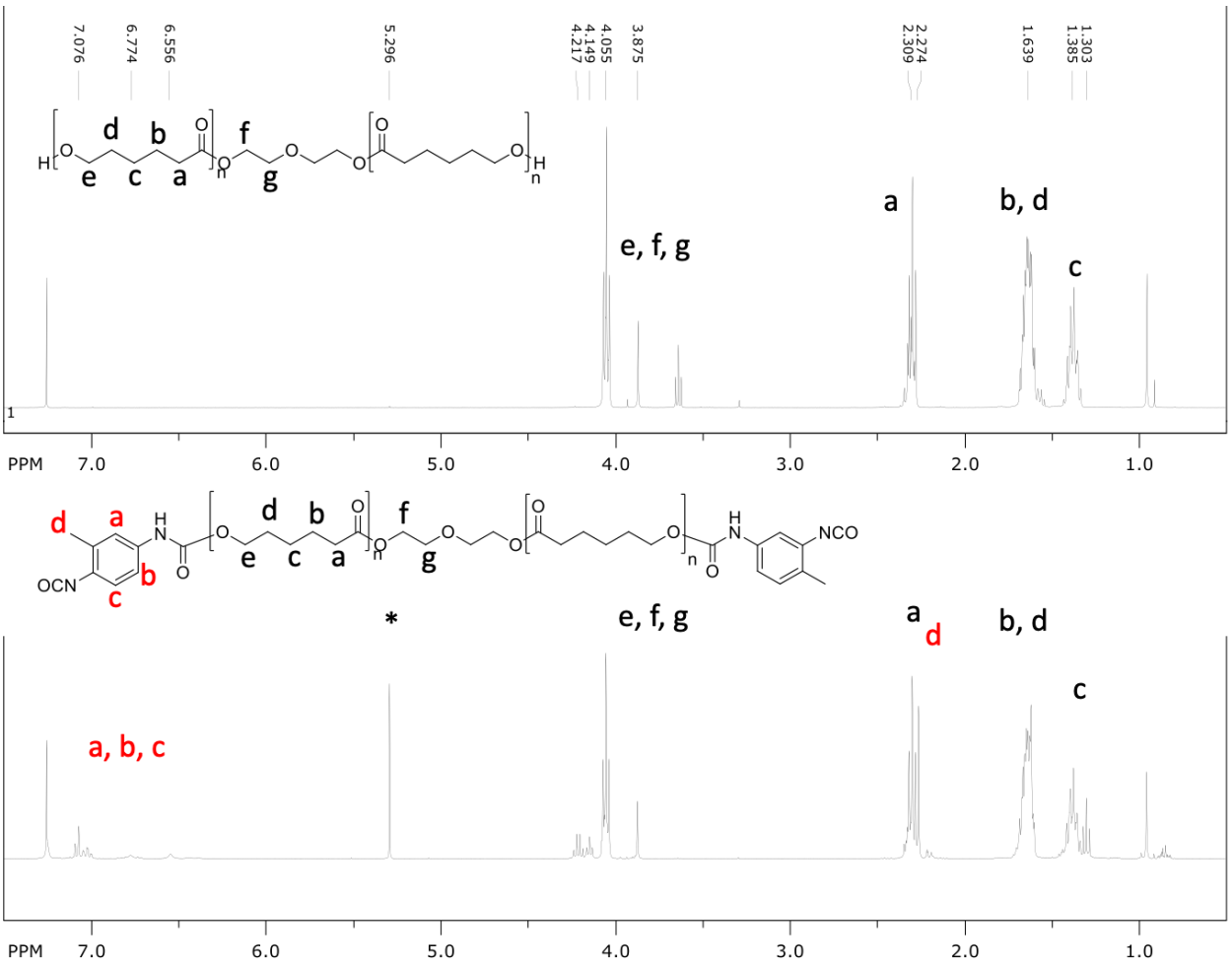

Figure 3.9. 1H-NMR spectra of polycaprolactone diol (PCL, top) and tolylene-2,4-diisocyanate difunctionalized polycaprolactone (TPCL, bottom).

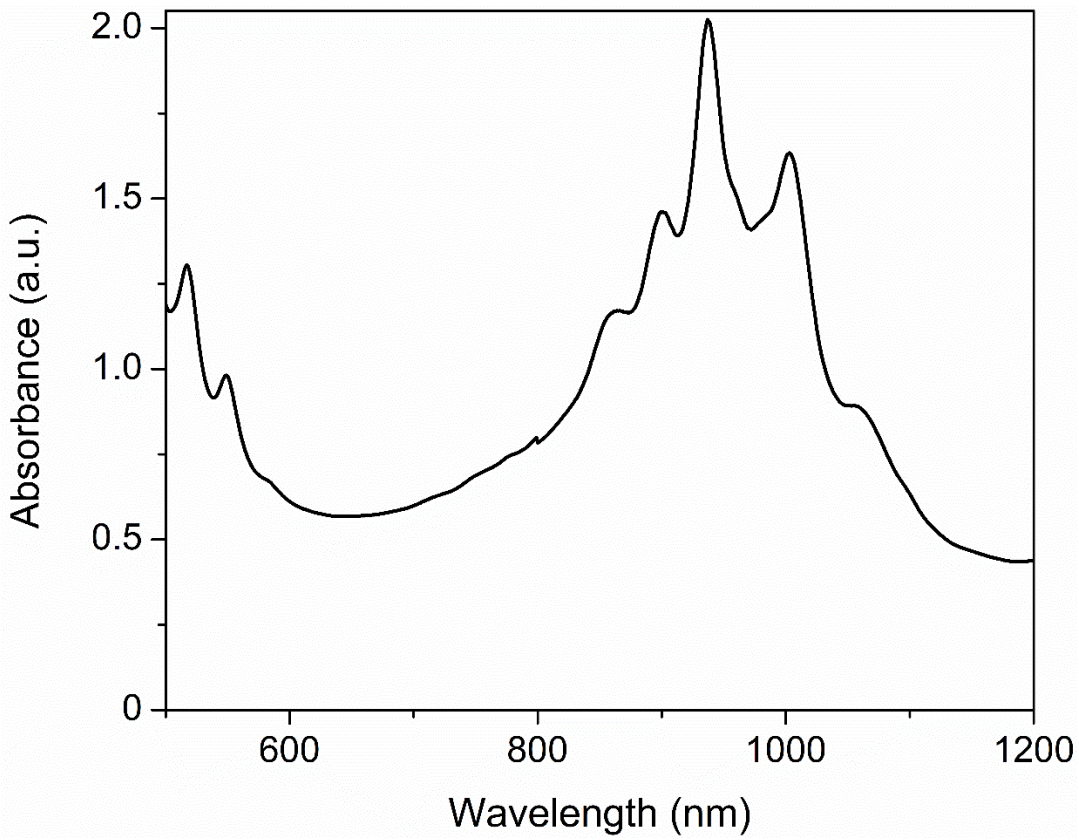

Figure 3.10. UV-Vis absorbance spectrum of S22 peaks for PCF-SWCNT dispersion in toluene (with excess unbound polymer) used to prepare OTFTs.

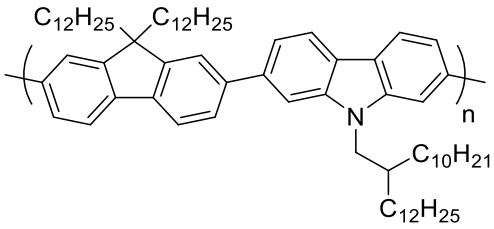

Figure 3.11. Structure of the PCF polymer used to sort the sc-SWCNTs.

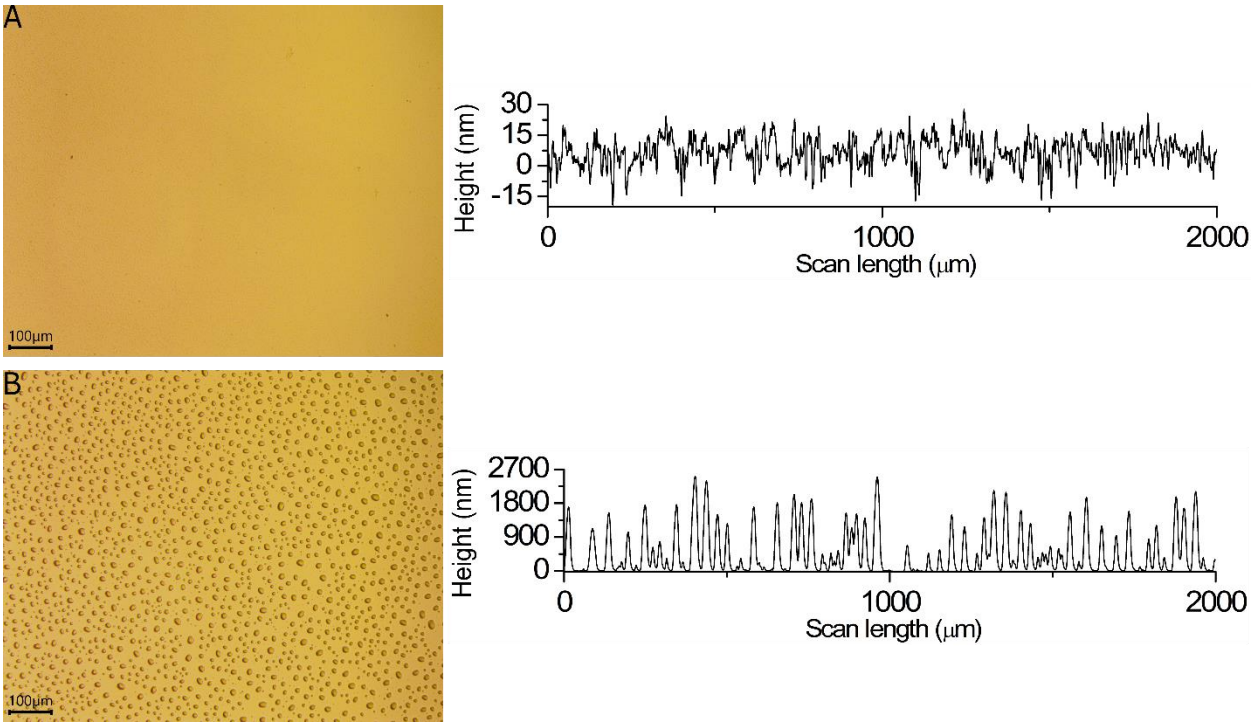

Figure 3.12. Microscope images (10x magnification) of 80 kDa PCL films (no crosslinker) deposited on top of a PVAC film, before (A) and after (B) annealing for 1h at 100 °C, with corresponding film height (as determined from optical profilometry) beside the images.

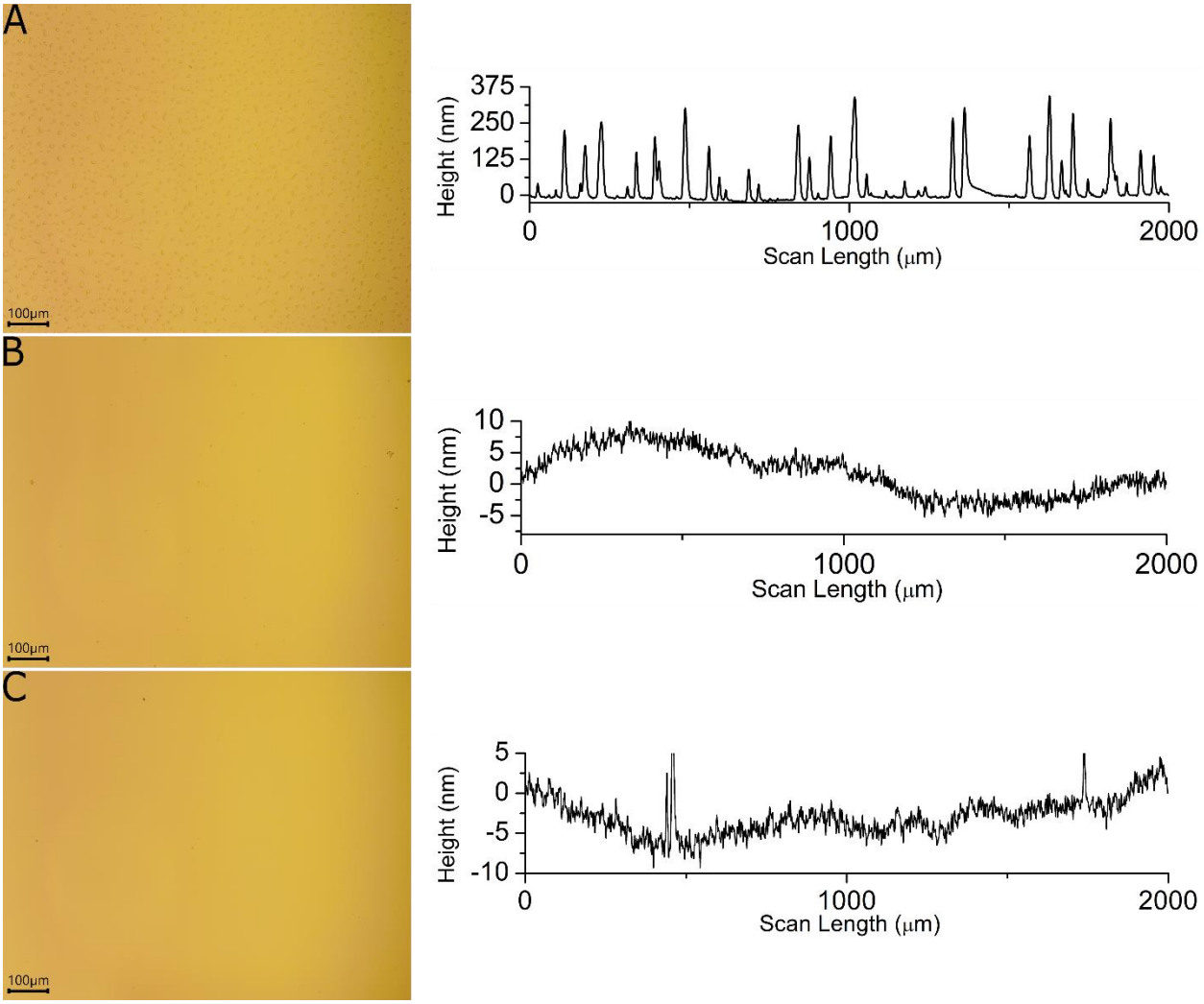

Figure 3.13. 10x microscope images of thermally crosslinked TPCL films spin-cast on top of PVAC at TPCL concentrations of (A) 10mg/ml, (B) 4mg/ml and (C) 2mg/ml. The corresponding film heights (as determined from optical profilometry) are shown beside the images.

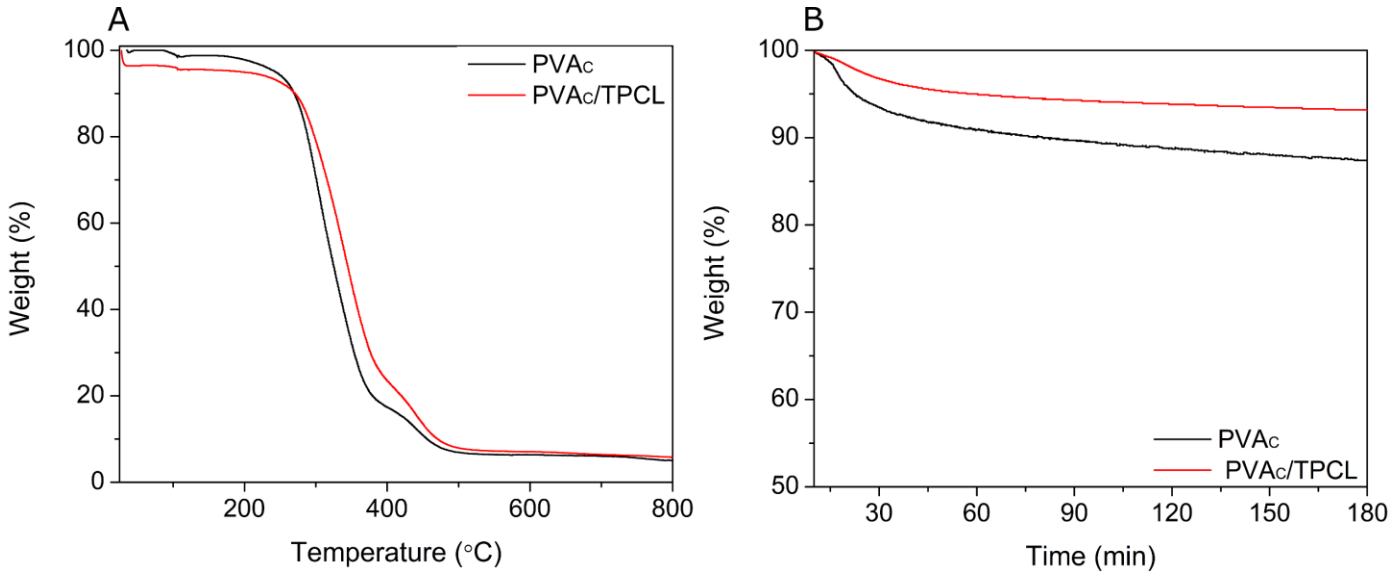

Figure 3.14. TGA measurements of PVAC and PVAC/TPCL for a (A) standard ramp at 10 °C/min in air and (B) heat and hold at 200°C in air for 3 h. The initial small mass loss in (B) for PVAC/TPCL is attributed to removal of moisture from the film.

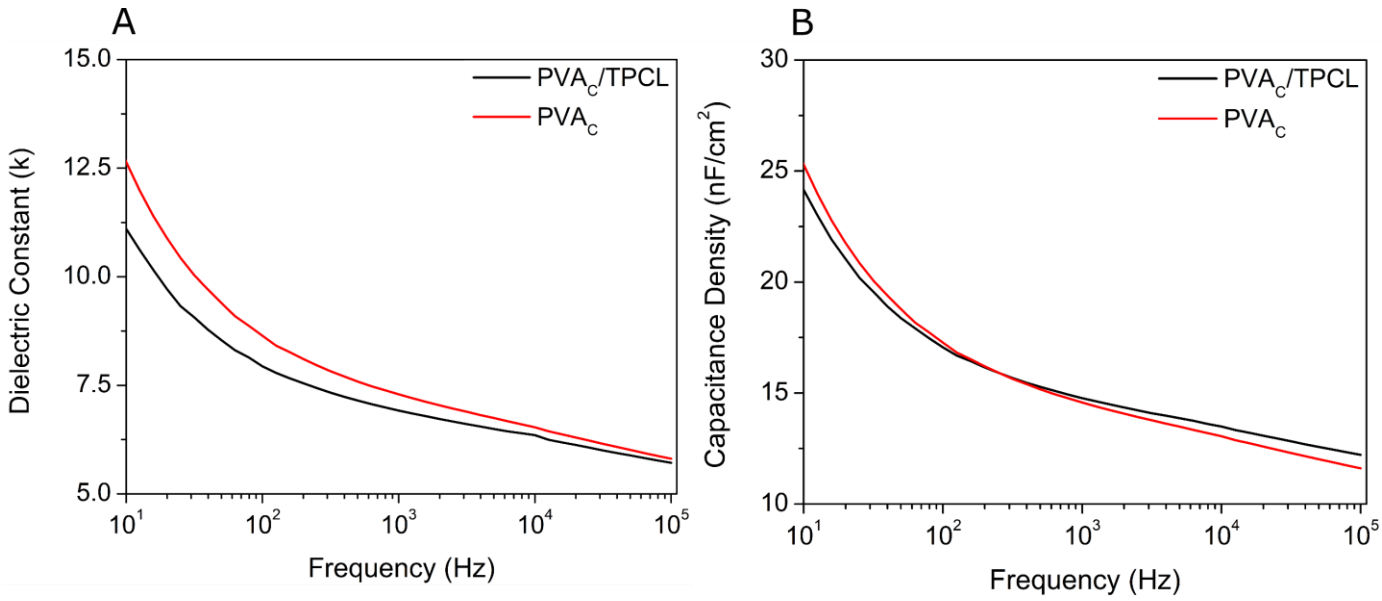

Figure 3.15. (A) Dielectric constant (k) and (B) capacitance density (nF/cm2) of PVAC and PVAC/TPCL2k between 105 and 10 Hz.

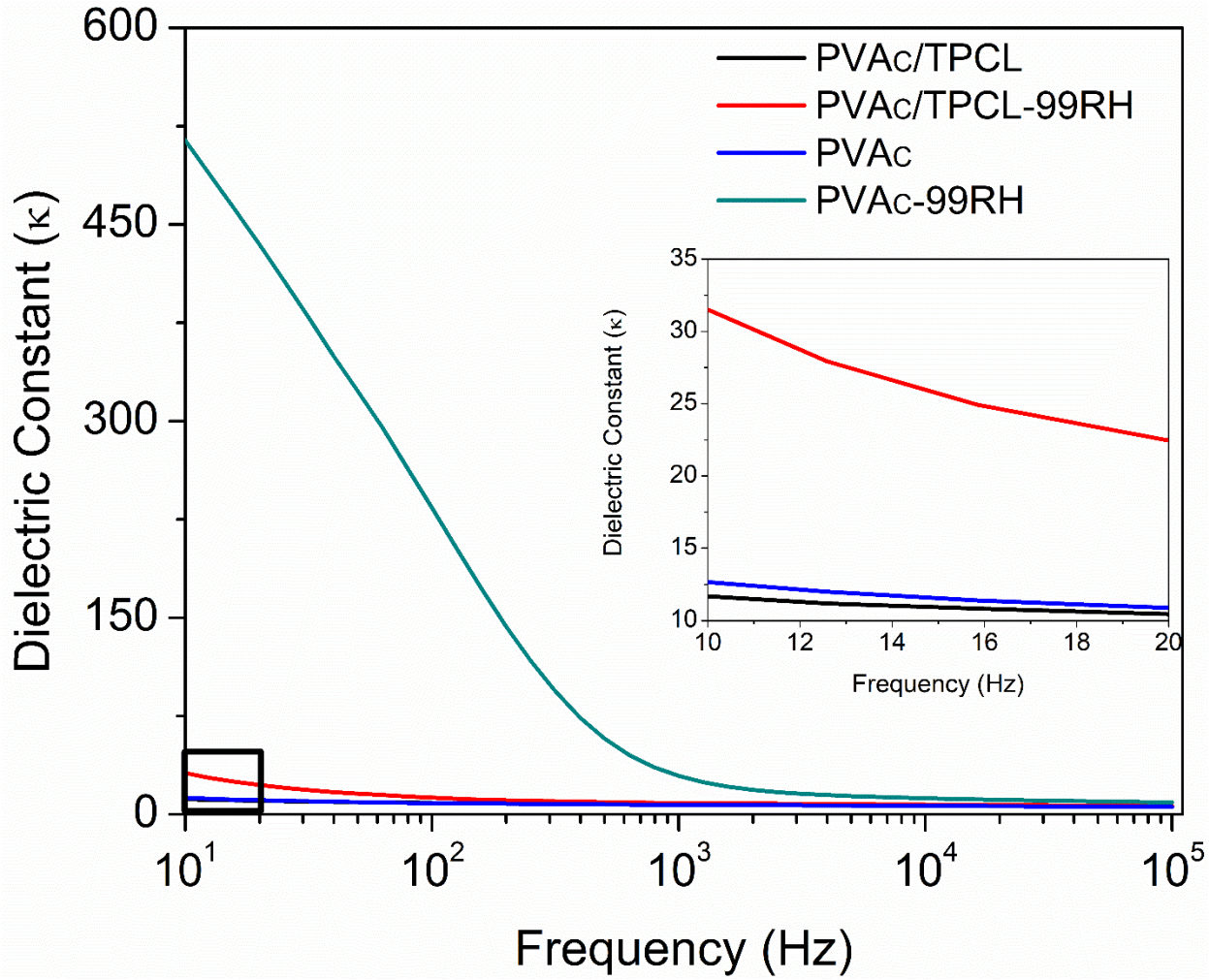

Figure 3.16. Frequency dependant dielectric constant of PVAC and PVAC/TPCL capacitors before and after exposure to 99% relative humidity (RH). The black box indicates the area of the inset graph.

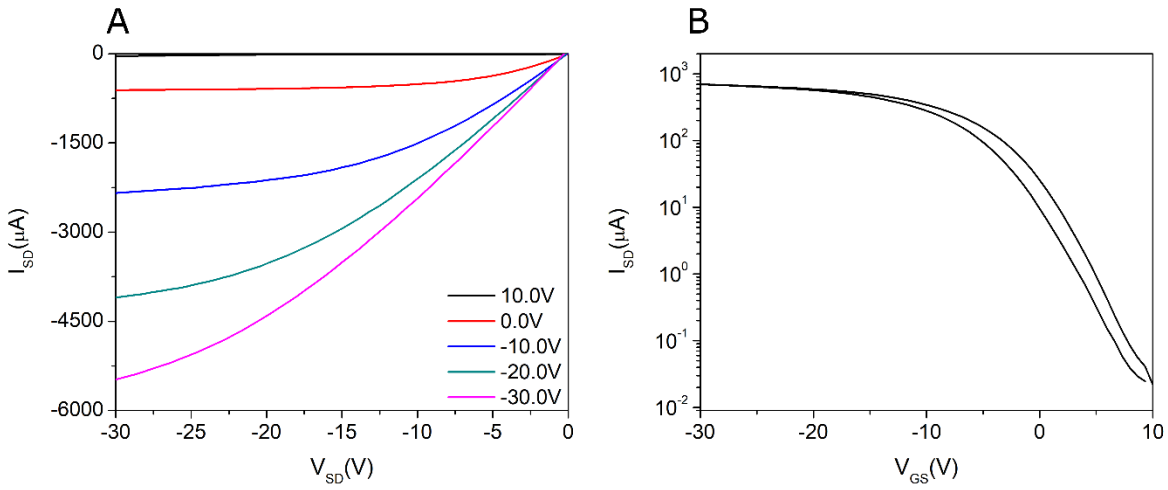

Figure 3.17. Output (A) and transfer (B) curves of sc-SWCNT OTFTs fabricated on a SiO2 dielectric at extended potential range, with VSD = -3 V for the transfer curve measurements.

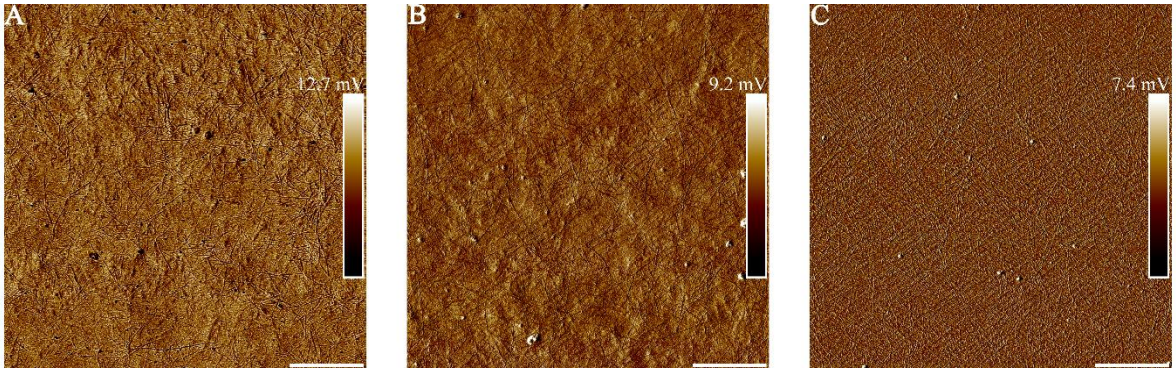

Figure 3.18. AFM inphase profiles demonstrating sc-SWCNTs network density on (A) PVAC, (B) PVAC/TPCL and (C) SiO2 dielectrics. The white scale bar in the lower right corner represents 1 μm.

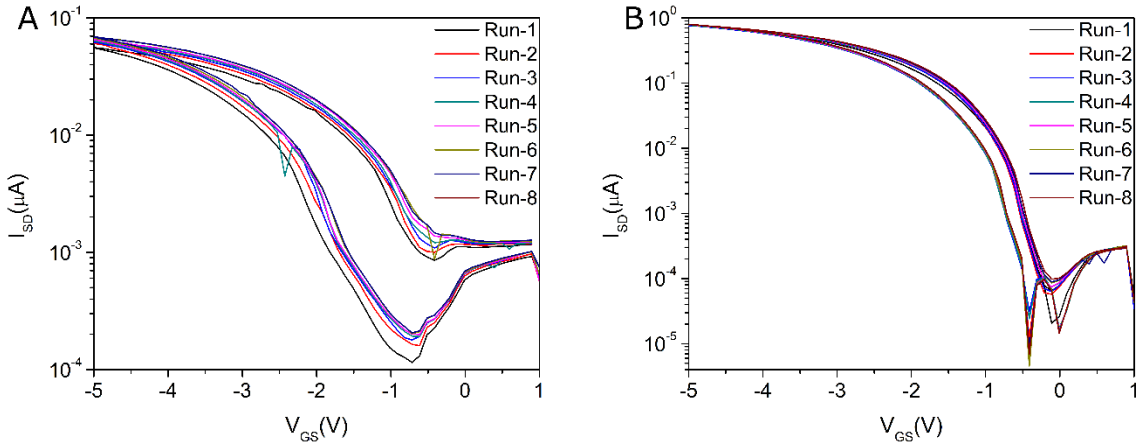

Figure 3.19. Transfer curve measurements of (A) PVAC and (B) PVAC/TPCL. Each device was measured sequentially (8 measurements) with VSD = -0.5 V for the transfer curve measurements.

3.8 References

1. Chen, S., Brahma, S., Mackay, J., Cao, C. & Aliakbarian, B. The role of smart packaging system in food supply chain. *J. Food Sci.* **85**, 517–525 (2020).

2. Schaefer, D. & Cheung, W. M. Smart Packaging: Opportunities and Challenges. *Procedia CIRP* **72**, 1022–1027 (2018).

3. Fattori, M. *et al.* A Fully-Printed Organic Smart Temperature Sensor for Cold Chain Monitoring Applications. *Proc. Cust. Integr. Circuits Conf.* **2020-March**, 3–6 (2020).

4. Comeau, Z. J. *et al.* On-the-Spot Detection and Speciation of Cannabinoids Using Organic Thin-Film Transistors. *ACS Sensors* **4**, 2706–2715 (2019).

5. Street, R. A. *et al.* From printed transistors to printed smart systems. *Proc. IEEE* **103**, 607–618 (2015).

6. Zhang, H. *et al.* Solution-processed organic field-effect transistors with cross-linked poly(4-vinylphenol)/polyvinyl alcohol bilayer dielectrics. *Appl. Surf. Sci.* **478**, 699–707 (2019).

7. Grau, G. & Subramanian, V. Dimensional scaling of high-speed printed organic transistors enabling high-frequency operation. *Flex. Print. Electron.* **5**, 014013 (2020).

8. Li, J. *et al.* Solution-processable organic and hybrid gate dielectrics for printed electronics. *Mater. Sci. Eng. R Reports* **127**, 1–36 (2018).

9. Karri, B. R. T. & Gupta, N. Hybrid bilayer gate dielectric-based organic thin film

transistors. *Bull. Mater. Sci.* **42**, 1–17 (2019).

10. Ortiz, R. P., Facchetti, A. & Marks, T. J. High-k organic, inorganic, and hybrid dielectrics for low-voltage organic field-effect transistors. *Chem. Rev.* **110**, 205–239 (2010).

11. Nketia-Yawson, B. & Noh, Y.-Y. Recent Progress on High-Capacitance Polymer Gate Dielectrics for Flexible Low-Voltage Transistors. *Adv. Funct. Mater.* **28**, 1802201 (2018).

12. Guo, X. *et al.* Current Status and Opportunities of Organic Thin-Film Transistor Technologies. *IEEE Trans. Electron Devices* **64**, 1906–1921 (2017).

13. Jin, S. H. *et al.* Pentacene OTFTS with PVA Gate Insulators on a Flexible Substrate. *J. Korean Phys. Soc.* **44**, 181–184 (2004).

14. Tousignant, M. N. *et al.* Improving Thin-Film Properties of Poly(vinyl alcohol) by the Addition of Low-Weight Percentages of Cellulose Nanocrystals. *Langmuir* **36**, (2020).

15. Wang, W., Ma, D., Pan, S. & Yang, Y. Hysteresis mechanism in low-voltage and high mobility pentacene thin-film transistors with polyvinyl alcohol dielectric. *Appl. Phys. Lett.* **101**, (2012).

16. Tsai, T.-D., Chang, J.-W., Wen, T.-C. & Guo, T.-F. Manipulating the Hysteresis in Poly(vinyl alcohol)-Dielectric Organic Field-Effect Transistors Toward Memory Elements. *Adv. Funct. Mater.* **23**, 4206–4214 (2013).

17. Lee, S. *et al.* Effects of hydroxyl groups in polymeric dielectrics on organic transistor performance. *Appl. Phys. Lett.* **88**, 162109 (2006).

18. Faraji, S., Hashimoto, T., Turner, M. L. & Majewski, L. A. Solution-processed nanocomposite dielectrics for low voltage operated OFETs. *Org. Electron.* **17**, 178–183 (2015).

19. Rullyani, C., Ramesh, M., Sung, C.-F., Lin, H.-C. & Chu, C.-W. Natural polymers for disposable organic thin film transistors. *Org. Electron.* **54**, 154–160 (2018).

20. Park, D. W. *et al.* Low hysteresis pentacene thin-film transistors using SiO 2/cross-linked poly(vinyl alcohol) gate dielectric. *Appl. Phys. Lett.* **89**, (2006).

21. Jin, S. H. *et al.* 34.2: PMMA Buffer-Layer Effects on Electrical Performance of Pentacene OTFTs with a Cross-linked PVA Gate Insulator on a Flexible Substrate. *SID Symp. Dig. Tech. Pap.* **34**, 1088 (2003).

22. Sun, Y. *et al.* Polymer gate dielectrics with self-assembled monolayers for high-mobility organic thin-film transistors based on copper phthalocyanine. *Appl. Phys. A* **95**, 777–780 (2009).

23. Vasimalla, S., Subbarao, N. V. V., Gedda, M., Goswami, D. K. & Iyer, P. K. Effects of Dielectric Material, HMDS Layer, and Channel Length on the Performance of the Perylenediimide-Based Organic Field-Effect Transistors. *ACS Omega* **2**, 2552–2560 (2017).

24. Tan, M. J. *et al.* Biodegradable electronics: cornerstone for sustainable electronics and transient applications. *J. Mater. Chem. C* **4**, 5531–5558 (2016).

25. Liu, K., Tran, H., Feig, V. R. & Bao, Z. Biodegradable and stretchable polymeric materials for transient electronic devices. *MRS Bull.* **45**, 96–102 (2020).

26. Yang, Y., Chen, H. & Li, H. Polymer single crystal dielectrics for organic field-effect transistors. *Polymer (Guildf).* **137**, 255–260 (2018).

27. Kuzma, M., Gerhard, E., Shan, D. & Yang, J. Advances in Bioresorbable Electronics and Uses in Biomedical Sensing. in *Interfacing Bioelectronics and Biomedical Sensing* 29–72 (Springer International Publishing, 2020). doi:10.1007/978-3-030-34467-2_2.

28. Wu, X. *et al.* Thermally Stable, Biocompatible, and Flexible Organic Field-Effect Transistors and Their Application in Temperature Sensing Arrays for Artificial Skin. *Adv. Funct. Mater.* **25**, 2138–2146 (2015).

29. Averous, L., Moro, L., Dole, P. & Fringant, C. Properties of thermoplastic blends: starch–polycaprolactone. *Polymer (Guildf).* **41**, 4157–4167 (2000).

30. De Prisco, N. *et al.* Preparation, physico-chemical characterization, and optical analysis of polyvinyl alcohol-based films suitable for protected cultivation. *J. Appl. Polym. Sci.* **86**, 622–632 (2002).

31. Malinconico, M. *et al.* Blends of polyvinylalcohol and functionalised polycaprolactone. A study on the melt extrusion and post-cure of films suitable for protected cultivation. *J. Mater. Sci.* **37**, 4973–4978 (2002).

32. She, X.-J., Liu, J., Zhang, J.-Y., Gao, X. & Wang, S.-D. Operational stability enhancement of low-voltage organic field-effect transistors based on bilayer polymer dielectrics. *Appl. Phys. Lett.* **103**, 133303 (2013).

33. Subbarao, N. V. V., Mandal, S., Gedda, M., Iyer, P. K. & Goswami, D. K. Effect of temperature on hysteresis of dipolar dielectric layer based organic field-effect transistors: A temperature sensing mechanism. *Sensors Actuators, A Phys.* **269**, 491–499 (2018).

34. Rice, N. A. *et al.* Polycarbazole-Sorted Semiconducting Single-Walled Carbon Nanotubes for Incorporation into Organic Thin Film Transistors. *Adv. Electron. Mater.* **5**, 1–11 (2019).

35. Mirka, B. *et al.* Excess Polymer in Single-Walled Carbon Nanotube Thin-Film Transistors: Its Removal Prior to Fabrication Is Unnecessary. *ACS Nano* **15**, 8252–8266 (2021).

36. Lee, H., You, J., Jin, H. J. & Kwak, H. W. Chemical and physical reinforcement behavior of dialdehyde nanocellulose in PVA composite film: A comparison of nanofiber and nanocrystal. *Carbohydr. Polym.* **232**, 115771 (2020).

37. Li, Y., Chen, S., Wu, M. & Sun, J. Rapid and efficient multiple healing of flexible

conductive films by near-infrared light irradiation. *ACS Appl. Mater. Interfaces* **6**, 16409–16415 (2014).

38. Huang, D. *et al.* Seawater degradable PVA/PCL blends with water-soluble polyvinyl alcohol as degradation accelerator. *Polym. Degrad. Stab.* **163**, 195–205 (2019).

39. Gao, Y. *et al.* Thermally Triggered Mechanically Destructive Electronics Based On Electrospun Poly(ϵ-caprolactone) Nanofibrous Polymer Films. *Sci. Rep.* **7**, 1–8 (2017).

40. Navarro-Baena, I. *et al.* Design of biodegradable blends based on PLA and PCL: From morphological, thermal and mechanical studies to shape memory behavior. *Polym. Degrad. Stab.* **132**, 97–108 (2016).

41. Facchetti, A., Yoon, M. H. & Marks, T. J. Gate Dielectrics for Organic Field-effect Transistors: New Opportunities for Organic Electronics. *Adv. Mater.* **17**, 1705–1725 (2005).

42. Van Etten, E. A. *et al.* Insulating characteristics of polyvinyl alcohol for integrated electronics. *Thin Solid Films* **568**, 111–116 (2014).

43. Hyung, G. W. *et al.* ZnO thin-film transistors with a polymeric gate insulator built on a polyethersulfone substrate. *Solid. State. Electron.* **69**, 27–30 (2012).

44. Egginger, M. *et al.* Mobile ionic impurities in poly (vinyl alcohol) gate dielectric: Possible source of the hysteresis in organic field-effect transistors. *Adv. Mater.* **20**, 1018–1022 (2008).

45. Aguilar, S. M. *et al.* Dielectric Characterization of PCL-Based Thermoplastic Materials for Microwave Diagnostic and Therapeutic Applications. *IEEE Trans. Biomed. Eng.* **59**, 627–633 (2012).

46. Lu, D. *et al.* Humidity dependent permittivity characterization of polyvinyl-alcohol film and its application in relative humidity RF sensor. *Eur. Microw. Week 2014 Connect. Futur. EuMW 2014 - Conf. Proceedings; EuMC 2014 44th Eur. Microw. Conf.* 163–166 (2014) doi:10.1109/EuMC.2014.6986395.

47. Amin, E. M., Karmakar, N. C. & Winther-Jensen, B. Polyvinyl-Alcohol (Pva)-Based RF Humidity Sensor in Microwave Frequency. *Prog. Electromagn. Res. B* **54**, 149–166 (2013).

48. Bergo, P., Moraes, I. C. F. & Sobral, P. J. A. Effects of Different Moisture Contents on Physical Properties of PVA-Gelatin Films. *Food Biophys.* **7**, 354–361 (2012).

49. Nawaz, A. & Hümmelgen, I. A. Poly(vinyl alcohol) gate dielectric in organic field-effect transistors. *J. Mater. Sci. Mater. Electron.* **30**, 5299–5326 (2019).

50. Endres, H. J. & Siebert-Raths, A. *Performance Profile of Biopolymers Compared to Conventional Plastics*. *Polymer Science: A Comprehensive Reference, 10 Volume Set* vol. 10 (Elsevier B.V., 2012).

51. Bettinger, C. J. & Bao, Z. Organic thin-film transistors fabricated on resorbable biomaterial substrates. *Adv. Mater.* **22**, 651–655 (2010).

52. Cao, J. *et al.* Polysiloxane-poly(vinyl alcohol) composite dielectrics for high-efficiency low voltage organic thin film transistors. *J. Mater. Chem. C* **7**, 4879–4886 (2019).

53. Lefebvre, J. *et al.* Hysteresis free carbon nanotube thin film transistors comprising hydrophobic dielectrics. *Appl. Phys. Lett.* **107**, (2015).

54. Lefebvre, J. & Ding, J. Carbon nanotube thin film transistors by droplet electrophoresis. *Mater. Today Commun.* **10**, 72–79 (2017).

55. Lefebvre, J. *et al.* High-Purity Semiconducting Single-Walled Carbon Nanotubes: A Key Enabling Material in Emerging Electronics. *Acc. Chem. Res.* **50**, 2479–2486 (2017).

56. Chung, S., Cho, K. & Lee, T. Recent Progress in Inkjet-Printed Thin-Film Transistors. *Adv. Sci.* **6**, (2019).

57. Li, J., Huang, C.-X. & Zhang, J.-H. Tuning the electrical performance and bias stability of a semiconducting SWCNT thin film transistor with an atomic layer deposited AlZrO x composite. *RSC Adv.* **7**, 52517–52523 (2017).

Chapter 4 : Interfacial Ultraviolet Cross-Linking of Green Bilayer Dielectrics

This chapter was published in the journal "Applied Materials Interfaces": Mathieu N Tousignant, Zheng Sonia Lin, Jaclyn Brusso, Benoît H Lessard. Interfacial Ultraviolet Cross-Linking of Green Bilayer Dielectrics. ACS Appl. Mater. Interfaces 15, 2, 3680–3688 (2023)

Context

This work builds on our previous findings that creating a TPCL/PVAc bilayer dielectric can be used to reduce moisture sensitivity and improve OTFT performance. However, the unprotected diisocyanate end groups of the TPCL make it unstable when left under ambient conditions. If it is not stored in a nitrogen environment or dissolved in anhydrous toluene it will react with moisture in the environment and no longer be able to react with PVAc or dissolve in solution. Another issue is that relying on a thermally activated reaction can limit the types of substrates that can be used when trying to scale this process with flexible and printable substrates. Therefore, we synthesized a benzodioxinone terminated PCL (UV-PCL) that when exposed to UV will undergo a ring opening reaction releasing acetone and exposing an NCO group that can react with the hydroxy groups of PVAc. The goal of this work was to provide a side-by-side comparison of this novel UV crosslinking PCL with the thermally crosslinking PCL. We found that the UV-PCL provided a similar barrier to moisture as that of TPCL and provided similar device performance when used as a bilayer dielectric within OTFTs.

Contribution

Dr. Lin synthesized the UV-PCL and TPCL and performed all the polymer characterization. I prepared all the thin films used within this study. I performed the AFM measurements and cleaned up the raw AFM images. I performed all the contact angle and surface energy measurements for this study. I performed all profilometry measurements and microscope imaging. I interpreted all the thin film characterization data. I fabricated, characterized, and interpreted all the capacitor data and all the organic thin film transistor data. Dr. Lin, Dr. Lessard and Dr. Brusso reviewed the manuscript. I wrote and reviewed the submitted manuscript.

4.1 Abstract

Electronic waste is a growing challenge which needs to be addressed through the integration of high-performance sustainable materials. Green dielectric polymers such as PVA have favourable electrical properties but are challenging to integrate into thin film electronics due to their physical properties. For example, PVA suffers from poor film formation and is hygroscopic. Bilayer dielectrics with interfacial crosslinking can enable the use of high performance PVA with favourable surface chemistry by using a hydrophobic PCL layer. In this study we developed a benzodioxinone terminated PCL layer which can be UV crosslinked to the hydroxy groups of the PVA dielectric. This air-stable UV-crosslinking PCL dielectric was able to effectively crosslink with PVA leading to high performance capacitors and SWCNT OTFTs. This UV crosslinking PCL dielectric led to significant improvements in shelf-life, ease of processing and similar device performance compared to our previously reported thermally crosslinking PCL layer. The UV crosslinking at the interface between these bilayers can allow for integration of high-speed roll-to-roll processing which enables low cost, sustainable, and high-performance electronics.

4.2 Introduction

From reducing the damage associated with E-waste to developing the next generation of wearable and implantable electronics, the need for green and sustainable electronics is becoming essential within society.[1–4] Unfortunately, the library of polymers that are biodegradable, sustainably sourced, have the desired mechanical properties and have the desired electrical properties are limited. These challenges have slowed the integration of green polymer layers into electronics. For example, the choice of the dielectric polymer material is important because it will determine the OTFT performance and the printing process which can be utilized for its manufacturing.[5,6] PS, PVP, PVA and PMMA are some of the most commonly used dielectrics within the field of organic and printed electronics.[3,6,7] However, these dielectrics have their drawbacks. For example, PVP has a low dielectric constant and requires sub 100 nm thin films for low voltage operation making it challenging to print.[5] PVA suffers from sensitivity to moisture which reduces the reliability and stability of the fabricated devices.[8,9] For printed electronic applications it is also favourable to process these materials using environmentally friendly solvents such as water and alcohol-based solvents.[10] Finally, the manufacturing of thin film electronics, such as transistors, requires the sequential deposition of different layers using

different (orthogonal) solvents which won't dissolve the previous layer.[11–14] To circumvent the issues of using orthogonal solvents the dielectric materials can be crosslinked, which has the added benefit of increasing the stability of the dielectric layer.[15–18] On the other hand, crosslinking can have a negative impact on the performance of the dielectric. For example, crosslinking PVA will reduce the dielectric constant of PVA by reducing the total amount of hydroxyl groups, which increases the necessary operating voltage and decreases OTFT performance.[15,19]

Recently, our group developed a high-*k*/low-*k* green bilayer dielectric by using a thin layer of PCL as the low-*k* dielectric which was crosslinked at the interface of a high-*k* PVA layer. High-*k*/low-*k* bilayer dielectrics have been found to reduce charge trapping, increase device stability, allow for orthogonal processing, and prevent the hydroxyl groups of PVA from interacting directly with the semiconductor.[7,20,21] The PCL layer also acts as an encapsulant for the PVA layer and creates a less polar environment at the dielectric/semiconductor interface.[22,23] The PCL was functionalized with toluene diisocyanate (TPCL) end groups enabling thermal crosslinking with the hydroxyl groups of PVA at the PVA/TPCL interface.[24] While effective, the unprotected NCO groups of toluene diisocyanate were not ideal due to being extremely reactive leading to a very short shelf life (**Figure 4.1**).[25] Finally, the crosslink between PVA and TPCL is a thermally induced reaction, which is relatively slow and not easily amenable to high throughput roll-to-roll printing processes.

In this study, to overcome the challenge of water sensitivity, stability, and to allow for better control and speed over the processibility of the fabricated devices, we employed a photocrosslinking strategy in which the toluene diisocyanate groups at the two termini of PCL were replaced with benzodioxinones (**Figure 4.1**). Benzodioxinones can be activated by UV-light to react with alcohols and phenols to form salicylate esters.[26] Since this process occurs under neutral conditions and can tolerate a wide range of sterically hindered alcohols, the Yagci group utilized the photochemistry 2,2-biphenyl benzodioxinones and its naphtho-derivative as well as the benzophenone by-product from these reactions to prepare oligoesters and networks of polymers containing hydroxyl groups.[27,28] Here, we have synthesized 2,2-dimethyl benzodioxinone terminated polycaprolactone (UV-PCL), which generated the ketene intermediate to react with hydroxyl groups on PVA upon UV-radiation. Acetone, the by-product

from this reaction, readily evaporated and did not form further crosslinks which could lead to a decrease in the number of available hydroxyl groups within the PVA layer. The use of UV-PCL as an alternative to TPCL allows for similar device performance with increased stability and processability all while still maintaining its encapsulation and moisture resistive properties.

4.3 Discussion

We have shown that the thermal interfacial crosslinking of TPCL (**Figure 4.1**) onto the PVAc dielectric layer leads to improved sc-SWNCTs OTFT performance.[24] This high-*k*/low-*k* bilayer dielectric reduces the moisture sensitivity, charge traps and provides a more hydrophobic interface improving the sc-SWNCT morphology. However, the unreacted TPCL polymer itself is highly reactive and has a short shelf life. The lifetime of the TPCL can be improved from 1-2 days up to 2-3 months by dissolving it in anhydrous toluene and storing it in a nitrogen environment; however, this is still unacceptable for most large-scale commercial applications. Therefore, we synthesized PCL polymers functionalized with benzodioxinone end groups (**Figure 4.1**) which are more stable under ambient conditions and can be activated to react with hydroxy groups through ultraviolet (UV) radiation.

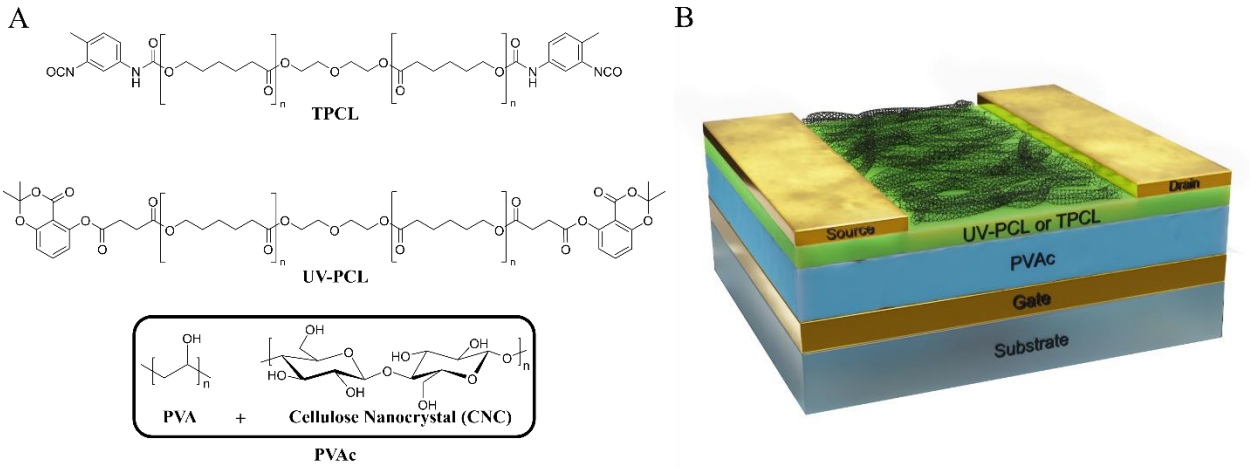

Figure 4.1. A) Chemical structures of the dielectric materials: TPCL or UV-PCL with PVAc; B) Representation of a BGTC bilayer dielectric OTFT.

Upon exposure to UV radiation the benzodioxinone end groups react with the hydroxyl groups of PVAc. This ring-opening process produces acetone and the ketene-containing UV-PCL intermediate, which further reacts with the hydroxyl groups of PVAc to form the photo-crosslinked product (**Figure 4.11A,** in the supporting information). When compared against the

thermal crosslinking reaction of the TPCL, the UV-PCL produces acetone as a by-product during the ketene formation; however, this isn't a large concern. The UV-PCL is only at a concentration of 2 mg/ml and acts as a thin low-*k* layer on top of the PVAc dielectric, making the amount of acetone produced negligeable. As a volatile solvent, acetone does not require a high temperature annealing step to be removed and has limited issues with sustainability.[10] **Figure 4.11B,** in the supporting information, demonstrates the thermal crosslinking reaction of TPCL with the hydroxyl groups of PVAc. The NCO groups in the TPCL are quite reactive and have been found to react with atmospheric moisture quite readily. Further, the characteristics that make substrates flexible and malleable also decrease their melting and glass transition (*Tg*) temperature. The *Tg* for many of the commonly used flexible plastic substrates range from 70 – 155 ºC, this leaves a relatively small window to perform thermal crosslinking reactions without damaging the substrate.[13,36,37] The increased stability and removal of a thermal processing step make the UV-PCL an attractive alternative to TPCL for the mass production of printed and flexible electronics.

Water contact angle measurements were performed to confirm that the UV-PCL had successfully crosslinked with the hydroxyl groups of the PVAc dielectric layer. Three different films were prepared: PVAc, PVAc/TPCL and PVAc/UV-PCL. The TPCL and UV-PCL coated films were thermally and UV crosslinked before contact angle measurements were performed. As demonstrated in **Figure 4.2A**, the contact angle of each film was measured followed by a rinsing step with toluene. The rinsed films were then dried under nitrogen and the contact angle was re-measured. The rinsing and measuring steps were repeated twice. Both TPCL and UV-PCL are soluble and dissolve in toluene before being crosslinked with the hydroxyl groups of PVAc. Because of this if the crosslinking reaction was unsuccessful both the TPCL and UV-PCL would be dissolved by the toluene during the rinsing step and the contact angle would drop to that of the bare PVAc film. The TPCL maintains a contact angle of approximately 62º while the UV-PCL has a contact angle of approximately 67º (**Figure 4.2A**). These values confirm that the films were successfully crosslinked. The crosslinking reaction between PCL and PVA also has the benefit of anchoring the PCL layer in place preventing aggregation.[24] This interfacial crosslinking technique also has the benefit of maintaining a large number of hydroxyl groups in the PVAc bulk while enabling further orthogonal processing, which is a critical requirement for printed electronics.[4,5,11] **Figure 4.2A** also demonstrates that the UV-PCL maintains a higher contact angle when compared against TPCL. This is beneficial in the fabrication of bottom gate

top contact OTFTs with sc-SWNCTs. Sc-SWCNTs are often suspended in toluene when fabricating semiconducting enriched dispersions.[38,39] When fabricating sc-SWCNT OTFTs the substrates are commonly treated with OTS.[38–41] OTS surface treatments increase the water contact angle of the substrates to approximately 100º.[42,43] The higher contact angle decreases the wettability of the toluene drops on the dielectric surface and increases the sc-SWCNT network density. Therefore, the higher water contact angle of the UV-PCL will help increase sc-SWCNT density and improve OTFT performance. The surface energy of OTS treated glass substrates is approximately 24.5 mJ/m^2 and the major component to the total surface energy is the dispersive portion (**Table 4.3,** in the supporting information). This suggests that a greater dispersive component leads to favourable SWCNT deposition. **Figure 4.2B** demonstrates the total surface energy of PVAc, PVAc/TPCL and PVAc/UV-PCL dielectrics. PVAc has the greatest surface energy of 55 mJ/m^2 where almost half of the surface energy is contributed by the polar component at 24 mJ/m^2. TPCL and UV-PCL both have lower surface energies of 51 and 49 mJ/m^2, respectively, where the dispersive component of the surface energy contributes to the majority of the total surface energy. The increase in the dispersive component for TPCL and UV-PCL, relative to PVAc makes them better suited for SWCNT deposition.

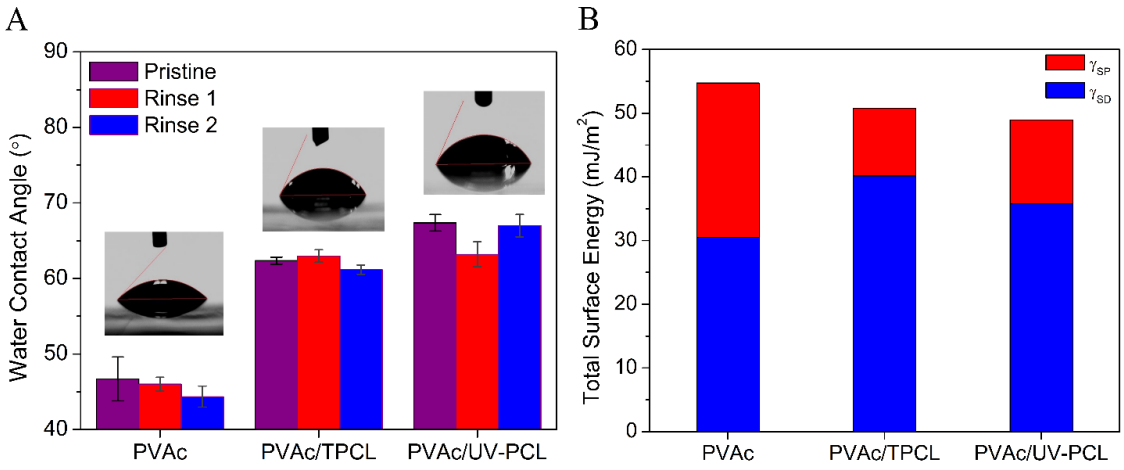

Figure 4.2. A) Water contact angle measurements for neat PVAc, PVAc/TPCL and PVAc/UV-PCL films. The water contact angle was measured for the pristine films, next the films were sequentially rinsed with toluene for 10s and dried using a stream of nitrogen. Contact angle measurements were performed after each rinsing step. B) Total surface energy for neat PVAc, PVAc/TPCL and PVAc/UV-PCL films. The polar component is represented in red (γ_{SP}) and the dispersive component in blue (γ_{SD}).

The impact of the increase in contact angle and changes in surface energy were further analysed using AFM. The AFM images shown in **Figure 4.3** represent characteristic sc-SWCNT network morphologies on top of the TPCL and UV-PCL dielectrics. The sc-SWCNTs network is less dense on the TPCL layer (**Figure 4.3A**) compared to when it is deposited on the UV-PCL layer (**Figure 4.3B**). Li et al. have shown that increasing the network density of SWCNTs is one of the factors that increase OTFT device performance,[44] suggesting a more favourable morphology is obtained when using UV-PCL instead of TPCL or PVA directly. It is interesting to note that the UV-PCL films (**Figure 4.3B and 4.3D**) exhibited pin pricks, or small bubbles in the film formation which we surmise is a result of the acetone formation and escape during UV crosslinking. These small pin pricks in the films lead to a small increase in surface roughness from 2.83 nm to 3.81 nm for the TPCL and UV-PCL, respectively. Regardless, the relatively small amount of acetone formation does not lead to significant film deformation and therefore the resulting OTFTs were still high performing.

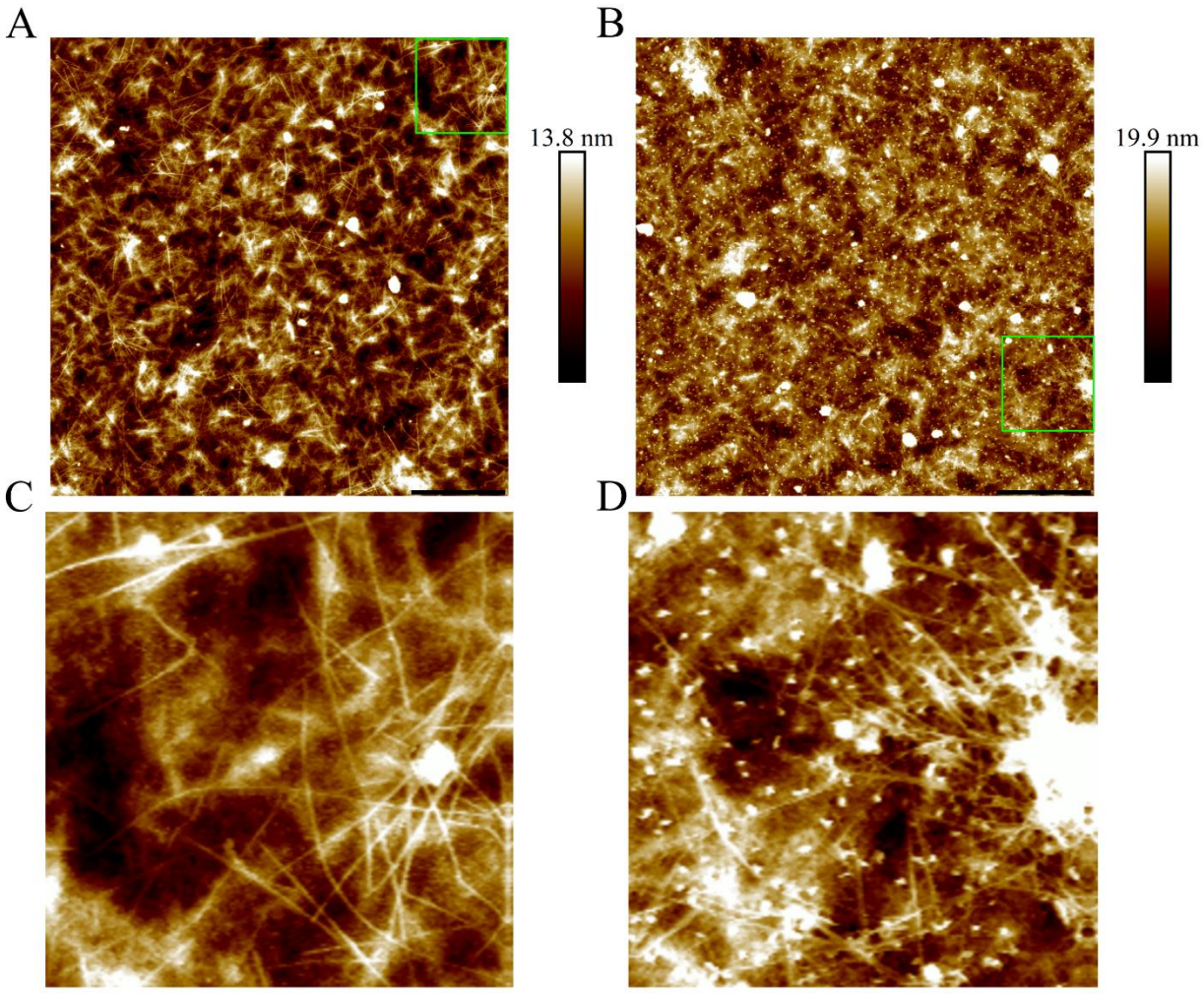

Figure 4.3. Atomic force microscopy images of sc-SWCNTs between the source and drain electrodes of A) TPCL and B) UV-PCL OTFTs. The green boxes represent a 1 µm x 1 µm area that was enlarged for both C) TPCL and D) UV-PCL. The black bar at the bottom right represents1 µm in length.

The TPCL/PVAc and the UV-PCL/PVAc bilayers were integrated into MIM capacitors and the dielectric properties were characterized by impedance spectroscopy. The dielectric constant and capacitance density at 10 Hz (and room temperature) were calculated and displayed in **Table 4.1**. The obtained values for the bilayer dielectrics are within the appropriate range for PVA.[21,45,46] The fabricated capacitors were also characterized after being exposed to 99% RH for 30 minutes. PVA is a hygroscopic polymer dielectric, and its capacitance density increased by up to 50 times at 10 Hz when exposed to moisture, as seen in **Figure 4.4B**. This is caused by the

moisture acting as a plasticizer facilitating the alignment of the hydroxyl groups with the applied electric field and increasing the capacitance of the PVAc layer. These results are also demonstrated within literature for PVA dielectrics when exposed to moisture.[8,16,47,48] The addition of a TPCL layer on top of PVAc provides a barrier to moisture and almost completely eliminated the impact of moisture on the performance of the PVAc dielectric.[24] As demonstrated in **Figure 4.4A**, both the UV-PCL and the TPCL have an almost identical response with only a slight increase in capacitance density after being exposed to 99% RH for 30 minutes. Both the TPCL and the UV-PCL provide a barrier to moisture, preventing it from penetrating into the PVAc films and making the films over 100 times less sensitive to moisture when comparing the capacitance densities at 10 Hz.

Table 4.1. Average dielectric properties of PVAc/TPCL and PVAc/UV-PCL at 10 Hz.

Dielectric Material	Effective Dielectric Constant [κ]	Capacitance Density [nF/cm^2]
PVAc/UV-PCL	14.5 ± 0.7	36.9 ± 2.1
PVAc/TPCL	13.6 ± 1.2	35.6 ± 3.0

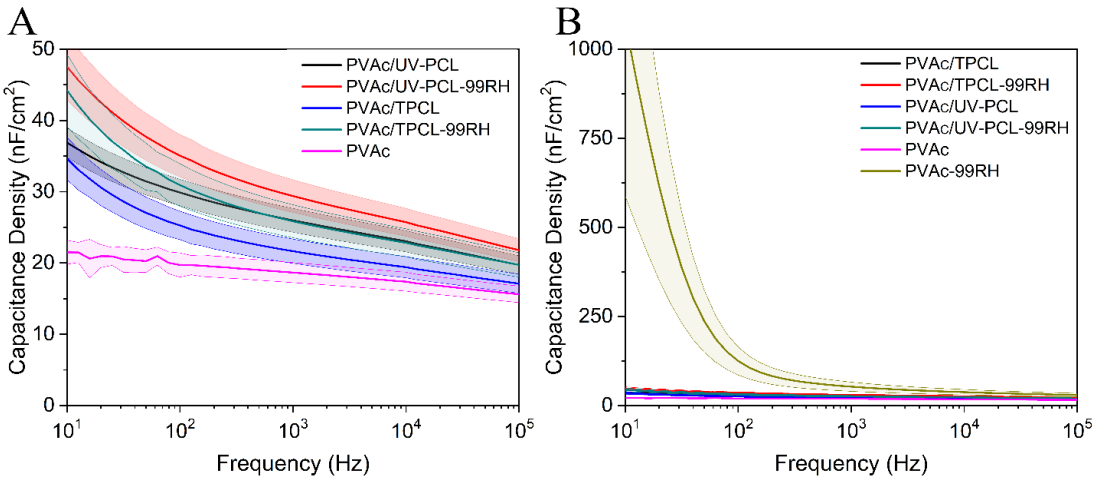

Figure 4.4. Frequency and moisture dependant capacitance density of PVAc, PVAc/TPCL and PVAc/UV-PCL. Capacitance measurements were performed before and after exposing the capacitors to 99% RH for 30 minutes. A) capacitance measurements excluding PVAc-99RH and B) capacitance measurements including PVAc-99RH. The shaded areas represent the standard deviations on the measured capacitance densities.

Sc-SWCNTs thin film transistors were fabricated in a bottom gate top contact architecture using PVAc, PVAc/TPCL and PVAc/UV-PCL as the dielectric layer. Tested under ambient conditions, both output and transfer characteristics for the different dielectrics are shown in **Figure 4.5**. The output characteristics immediately show the benefit of the bilayer dielectric, which increased the current by up to 6 times when compared against PVAc. This is caused by a reduction in the polarity at the dielectric/semiconductor interface reducing the amount of charge trapping and improving device performance.[6,17,20,49] The same trend is mirrored for the transfer curves where PVAc (**Figure 4.5B**) also has a lower current compared to the bilayer device of **Figure 4.5D** and **4.5E**. When comparing the output and transfer curves of TPCL with UV-PCL they both have similar performances. However, the TPCL has slightly higher output currents even though the observed network density in **Figure 4.3** is slightly lower compared to the UV-PCL. The sc-SWCNTs appear to be better aligned tail to tail on the TPCL dielectric **Figure 4.3A** while the SWCNT network for the UV-PCL is less ordered, **Figure 4.3B**. This is further highlighted in **Figure 4.12A** (in the supporting information) where the peak force images bring out the tail-to-tail alignment of the SWCNTs on the TPCL dielectric compared to the randomized denser network for the UV-PCL in **Figure 4.12B** (in the supporting information). For SWCNT performance both these parameters are important for increasing device performance.[41,50] **Table 4.2** also highlights that the use of TPCL and UV-PCL layers when compared to a neat PVAc layer leads to greater μ_h and $I_{on/off}$ which is consistent with the use of high-*k*/low-*k* bilayer dielectrics with SWCNTs.[41,51] TPCL and UV-PCL have average $\mu_{h's}$ of 3.6 and 2.8 cm^2/Vs respectively, while dipolar disorder and charge trapping at the semiconductor/dielectric interface reduces the average μ_h of PVAc to 0.63 cm^2/Vs. Both the TPCL and UV-PCL dielectrics also increase the on-state current as seen in **Figure 4.5** allowing for an order of magnitude increase in $I_{on/off}$ for the fabricated devices. Hysteresis is observed for every transfer curve in **Figure 4.5**. Hysteresis is common among polar dielectrics as well as PVA where the degree of hysteresis can be influenced by moisture, temperature as well as impurities within PVA.[16,21,52,53] Hysteresis is often reduced as PVA absorbs moisture, however TPCL and UV-PCL both provide a strong barrier to moisture, suggesting moisture is not the only cause for device hysteresis.[16,53] Hysteresis is likely due to the polar nature of the hydroxyl groups which can vary the hysteresis as a function of temperature.[21] The hysteresis is related to how easily the polar hydroxyl groups can orient themselves with the applied electric field between the source and the gate electrodes.

When the hydroxyl groups can follow the applied field there is no observed hysteresis.[54,55] Therefore, the effect of polarization on the PVA bilayers hysteresis was characterized by changing the pulse frequency during OTFT operation. Decreasing the pulse frequency enabled polarization effects to complete their cycles prior to subsequent pulses leading to decreases in the observed hysteresis.[55] **Figure 4.13**, in the supporting information demonstrates that by decreasing the pulsing frequency almost all measured hysteresis can be eliminated. These results indicate that UV-PCL is a promising green hydrophobic polymer which can be used to improve PVA based dielectrics in sc-SWCNT OTFTs.

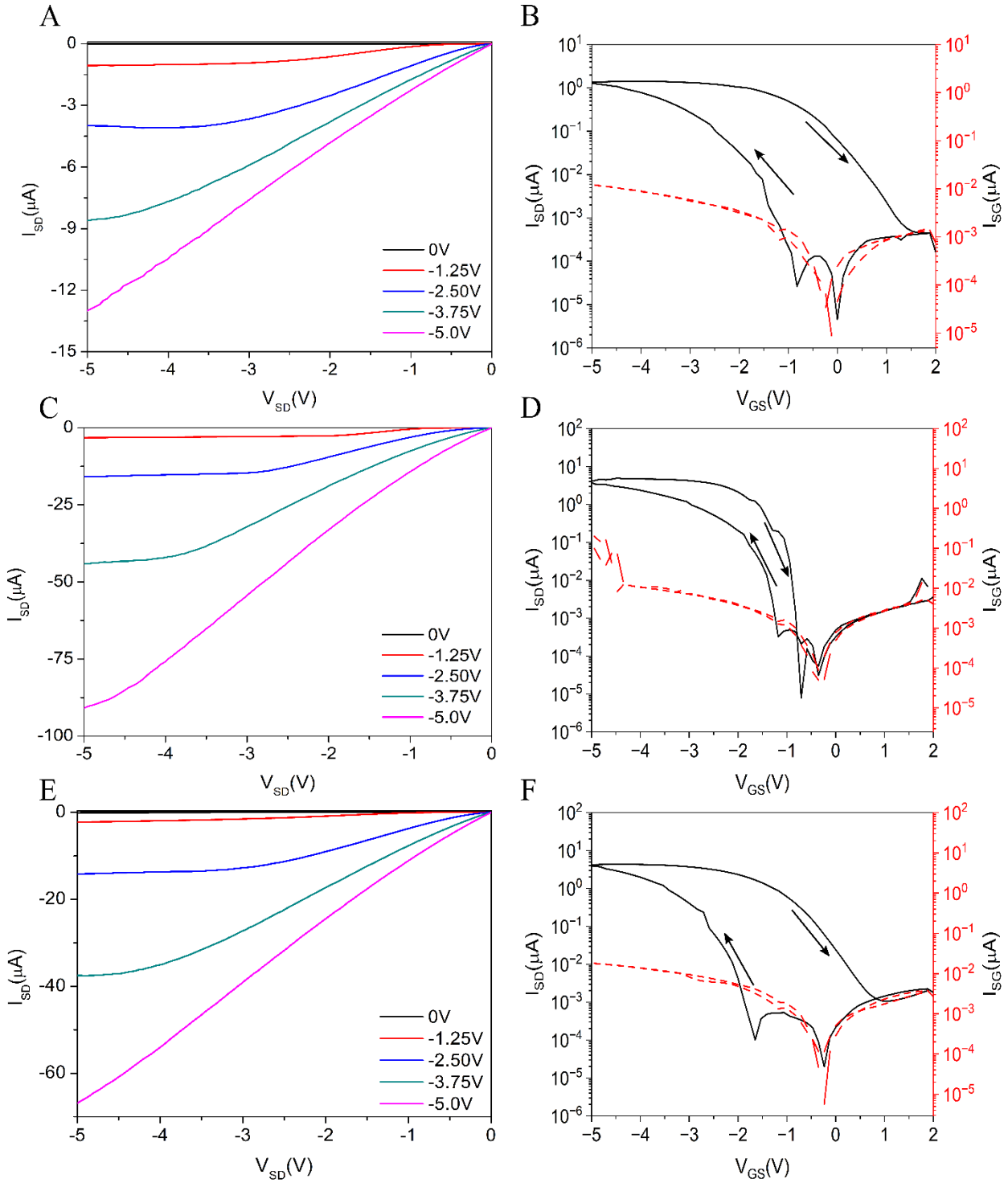

Figure 4.5. Representative output and transfer curves of OTFTs fabricated with sc-SWCNTs using a PVAc (A,B), PVAc/TPCL (C,D) and PVAc/UV-PCL (E,F) dielectric with a 10 Hz pulsing frequency. The transfer curves were measured using a -1 V source-drain bias. The red dotted lines on the transfer curves represent the measured source-gate current (I_{GS}).

Table 4.2. TFT properties for the PVAc, PVAc/TPCL and PVAc-UV-PCL dielectrics at 10 Hz.

Dielectric	Mobility (cm^2/Vs)	$I_{on/off}$	V_T (V)
PVAc	0.63 ± 0.3	10^4	-2.1 ± 0.5
PVAc/TPCL	3.6 ± 2.5	10^5	-1.6 ± 0.4
PVAc/UV-PCL	2.8 ± 1.9	10^5	-2.2 ± 0.4

4.4 Conclusion

We report the synthesis of a novel end-functionalized benzodioxinone PCL dielectric which can be used to photo crosslink PVAc at the PVAc/UV-PCL interface and be incorporated as the dielectric in capacitors and transistors. We demonstrated that this UV crosslinked PCL improves the sc-SWCNT OTFT performance by providing a hydrophobic surface that allows for a higher sc-SWCNT network density. This also highlighted the impact of increasing the dispersive component of the surface energy as well as increasing the water contact angle on OTFT performance. Further, the PVAc/UV-PCL dielectric eliminates charge traps caused by the exposed hydroxy groups of bare PVAc and provides moisture barrier properties. The UV-PCL is also compared to previously published thermally crosslinked PCL (TPCL). UV-PCL provides similar improvements to OTFT performance as TPCL while providing improved shelf life and less stringent storage requirements. The use of UV as the crosslinking activation step is also favourable to a thermal trigger due to the potential for integration into high throughput roll-to-roll manufacturing.

4.5 Experimental

PCL diol (M_w = 2000 Da), toluene-2,4-diisocyante (95%) and PVA M_w = 31 000 – 50 000 Da; 98-99% hydrolyzed were purchased through Sigma-Aldrich. Chromium coated tungsten rods (Cr) and Gold (Au, 99.99%) were purchased through Angstrom Engineering. CNC aqueous dispersion at 2 wt% was donated by FP innovations. 15 X 20 mm^2 quartz coated glass substrates were purchased from Ossila Limited. 1 in^2 pre diced glass substrates were purchased from University Wafers.

Synthetic and characterization methods TPCL

The toluene diisocyanate-terminated polycaprolactone was synthesized following a previously reported procedure.[24] The fabricated TPCL was dissolved in anhydrous toluene at a concentration of 2 mg/ml and stored in a moisture free nitrogen environment.

Synthetic and characterization methods UV-PCL

All reactions were performed under a nitrogen atmosphere unless otherwise indicated. The glassware was flame- or oven-dried. All chemicals were purchased from commercial sources (Aldrich and TCI America) unless otherwise indicated. Column chromatography was performed using silica gel (Silicycle, Siliaflash F60, 40−63 μm, 230−400 mesh). Thin layer chromatography (TLC) was performed using SiliCycle Aluminium Backed Silica gel 200 μm F254 plates. TLC plates were visualized using UV light at a wavelength of 254 nm. NMR experiments were performed on a Bruker Advance II 400 spectrometer (400 MHz for ^{1}H and 100 MHz for ^{13}C). All spectra were recorded at room temperature. For NMR spectra, chemical shifts were measured in parts per million (δ scale). The coupling constants are reported in hertz. Multiplicities are reported as follows: s, singlet; d, doublet; t, triplet; q, quartet; dd, doublet of doublet; dt, doublet of triplet; p, pentet; m, multiplet; br, broad singlet.

5-Hydroxy-2,2-dimethyl-4H-1,3-benzodioxin-4-one (**4**)

A round bottom flask containing a stirred solution of 2,6-dihydroxybenzoic acid (2.00 g, 13.0 mmol), 4-dimethylaminopyridine (4-DMAP) (79 mg, 0.65 mmol), and acetone (1.22 mL, 16.5 mmol) in dimethyl ether (DME) (6.6 mL) was cooled to 0 °C. Acetone (1.22 mL, 16.5 mmol) was added to the stirred solution followed by the dropwise addition of $SOCl_2$ (1.21 mL, 16.7 mmol). After the mixture was stirred for 1 h at 0 °C, it was gradually warmed up to room temperature and stirred overnight. The resulting red solution was neutralized using 6.5 mL of aqueous sodium bicarbonate and extracted using three 8 mL portions of diethyl ether. The combined organic layers were washed with brine, dried over Na_2SO_4, and the solvent of the organic layer was removed under reduced pressure to afford a crude orange yellow solid. Purification using silica gel chromatography with 85: 15 (hexane: ethyl acetate) gave the product as a white solid (1.23g, 49% yield). The ^{1}H NMR spectrum is consistent with the previously reported spectrum.[29] ^{1}H NMR δ 10.3 (1H, s), 7.4 (1H, t, J = 7.4 Hz), 6.6 (1H, dd, J = 8.4, 0.9 Hz), 6.4 (1H, dd, J = 8.3, 0.8 Hz), 1.7 (6H, s).

Carboxyl telechelic PCL (**2**)

Compound **2** was prepared according to literature procedures.[30] 2.0g PCL-diol (Mw = 2000) was dissolved in 25 mL DCM in a round bottom flask equipped with a magnetic stir bar.

To this stirring solution at room temperature, triethylamine (0.28 mL, 2.0 eq.), 4-DMAP (244.4mg, 2.0 eq.) and succinic anhydride (205.2 mg, 2.05 eq.) was added. The reaction was stirred at room temperature for 24 h. The reaction mixture was washed with saturated $NaHCO_3$, aqueous HCl (5% v/v), and brine. The organic layer was dried over Na_2SO_4, filtered and concentrated to give the product as a waxy off white solid (1.8g, 2% yield). ^{1}H NMR δ 4.00-4.07 (m, CH_2CH_2-OC=O, -O-CH_2CH_2-OC=O), 3,84 (s, br, O-CH_2CH_2OC=O), 2.60 (m, O=CCH_2CH_2 COOH, O=CCH_2CH_2COOH), 2.27 (m, O=C-CH_2CH_2-), 1.60 (m, O=$CCH_2CH_2CH_2$- and -$CH_2CH_2CH_2O$), 1.35 (m, -$CH_2CH_2CH_2CH_2$-).[30]

Bisbenzodioxionone-PCL (**5**)

1.06 g of compound **2** (1.0 eq.), 116.1 mg of 4-DMAP (2.0 eq.), 196.0 mg of *N, N′*-Dicyclohexylcarbodiimide (DCC) (2.0 eq.), and 203.6 mg of compound **4** (2.2 eq.) were dissolved in 8 mL of dry DCM in a 50 mL round bottom flask. The reaction was stirred at room temperature for 24 hr. The reaction mixture was filtered, washed with 10% citric acid and brine. The organic layer was concentrated, and the resulting off-white solid was washed three times with EtOH. The precipitate was dried under high vacuum to give the final 538 mg of the final product (isolated yield = 45.7%). ^{1}H NMR δ 7.50 (2H, t, J = 8.5 Hz), 6.84 (2H, d, J = 8.5, 0.9 Hz), 6.79 (2H d, J = 8.1, 0.9 Hz), 4.07 (m, CH_2CH_2-OC=O), 4.03 (m, -O-CH_2CH_2-OC=O), 3.85 (s, br, O-CH_2CH_2OC=O), 2.96 (t, J = 6.9 Hz, O=CCH_2CH_2 COO-), 2.74 (t, J = 6.5 Hz, O=CCH_2CH_2COO-), 2.27 (m, m, O=C-CH_2CH_2-), 1.69 (s, 6H), 1.61 (m, O=$CCH_2CH_2CH_2$- and -$CH_2CH_2CH_2O$), 1.35 (m, -$CH_2CH_2CH_2CH_2$-). ^{13}C NMR δ 173.7, 173.5, 172.5, 172.4, 171.1, 158.4, 157.2, 151.5, 136.4, 117.4, 115.3, 107.7, 106.4, 69.2, 64.8, 64.3, 34.9, 34.3, 29.5, 29.1, 28.5, 25.8, 25.7, 24.8, 22.0.

Preparation of dielectric and SWCNTs

To improve the solution viscosity, 0.75 wt% of CNCs were added to the PVA water solution and is referred to as PVAc.[31] The PVAc and TPCL solutions were prepared following previously reported procedures.[24] UV-PCL was weight out into an opaque vial and dissolved in toluene at a concentration of 2 mg/ml. Next, the UV-PCL was left on a hot plate at 60 ºC for 1 h to fully dissolve. The UV-PCL solution was then filtered into another opaque vial using a 0.45 µm PTFE filter. All these steps were done under ambient conditions. sc-SWCNTs were prepared

following a previously reported procedure using a PCF polymer.[24] The synthesis of the PCF polymer has also been previously reported.[32] Raymore NanoIntegris plasma grown SWCNTs were purchased and used in the fabrication of the ultra pure sc-SWCNTs. The concentration of the sc-SWCNTs suspensions were adjusted so that the 937 nm peak had an absorbance of 2.0 a.u.

Thin film characterization and fabrication

Thin films of PVAc, UV-PCL and TPCL were fabricated using a Laurell WS-650-23 spin coater. These films were deposited on 1 in^2 glass substrates. The substrates were cleaned using a four-step cleaning procedure where the substrates are immersed in detergent, distilled water, acetone and methanol. The substrates were sonicated for 5 minutes at each step. PVAc films were then dynamically spun at 3000 RPM for 90 s under ambient conditions. The PVAc films were then annealed under vacuum at 150 ºC for 1 h, removing any excess moisture in the film. The TPCL layer is then statically dispensed on top of the PVAc layer and spun at 2000 RPM for 90 s. The PVAc/TPCL substrates were then annealed under vacuum at 200 ºC for 15 minutes to crosslink the TPCL with the hydroxyl groups of the PVAc. The UV-PCL films were statically dispensed on top of the PVAc layer and spun at 2000 rpm for 90 s. Next, these films were left under a UV lamp (254 nm, 4 W) for 30 minutes to crosslink the UV-PCL with the hydroxyl groups of the PVAc. These films were then annealed under vacuum at 100 ºC for 30 minutes. All the prepared films had a dielectric thickness between 350 - 400 nm characterized using a Bruker Dektak XT profilometer.

Atomic force microscopy images were taken using a Bruker dimension Icon with scan assists tips using the scan assist mode. The images were flattened and cleaned up using the Bruker Nanoscope analysis software.

A VSA Optima goniometer was used with a 1 µL drop size to measure the distilled water and diidomethane contact angle of the fabricated dielectric films. For the water contact angle, multiple measurements were taken on each film before they were rinsed with toluene for approximately 10 s, dried under nitrogen and the measurements were repeated. A five-point curve fitting was used to measure the contact angle from the images of the drops. Both the dispersive (γ^d) and the polar component (γ^p) of the surface energy were calculated using a system

of two equations, these equations have the same form (eq. 1) and are solved simultaneously with the obtained contact angle values of diidomethane and distilled water.[33]

$$1 + \cos\theta = \frac{2(\gamma_s^d)^{\frac{1}{2}}(\gamma_{lv}^d)^{\frac{1}{2}}}{\gamma_{lv}} + \frac{2(\gamma_s^p)^{\frac{1}{2}}(\gamma_{lv}^p)^{\frac{1}{2}}}{\gamma_{lv}} \qquad Eq\ 4.1$$

For equation 4.1, cosθ is the contact angle for either the distilled water or diidomethane on the polymer coated substrates, γ_{lv}^d and γ_{lv}^p are the liquid dispersive and polar components for the surface energy of the reference liquid with γ_{lv} being the total surface energy of the reference liquid. The surface energy is calculated as the sum of the polar and dispersive components. For diidomethane the following parameters are known: $\gamma_{lv}^d = 49.5\, mJ/m^2$, $\gamma_{lv}^p = 1.3\, mJ/m^2$ and $\gamma_{lv} = 50.8\, mJ/m^2$. For distilled water these are the known parameters: $\gamma_{lv}^d = 21.8\, mJ/m^2$, $\gamma_{lv}^p = 51.0\, mJ/m^2$ and $\gamma_{lv} = 72.8\, mJ/m^2$.[33–35]

Metal-insulator-metal capacitor fabrication, characterization, and moisture study

The dielectric properties of the films were characterized using MIM capacitors. The capacitors were fabricated on cleaned 1 in^2 glass substrates. PVD techniques and a shadow mask were used to deposit the bottom electrodes 5 nm Cr at 0.5 Å s^{-1} and 50 nm of Au at 1 Å s^{-1}. Next the PVAc, PVAc/TPCL and PVAc/UV-PCL films were deposited on top of the bottom electrodes using spin coating techniques as outlined in the thin film fabrication section. PVD was then used to deposit the top electrodes, 50 nm Au at 1 Å s^{-1} through a shadow mask. This allows for the fabrication of 10 individual capacitors per substrate with areas from 0.35-2.88 mm^2.

Impedance measurements were then performed on the MIM capacitors using a Mehtrom PGSTAT204. Potentiostatic measurements were done with an AC amplitude of 10 mV, between 10^{-1} to 10^5 Hz under ambient conditions. Next the MIM capacitors were put into a humidity chamber at 99% relative humidity (RH) and left for 30 minutes before repeating the impedance measurements. Equations 4.2 and 4.3 are used to calculate the κ and c_i of the fabricated MIM capacitors.

$$\kappa = \frac{t}{\omega A \varepsilon_0} \frac{Z''}{Z''^2 + Z'^2} \qquad Eq\ 4.2$$

$$c_i = \frac{\kappa \varepsilon_0}{t} \qquad Eq\ 4.3$$

For these equations t is the thickness of the polymer dielectric layers, ω is the angular frequency (2πf), A is the surface area of the fabricated capacitor, ε_0 is the permittivity of vacuum, Z" is the imaginary portion of the impedance and Z' is the real portion of the impedance.

OTFT fabrication and characterization

Thin film transistors were fabricated in a BGTC architecture on 15 X 20 mm^2 quarts coated glass substrates. The substrates were cleaned following a 4-step cleaning process where the substrates were immersed and sonicated for 5 minutes in detergent, distilled water, acetone and methanol, sequentially. The cleaned substrates were dried under a stream of nitrogen and the gate electrodes (Cr 5nm, Au 50 nm) were then deposited using PVD and a shadow mask. Next, PVAc, PVAc/TPCL and PVAc/UV-PCL films were deposited on top of the gate electrodes using the spin coating techniques outlined in the thin film fabrication section. 0.2 µL of sc-SWCNT solution is then drop casted onto the gate electrode at the location of each transistor using a drop casting machine: Musashi SHOT mini 200Sx, dispenser: Nano Master SMP-III. The entire substrate is then rinsed twice at a 45º angle with 1000 µL of toluene and dried under nitrogen. This process is then repeated for each substrate. The substrates were then annealed in air at 200 ºC for 1 h. The source and drain electrodes were deposited through PVD (Au 50 nm) using a shadow mask. This results in the fabrication of 20 individual transistors per substrate (L = 30 µm, W = 1000 µm).

OTFT measurements were performed using a Keithley 2614B with a custom Labview software. The OTFTs are characterized on a custom-made probe station (oesProbe A10000-P290) from Element Instrumentation inc. and Kreus Design. The OTFT measurements were all performed under ambient conditions and all transfer curve measurements were performed in the linear region. Equations 4.4 to 4.6 were used to calculate the I_{SD} and μ_h.

$$I_{SD} = \frac{W\mu_h C_i}{L}\left((V_{GS} - V_T)V_{SD} - \frac{V_{SD}^2}{2}\right) \qquad Eq\ 4.4$$

$$\mu = \frac{L}{WC_iV_{SD}}\frac{dI_{SD}}{dV_{GS}} \qquad Eq\ 4.5$$

$$V_T = V_{GS}(x\text{-}intercept) - \frac{V_{SD}}{2} \qquad Eq\ 4.6$$

V_T is the threshold voltage, V_{SD} and V_{GS} are the source-drain and the gate source voltages, c_i is the capacitance density (A parallel plate capacitor is used to estimate the capacitance density of the fabricated OTFTs, with the dielectric thickness of 350-400 nm for the fabricated OTFTs, L is the channel Length and W is the channel width. The OTFTs were tested at various pulsing frequencies from 0.1 to 100 Hz.

4.6 Acknowledgement

This work was supported by the NSERC Green Electronics Network (GreEN) (grant number: NETGP 508526-17) and NSERC CGS to M.T. We thank Prof. Alex Adronov (McMaster University) for providing the PCF polymer.

4.7 Supporting Information

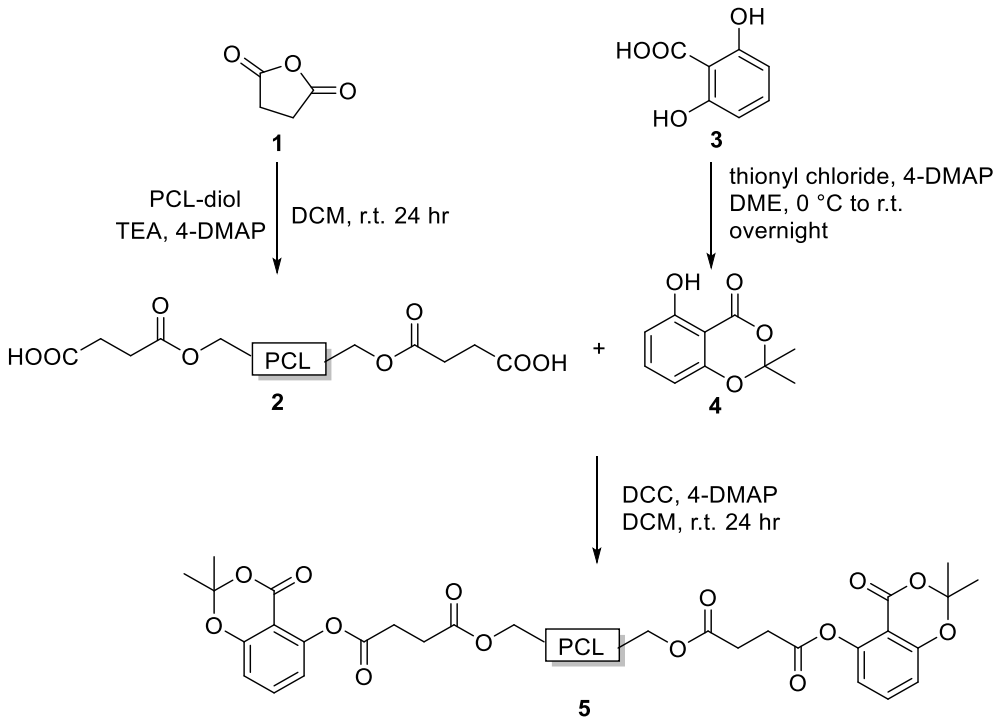

Figure 4.6. Synthesis of benzodioxinone incorporated polycaprolactone.

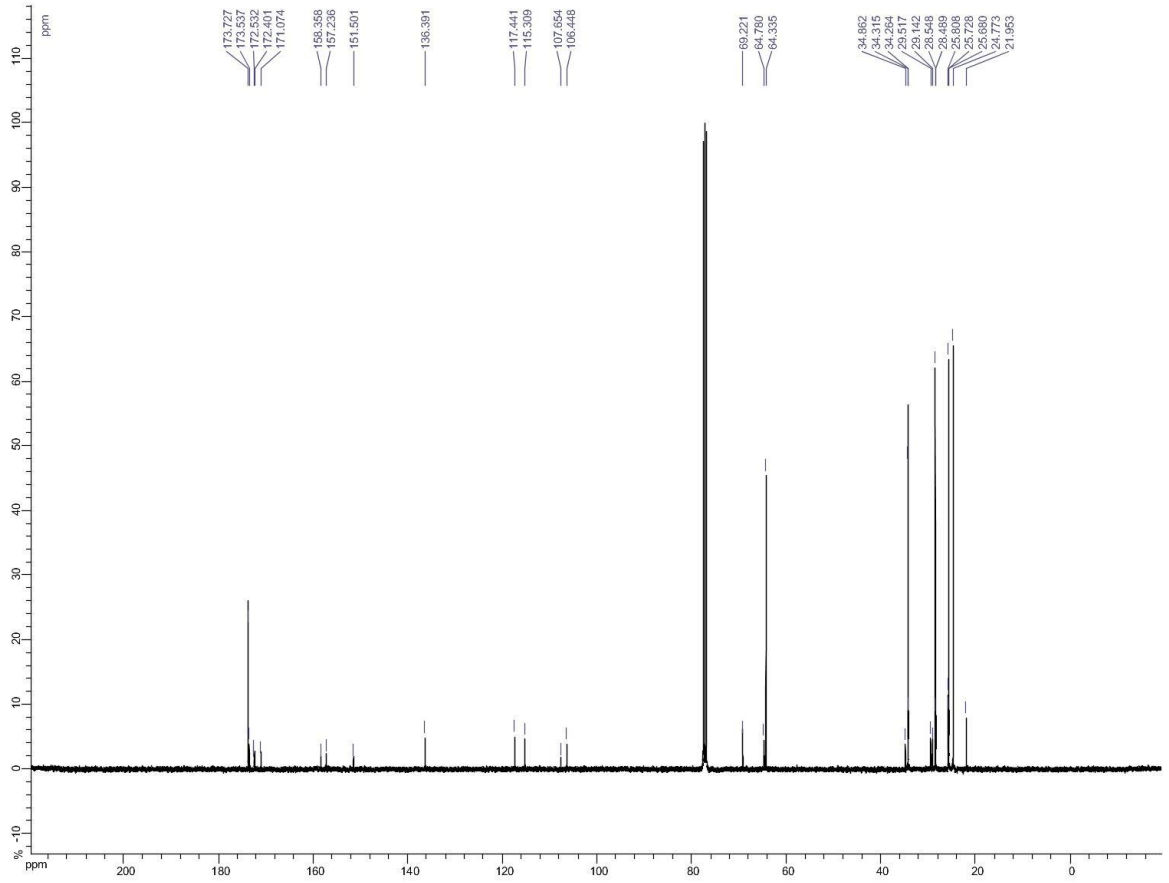

Figure 4.7. ^{13}C NMR ($CDCl_3$) of benzodioxinone incorporated polycaprolactone **5** (in **Figure 4.6**).

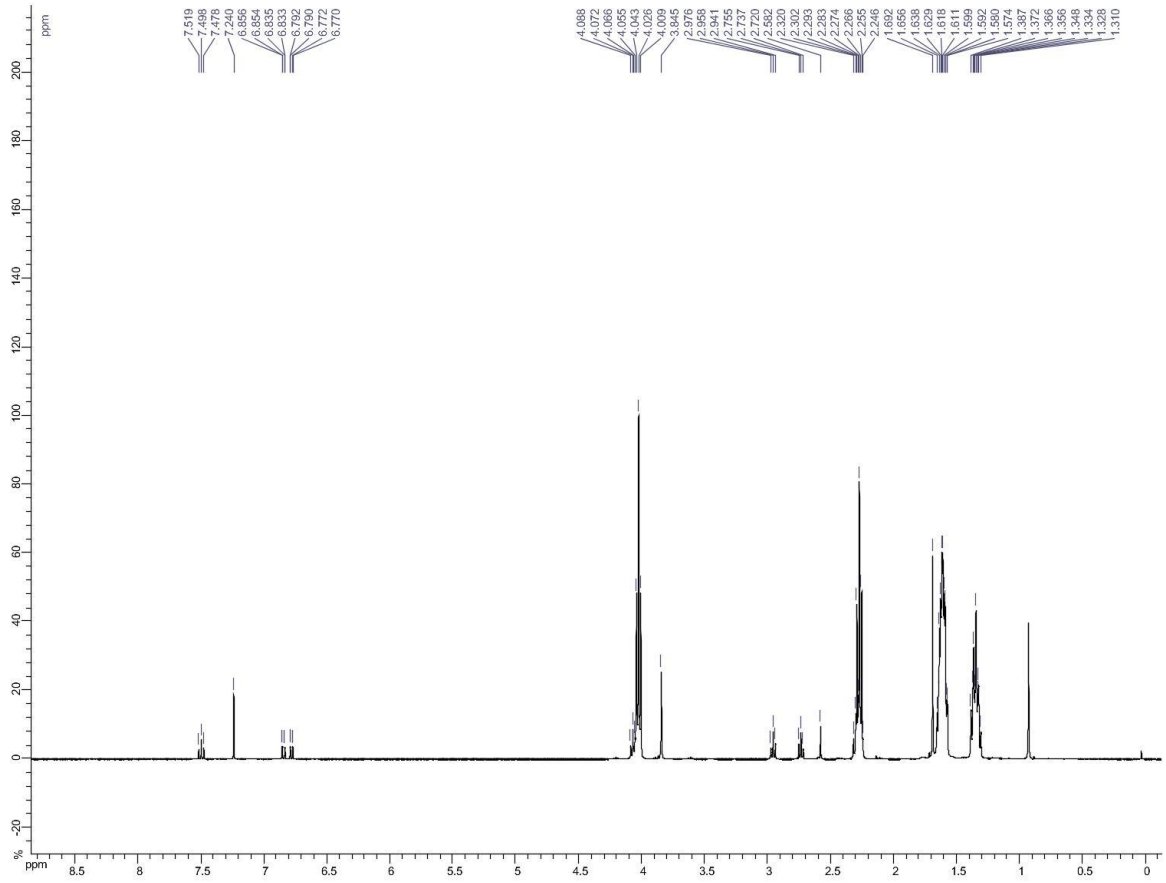

Figure 4.8. ^{1}H NMR ($CDCl_3$) of benzodioxinone incorporated polycaprolactone **5** (in **Figure 4.6**).

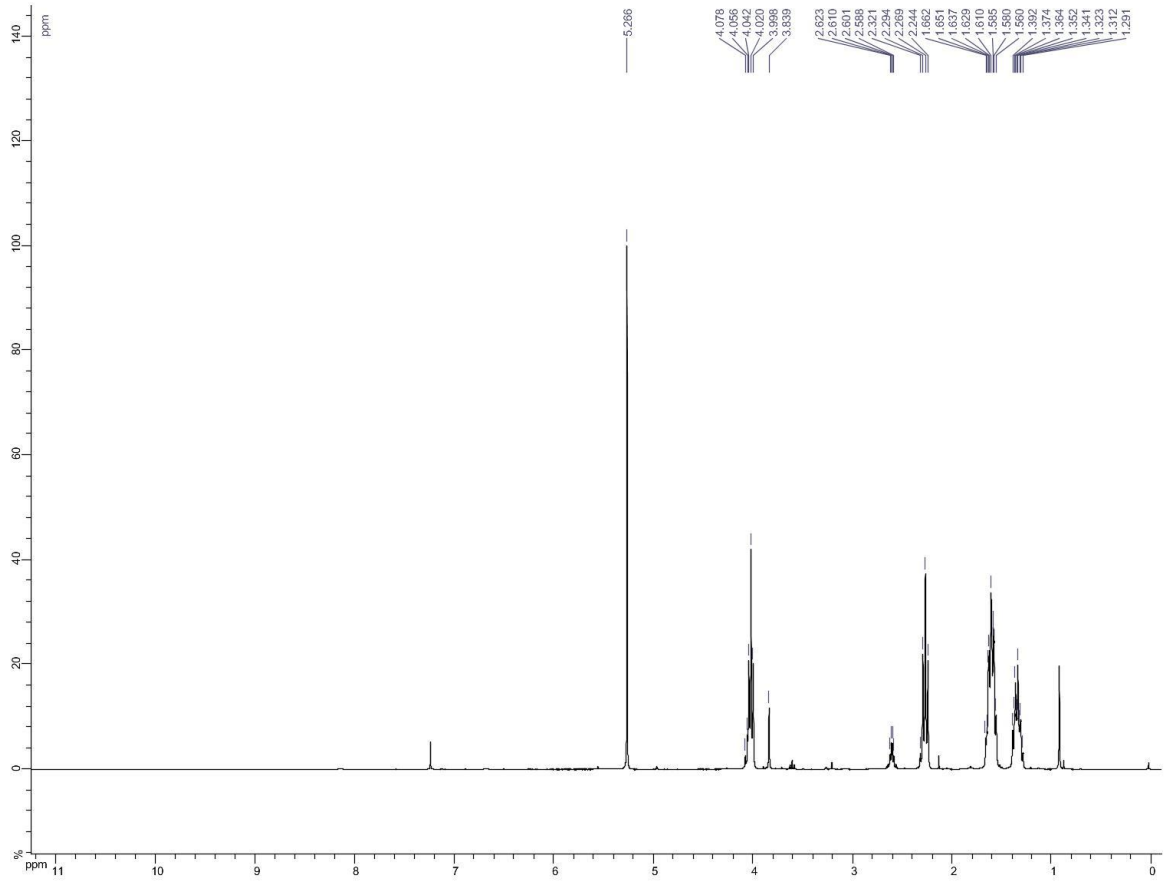

Figure 4.9. ^{1}H NMR ($CDCl_3$) of **Figure 4.6** Compound **2**.

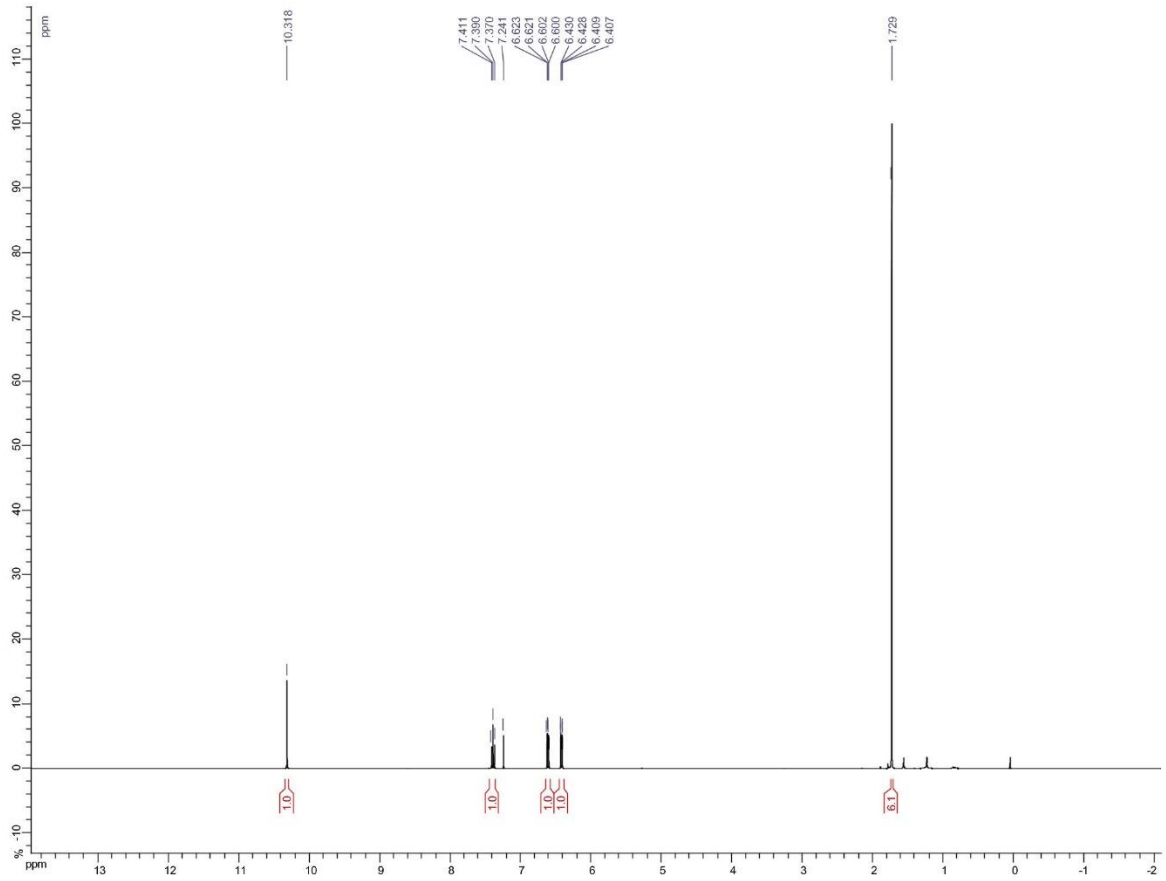

Figure 4.10. ^{1}H NMR ($CDCl_3$) of **Figure 4.6** Compound **4.**

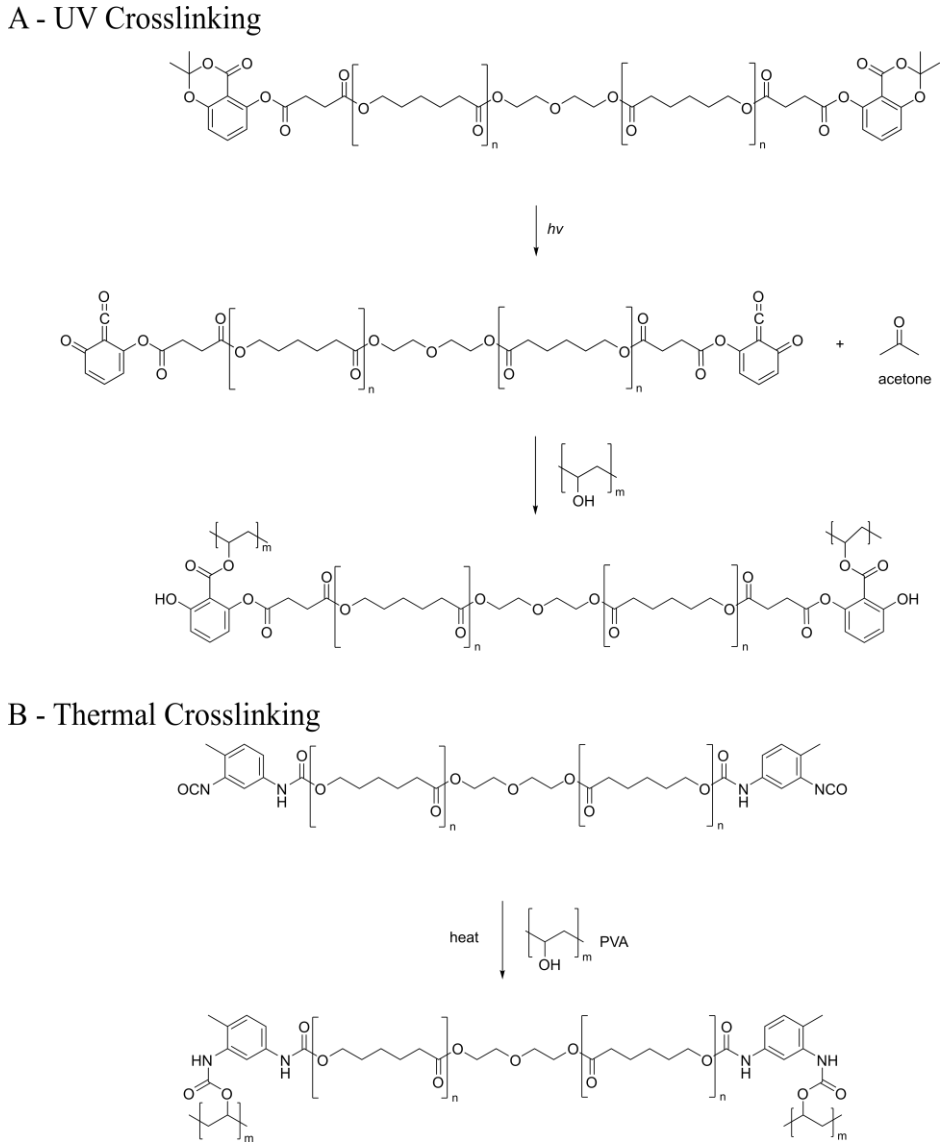

Figure 4.11. A) UV reaction for the UV-PCL with PVA including by-products of the ring opening reaction. B) Thermal reaction for the TPCL with PVA.

Table 4.3. Surface energy on the dielectric surfaces. γ_{sd} is the dispersive component of the surface energy, γ_{sp} is the polar component and γ_{total} is the total surface energy.

Surface	γ_{sd} (mJ/m^2)	γ_{sp} (mJ/m^2)	γ_{total} (mJ/m^2)
PVAc	30.54	24.19	54.74
TPCL	40.16	10.61	50.77
UV-PCL	35.75	13.18	48.93
OTS	24.45	0.04	24.49

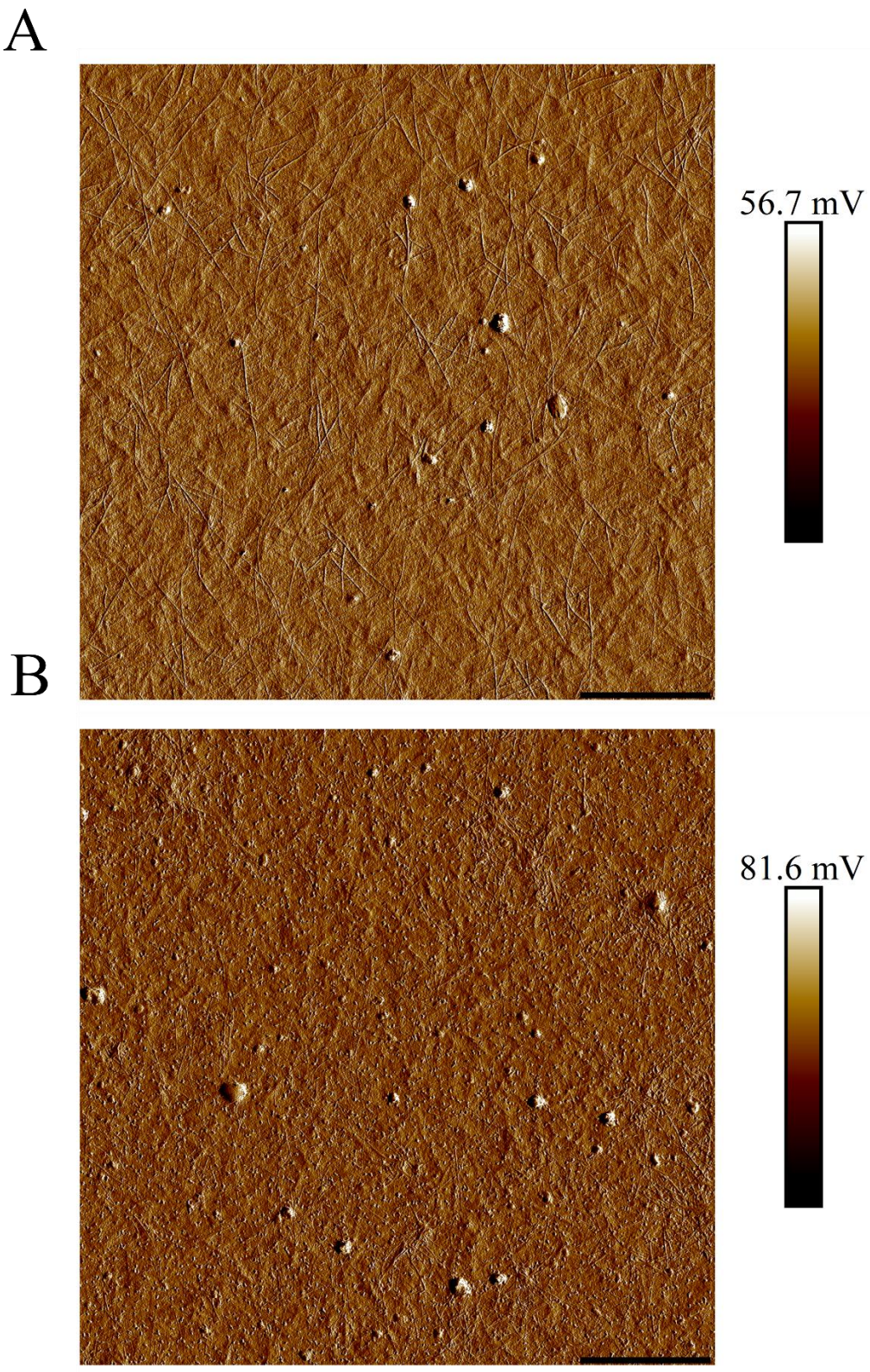

Figure 4.12. Atomic force microscopy peak force images of sc-SWCNTS between the source and drain electrodes of A) TPCL and B) UV-PCL TFTs. The black bar represents 1 μm in length.

OTFT transistor measurements were performed at various on and off pulse frequencies to highlight the reduction in hysteresis. Equation 4.7 was used to determine the pulse frequency. The on times used were set at 2, 20, 200 or 2000 ms and the off time used were set at 8, 80, 800 or 8000 ms for frequencies of 100, 10, 1 and 0.1 Hz.

$$f(Hz) = \frac{1000}{(on_{time} + off_{time})ms} \qquad Eq\ 4.7$$

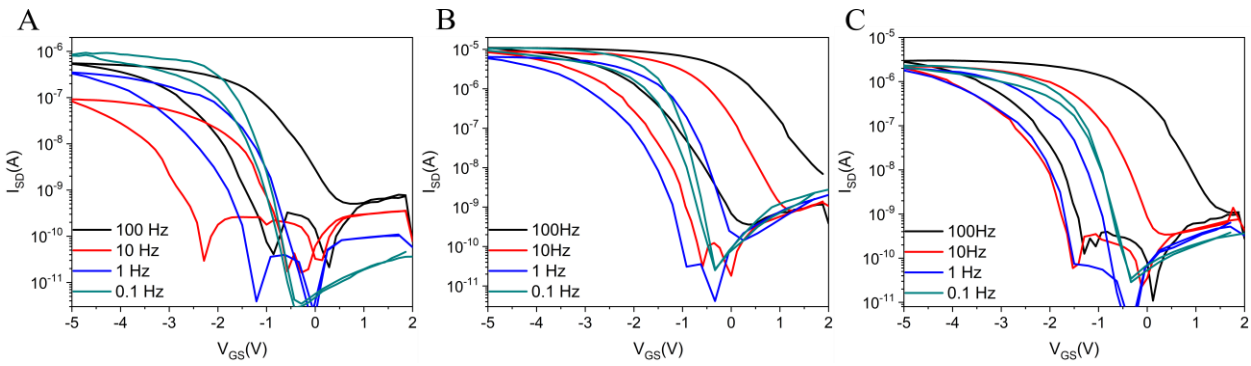

Figure 4.13. Transfer curves at various pulsing frequencies for A) PVAc B) TPCL/PVAc and C) UV-PCL/PVAc. The transfer curves were measured using a -1 V source-drain bias.

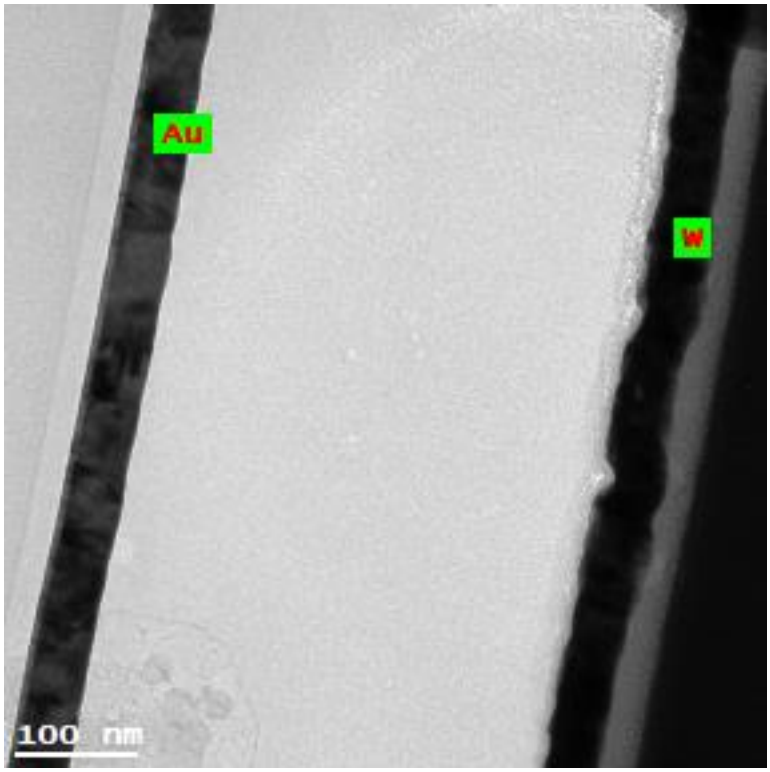

Figure 4.14. TEM image of the PVAc/TPCL dielectric on top of an Au gate electrode. Au represents the location of the gold electrode and w is a protective coating placed on top of the OTFT films for the TEM imaging process.

4.8 References

1. Tan, M. J. *et al.* Biodegradable electronics: cornerstone for sustainable electronics and transient applications. *J. Mater. Chem. C* **4**, 5531–5558 (2016).

2. Kumar, A., Holuszko, M. & Espinosa, D. C. R. E-waste: An overview on generation, collection, legislation and recycling practices. *Resour. Conserv. Recycl.* **122**, 32–42 (2017).

3. Wiklund, J. *et al.* A Review on Printed Electronics: Fabrication Methods, Inks, Substrates, Applications and Environmental Impacts. *J. Manuf. Mater. Process.* **5**, 89 (2021).

4. Khan, Y. *et al.* A New Frontier of Printed Electronics: Flexible Hybrid Electronics. *Adv. Mater.* **32**, 1–29 (2020).

5. Grau, G. & Subramanian, V. Dimensional scaling of high-speed printed organic transistors enabling high-frequency operation. *Flex. Print. Electron.* **5**, 014013 (2020).

6. Nketia-Yawson, B. & Noh, Y.-Y. Recent Progress on High-Capacitance Polymer Gate Dielectrics for Flexible Low-Voltage Transistors. *Adv. Funct. Mater.* **28**, 1802201 (2018).

7. TEJA KARRI, B. R. & GUPTA, N. Hybrid bilayer gate dielectric-based organic thin film transistors. *Bull. Mater. Sci.* **42**, 2 (2019).

8. Jin, S. H. *et al.* Pentacene OTFTS with PVA Gate Insulators on a Flexible Substrate. *J. Korean Phys. Soc.* **44**, 181–184 (2004).

9. Jin, S. H. *et al.* 34.2: PMMA Buffer-Layer Effects on Electrical Performance of Pentacene OTFTs with a Cross-linked PVA Gate Insulator on a Flexible Substrate. *SID Symp. Dig. Tech. Pap.* **34**, 1088 (2003).

10. Larsen, C. *et al.* A tool for identifying green solvents for printed electronics. *Nat. Commun.* **12**, 1–7 (2021).

11. Gaikwad, A. M. *et al.* Identifying orthogonal solvents for solution processed organic transistors. *Org. Electron. physics, Mater. Appl.* **30**, 18–29 (2016).

12. Søndergaard, R. R., Hösel, M. & Krebs, F. C. Roll-to-Roll fabrication of large area functional organic materials. *J. Polym. Sci. Part B Polym. Phys.* **51**, 16–34 (2013).

13. Matsui, H., Takeda, Y. & Tokito, S. Flexible and printed organic transistors: From materials to integrated circuits. *Org. Electron.* **75**, 105432 (2019).

14. Li, J. *et al.* Solution-processable organic and hybrid gate dielectrics for printed electronics. *Mater. Sci. Eng. R Reports* **127**, 1–36 (2018).

15. Van Etten, E. A. *et al.* Insulating characteristics of polyvinyl alcohol for integrated electronics. *Thin Solid Films* **568**, 111–116 (2014).

16. Tsai, T.-D., Chang, J.-W., Wen, T.-C. & Guo, T.-F. Manipulating the Hysteresis in Poly(vinyl alcohol)-Dielectric Organic Field-Effect Transistors Toward Memory Elements. *Adv. Funct. Mater.* **23**, 4206–4214 (2013).

17. Nawaz, A. & Hümmelgen, I. A. Poly(vinyl alcohol) gate dielectric in organic field-effect transistors. *J. Mater. Sci. Mater. Electron.* **30**, 5299–5326 (2019).

18. MacHado, W. S. & Hummelgen, I. A. Low-voltage poly(3-Hexylthiophene)/Poly(Vinyl Alcohol) field-effect transistor and inverter. *IEEE Trans. Electron Devices* **59**, 1529–1533 (2012).

19. Lee, S. *et al.* Effects of hydroxyl groups in polymeric dielectrics on organic transistor performance. *Appl. Phys. Lett.* **88**, (2006).

20. Zhang, H. *et al.* Solution-processed organic field-effect transistors with cross-linked poly(4-vinylphenol)/polyvinyl alcohol bilayer dielectrics. *Appl. Surf. Sci.* **478**, 699–707 (2019).

21. Subbarao, N. V. V., Mandal, S., Gedda, M., Iyer, P. K. & Goswami, D. K. Effect of temperature on hysteresis of dipolar dielectric layer based organic field-effect transistors: A temperature sensing mechanism. *Sensors Actuators, A Phys.* **269**, 491–499 (2018).

22. She, X.-J., Liu, J., Zhang, J.-Y., Gao, X. & Wang, S.-D. Operational stability enhancement of low-voltage organic field-effect transistors based on bilayer polymer dielectrics. *Appl. Phys. Lett.* **103**, 133303 (2013).

23. Rullyani, C., Ramesh, M., Sung, C.-F., Lin, H.-C. & Chu, C.-W. Natural polymers for disposable organic thin film transistors. *Org. Electron.* **54**, 154–160 (2018).

24. Tousignant, M. N. *et al.* High Performance Organic Electronic Devices Based on a Green Hybrid Dielectric. *Adv. Electron. Mater.* **7**, 2100700 (2021).

25. Kv, S. B. *et al.* Methods of Decontamination of Toluene Di-Isocyanate (TDI) spills and leftovers. **4**, 89–93 (2014).

26. Soltani, O. & De Brabander, J. K. Synthesis of Functionalized Salicylate Esters and Amides by Photochemical Acylation. *Angew. Chemie Int. Ed.* **44**, 1696–1699 (2005).

27. Kumbaraci, V., Talinli, N. & Yagci, Y. Photoinduced Crosslinking of Polymers Containing Pendant Hydroxyl Groups by Using Bisbenzodioxinones. *Macromol. Rapid Commun.* **28**, 72–77 (2007).

28. Kumbaraci, V., Talinli, N. & Yagci, Y. Photoinduced Synthesis of Oligoesters. *Macromolecules* **39**, 6031–6035 (2006).

29. Sugimoto, K., Kobayashi, A., Kohyama, A., Sakai, H. & Matsuya, Y. Divinylcarbinol Desymmetrization Strategy: A Concise and Reliable Approach to Chiral Hydroxylated Fatty Acid Derivatives. *J. Org. Chem.* **86**, 3970–3980 (2021).

30. Panwiriyarat, W. Preparation and properties of bio-based polyurethane made from natural rubber and poly (Ɛ-caprolactone). (2013).

31. Tousignant, M. N. *et al.* Improving Thin-Film Properties of Poly(vinyl alcohol) by the Addition of Low-Weight Percentages of Cellulose Nanocrystals. *Langmuir* **36**, (2020).

32. Rice, N. A. *et al.* Polycarbazole-Sorted Semiconducting Single-Walled Carbon Nanotubes for Incorporation into Organic Thin Film Transistors. *Adv. Electron. Mater.* **5**, 1–11 (2019).

33. Owens, D. K. & Wendt, R. C. Estimation of the surface free energy of polymers. *J. Appl. Polym. Sci.* **13**, 1741–1747 (1969).

34. Umeda, T., Kumaki, D. & Tokito, S. Surface-energy-dependent field-effect mobilities up to 1 cm2/V s for polymer thin-film transistor. *J. Appl. Phys.* **105**, 024516 (2009).

35. Zhao, C., Li, A., Chen, X., Ali, M. U. & Meng, H. Hysteresis effect in organic thin film transistors based on naphthalene tetracarboxylic diimide derivatives. *Appl. Phys. Lett.* **118**, 193302 (2021).

36. Cruz, S. M. F., Rocha, L. A. & Viana, J. C. *Flexible Electronics*. *Flexible Electronics* (InTech, 2018). doi:10.5772/intechopen.72522.

37. Douglas, S. P., Mrig, S. & Knapp, C. E. MODs vs. NPs: Vying for the Future of Printed Electronics. *Chem. - A Eur. J.* **27**, 8062–8081 (2021).

38. Rice, N. A. *et al.* Organic Thin Film Transistors: Polycarbazole-Sorted Semiconducting Single-Walled Carbon Nanotubes for Incorporation into Organic Thin Film Transistors. *Adv. Electron. Mater.* **5**, 1970002 (2019).

39. Mirka, B. *et al.* Excess Polymer in Single-Walled Carbon Nanotube Thin-Film Transistors: Its Removal Prior to Fabrication Is Unnecessary. *ACS Nano* **15**, 8252–8266 (2021).

40. Mirka, B. *et al.* Polyfluorene-Sorted Semiconducting Single-Walled Carbon Nanotubes for Applications in Thin-Film Transistors. *Chem. Mater.* **31**, 2863–2872 (2019).

41. Li, Q. *et al.* Designing hybrid gate dielectric for fully printing high-performance carbon nanotube thin film transistors. *Nanotechnology* **28**, (2017).

42. Melville, O. A., Rice, N. A., Therrien, I. & Lessard, B. H. Organic thin-film transistors incorporating a commercial pigment (Hostasol Red GG) as a low-cost semiconductor. *Dye. Pigment.* **149**, 449–455 (2018).

43. Vosgueritchian, M., LeMieux, M. C., Dodge, D. & Bao, Z. Effect of Surface Chemistry on Electronic Properties of Carbon Nanotube Network Thin Film Transistors. *ACS Nano* **4**, 6137–6145 (2010).

44. Lefebvre, J. *et al.* Hysteresis free carbon nanotube thin film transistors comprising hydrophobic dielectrics. *Appl. Phys. Lett.* **107**, (2015).

45. Ortiz, R. P., Facchetti, A. & Marks, T. J. High-k organic, inorganic, and hybrid dielectrics for low-voltage organic field-effect transistors. *Chem. Rev.* **110**, 205–239 (2010).

46. Van Etten, E. A. *et al.* Insulating characteristics of polyvinyl alcohol for integrated electronics. *Thin Solid Films* **568**, 111–116 (2014).

47. Amin, E. M., Karmakar, N. C. & Winther-Jensen, B. Polyvinyl-Alcohol (Pva)-Based RF Humidity Sensor in Microwave Frequency. *Prog. Electromagn. Res. B* **54**, 149–166 (2013).

48. Bergo, P., Moraes, I. C. F. & Sobral, P. J. A. Effects of Different Moisture Contents on Physical Properties of PVA-Gelatin Films. *Food Biophys.* **7**, 354–361 (2012).

49. Sun, Y. *et al.* Polymer gate dielectrics with self-assembled monolayers for high-mobility organic thin-film transistors based on copper phthalocyanine. *Appl. Phys. A* **95**, 777–780 (2009).

50. Timmermans, M. Y. *et al.* Effect of carbon nanotube network morphology on thin film transistor performance. *Nano Res.* **5**, 307–319 (2012).

51. Lee, S. H., Kim, D. Y. & Noh, Y. Y. Solution-processed polymer-sorted semiconducting carbon nanotube network transistors with low- k/high- k bilayer polymer dielectrics. *Appl. Phys. Lett.* **111**, (2017).

52. Egginger, M. *et al.* Mobile ionic impurities in poly (vinyl alcohol) gate dielectric: Possible source of the hysteresis in organic field-effect transistors. *Adv. Mater.* **20**, 1018–1022 (2008).

53. Subbarao, N. V. V., Gedda, M., Iyer, P. K. & Goswami, D. K. Organic field-effect transistors as high performance humidity sensors with rapid response, recovery time and remarkable ambient stability. *Org. Electron.* **32**, 169–178 (2016).

54. Georgiou, V. *et al.* Ferroelectricity in Polar Polymer-Based FETs: A Hysteresis Analysis. *Adv. Funct. Mater.* **28**, 1705250 (2018).

55. Egginger, M., Bauer, S., Schwödiauer, R., Neugebauer, H. & Sariciftci, N. S. Current versus gate voltage hysteresis in organic field effect transistors. *Monatshefte fur Chemie* **140**, 735–750 (2009).

Chapter 5 : N-type Single Walled Carbon Nanotube Thin Film Transistors using Green Tri-layer Polymer Dielectric

This chapter was published in the journal "Advanced Materials Interfaces": Tousignant, M. N., Ronnasi, B., Tischler, V. & Lessard, B. H. N-Type Single Walled Carbon Nanotube Thin Film Transistors Using Green Tri-Layer Polymer Dielectric. Adv. Mater. Interfaces 2300079, 1–8 (2023)

Context

One of the major issues encounter during the studies of Chapter 3 and Chapter 4 involved the density of the SWCNT networks. Both UV-PCL and TPCL have water contact angles of 60-70° while SWCNTs form denser networks on more hydrophobic surfaces. Because of this octyl trichloro silanes are commonly used to increase the water contact angle of a substrate prior to SWCNT deposition. For this study, we wanted to take advantage of the increased SWCNT network density caused by the OTS surface treatment and see if we could produce n-type OTFTs. To accomplish this the device architecture was change to a TGBC architecture allowing the SWCNTs to be deposited directly on the OTS treated substrate and encapsulated by the dielectric. When designing the dielectric system it was apparent that water soluble PVAc would not be a good candidate polymer to be deposited on an OTS treated surface. Therefore, we decided to explore a tri-layer architecture using poly lactic acid as an additional low-*k* layer. This would allow us to improve the deposition surface for PVAc and further reduce the leakage currents and polar interactions between PVAc and the SWCNTs. The TPCL layer is still used as the top low-*k* layer providing a barrier to moisture. The TGBC architecture allowed for air stable n-type SWCNT OTFTs and improved performance when compared to the bilayer system.

Contribution

Bahar Ronnasi prepared the TPCL and helped with the fabrication and characterization of the OTFTs. Dr. Tischler performed all PVA ink blade coating experiments. I prepared all the thin films used within this study. I performed the AFM measurements and cleaned up the raw AFM images. I performed all the contact angle and surface energy measurements for this study. I interpreted all thin film characterization data. I fabricated, characterized, and interpreted all the capacitor data. Bahar Ronnasi, Dr. Tischler and Dr. Lessard reviewed the manuscript. I wrote and reviewed the manuscript.

5.1 Abstract

The proliferation of disposable, wearable and implantable printable electronics requires the development of high-performance biodegradable and sustainable electronic components. Often green materials don't have the necessary properties for high performance electronics, therefore obtaining the ideal properties requires a combination of multiple green materials. We report a tri-layer dielectric using PLA, PVAc and TPCL which we integrated into sc-SWCNT based thin film transistors in a top gate bottom contact architecture. The PVA provides a high dielectric constant due to the hydroxy groups, the cellulose is used to optimize the viscosity, the TPCL layer provides a robust hydrophobic surface, and the PLA eliminates the interfacial charge traps present in the PVAc and improves the adhesion between PVAc and the substrate. This leads to a decrease in leakage currents and reduces the polarity at the dielectric/semiconductor interface. The OTFTs fabricated using tri-layer dielectrics led to air stable n-type devices with higher overall performance when compared against the PVAc/TPCL bilayer devices.

5.2 Introduction

The need is growing for high performance environmentally friendly materials that can be used in printed electronic applications such as wearable sensors, disposable circuitry and implantable electronics.[1] Unfortunately, the choice of green materials is limited and many of the existing materials represent a compromise in performance. OTFTs are three electrode logic gate operators including a semiconductive layer with a dielectric layer and are a common example of electronic devices used in flexible electronic and sensing applications.[2–5] The desired properties of these OTFTs are low voltage operation, low leakage currents and high on state currents.[6–8] SWCNTs are promising semiconductors achieving high mobilities in low-voltage flexible, printed OTFTs.[9–12] High performance OTFTs are obtained through achieving good SWCNT density as well as selection of high-*k* dielectrics increasing the capacitance density and ultimately the performance of the OTFTs.[13] For example, PVA is a common environmentally friendly high-*k* dielectric.[14–16] However, often high-*k* materials are plagued with increased leakage currents and charge trapping at the semiconductor/dielectric interface.[16] When used in the fabrication of SWCNT OTFTs, PVA can prevent saturation of the output curves, increase leakage currents and create a polar environment at the SWCNT/PVA interface reducing device performance.[17,18] To circumvent this challenge the dielectric layer can be modified by adding a thin low-*k* dielectric material on top of the high-*k* dielectric creating a bilayer dielectric. Low-*k* dielectric materials

are better for the deposition of the semiconducting material and reduce the polarity at the dielectric/semiconductor interface leading to higher operating currents and mobilities.[15,17–24] Furthermore this bilayer approach can also be used to change the hydrophobicity of the surface, similar to the use of OTS, leading to reduced wettability of the solvent and resulting in a better SWCNT network density.[12,25] Studies have also shown that the addition of a third low-*k* layer can be used to sandwich the high-*k* dielectric material further improving device performance by reducing leakage currents between the source and the gate.[20,26,27]

Within this study we report the use of an environmentally friendly tri-layer dielectric composed of low-*k* PLA bottom layer, high-*k* PVAc and low-*k* TPCL top layer. PLA is a biodegradable polymer that has been used with other green dielectric bilayer systems while PVA/TPCL blends have been used as biodegradable solarizing films in agricultural applications which makes them ideal environmentally friendly dielectric materials.[24,28,29] This tri-layer dielectric was used with sc-SWCNTs in a TGBC architecture to fabricate n-type OTFTs that functioned under ambient conditions. Depositing PLA on top of the sc-SWCNTs encapsulates them reducing leakage currents and forming a better surface for the deposition of PVAc. The top layer is a low-*k* TPCL layer that prevents moisture from impacting the performance of the PVAc layer and helps enable air stable operation.

5.3 Discussion

Thin film characterization

PVA is a promising dielectric due to its polar hydroxyl groups and low environmental impact,[1] however, it does suffer from moisture sensitivity.[35,36] Therefore, several techniques have been adopted to improve the performance of PVA while maintaining it's high dielectric constant. For example, Zhang et al. used PVP/PVA and She et al. used PMMA/PVA as low-*k*/PVA bilayer dielectrics reducing leakage currents and reducing the polarity at the dielectric/semiconductor interface.[19,20] Our group reported the use of TPCL (**Figure 5.1A)** as a low-*k* top encapsulating layer, which was crosslinked at the PVA interface, providing a resistance to moisture, reducing the gate leakage while also enabling a thin hydrophobic layer which was impervious to dissolution from sequential solution deposition of the semiconductor.[18] We have also reported that the use of cellulose nanocrystals can increase the viscosity of the PVA layer during deposition, reducing the chance of fingering and providing a more uniform

film and less short circuited devices.[37] However, the leakage current of these bilayer devices can be further reduced through a tri-layer architecture. Therefore, we designed a tri-layer dielectric with the structure PLA/PVAc/TPCL. Furthermore, our initial studies suffered from relatively low OTFT performance due to the low sc-SWCNT density on the TPCL.[18,38] Therefore we are targeting a TGBC architecture allowing for the substrates to be treated with OTS prior to sc-SWCNT deposition, leading to higher sc-SWCNTs network densities.[39,40] TPCL does not form uniform films on glass or OTS treated substrates due to its tendency to aggregate.[18] Therefore, PLA was implemented as an alternative, environmentally friendly low-*k* layer that could be deposited above the sc-SWCNT and below the PVAc, acting as an intermediate layer between OTS and PVAc. Because PLA is insoluble in water it can be deposited without the risk of being rinsed away during the PVAc deposition. Some examples of tri-layer dielectrics structures similar to **Figure 5.1B** have also been reported. Subbarao et al. used a PMMA/PVA/Al_2O_3 dielectric to further reduce leakage currents and encapsulate the PVA protecting it from moisture.[26,27] To the best of our knowledge, this is the first report of completely green tri-layer dielectrics being used in sc-SWCNT OTFTs.

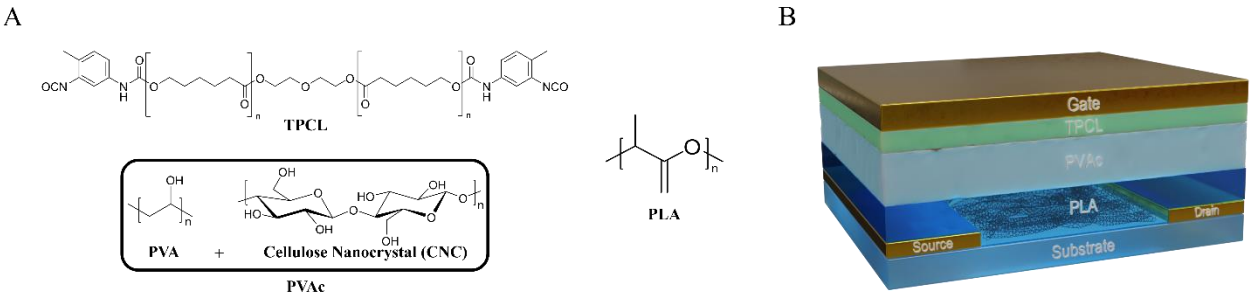

Figure 5.1. A) Chemical structures of TPCL, PVAc and PLA. B) TGBC OTFT with a tri-layer PLA/PVAc/TPCL dielectric.

In our previous work involving sc-SWCNTs and our PVAc/TPCL bilayer dielectrics the devices were fabricated in a BGTC architecture. However, this architecture has certain limitations. For example, in a BGTC architecture the sc-SWCNTs are exposed to the ambient environment which causes oxygen doping and supresses any n-type performance.[41,42] Further the TPCL surface does not allow for dense networks of sc-SWCNTs due to a miss match in both water contact angle and surface energies. Sc-SWCNTs are commonly dispersed in toluene and have been demonstrated to form dense randomized networks when deposited on OTS

surfaces.[12,31,40,43] **Figure 5.2** shows AFM images of drop casted sc-SWCNTs and their varying network densities and alignments when deposited on quartz coated glass (**Figure 5.2A**), OTS treated quartz coated glass (**Figure 5.2B**) and TPCL (**Figure 5.2C**). Both AFM images of **Figure 5.2A** and **Figure 5.2B** demonstrate a much higher network density when compared to the TPCL network in **Figure 5.2C**. When fabricating sc-SWCNT transistors both network density and alignment are important.[12,44] The use of OTS improves the tail to tail alignment creating a webbed network unlike the SWCNTs on quartz coated glass. This leads to better overall OTFT performance for the OTS treated surfaces. By switching from a BGTC architecture to a TGBC architecture it is possible to use an OTS surface treatment to improve the deposition of the sc-SWCNTs while encapsulating the nanotubes allowing them to operate as n-type OTFTs.

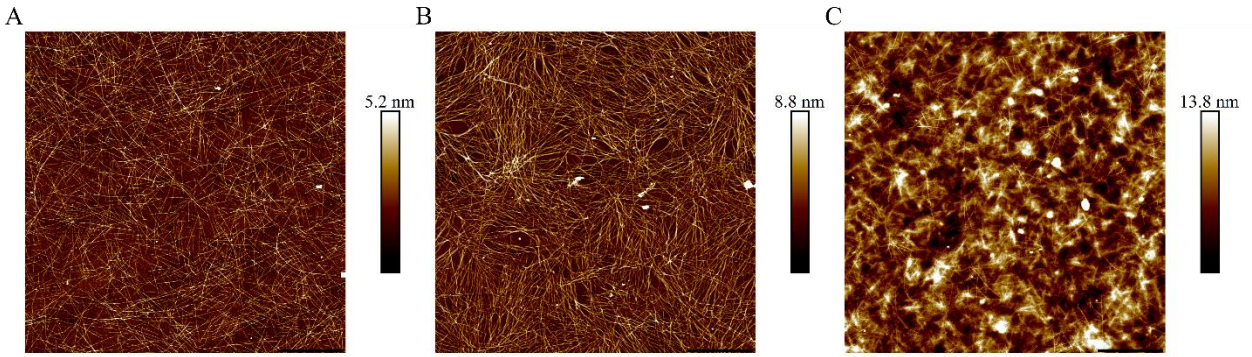

Figure 5.2. AFM height images of SWCNTs on A) quartz B) OTS and C) PVAc/TPCL.

The properties of each layer were further analysed through contact angle and surface energy measurements as seen in **Table 5.1**. The use of surface energy measurements allows for a better understanding of why sc-SWCNTs form denser networks on OTS treated surfaces and can be used to help determine how to improve the sequential deposition of layers on top of an OTS treated surface. Low surface energy materials are usually used as anti-adhesive layers.[45] This property is favorable for drop casting sc-SWCNTs from toluene because it allows the drops to bead and form dense sc-SWCNT networks. However, it poses a challenge for orthogonal processing. There are two main factors contributing towards the adhesion between two materials one of which is the total surface energy of the material, and the other is the ratio between the polar and dispersive components of the material.[46] First, when orthogonally processing materials it's important to try and match their surface energies. The closer the surface energies of the materials the better the two layers will adhere to each other.[47] The total surface energies can be

seen in **Table 5.1** and **Figure 5.3**. The large difference between PVAc and OTS demonstrates that both these materials are incompatible for sequential deposition. However, the addition of a PLA interlayer with a lower total surface energy of 41.5 mJ/m^2 makes it a better material for deposition on top of the OTS treated substrates. Next, both the dispersive and polar components of the total surface energy can be seen in **Table 5.1** and **Figure 5.3**. This metric is also important when determining the adhesion between materials. At the interface between both materials the polar portion of one material will only interact with the polar portion of the other material and it is the same for the dispersive portion.[46] This can be seen in **Figure 5.3** where 55% of the total surface energy is dispersive for PVAc whereas OTS is 99% dispersive. This can be improved by using PLA where 82% of the total surface energy is dispersive increasing its adhesion to OTS when compared to PVAc. Further we also analyzed the deposition of PVA on top of PLA and silver using blade coating techniques and found that depositing PVA on top of PLA leads to lower variations in film thickness (**Figure 5.6 and 5.7,** in the supporting information). When comparing the surface energies, we see that the low surface energy of OTS allows the toluene drops to bead and increase the density of the sc-SWCNTs networks. The increase in network density is vital for improving OTFT performance however it complicated the sequential deposition of PVAc. Therefore, the addition of a thin PLA layer can act as an intermediate between the OTS and the PVAc increasing the adhesion between each layer.

Table 5.1. Dispersive (γ_{sd}), polar (γ_{sp}) and total (γ_{tot}) surface energy of PVAc, PVAc/TPCL, PLA and OTS with their associated water and diiodomethane contact angles.

Surface	γ_{sd} (mJ/m^2)	γ_{sp} (mJ/m^2)	γ_{tot} (mJ/m^2)	**H_2O** (°)	**DIIM** (°)
PVAc	30.5	24.2	54.7	47.6	41.3
PVAc/TPCL	40.2	10.6	50.8	63.1	25.6
PLA	34.3	7.1	41.5	74.0	42.0
OTS	24.4	0.04	24.5	93.5	41.1

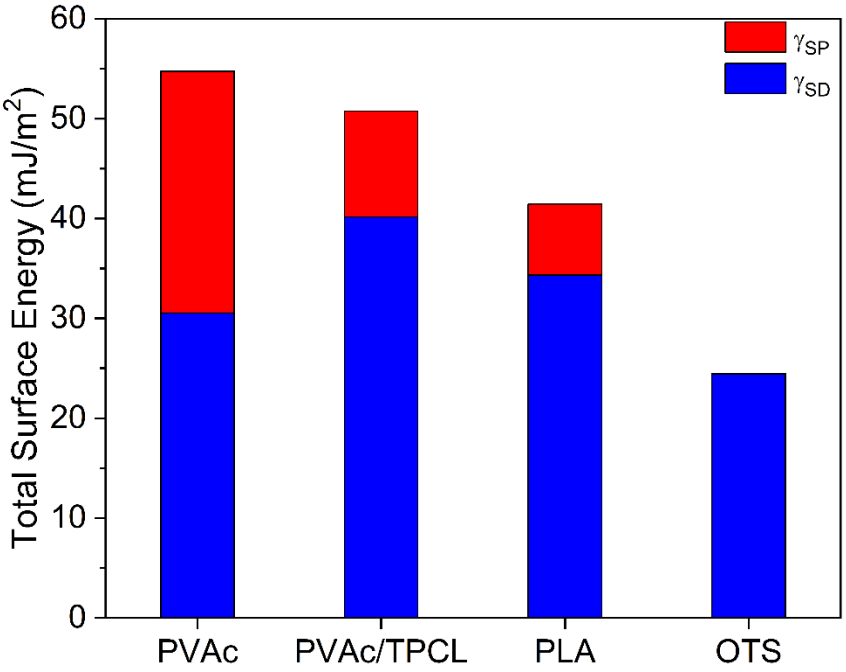

Figure 5.3. Polar and dispersive components of the total surface energy for PVAc, PVAc/TPCL, PLA and OTS.

Capacitor characterization

MIM capacitors were fabricated for both the PVAc/TPCL and PLA/PVAc/TPCL bi and tri-layers. The dielectric properties were characterized under ambient conditions, between 10^{-1}-10^{5} Hz. The capacitance density of the PVAc/TPCL dielectric stack is slightly higher at 85.5 nF/cm^2 compared to 36.3 nF/cm^2 for the PLA/PVAc/TPCL tri-layer dielectric as seen in **Table 5.1**. This is to be expected as the decrease in capacitance density is caused by the introduction of an additional low-*k* dielectric layer.[12] The capacitance is calculated as:

$$\frac{1}{c_{tot}} = \frac{1}{c_1} + \frac{1}{c_2} + \frac{1}{c_3} \qquad Eq\ 5.1$$

where c_{tot} is the total capacitance of the tri-layer dielectric and c_1 to c_3 is the capacitance of each material in the tri-layer dielectric. For standard dielectric materials increasing the thickness will reduce the capacitance.[15] Therefore, the addition of PLA as a low capacitance material reduces the overall capacitance density. This highlights the importance of keeping the PLA layer thin to limit its impact on the capacitance of the tri-layer dielectric. The PLA layer is deposited at a concentration of 2 mg/ml allowing for films of approximately 30 nm measured

using profilometry. By keeping the PLA layer thin we can limit the impact it has on the capacitance density of the fabricated dielectrics. The change in capacitance density with frequency is also demonstrated in **Figure 5.4**. This highlights the frequency dependence cause by the polarization of the hydroxy groups in the PVAc dielectric. **Figure 5.4** also demonstrates that the introduction of the PLA layer helps reduce variability in both the dielectric and capacitance density measurements.

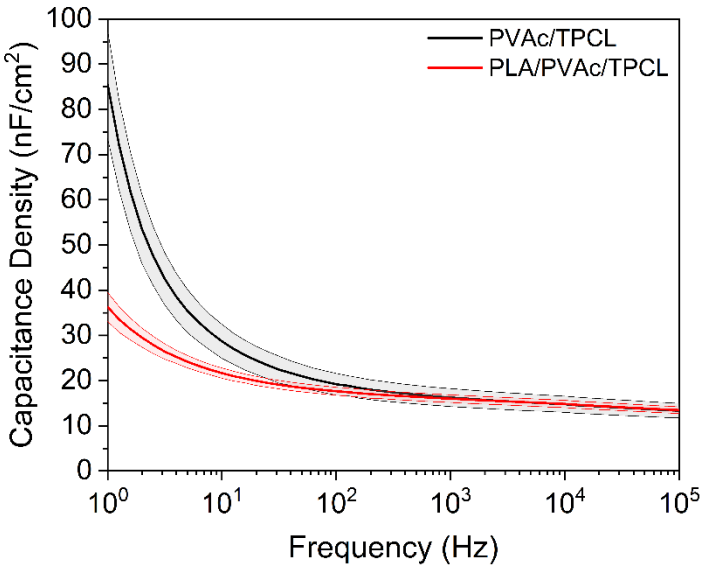

Figure 5.4. Frequency dependant capacitance density for PVAc/TPCL and PLA/PVAc/TPCL. The transparent areas around the lines represent the standard deviation. The averages and standard deviations calculated using 20 MIM capacitors per condition.

Table 5.2. The effective dielectric constant and capacitance density of PVAc/TPCL and PLA/PVAc/TPCL at 1 Hz. The averages and standard deviations were calculated using 20 MIM capacitors per condition.

Dielectric Material	Dielectric Constant [κ]	Capacitance Density [nF/cm^2]
PVAc/TPCL	37.5 ± 5.2	85.5 ± 11.9
PLA/PVAc/TPCL	15.2 ± 1.3	36.3 ± 3.2

Organic thin film transistor characterization

TGBC sc-SWCNT OTFTs were assembled using PVAc/TPCL bilayer and PLA/PVAc/TPCL tri-layer dielectrics. The transfer and output behaviour of devices with both bilayer and tri-layer dielectrics were characterized under n-type operation. The devices were operated in their linear regime and the transfer curves were used to calculate V_T, $I_{on/off}$ and g_m values summarized in **Table 5.2**. The OTS modified substrate led to the desired increase in sc-SWCNT network density as seen in **Figure 5.2**. Although a hydrophobic substrate improves the sc-SWCNT deposition, it introduced a challenge for coating a uniform film of hydrophilic PVAc using an aqueous solution. The poor adhesion between the OTS surface and PVAc dielectric led to a reduction in functioning OTFTs. This was improved using a PLA layer which formed a more uniform film on the OTS treated substrate increasing the total surface area of the substrates that was covered by the tri-layer dielectric. The use of a tri-layer dielectric in TGBC devices led to an order of magnitude increase in $I_{on/off}$ for the fabricated devices as seen in **Table 5.3**. The increase in $I_{on/off}$ is caused by the introduction of a second low-*k* barrier between the semiconductor and the PVAc dielectric, further reducing the leakage currents.[26] This is consistent with previous reports showing significant improvements in $I_{on/off}$ by adding low-*k* interlayers.[17,18,20] The transconductance of sc-SWCNT OTFTs have been recorded between 0.001 to 5 μS/μm with many studies between 0.1 to 1 μS/μm.[48] In this study the bi and tri-layer OTFTs have transconductances of 0.204 and 0.159 μS/μm as seen in **Table 5.3**. These values for the bi and tri-layer OTFTs are within the average range for SWCNT OTFTs. Further, within **Table 5.3** the bilayer dielectrics have a higher transconductance which matches literature.[49] For example, Kim et al.[50] demonstrate that hydroxyl groups can be used to enhance n-type performance. The μ of the fabricated OTFTs were also estimated and shown in **Table 5.4,** in the supporting information**.** The use of a TGBC architecture along with the bi and tri-layer dielectrics also enables stable n-type OTFTs under ambient conditions. This is due to the dielectric encapsulating the sc-SWCNTs and protecting them from degradation by oxygen and moisture.[51–53] The characteristic output and transfer curves of the bilayers and tri-layers are presented in **Figure 5.5A,B,C and 5.5D**. The output curves for the tri-layers have a more stable saturation plateau compared to the bilayers, in which PVAc is directly in contact with the sc-SWCNT layer. The instability and non–ideal OTFT behaviour is caused by charge trapping between the sc-SWCNTs and PVAc and can be seen for the bilayer devices at all source gate

voltages while the increased leakage currents can also be perceived at the 0 V source-gate measurement. The transfer curve measurements also demonstrate similar performance between both the bi and tri-layer devices. The major difference in the transfer curves is the difference in off state and source-gate leakage currents. The low-*k* PLA layer helps reduce leakage currents between the source and the gate while the TPCL layer prevents charge injection through the gate into the PVAc dielectric. The use of two low-*k* dielectric layers sandwiching the high-*k* layer compared to a single layer helps further reduce the off-state current of the fabricated OTFTs while still allowing for similar device performance. Large gate leakage is a known issue with polymer dielectrics. Some of the ways to mitigate leakage currents are by increasing the thickness of the low-*k* layer or by increasing the band gap by selecting a polymer with a lower dielectric constant.[54,55] However, both these techniques can also reduce OTFT performance. Overall, for TGBC architecture both bilayer and tri-layer dielectrics have a high n-type performance under ambient conditions with the tri-layer reducing leakage currents and allowing for better $I_{on/off}$.

Table 5.3. OTFT properties of the tri-layer and bilayer dielectrics under n-type operation.

Layers	**gm (μS)**	**gm (S/m)**	$I_{on/off}$	V_T **(V)**
PLA/PVAc/TPCL	159 ± 40	0.159 ± 0.04	10^5	-0.4 ± 0.4
PVAc/TPCL	204 ± 51	0.204 ± 0.05	10^4	0.2 ± 0.3

*The averages and standard deviations were calculated over 30 – 40 OTFTs per conditions, each of which were measured 3 times.

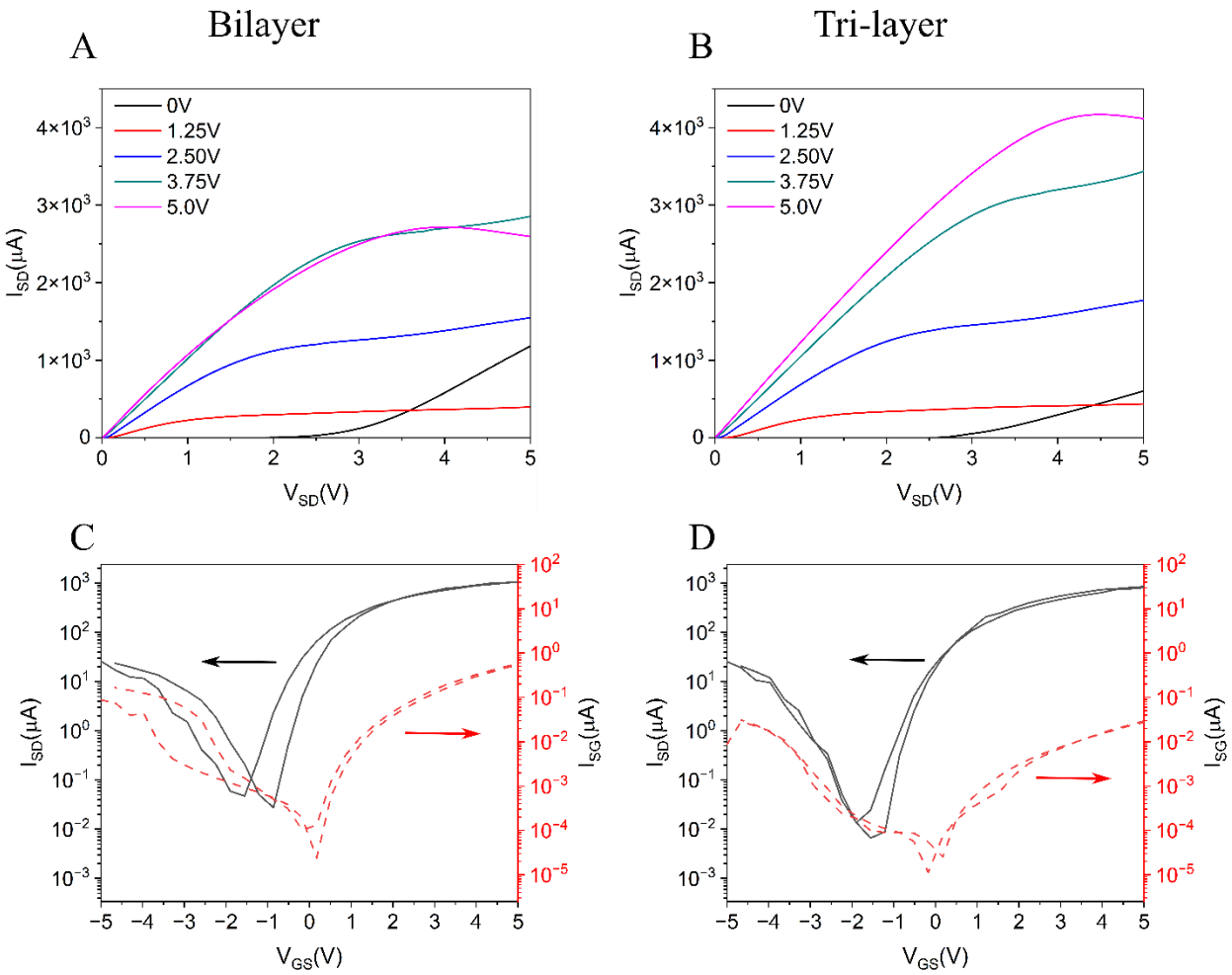

Figure 5.5. Representative output (A, B) and transfer (C, D) curves for the n-type bilayer and tri-layer OTFTs fabricated using sc-SWCNTs, V_{sd} = 1 V. The red dotted lines represent the source-gate leakage currents.

5.4 Conclusion

We demonstrated the use of a high-performance green tri-layer dielectric with sc-SWCNT OTFTs. The use of a TGBC architecture allowed for the substrates to be treated with OTS increasing sc-SWCNT network density which led to increased OTFT performance. The TGBC architecture also allowed for n-type operation under ambient conditions. Furthermore, we demonstrated that the addition of a PLA layer can act as an intermediate layer between the OTS surface treatment and PVAc, improving the layer adhesion for orthogonal processing. The PLA layer also supressed the charge trapping and polar effects caused by PVAc at the dielectric/semiconductor interface and reduced the leakage current of the fabricated OTFTs. In

this work we managed to use a change in architecture along with an environmentally friendly tri-layer dielectric system to improve n-type sc-SWCNT OTFT performance.

5.5 Experimental

Materials

PVA 98-99% hydrolyzed; (M_w = 31 000 – 50 000 Da), PCL diol (M_w = 2000 Da), tolylene-2,4-diisocyante (95%) and PLA (M_n=40,000 Da) was purchased from Sigma-Aldrich. Gold (Au, 99.99%) and chromium coated tungsten rods were purchased from Angstrom Engineering. A 2 wt% aqueous dispersion of CNCs was donated by FP innovations. Quartz coated glass substrates (15 X 20 mm^2) were purchased from Ossila Limited. Pre diced 1 in^2 glass substrates were purchased from University Wafers.

Preparation of dielectric and sc-SWCNTs

PLA was dissolved in chloroform at a concentration of 2 mg/ml. Once fully dissolved the PLA was filtered into another vial using a 0.45 μm PTFE filter. PVA was dissolved in water, filtered with a 0.45 μm cellulose filter and mixed with a 2 wt% suspension of CNCs to form a PVAc suspension. The PVAc suspensions were fabricated based on previously reported procedures producing a suspension at a concentration of 80mg/ml with 0.75 wt% CNCs.[30] TPCL was synthesized following previously reported procedures.[18] The TPCL was dissolved in anhydrous toluene at 2mg/ml and heated to 60 °C for 1h before being filtered through a 0.45 μm PTFE filter into a new vial. The filtered TPCL solution was stored in a nitrogen environment and small volumes of the stock solution were removed for spin coating under ambient conditions. SWCNTs were purchased from Raymor Nanointegris (D = 1.5 nm). The SWCNTs were selectively wrapped with a PCF polymer and dispersed in toluene following a previously reported procedure to create semiconducting enriched single walled carbon nanotube dispersion.[31] The concentration of the sc-SWCNTs was adjusted so that then 957 nm peak had an absorbance of 2.0 a.u via UV-Vis spectroscopy.

Thin film Characterization

Both the dispersive (γ^d) and the polar component (γ^p) of the surface energies were calculated using a system of two equations where a curve fitting was used to measure contact

angles from images of the drops. These equations have the same form as shown in equation 5.2 and are solved simultaneously with the contact angles of diidomethane and distilled water. [32]

$$1 + \cos\theta = \frac{2(\gamma_s^d)^{\frac{1}{2}}(\gamma_{lv}^d)^{\frac{1}{2}}}{\gamma_{lv}} + \frac{2(\gamma_s^p)^{\frac{1}{2}}(\gamma_{lv}^p)^{\frac{1}{2}}}{\gamma_{lv}} \qquad Eq\ 5.2$$

For equation 5.2, γ_{lv}^d and γ_{lv}^p are the liquid dispersive and polar components for the surface energy of the reference liquid with γ_{lv} being the total surface energy of the reference liquid, cosθ is the contact angle for the distilled water or diidomethane, The surface energy is calculated as the sum of the polar and dispersive components. The following parameters are known for diidomethane: $\gamma_{lv}^d = 49.5\, mJ/m^2$, $\gamma_{lv}^p = 1.3\, mJ/m^2$ and $\gamma_{lv} = 50.8\, mJ/m^2$. Next, these are the known parameters for distilled water: $\gamma_{lv}^d = 21.8\, mJ/m^2$, $\gamma_{lv}^p = 51.0\, mJ/m^2$ and $\gamma_{lv} = 72.8\, mJ/m^2$.[32–34]

A Bruker dimension Icon was used to perform atomic force microscopy images with ScanAsyst tips while using the ScanAsyst mode. The images were flattened and cleaned up using the Bruker Nanoscope software.

Metal-insulator-metal capacitor fabrication and characterization

MIM capacitors were fabricated using 1 in^2 glass substrates that were purchased from University Wafers. The glass substrates were cleaned using a 4-step cleaning procedure where the substrates were sonicated for 5 minutes while immersed in detergent, distilled water, acetone and methanol sequentially. Next, the substrates were dried using a stream of nitrogen. Both a 5 nm layer of chromium (0.5 Å/s) and a 50 nm layer of gold (1 A/s) were then deposited on to the substrates using a shadow mask and PVD. The PVD system was built by Angstrom Engineering. The PLA for the tri-layer capacitors and PVA for the bilayer devices was then deposited onto the patterned substrates through spin coating. The PLA solution was statically dispensed onto the substrate and spun at 2000 RPM for 90s under ambient conditions. Next the PVAc dispersion was dynamically spun on top of the PLA layer at 2000 RPM for 90s under ambient conditions. For the bilayer dielectrics the PVAc suspension was spun dynamically onto the patterned substrate at 2000 RPM for 90s. Both the substrate/PLA/PVAc and substrate/PVAc films were then annealed under vacuum at 150 °C for 1h to remove any excess moisture within the PVAc. Next the TPCL layer was statically dispensed on top of the PVAc layer for both the bi and tri-

layer devices. The TPCL layer was spun at 2000 RPM for 90s and annealed under vacuum at 200 °C for 15 minutes to crosslink the TPCL with the PVAc film. The top electrode (Au, 50nm, 1 Å/s) was then deposited above of the TPCL films using a shadow mask and PVD. This yielded 10 individual MIM capacitors per substrates with areas from 0.35-2.88 mm^2.

The dielectric properties of the fabricated MIM capacitors were then characterised using impedance spectroscopy. A Methrohm PGSTAT204 was used to perform potentiostatic impedance measurements with a 10mv amplitude within the range of 10^{-1} to 10^5 Hz. The κ as well as the c_i in relation to frequency was then calculated using the potentiostatic measurements and the following equations.

$$\kappa = \frac{t}{\omega A \varepsilon_0} \frac{Z''}{Z''^2 + Z'^2} \qquad Eq\ 5.3$$

$$C_i = \frac{\kappa \varepsilon_0}{t} \qquad Eq\ 5.4$$

In the above equations t represents the dielectric thickness, ω the angular frequency, A the surface area, ε_0 the permittivity of vacuum, Z" the imaginary portion of the impedance and Z' the real portion of the impedance.

OTFT fabrication and characterization

OTFTs were fabricated on 15 X 20 mm quartz coated glass substrates purchased from Ossila. The substrates were cleaned using a 4-step cleaning procedure where the substrates were immersed in detergent, distilled water, acetone, and methanol. For each step the substrates are sonicated for 5 minutes then dried under a stream of nitrogen. Next the bottom source drain electrodes (Cr 5nm 0.5 Å/s, Au 50nm, 1 Å/s) were deposited onto the substrates through a shadow mask by PVD. The patterned substrates were rinsed with distilled water and isopropyl alcohol, dried under nitrogen and plasma treated for 15 minutes. The substrates were then submerged in a 1% solution of toluene and OTS at 70 °C overnight. Once the OTS reaction was completed the substrates were rinsed with toluene, dried with nitrogen and annealed under vacuum at 100 °C for 1 h. With the OTS surface treatment complete the sc-SWCNTs were deposited onto the surface using a Musashi SHOT mini 200Sx (dispenser: Nano Master SMP-III) drop casting machine. 0.2 μL drops were deposited between the source drain electrodes. The

substrates were then rinsed at a 45° angle 4 times with 1 ml of toluene and dried under nitrogen to remove any excess unbound polymer. Following the sc-SWCNT deposition the bi and tri-layer dielectrics were deposited through spin coating techniques using the same procedure as the MIM fabrication section. Finally, the gate electrode (Au, 50nm, 1 Å/s) was deposited on top of the TPCL dielectric through a shadow mask using PVD. This yielded 20 OTFTs per substrates (W = 1000 μm and L = 30 μm).

The fabricated OTFTs were then tested on a custom testing station built by Element Instrumentation inc. and Kreus Design (oesProbe A10000-P290) using a Keithley 2614B and a custom labview software. All the output and transfer characteristics of the fabricated OTFTs were tested under ambient conditions and their transfer characteristics were measured in the linear regime. The following equations were used for the calculation of V_T and g_m

$$g_m = \frac{dI_{SD}}{dV_{GS}} \qquad Eq\ 5.5$$

$$V_T = V_{GS}(x\text{-}intercept) - \frac{V_{SD}}{2} \qquad Eq\ 5.6$$

V_{GS} and V_{SD} are the gate-source and the source-drain voltages, c_i is the capacitance density, L is the channel Length and W is the channel width.

Statistical analysis

The capacitance density is averaged over 20 functioning capacitors per conditions and the standard deviation is shown as a semi-transparent line around the average for both bi and tri-layer devices. The OTFT properties are characterized over 30-40 functioning OTFTs per condition. The OTFTs are measured 3 times and each time the μ, gm, V_T and $I_{on/off}$ are collected or calculated for each run. The average values are shown with their standard deviation. The transfer and output curves are representative curves of a thin film transistor with performance close to the average for both the bi and tri-layer devices.

5.6 Acknowledgement

This work was supported by the NSERC Green Electronics Network (GreEN) (grant number: NETGP 508526-17) and NSERC CGS to M.T. We thank Prof. Alex Adronov (McMaster University) for providing the PCPF polymer.

5.7 Supporting information

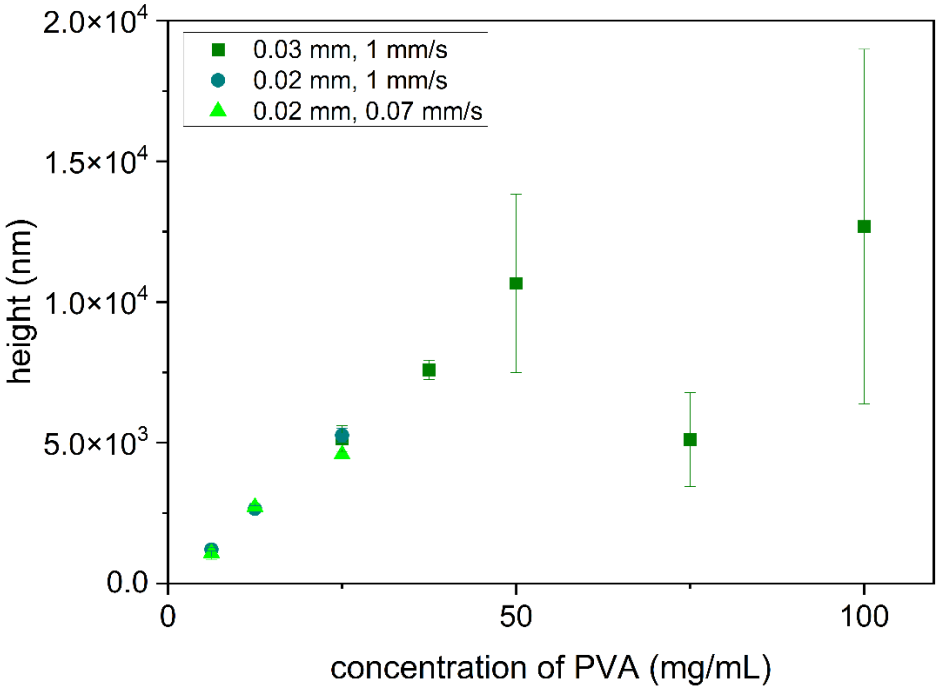

Figure 5.6. Thickness dependence on concentration for PVA blade coated on PLA using various blade heights and speeds.

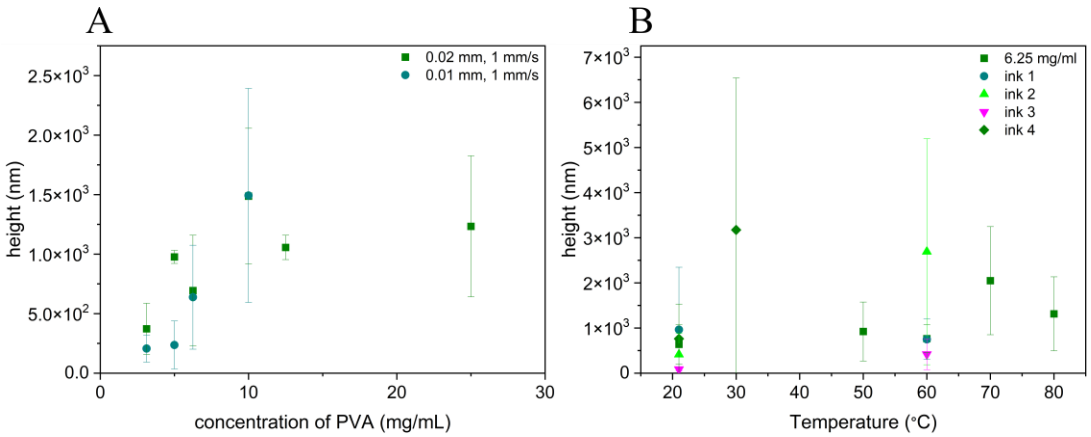

Figure 5.7. A) Thickness dependence on concentration for PVA blade coated on silver using various blade heights and speeds. B) Thickness dependence of PVA inks blade coated on silver at various temperatures.

Table 5.4. Different PVA ink formulations used to optimize the blade coating of PVA on silver.

Ink number	PVA in DI		Co-solvent 1	Co-solvent 2	Ink volume
	Volume	concentration			
1	2 mL	12.5 mg/mL	0.5 mL IPA	0.5 mL toluene	3 mL
2	6.154 mL	10 mg/mL	2.011 mL IPA	1.825 mL toluene	9.9 mL
3	5.152 mL	10 mg/mL	2.542 mL IPA	2.307 mL toluene	10.001 mL
4	750 µL	5 mg/mL	250 µL acetone		1 mL

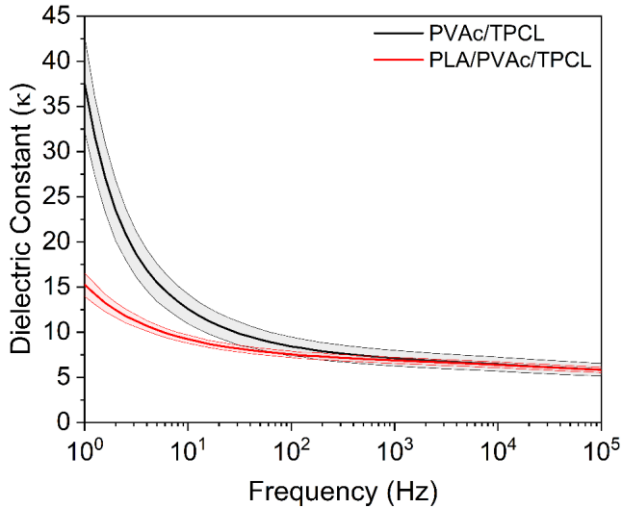

Figure 5.8. Frequency dependant effective dielectric constant for PVAc/TPCL and PLA/PVAc/TPCL. The transparent areas around the lines represent the standard deviation.

Equation 5.7 was used to correct for the capacitance based on the linear density of the SWCNTs.

$$C_{Cyl} = \frac{\Lambda_0^{-1}}{\left\{C_Q^{-1} + \frac{1}{2\pi\kappa\varepsilon_0} \ln\left[\frac{\Lambda_0}{R\pi} \sinh\left(\frac{2\pi t}{\Lambda_0}\right)\right]\right\}} \qquad Eq\ 5.7$$

Within **equation 5.7** K is the dielectric constant, ε_0 is the permittivity of vacuum, C_Q is the quantum capacitance, t is the dielectric thickness and Λ_0^{-1} is the linear density estimated using a custom computer vision software with an average value of 14.3 μm^{-1}, **Figure 5.9**.

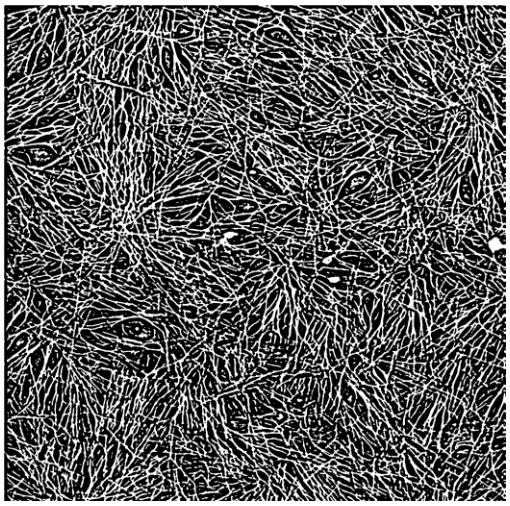

Figure 5.9. Segmented SWCNT image on OTS treated quartz coated glass used with a custom computer program to calculate the linear density.

Table 5.5. N-type μ estimates calculated using the linear density model by Cao et al.

Dielectric Material	Estimated n-type mobility [cm^2/Vs]
PVAc/TPCL	102.8 ± 22.1
PLA/PVAc/TPCL	130.2 ± 40.1

5.8 References

1. Wiklund, J. *et al.* A Review on Printed Electronics: Fabrication Methods, Inks, Substrates, Applications and Environmental Impacts. *J. Manuf. Mater. Process.* **5**, 89 (2021).

2. Wang, X. *et al.* Large-Area Flexible Printed Thin-Film Transistors with Semiconducting Single-Walled Carbon Nanotubes for NO2 Sensors. *ACS Appl. Mater. Interfaces* **12**, 51797–51807 (2020).

3. Comeau, Z. J. *et al.* On-the-Spot Detection and Speciation of Cannabinoids Using Organic Thin-Film Transistors. *ACS Sensors* (2019) doi:10.1021/acssensors.9b01150.

4. Fattori, M. *et al.* A Fully-Printed Organic Smart Temperature Sensor for Cold Chain Monitoring Applications. in *2020 IEEE Custom Integrated Circuits Conference (CICC)* vols 2020-March 1–4 (IEEE, 2020).

5. Zhu, C., Wu, H. C., Nyikayaramba, G., Bao, Z. & Murmann, B. Intrinsically Stretchable Temperature Sensor Based on Organic Thin-Film Transistors. *IEEE Electron Device Lett.* **40**, 1630–1633 (2019).

6. Sung, S. *et al.* Large-area printed low-voltage organic thin film transistors: Via minimal-solution bar-coating. *J. Mater. Chem. C* **8**, 15112–15118 (2020).

7. Nketia-Yawson, B. & Noh, Y.-Y. Recent Progress on High-Capacitance Polymer Gate Dielectrics for Flexible Low-Voltage Transistors. *Adv. Funct. Mater.* **28**, 1802201 (2018).

8. Lei, T. *et al.* Low-voltage high-performance flexible digital and analog circuits based on ultrahigh-purity semiconducting carbon nanotubes. *Nat. Commun.* **10**, 2161 (2019).

9. Lefebvre, J. *et al.* High-Purity Semiconducting Single-Walled Carbon Nanotubes: A Key Enabling Material in Emerging Electronics. *Acc. Chem. Res.* **50**, 2479–2486 (2017).

10. Chung, S., Cho, K. & Lee, T. Recent Progress in Inkjet-Printed Thin-Film Transistors. *Adv. Sci.* **6**, 1801445 (2019).

11. Heimfarth, D. *et al.* Enhancing Electrochemical Transistors Based on Polymer-Wrapped (6,5) Carbon Nanotube Networks with Ethylene Glycol Side Chains. *ACS Appl. Mater. Interfaces* **14**, 8209–8217 (2022).

12. Li, Q. *et al.* Designing hybrid gate dielectric for fully printing high-performance carbon nanotube thin film transistors. *Nanotechnology* **28**, (2017).

13. Lopinski, G. *et al.* Cyanoethylated pullulan as a high-k solution processable polymer gate dielectric for SWCNT TFTs. *Org. Electron.* **42**, 329–336 (2017).

14. Nawaz, A. & Hümmelgen, I. A. Poly(vinyl alcohol) gate dielectric in organic field-effect transistors. *J. Mater. Sci. Mater. Electron.* **30**, 5299–5326 (2019).

15. TEJA KARRI, B. R. & GUPTA, N. Hybrid bilayer gate dielectric-based organic thin film transistors. *Bull. Mater. Sci.* **42**, 2 (2019).

16. Wang, B. *et al.* High- k Gate Dielectrics for Emerging Flexible and Stretchable Electronics. *Chem. Rev.* **118**, 5690–5754 (2018).

17. Lee, S. H., Kim, D. Y. & Noh, Y. Y. Solution-processed polymer-sorted semiconducting

carbon nanotube network transistors with low- k/high- k bilayer polymer dielectrics. *Appl. Phys. Lett.* **111**, (2017).

18. Tousignant, M. N. *et al.* High Performance Organic Electronic Devices Based on a Green Hybrid Dielectric. *Adv. Electron. Mater.* **7**, 2100700 (2021).

19. She, X.-J., Liu, J., Zhang, J.-Y., Gao, X. & Wang, S.-D. Operational stability enhancement of low-voltage organic field-effect transistors based on bilayer polymer dielectrics. *Appl. Phys. Lett.* **103**, 133303 (2013).

20. Zhang, H. *et al.* Solution-processed organic field-effect transistors with cross-linked poly(4-vinylphenol)/polyvinyl alcohol bilayer dielectrics. *Appl. Surf. Sci.* **478**, 699–707 (2019).

21. Yang, F. Y., Chang, K. J., Hsu, M. Y. & Liu, C. C. Low-operating-voltage polymeric transistor with solution-processed low-k polymer/high-k metal-oxide bilayer insulators. *Org. Electron.* **9**, 925–929 (2008).

22. Faraji, S., Hashimoto, T., Turner, M. L. & Majewski, L. A. Solution-processed nanocomposite dielectrics for low voltage operated OFETs. *Org. Electron.* **17**, 178–183 (2015).

23. Rullyani, C., Ramesh, M., Sung, C.-F., Lin, H.-C. & Chu, C.-W. Natural polymers for disposable organic thin film transistors. *Org. Electron.* **54**, 154–160 (2018).

24. Ronnasi, B., Tousignant, M. & Lessard, B. H. Chitosan based dielectrics for use in single walled carbon nanotube-based thin film Transistors. *J. Mater. Chem. C* (2023) doi:10.1039/D2TC04458G.

25. Melville, O. A., Rice, N. A., Therrien, I. & Lessard, B. H. Organic thin-film transistors incorporating a commercial pigment (Hostasol Red GG) as a low-cost semiconductor. *Dye. Pigment.* **149**, 449–455 (2018).

26. Subbarao, N. V. V., Gedda, M., Iyer, P. K. & Goswami, D. K. Organic field-effect transistors as high performance humidity sensors with rapid response, recovery time and remarkable ambient stability. *Org. Electron.* **32**, 169–178 (2016).

27. Subbarao, N. V. V., Mandal, S., Gedda, M., Iyer, P. K. & Goswami, D. K. Effect of temperature on hysteresis of dipolar dielectric layer based organic field-effect transistors: A temperature sensing mechanism. *Sensors Actuators, A Phys.* **269**, 491–499 (2018).

28. Mattana, G., Briand, D., Marette, A., Vásquez Quintero, A. & de Rooij, N. F. Polylactic acid as a biodegradable material for all-solution-processed organic electronic devices. *Org. Electron.* **17**, 77–86 (2015).

29. Malinconico, M. *et al.* Blends of polyvinylalcohol and functionalised polycaprolactone. A study on the melt extrusion and post-cure of films suitable for protected cultivation. *J. Mater. Sci.* **37**, 4973–4978 (2002).

30. Tousignant, M. N. *et al.* Improving Thin-Film Properties of Poly(vinyl alcohol) by the Addition of Low-Weight Percentages of Cellulose Nanocrystals. *Langmuir* **36**, 3550–3557 (2020).

31. Rice, N. A. *et al.* Organic Thin Film Transistors: Polycarbazole-Sorted Semiconducting Single-Walled Carbon Nanotubes for Incorporation into Organic Thin Film Transistors. *Adv. Electron. Mater.* **5**, 1970002 (2019).

32. Owens, D. K. & Wendt, R. C. Estimation of the surface free energy of polymers. *J. Appl. Polym. Sci.* **13**, 1741–1747 (1969).

33. Umeda, T., Kumaki, D. & Tokito, S. Surface-energy-dependent field-effect mobilities up to 1 cm2/V s for polymer thin-film transistor. *J. Appl. Phys.* **105**, 024516 (2009).

34. Zhao, C., Li, A., Chen, X., Ali, M. U. & Meng, H. Hysteresis effect in organic thin film transistors based on naphthalene tetracarboxylic diimide derivatives. *Appl. Phys. Lett.* **118**, 193302 (2021).

35. Amin, E. M., Karmakar, N. C. & Winther-Jensen, B. Polyvinyl-Alcohol (Pva)-Based RF Humidity Sensor in Microwave Frequency. *Prog. Electromagn. Res. B* **54**, 149–166 (2013).

36. Tsai, T.-D., Chang, J.-W., Wen, T.-C. & Guo, T.-F. Manipulating the Hysteresis in Poly(vinyl alcohol)-Dielectric Organic Field-Effect Transistors Toward Memory Elements. *Adv. Funct. Mater.* **23**, 4206–4214 (2013).

37. Tousignant, M. N. *et al.* Improving Thin-Film Properties of Poly(vinyl alcohol) by the Addition of Low-Weight Percentages of Cellulose Nanocrystals. *Langmuir* **36**, (2020).

38. Tousignant, M. N., Lin, Z. S., Brusso, J. & Lessard, B. H. Interfacial Ultraviolet Cross-Linking of Green Bilayer Dielectrics. *ACS Appl. Mater. Interfaces* **15**, 3680–3688 (2023).

39. Li, Z., Ding, J., Lefebvre, J. & Malenfant, P. R. L. Surface effects on network formation of conjugated polymer wrapped semiconducting single walled carbon nanotubes and thin film transistor performance. *Org. Electron.* **26**, 15–19 (2015).

40. Mirka, B. *et al.* Excess Polymer in Single-Walled Carbon Nanotube Thin-Film Transistors: Its Removal Prior to Fabrication Is Unnecessary. *ACS Nano* **15**, 8252–8266 (2021).

41. Li, H. & Zhou, L. Effects of Ambient Air and Temperature on Ionic Gel Gated Single-Walled Carbon Nanotube Thin-Film Transistor and Circuits. *ACS Appl. Mater. Interfaces* **7**, 22881–22887 (2015).

42. Brownlie, L. & Shapter, J. Advances in carbon nanotube n-type doping: Methods, analysis and applications. *Carbon N. Y.* **126**, 257–270 (2018).

43. Mirka, B. *et al.* Polyfluorene-Sorted Semiconducting Single-Walled Carbon Nanotubes for Applications in Thin-Film Transistors. *Chem. Mater.* **31**, 2863–2872 (2019).

44. Timmermans, M. Y. *et al.* Effect of carbon nanotube network morphology on thin film transistor performance. *Nano Res.* **5**, 307–319 (2012).

45. Song, Y., Premachandran Nair, R., Zou, M. & Wang, Y. A. Adhesion and friction properties of micro/nano-engineered superhydrophobic/hydrophobic surfaces. *Thin Solid Films* **518**, 3801–3807 (2010).

46. Lugscheider, E. & Bobzin, K. The influence on surface free energy of PVD-coatings. *Surf. Coatings Technol.* **142**–**144**, 755–760 (2001).

47. Yip, H. L. & Jen, A. K. Y. Recent advances in solution-processed interfacial materials for efficient and stable polymer solar cells. *Energy Environ. Sci.* **5**, 5994–6011 (2012).

48. Zhang, H. *et al.* High-Performance Carbon Nanotube Complementary Electronics and

Integrated Sensor Systems on Ultrathin Plastic Foil. *ACS Nano* **12**, 2773–2779 (2018).

49. Lockhart De La Rosa, C. J. *et al.* Highly efficient and stable MoS2 FETs with reversible n-doping using a dehydrated poly(vinyl-alcohol) coating. *Nanoscale* **9**, 258–265 (2017).

50. Kim, S., Baek, G. W., Jeong, J., Seo, S. G. & Jin, S. H. Scalable and selective N-type conversion for carbon nanotube transistors via patternable polyvinyl alcohol stacked with hydrophobic layers and their application to complementary logic circuits. *J. Mater. Res. Technol.* **12**, 243–256 (2021).

51. Zorn, N. F. & Zaumseil, J. Charge transport in semiconducting carbon nanotube networks. *Appl. Phys. Rev.* **8**, (2021).

52. Kim, W. *et al.* Hysteresis Caused by Water Molecules in Carbon Nanotube Field-Effect Transistors. *Nano Lett.* **3**, 193–198 (2003).

53. Aguirre, C. M. *et al.* The Role of the Oxygen/Water Redox Couple in Suppressing Electron Conduction in Field-Effect Transistors. *Adv. Mater.* **21**, 3087–3091 (2009).

54. Su, Y. *et al.* Low-Voltage Organic Field-Effect Transistors (OFETs) with Solution-Processed Metal-Oxide as Gate Dielectric. 4662–4667 (2011).

55. Subbarao, N. V. V, Gedda, M., Iyer, P. K. & Goswami, D. K. Enhanced environmental stability induced by effective polarization of a polar dielectric layer in a trilayer dielectric system of organic field-effect transistors: A quantitative study. *ACS Appl. Mater. Interfaces* **7**, 1915–1924 (2015).

Chapter 6 : Conclusion and Recommended Future work

6.1 Overall Conclusion

Designing new materials and techniques that can be used to fabricate environmentally friendly printed electronics is necessary for the continued growth of this field. Ideally the materials need to be sustainable and available on the ton scale which is necessary for mass production. Developing strategies that utilize already available commercial polymers that are environmentally friendly and high performance is an effective way to enable sustainable electronics. This thesis explored strategies that enable sustainable green electronics through the combination of commercially available polymers and simple chemistry to provide robust, high-performance electronics.

Chapter 2 investigated the use of CNCs as an environmentally friendly additive to increase the viscosity of PVA solutions. I demonstrated that the addition of low weight percentages of CNCs could lead to a significant increase in viscosity. This improved the deposition of these thin polymer films without negatively impacting the performance of PVA as a dielectric material in both capacitors and OTFTs.

Chapter 3 built on the findings of Chapter 2 as we tried to determine a way to improve the semiconductor/dielectric interface and reduce the moisture sensitivity of PVAc. By using the combination of a low-*k* PCL material with the high-*k* PVAc it was possible to take advantage of the improve semiconductor/dielectric interface caused by the low-*k* PCL layer while still taking advantage of the high capacitance of the PVAc layer. Further by functionalizing the end groups of the PCL polymer it was possible to thermally crosslink the PCL at the PVAc/PCL interface allowing for further orthogonal processing and encapsulating the PVAc layer protecting it from moisture. However, the thermally activated reaction was sensitive to moisture in the ambient environment limiting the shelf life and stability of the unreacted polymer.

Chapter 4 was used to address these issues from Chapter 3. We investigated the use of UV crosslinking end units as an alternative to the thermally activated end units. The advantage of the UV end units is that if the undissolved polymer is stored in an opaque container it remains stable and unreacted even under ambient conditions. Further, many flexible substrates have low melting points limiting the use of thermally activated reactions and many printing processes

already use UV curing systems alleviating the need for modifications to the existing printing infrastructure. This chapter compared the use of both TPCL/PVAc and UV-PCL/PVAc bilayer dielectrics in capacitors and OTFTs. The findings demonstrate that both the TPCL and UV-PCL devices have similar performance meaning that UV-PCL can be used as an effective alternative to TPCL for PCL/PVAc bilayer systems.

Chapter 5 focused on the interactions between the previously optimized dielectrics systems and hydrophobic OTS treated surfaces. PLA was investigated as an additional layer between the SWCNTs and PVAc in the fabrication of tri-layer dielectric OTFTs. PLA demonstrated improved adhesion to OTS treated substrates when compared to PVAc allowing for a larger number of functioning OTFTs. The PLA layer also works as a low-*k* layer between the SWCNTs and PVAc improving the semiconductor/dielectric interface and in turn the OTFT performance. In this work we demonstrate that higher SWCNT densities could be achieved by changing the OTFT architecture and the use of a low-*k* PLA layer could be used to improve surface adhesion and OTFT performance.

To summarize, the use of both blending and stacking dielectric materials can be used to improve the dielectric and physical properties of already commercially available and mass produced PVA. These studies have demonstrated that the viscosity can be adjusted to accommodate various fabrication techniques and low-*k* polymer layer can be added to reduce the impact of moisture and improve the interface between the dielectric and the semiconductor. Further, matching the surface energies can help improve the film adhesion for use on various substrates. This thesis demonstrates the application of these techniques and how they can be used to incorporate already mass produced environmentally friendly polymer dielectrics into printed electronic applications.

6.2 Recommendation for Future Work

This thesis has demonstrated techniques that can be used to improve the performance of PVA. However, there is still a lot of optimization work that needs to be performed to improve both the performance and printability of PVA. For example, when blade coating PVAc our group has noticed that it has a strong coffee ring effect which led to poor film uniformity. These findings demonstrate that our PVAc system can still be improved to help with film uniformity when using techniques such as blade coating, screen printing and inkjet printing. To improve the

uniformity of these films techniques have been used such as increasing the boiling point and viscosity of the solvent, reducing the substrate temperature and gelling the polymer.[1] Although the addition of 0.75 wt% CNCs into the PVA dispersion provided enough of an increase in viscosity for spin coating, I believe further work can be done to optimize the viscosity of PVA for other printing techniques. For example, higher weight percentages of CNCs could be added into the PVA solution to further gel the PVA and help mitigate coffee ring effects or cooling the substrate could be investigated as a method to improve thin film deposition.

Apart from the addition of CNCs other techniques could be investigated to improve both the electrical properties and increase the viscosity of the PVA solutions. This could be done through the addition of various salts. One example is the addition of NaCl to PVA. At low concentration NaCl will increase the viscosity of PVA and have a gelling effect which could be used to help reduce the coffee ring effect and improve thin film uniformity.[2] Further the addition of NaCl will allow an EDL to form within the PVA film and increase the capacitance. Usually, this would also have the draw back of allowing the Na^+ and Cl^- ions to diffuse and interact with the semiconductor. However, using these films in combination with TPCL and PLA in a bi or tri-layer stacked dielectric would allow for the PVA/NaCl blend to be fully encapsulated and protected from interacting with the semiconductor. This could have the potential to further improve the thin film uniformity of PVA when deposited using printing techniques as well as increase the total capacitance of the dielectric system, improving OTFT performance.

On a similar note, metallic nanoparticles could be used as an additive for increased dielectric performance. For example, Zinc oxide (ZnO) has been shown to increase the dielectric constant and capacitance of PVA.[3] ZnO nanoparticles have also been blended with PVA to create UV and oxygen blocking films for food packaging.[4] These films are biodegradable and increased the shelf life of the products. This demonstrates that the addition of ZnO has a positive impact on both the packaged product and the dielectric properties for PVA films. When building sensors into product packaging the substrate itself can also be used as the dielectric layer. However, for native PVA this can pose an issue because the thickness of the product packaging leads to a significant decrease in capacitance and performance. By using ZnO metallic nanoparticles it could be possible to circumvent this issue allowing for thicker high capacitance films where the plastic packaging also acts as the dielectric. This is an example of a way that

ZnO could be used to improve the performance of PVA as a biodegradable substrate/dielectric for smart packaging in the food and beverage industry. Further, TPCL could also be added as a layer in this system allowing for a reduction in moisture sensitivity and permittivity, further improving these films for product packaging applications.

Finally, PVA itself also has the potential to be used in the fabrication of fully biodegradable temperature sensors. There have been studies that have demonstrated that PVA has a temperature response when used in both capacitors and transistors.[5,6] This response has been amplified within literature using both metallic nanoparticle blends or semiconductors. Therefore, SWCNTs could be used to amplify a temperature response from native or blended PVA. Using these techniques, we could fabricate fully biodegradable temperature sensors for product packaging or biosensing applications.

6.3 References

1. Yu, X. *et al.* To inhibit coffee ring effect in inkjet printing of light-emitting polymer films by decreasing capillary force. *Chinese Chem. Lett.* **30**, 135–138 (2019).

2. Briscoe, B. & Luckham, P. The effects of hydrogen bonding upon the viscosity of aqueous poly(vinyl alcohol) solutions. *Polymer (Guildf).* **41**, 3851–3860 (2000).

3. Sugumaran, S. *et al.* Novel hybrid PVA-InZnO transparent thin films and sandwich capacitor structure by dip coating method: Preparation and characterizations. *RSC Adv.* **5**, 10599–10610 (2015).

4. Channa, I. A. *et al.* UV Blocking and Oxygen Barrier Coatings Based on Polyvinyl Alcohol and Zinc Oxide Nanoparticles for Packaging Applications. *Coatings* **12**, (2022).

5. Kim, S. W. *et al.* Encapsulation of polyvinyl alcohol based flexible temperature sensor through spatial atmospheric atomic layer deposition system to enhance its lifetime. *Thin Solid Films* **673**, 44–51 (2019).

6. Subbarao, N. V. V., Mandal, S., Gedda, M., Iyer, P. K. & Goswami, D. K. Effect of temperature on hysteresis of dipolar dielectric layer based organic field-effect transistors: A temperature sensing mechanism. *Sensors Actuators, A Phys.* **269**, 491–499 (2018).

Chapter 7 : Additional Contributions

During my graduate I was involved in many other projects where I performed AFM imaging, device fabrication and characterization or complete studies. The following list summarizes the additional first author and non-first author publications I contributed towards during my PhD.

7.1 Contact Engineering Using Manganese, Chromium, and Bathocuproine in Group 14 Phthalocyanine Organic Thin-Film Transistors.

Owen A. Melville, Trevor M. Grant, Kate Lochhead, Benjamin King, Ryan Ambrose, Nicole A. Rice, Nicholas T. Boileau, Alexander J. Peltekoff, Mathieu Tousignant, Ian G. Hill, and Benoît H. Lessard*

Publication date: March 20th 2020
Citation: ACS Appl. Electron. Mater. 2020, 2, 5, 1313–1322
DOI: https://doi.org/10.1021/acsaelm.0c00104

Abstract

Silicon and tin(IV) phthalocyanines, which have been demonstrated as simple-to-synthesize materials for n-type organic thin-film transistors (OTFTs), have relatively shallow lowest unoccupied molecular orbital (LUMO) levels that create a Schottky barrier with the gold source–drain contacts typically used in device fabrication. To reduce the contact resistance (RC) associated with this barrier and improve the OTFT performance, we fabricated bottom-gate top-contact (BGTC) devices using low-work-function metals (Mn/Cr) and an electron dopant material (bathocuproine, BCP) as contact interlayers. We characterized two tin phthalocyanines (SnPcs), tin bis(pentafluorophenoxy)phthalocyanine (F10-SnPc) and tin bis(2,4,6-trifluorophenoxy)phthalocyanine (246F-SnPc), as organic semiconductors (OSCs) and compared them to their silicon phthalocyanine (SiPc) analogues. We found that using Mn and Cr interlayers with SiPc OTFTs reduces RC to as low as 11.8 kΩ cm and reduces the V_T to as low as 7.8 V while improving linear region characteristics compared to devices using silver or gold electrodes only. BCP interlayers appear to reduce V_T in all SiPc and SnPc devices and increase the off-state conductivity of SnPc devices if covering the entire OSC. Overall, this work demonstrates the potential for metal interlayers and solid-state organic interlayers for improving electron transport in low-cost, n-type OTFTs using group 14 phthalocyanines.

Contribution

I aided in the fabrication and Characterization of some of the thin film transistors and helped review the final manuscript before submission.

7.2 Controlled synthesis of poly(pentafluorostyrene-ran-methyl methacrylate) copolymers by nitroxide mediated polymerization and their use as dielectric layers in organic thin-film transistors.

A.J. Peltekoff, M.N. Tousignant, V.E. Hiller, O.A. Melville, B.H. Lessard
Publication date: May 29th 2020
Citation: Polymers (Basel). 12 (2020)
DOI: https://doi.org/10.3390/polym12061231

Abstract

A library of statistically random pentafluorostyrene (PFS) and methyl methacrylate (MMA) copolymers with narrow molecular weight distributions was produced, using nitroxide mediated polymerization (NMP) to study the effect of polymer composition on the performance of bottom-gate top-contact organic thin-film transistors, when utilized as the dielectric medium. Contact angle measurements confirmed the ability to tune the surface properties of copolymer thin films through variation of its PFS/MMA composition, while impedance spectroscopy determined the effect of this variation on dielectric properties. Bottom-gate, top-contact copper phthalocyanine (CuPc) based organic thin-film transistors were fabricated using the random copolymers as a dielectric layer. We found that increasing the PFS content led to increased field-effect μ, until a point after which the CuPc no longer adhered to the polymer dielectric.

Contribution

I deposited the CuPc semiconductor on various PFS/MMA surfaces to perform X-ray diffraction measurements, I fabricated and characterized the metal insulator metal capacitors, I fabricated and characterized the organic thin film transistors. I helped interpret the collected capacitor and OTFT data and reviewed the prepared manuscript.

7.3 1,2,3-triazole based poly(ionic liquids) as solid dielectric materials.

Brendan Mirka, Nicole A Rice, Phillip Williams, Mathieu N Tousignant, Nicholas T Boileau, William J Bodnaryk, Darryl Fong, Alex Adronov, Benoît H Lessard
Publication date: April 8th 2021
Citation: ACS Nano 2021, 15, 5, 8252–8266
DOI: https://doi.org/10.1021/acsnano.0c08584

Abstract

Ultrapure semiconducting single-walled carbon nanotube (sc-SWNT) dispersions produced through conjugated polymer sorting are ideal candidates for the fabrication of solution-processed organic electronic devices on a commercial scale. Protocols for sorting and dispersing ultrapure sc-SWNTs with conjugated polymers for thin-film transistor (TFT) applications have been well refined. Conventional wisdom dictates that removal of excess unbound polymer through filtration or centrifugation is necessary to produce high-performance TFTs. However, this is time-consuming, wasteful, and resource-intensive. In this report, we challenge this paradigm and demonstrate that excess unbound polymer during semiconductor film fabrication is not necessarily detrimental to device performance. Over 1200 TFT devices were fabricated from 30 unique polymer-sorted SWNT dispersions, prepared using two different alternating copolymers. Detailed Raman spectroscopy, x-ray photoelectron spectroscopy (XPS), and atomic force microscopy (AFM) studies of the random-network semiconductor films demonstrated that a simple solvent rinse during TFT fabrication was sufficient to remove unbound polymer from the sc-SWNT films, thus eliminating laborious polymer removal before TFT fabrication. Furthermore, below a threshold polymer concentration, the presence of excess polymer during fabrication did not significantly impede TFT performance. Preeminent performance was achieved for devices prepared from native polymer-sorted SWNT dispersions containing the "original" amount of excess unbound polymer (immediately following enrichment). Lastly, we developed an open-source Machine Learning algorithm to quantitatively analyze AFM images of SWNT films for surface coverage, number of tubes, and tube alignment.

Contribution

I designed and fabricated a 3D printed drop casting aid that allowed for the authors to drop cast the SWCNTs by hand directly where the SD electrodes would later be deposited on the substrate. This aid led to a large increase in the number of functioning TFTs. I reviewed the prepared manuscript.

7.4 Excess Polymer in Single-Walled Carbon Nanotube Field-Effect Transistors: Does It Really Need to be Removed Prior to Fabrication?

Jukka Niskanen, Mathieu N. Tousignant, Alexander J. Peltekoff, Benoît H. Lessard
Publication date: October 12th 2021
Citation: Polymer Volume 212, 6 January 2021, 123144
DOI: https://doi.org/10.1016/j.polymer.2020.123144

Abstract

1,2,3-triazole based polyionic liquids (PIL) are an emerging field among polymeric dielectrics in organic electronics. 1,2,3-triazole based PILs can be obtained from poly(4-vinylbenzylchloride) by copper-catalyzed azide-alkyne cycloaddition (CuAAC) 'click' reaction. The polymer architecture and the charge of the PILs can be manipulated by choosing a suitable alkyne, azide containing moiety, and by the alkylation of the 1,2,3-triazole group. Thus, we were able to prepare PILs carrying either inorganic (Na+ or Cl−) or the organic counterions 1-butyl-3-methyl-imidazolium (C4mim+) or 1-butyl-3-methyl-imidazolium (TFSI−). Metal-insulator-metal capacitors were fabricated and the dielectric properties were characterized through electrochemical impedance spectroscopy. The PILs demonstrated an increase in capacitance density with decreasing frequency, characteristic for the polarization of the polymer layer and electrical double layer formation. Substitution of inorganic counterions with organic counterions improved the transition frequency of the capacitors and the conductivity of the polymers. This was due to increased ion mobility and decreased glass transition temperatures.

Contribution

I fabricated and characterized the metal insulator metal capacitors. I performed the conductivity measurements of the fabricated capacitors. I interpreted the capacitor and conductivity results and wrote the sections of the manuscript involving these results. I reviewed the prepared manuscript.

7.5 Improving Latex-Based Pressure-Sensitive Adhesive Properties Using Carboxylated Cellulose Nanocrystals.

Vida A. Gabriel, Mathieu N. Tousignant, Sean M.W. Wilson, Marie D.M. Faure, Emily D. Cranston, Michael F. Cunningham, Benoît H. Lessard, Marc A. Dubé
Publication date: December 27th 2021
Citation: Volume16, Issue 3, Special Issue: Green Macromolecular Reaction Engineering June 2022, 2100051
DOI: https://doi.org/10.1002/mren.202100051

Abstract

Cellulose nanocrystals (CNCs) are becoming a popular option when producing polymer nanocomposites because they are a green alternative to petroleum-based performance enhancers and provide significant matrix reinforcement at low loadings. DextraCel is a commercial grade CNC with carboxylate surface groups that can be dispersed in water without sonication. These carboxylated CNCs (cCNCs) can be incorporated in situ via seeded semi-batch emulsion polymerization to produce latexes for adhesive applications. The resulting nanocomposite films exhibit 26x higher peel strength, 4.5x higher tack, and 7.7x higher shear strength relative to base case films. Curiously, adhesives produced from latexes containing cCNCs that do not undergo ultrasonication display greater adhesive property improvements relative to films produced with cCNCs that are ultrasonicated. Atomic force microscopy images reveal that cCNCs have stronger self interactions than their sulfated CNCs counterparts; cCNCs display side-by-side and end-to-end association in films when they are not ultrasonicated, which increases their "apparent" aspect ratio—an important characteristic attributed to matrix reinforcement. Omitting ultrasonication preserves cCNC-cCNC interactions that cause them to behave like nanofibers rather than discrete nanocrystals; this allows them to display greater mechanical enhancements, similar to reinforcements provided by nanofibrils, without the technical challenges associated with producing composite latexes with nanofibrils.

Contribution

I performed all the atomic force microscopy imaging for this study. I processed and cleaned up the raw AFM images and helped with their interpretation. I reviewed the prepared manuscript.

7.6 Poly (ethylene glycol)-Based Poly (ionic liquid) Block Copolymers through 1, 2, 3-Triazole Click Reactions.

A.J. Peltekoff, M.N. Tousignant, V.E. Hiller, O.A. Melville, B.H. Lessard
Publication date: Febuary 7th 2022
Citation: ACS Appl. Polym. Mater. 2022, 4, 3, 1559–1564
DOI: https://doi.org/10.1021/acsapm.1c01678

Abstract

1,2,3-Triazolium-based polyionic liquids (PILs) were made by a copper-catalyzed azide–alkyne cycloaddition (CuAAC) “click” reaction from poly(4-vinylbenzyl chloride). The click reaction facilitates the design and manipulation of the polymer architecture by selecting the desired alkynes, the azide-containing moieties, and the alkylating group of the 1,2,3-triazole group. Using this versatile chemistry and design, we prepared PILs with comblike homo- and block copolymer architectures using bistrifluoromethanesulfonimidate (TFSI-) as counterions. The block copolymer self-assembles into an ordered morphology. The block copolymer was integrated into metal–insulator–metal capacitors and found to display a prominent electrical double layer when characterized by electrochemical impedance spectroscopy.

Contribution

I fabricated and characterized the metal insulator metal capacitors. I performed the conductivity measurements of the fabricated capacitors. I interpreted the capacitor and conductivity results and wrote the sections of the manuscript involving these results. I reviewed the submitted manuscript.

7.7 Poly (ionic liquid) Gating Materials for High-Performance Organic Thin-Film Transistors: The Role of Block Copolymer Self-Assembly at the Semiconductor Interface.

Samantha Brixi, Chase L Radford, Mathieu N Tousignant, Alexander J Peltekoff, Joseph G Manion, Timothy L Kelly, Benoît H Lessard

Publication date: August 23rd 2022
Citation: ACS Appl. Mater. Interfaces 2022, 14, 35, 40361–40370
DOI: https://doi.org/10.1021/acsami.2c07912

Abstract

The widespread realization of wearable electronics requires printable active materials capable of operating at low voltages. Polymerized ionic liquid (PIL) block copolymers exhibit a thickness-independent double-layer capacitance that makes them a promising gating medium for the development of organic thin-film transistors (OTFTs) with low operating voltages and high switching speed. PIL block copolymer structure and self-assembly can influence ion conductivity and the resulting OTFT performance. In an OTFT, self-assembly of the PIL gate on the semiconducting polymer may differ from bulk self-assembly, which would directly influence electrical double-layer formation. To this end, we used poly{[N,N′-bis(2-octyldodecyl)-naphthalene-1,4,5,8-bis(dicarboximide)-2,6-diyl]-alt-5,5′-(2,2′-bithiophene)} (P(NDI2OD-T2)) as a model semiconductor for our OTFTs, on which our PILs exhibited self-assembly. In this study, we explore this critical interface by grazing-incidence small-angle X-ray scattering (GISAXS) and atomic force microscopy (AFM) of P(NDI2OD-T2) and a series of poly(styrene)-b-poly(1-(4-vinylbenzyl)-3-butylimidazolium-random-poly(ethylene glycol) methyl ether methacrylate) (poly(S)-b-poly(VBBI+[X]-r-PEGMA)) block copolymers with varying PEGMA/VBBI+ ratios and three different mobile anions (where X = TFSI–, PF6–, or BF4–). We investigate the thin-film self-assembly of block copolymers as a function of device performance. Overall, a mixed orientation at the interface leads to improved device performance, while predominantly hexagonal packing leads to nonfunctional devices, regardless of the anion present. These PIL gated OTFTs were characterized with a threshold voltage below 1 V, making understanding of their structure–property relationships crucial to enabling the further development of high-performance gating materials.

Contribution

I characterized the various PILs using atomic force microscopy. I aided with the AFM interpretation and post processing of the raw AFM images. I reviewed the submitted manuscript.

7.8 Poly (ionic liquid) Dielectric for High performing P-and N-type Single Walled Carbon Nanotube Transistors.

Mathieu N Tousignant, May Ourabi, Jukka Niskanen, Brendan Mirka, William J Bodnaryk, Alex Adronov and Benoît H Lessard
Publication date: 29th May 2020
Citation: 2022 Flex. Print. Electron. 7 034004
DOI: 10.1088/2058-8585/ac928f

Abstract

There is an increasing demand for low-cost and high-performance electronics which has stimulated a need for new high-performance dielectric materials. We have developed a facile synthesis of poly(2-(methacryloyloxy)ethyl trimethylammonium bis(trifluoromethylsulfonyl)azanide-ran-methyl methacrylate) (P(METATFSI-MMA)), a polymeric ionic liquid that can be used as a high-performance dielectric for semiconducting single walled carbon nanotube (SWCNTs) thin film transistors (TFTs). The P(METATFSI-MMA) polymer was synthesized at both 35 and 62 mol% of 2-(methacryloyloxy)ethyl trimethylammonium bis(trifluoromethylsulfonyl)azanide and produced p- and n-type devices that functioned under ambient conditions. These TFTs were then used to study the impact of electrochemical doping on the performance of SWCNT TFTs when switching from n-type, where an electrical double layer is formed, to p-type, where the TFSI− anions are free to interact with the SWCNTs. The TFTs operating in p-type had higher current on/off ratios and a larger transconductance than those operating in n-type, which is characteristic of electrochemically doped transistors. Furthermore, we tested the impact of operating frequency on device performance and discovered that decreasing the operating frequency of the TFTs resulted in a decreased hysteresis. The decrease in hysteresis was also observed to be more significant for the 35 mol% polymer.

Contribution

I aided with the capacitor fabrication and characterization. I helped interpret the capacitor results. I fabricated and characterized the thin film transistors. I prepared the figures and wrote and reviewed the manuscript for this study.

7.9 From P-type to N-type: Peripheral Fluorination of Axially Substituted Silicon Phthalocyanines Enables Fine Tuning of Charge Transport.

Mário C. Vebber, Benjamin King, Callum French, Mathieu Tousignant, Bahar Ronnasi, Chloé Dindault, Guillaume Wantz, Lionel Hirsch, Jaclyn Brusso, Benoît H. Lessard
Publication date: January 15th 2023
Citation: Can J Chem Eng. 2023;1–13.
DOI: https://doi.org/10.1002/cjce.24843

Abstract

Silicon phthalocyanines (R2-SiPcs) are a family of promising tunable materials for organic electronic applications. We report the chemistry of the synthesis of axially substituted fluorinated SiPcs (tb-Ph)2-FxSiPc (where X = 0, 4, 8, or 16) and explore how the degree of fluorination effects optical and electronic properties. A new treatment with boron trichloride was included to obtain Cl2-FXSiPcs from F2-FXSiPcs, activating the axial position for further functionalization. We observed that as the degree of fluorination increased, so did the electron affinity of the compounds, leading to a drop in frontier orbital levels, as measured by electrochemistry and ultraviolet photoelectron spectroscopy (UPS). The deeper energy levels enabled successful (tb-Ph)2-F4SiPc and poly [[6,7-difluoro[(2-hexyldecyl)oxy]-[5,8-quinoxalinediyl]-2,5-thiophenediyl]] (PTQ10) blends for organic photovoltaics and photodetectors. All four compounds were incorporated in organic thin-film transistors (OTFTs), where the degree of fluorination influenced device operation, changing it from p-type conduction for (tb-Ph)2-F0SiPc, to ambipolar for (tb-Ph)2-F4SiPc, and n-type for (tb-Ph)2-F8SiPc and (tb-Ph)2-F16SiPc. The OTFT devices made with (tb-Ph)2-F16SiPc achieved a low average threshold voltage of 7.0 V in N2 and retained its n-type μ when exposed to air.

Contribution

I performed all the atomic force microscopy imaging for this study. I processed and cleaned up the raw AFM images and helped with their interpretation. I reviewed the prepared manuscript.

7.10 Chitosan based dielectrics for use in single walled carbon nanotube-based thin film Transistors.

Bahar Ronnasi, Mathieu N. Tousignanta and Benoît H. Lessard
Publication date: January 30th 2023
Citation: J. Mater. Chem. C, 2023,11, 3197-3205
DOI: https://doi.org/10.1039/D2TC04458G

Abstract

Chitosan, a sustainable biopolymer, is a naturally occurring solution processable polyelectrolyte that can form electrical double layers at high frequencies (<1 kHz) and can be integrated as the dielectric in metal–insulator–metal (MIM) capacitors and thin-film transistors (TFTs). In this study, we achieved capacitance densities as high as 11.1 nF mm−2 for the fabricated MIM capacitors. This was achieved through optimization of the chitosan content and the acid concentration of solutions during thin-film fabrication. We report the first chitosan-based TFT using semiconducting single-walled carbon nanotubes (SWCNTs). SWCNTs are emerging printable air-stable semiconductors that yield high hole mobility values in TFTs and can function at low voltages when paired with a high-*k* dielectric. A low-*k* PLA encapsulating layer was introduced between chitosan and the semiconducting channel in a top gate bottom contact architecture. The PLA layer suppresses unfavourable charge trapping phenomena between the polar hydroxyl groups of chitosan and SWCNTs as well as minimizes degradation of SWCNTs by moisture and oxygen. The PLA/chitosan devices achieved a high mobility upwards of 20 cm2 V−1 s−1 with an on/off current ratio in the 104 range and a low threshold voltage of −1.6 V. The mobility values achieved in this work are 100–1000 fold greater than previously reported values for blends of chitosan, making SWCNT TFTs with a PLA/chitosan bilayer dielectric a promising dielectric for fast and low power applications within the field of printed electronics.

Contribution

I helped with the capacitor fabrication, characterization, and data interpretation. I also helped with the thin film transistor fabrication, characterization, and data interpretation. I reviewed the submitted manuscript.